Multi-Magnon Excitations in One-Dimensional Quantum Spin Chains with NNN Interactions

by

Sandra Leigh Mary Cyr

A Thesis

Submitted to the Faculty of Graduate Studies

in Partial Fulfillment of the Requirements

for the Degree of

MASTER OF SCIENCE

Department of Physics

University of Manitoba

Winnipeg, Manitoba

ISBN 0-315-99038-4

Name Sandra Cyc

Dissertation Abstracts International is arranged by broad, general subject categories. Please select the one subject which most nearly describes the content of your dissertation. Enter the corresponding four-digit code in the spaces provided.

Physics, General
SUBJECT TERM

0605
SUBJECT CODE

U·M·I

Subject Categories

THE HUMANITIES AND SOCIAL SCIENCES

COMMUNICATIONS AND THE ARTS
Architecture 0729
Art History 0377
Cinema 0900
Dance 0378
Fine Arts 0357
Information Science 0723
Journalism 0391
Library Science 0399
Mass Communications 0708
Music 0413
Speech Communication 0459
Theater 0465

EDUCATION
General 0515
Administration 0514
Adult and Continuing 0516
Agricultural 0517
Art 0273
Bilingual and Multicultural 0282
Business 0688
Community College 0275
Curriculum and Instruction 0727
Early Childhood 0518
Elementary 0524
Finance 0277
Guidance and Counseling 0519
Health 0680
Higher 0745
History of 0520
Home Economics 0278
Industrial 0521
Language and Literature 0279
Mathematics 0280
Music 0522
Philosophy of 0998
Physical 0523
Psychology 0525
Reading 0535
Religious 0527
Sciences 0714
Secondary 0533
Social Sciences 0534
Sociology of 0340
Special 0529
Teacher Training 0530
Technology 0710
Tests and Measurements 0288
Vocational 0747

LANGUAGE, LITERATURE AND LINGUISTICS
Language
- General 0679
- Ancient 0289
- Linguistics 0290
- Modern 0291

Literature
- General 0401
- Classical 0294
- Comparative 0295
- Medieval 0297
- Modern 0298
- African 0316
- American 0591
- Asian 0305
- Canadian (English) 0352
- Canadian (French) 0355
- English 0593
- Germanic 0311
- Latin American 0312
- Middle Eastern 0315
- Romance 0313
- Slavic and East European 0314

PHILOSOPHY, RELIGION AND THEOLOGY
Philosophy 0422
Religion
- General 0318
- Biblical Studies 0321
- Clergy 0319
- History of 0320
- Philosophy of 0322

Theology 0469

SOCIAL SCIENCES
American Studies 0323
Anthropology
- Archaeology 0324
- Cultural 0326
- Physical 0327

Business Administration
- General 0310
- Accounting 0272
- Banking 0770
- Management 0454
- Marketing 0338

Canadian Studies 0385
Economics
- General 0501
- Agricultural 0503
- Commerce-Business 0505
- Finance 0508
- History 0509
- Labor 0510
- Theory 0511

Folklore 0358
Geography 0366
Gerontology 0351
History
- General 0578
- Ancient 0579
- Medieval 0581
- Modern 0582
- Black 0328
- African 0331
- Asia, Australia and Oceania 0332
- Canadian 0334
- European 0335
- Latin American 0336
- Middle Eastern 0333
- United States 0337

History of Science 0585
Law 0398
Political Science
- General 0615
- International Law and Relations 0616
- Public Administration 0617

Recreation 0814
Social Work 0452
Sociology
- General 0626
- Criminology and Penology 0627
- Demography 0938
- Ethnic and Racial Studies 0631
- Individual and Family Studies 0628
- Industrial and Labor Relations 0629
- Public and Social Welfare 0630
- Social Structure and Development 0700
- Theory and Methods 0344

Transportation 0709
Urban and Regional Planning 0999
Women's Studies 0453

THE SCIENCES AND ENGINEERING

BIOLOGICAL SCIENCES
Agriculture
- General 0473
- Agronomy 0285
- Animal Culture and Nutrition 0475
- Animal Pathology 0476
- Food Science and Technology 0359
- Forestry and Wildlife 0478
- Plant Culture 0479
- Plant Pathology 0480
- Plant Physiology 0817
- Range Management 0777
- Wood Technology 0746

Biology
- General 0306
- Anatomy 0287
- Biostatistics 0308
- Botany 0309
- Cell 0379
- Ecology 0329
- Entomology 0353
- Genetics 0369
- Limnology 0793
- Microbiology 0410
- Molecular 0307
- Neuroscience 0317
- Oceanography 0416
- Physiology 0433
- Radiation 0821
- Veterinary Science 0778
- Zoology 0472

Biophysics
- General 0786
- Medical 0760

EARTH SCIENCES
Biogeochemistry 0425
Geochemistry 0996
Geodesy 0370
Geology 0372
Geophysics 0373
Hydrology 0388
Mineralogy 0411
Paleobotany 0345
Paleoecology 0426
Paleontology 0418
Paleozoology 0985
Palynology 0427
Physical Geography 0368
Physical Oceanography 0415

HEALTH AND ENVIRONMENTAL SCIENCES
Environmental Sciences 0768
Health Sciences
- General 0566
- Audiology 0300
- Chemotherapy 0992
- Dentistry 0567
- Education 0350
- Hospital Management 0769
- Human Development 0758
- Immunology 0982
- Medicine and Surgery 0564
- Mental Health 0347
- Nursing 0569
- Nutrition 0570
- Obstetrics and Gynecology 0380
- Occupational Health and Therapy 0354
- Ophthalmology 0381
- Pathology 0571
- Pharmacology 0419
- Pharmacy 0572
- Physical Therapy 0382
- Public Health 0573
- Radiology 0574
- Recreation 0575
- Speech Pathology 0460
- Toxicology 0383

Home Economics 0386

PHYSICAL SCIENCES
Pure Sciences
Chemistry
- General 0485
- Agricultural 0749
- Analytical 0486
- Biochemistry 0487
- Inorganic 0488
- Nuclear 0738
- Organic 0490
- Pharmaceutical 0491
- Physical 0494
- Polymer 0495
- Radiation 0754

Mathematics 0405
Physics
- General 0605
- Acoustics 0986
- Astronomy and Astrophysics 0606
- Atmospheric Science 0608
- Atomic 0748
- Electronics and Electricity 0607
- Elementary Particles and High Energy 0798
- Fluid and Plasma 0759
- Molecular 0609
- Nuclear 0610
- Optics 0752
- Radiation 0756
- Solid State 0611

Statistics 0463

Applied Sciences
Applied Mechanics 0346
Computer Science 0984
Engineering
- General 0537
- Aerospace 0538
- Agricultural 0539
- Automotive 0540
- Biomedical 0541
- Chemical 0542
- Civil 0543
- Electronics and Electrical 0544
- Heat and Thermodynamics 0348
- Hydraulic 0545
- Industrial 0546
- Marine 0547
- Materials Science 0794
- Mechanical 0548
- Metallurgy 0743
- Mining 0551
- Nuclear 0552
- Packaging 0549
- Petroleum 0765
- Sanitary and Municipal 0554
- System Science 0790

Geotechnology 0428
Operations Research 0796
Plastics Technology 0795
Textile Technology 0994

PSYCHOLOGY
General 0621
Behavioral 0384
Clinical 0622
Developmental 0620
Experimental 0623
Industrial 0624
Personality 0625
Physiological 0989
Psychobiology 0349
Psychometrics 0632
Social 0451

Nom _____

Dissertation Abstracts International est organisé en catégories de sujets. Veuillez s.v.p. choisir le sujet qui décrit le mieux votre thèse et inscrivez le code numérique approprié dans l'espace réservé ci-dessous.

_____ ☐☐☐ U·M·I

SUJET — CODE DE SUJET

Catégories par sujets

HUMANITÉS ET SCIENCES SOCIALES

COMMUNICATIONS ET LES ARTS
Architecture 0729
Beaux-arts 0357
Bibliothéconomie 0399
Cinéma 0900
Communication verbale 0459
Communications 0708
Danse 0378
Histoire de l'art 0377
Journalisme 0391
Musique 0413
Sciences de l'information 0723
Théâtre 0465

ÉDUCATION
Généralités 515
Administration 0514
Art 0273
Collèges communautaires 0275
Commerce 0688
Économie domestique 0278
Éducation permanente 0516
Éducation préscolaire 0518
Éducation sanitaire 0680
Enseignement agricole 0517
Enseignement bilingue et multiculturel 0282
Enseignement industriel 0521
Enseignement primaire. 0524
Enseignement professionnel 0747
Enseignement religieux 0527
Enseignement secondaire 0533
Enseignement spécial 0529
Enseignement supérieur 0745
Évaluation 0288
Finances 0277
Formation des enseignants 0530
Histoire de l'éducation 0520
Langues et littérature 0279
Lecture 0535
Mathématiques 0280
Musique 0522
Orientation et consultation 0519
Philosophie de l'éducation 0998
Physique 0523
Programmes d'études et enseignement 0727
Psychologie 0525
Sciences 0714
Sciences sociales 0534
Sociologie de l'éducation 0340
Technologie 0710

LANGUE, LITTÉRATURE ET LINGUISTIQUE
Langues
- Généralités 0679
- Anciennes 0289
- Linguistique 0290
- Modernes 0291

Littérature
- Généralités 0401
- Anciennes 0294
- Comparée 0295
- Médiévale 0297
- Moderne 0298
- Africaine 0316
- Américaine 0591
- Anglaise 0593
- Asiatique 0305
- Canadienne (Anglaise) 0352
- Canadienne (Française) 0355
- Germanique 0311
- Latino-américaine 0312
- Moyen-orientale 0315
- Romane 0313
- Slave et est-européenne 0314

PHILOSOPHIE, RELIGION ET THÉOLOGIE
Philosophie 0422
Religion
- Généralités 0318
- Clergé 0319
- Études bibliques 0321
- Histoire des religions 0320
- Philosophie de la religion 0322

Théologie 0469

SCIENCES SOCIALES
Anthropologie
- Archéologie 0324
- Culturelle 0326
- Physique 0327

Droit 0398
Économie
- Généralités 0501
- Commerce-Affaires 0505
- Économie agricole 0503
- Économie du travail 0510
- Finances 0508
- Histoire 0509
- Théorie 0511

Études américaines 0323
Études canadiennes 0385
Études féministes 0453
Folklore 0358
Géographie 0366
Gérontologie 0351
Gestion des affaires
- Généralités 0310
- Administration 0454
- Banques 0770
- Comptabilité 0272
- Marketing 0338

Histoire
- Histoire générale 0578
- Ancienne 0579
- Médiévale 0581
- Moderne 0582
- Histoire des noirs 0328
- Africaine 0331
- Canadienne 0334
- États-Unis 0337
- Européenne 0335
- Moyen-orientale 0333
- Latino-américaine 0336
- Asie, Australie et Océanie 0332

Histoire des sciences 0585
Loisirs 0814
Planification urbaine et régionale 0999
Science politique
- Généralités 0615
- Administration publique 0617
- Droit et relations internationales 0616

Sociologie
- Généralités 0626
- Aide et bien-être social 0630
- Criminologie et établissements pénitentiaires 0627
- Démographie 0938
- Études de l' individu et de la famille 0628
- Études des relations interethniques et des relations raciales 0631
- Structure et développement social 0700
- Théorie et méthodes. 0344
- Travail et relations industrielles 0629

Transports 0709
Travail social 0452

SCIENCES ET INGÉNIERIE

SCIENCES BIOLOGIQUES
Agriculture
- Généralités 0473
- Agronomie. 0285
- Alimentation et technologie alimentaire 0359
- Culture 0479
- Élevage et alimentation 0475
- Exploitation des pâturages 0777
- Pathologie animale 0476
- Pathologie végétale 0480
- Physiologie végétale 0817
- Sylviculture et faune 0478
- Technologie du bois 0746

Biologie
- Généralités 0306
- Anatomie 0287
- Biologie (Statistiques) 0308
- Biologie moléculaire 0307
- Botanique 0309
- Cellule 0379
- Écologie 0329
- Entomologie 0353
- Génétique 0369
- Limnologie 0793
- Microbiologie 0410
- Neurologie 0317
- Océanographie 0416
- Physiologie 0433
- Radiation 0821
- Science vétérinaire 0778
- Zoologie 0472

Biophysique
- Généralités 0786
- Medicale 0760

SCIENCES DE LA TERRE
Biogéochimie 0425
Géochimie 0996
Géodésie 0370
Géographie physique 0368
Géologie 0372
Géophysique 0373
Hydrologie 0388
Minéralogie 0411
Océanographie physique 0415
Paléobotanique 0345
Paléoécologie 0426
Paléontologie 0418
Paléozoologie 0985
Palynologie 0427

SCIENCES DE LA SANTÉ ET DE L'ENVIRONNEMENT
Économie domestique 0386
Sciences de l'environnement 0768
Sciences de la santé
- Généralités 0566
- Administration des hôpitaux 0769
- Alimentation et nutrition 0570
- Audiologie 0300
- Chimiothérapie 0992
- Dentisterie 0567
- Développement humain 0758
- Enseignement 0350
- Immunologie 0982
- Loisirs 0575
- Médecine du travail et thérapie 0354
- Médecine et chirurgie 0564
- Obstétrique et gynécologie 0380
- Ophtalmologie 0381
- Orthophonie 0460
- Pathologie 0571
- Pharmacie 0572
- Pharmacologie 0419
- Physiothérapie 0382
- Radiologie 0574
- Santé mentale 0347
- Santé publique 0573
- Soins infirmiers 0569
- Toxicologie 0383

SCIENCES PHYSIQUES
Sciences Pures
Chimie
- Généralités 0485
- Biochimie 487
- Chimie agricole 0749
- Chimie analytique 0486
- Chimie minérale 0488
- Chimie nucléaire 0738
- Chimie organique 0490
- Chimie pharmaceutique 0491
- Physique 0494
- PolymÈres 0495
- Radiation 0754

Mathématiques 0405
Physique
- Généralités 0605
- Acoustique 0986
- Astronomie et astrophysique 0606
- Électronique et électricité 0607
- Fluides et plasma 0759
- Météorologie 0608
- Optique 0752
- Particules (Physique nucléaire) 0798
- Physique atomique 0748
- Physique de l'état solide 0611
- Physique moléculaire 0609
- Physique nucléaire 0610
- Radiation 0756

Statistiques 0463

Sciences Appliqués Et Technologie
Informatique 0984
Ingénierie
- Généralités 0537
- Agricole 0539
- Automobile 0540
- Biomédicale 0541
- Chaleur et thermodynamique 0348
- Conditionnement (Emballage) 0549
- Génie aérospatial 0538
- Génie chimique 0542
- Génie civil 0543
- Génie électronique et électrique 0544
- Génie industriel 0546
- Génie mécanique 0548
- Génie nucléaire 0552
- Ingénierie des systèmes 0790
- Mécanique navale 0547
- Métallurgie 0743
- Science des matériaux 0794
- Technique du pétrole 0765
- Technique minière 0551
- Techniques sanitaires et municipales 0554
- Technologie hydraulique 0545

Mécanique appliquée 0346
Géotechnologie 0428
Matières plastiques (Technologie) 0795
Recherche opérationnelle 0796
Textiles et tissus (Technologie) 0794

PSYCHOLOGIE
Généralités 0621
Personnalité 0625
Psychobiologie 0349
Psychologie clinique 0622
Psychologie du comportement 0384
Psychologie du développement 0620
Psychologie expérimentale 0623
Psychologie industrielle 0624
Psychologie physiologique 0989
Psychologie sociale 0451
Psychométrie 0632

MULTI-MAGNON EXCITATIONS IN ONE-DIMENSIONAL QUANTUM SPIN CHAINS WITH NNN INTERACTIONS

BY

SANDRA LEIGH MARY CYR

A Thesis submitted to the Faculty of Graduate Studies of the University of Manitoba in partial fulfillment of the requirements for the degree of

MASTER OF SCIENCE

Abstract

The two and three-magnon excitation spectra are calculated and analyzed for one-dimensional Hamiltonians with general two-spin interactions plus interactions extending to second neighbors. The specific cases studied are the Heisenberg Hamiltonian with both nearest neighbor and next nearest neighbor (NNN) interactions, the Takhtajan and Babujian model ([7], [8]) with both nearest neighbor and next nearest neighbor interactions and a nearest neighbor Heisenberg Hamiltonian with the addition of a term involving interactions between three adjacent spins on the chain (Tsvelik [9]). The two-magnon spectra are studied using both analytical and numerical rescaling methods and the three-magnon spectra are studied using the recursion method. The complete dispersion diagrams for both two and three-magnons are found for varying strengths of the next nearest neighbor interactions consistent with a ferromagnetic ground state.

Ackowledgements

I wish to thank Dr. B.W. Southern for his guidance, kindness and patience in supervising this research. The financial support of the Natural Sciences and Engineering Research Council of Canada is gratefully acknowledged.

Contents

List of Figures

List of Tables

Chapter 1

Introduction

Magnetism has always been a fascinating topic. The Greeks first discovered magnetism in naturally occurring rocks called magnetite over 2000 years ago. Their interest in the 'mysterious' force, which arises when you try to push two magnets together in the way they do not want to go, has led to much interest and study in magnetism. It is now known that magnetism is inseparably related to electricity, and the union of the two is called electromagnetism.

The source of the magnetic interaction is purely quantum mechanical. For a two electron system, the Pauli principle states that the total wavefunction must be antisymmetric under a particle interchange. Since the total wavefunction involves both spatial and spin degrees of freedom, the spatial and spin parts of the wavefunction cannot have the same symmetry under exchange. Two hydrogen-like atoms can be in a state with total spin $S = 0$ (known as the singlet state) with a symmetric spatial wavefunction, or in one of three states with total spin $S = 1$ (known as the triplet states) with an antisymmetric spatial wavefunction. These states in general have different energies due to the spatially dependent Coulomb forces, and the difference can be expressed by a Hamiltonian of the form:

$$\widehat{H}^{spin} = -J\widetilde{S}_1 \cdot \widetilde{S}_2 \tag{1.1}$$

The $\widetilde{S}_1$ and $\widetilde{S}_2$ are spin operators and J is known as the exchange integral. If J

is positive parallel alignment of the spins are favored (ferromagnetic), and if J is negative antiparallel alignment of the spins are favored (antiferromagnetic).

Dirac [1] and Heisenberg [2] extended the above spin Hamiltonian to include the interactions between all pairs of ions on a lattice:

$$\widehat{H}^{Heis} = -\sum_{i,j} J_{ij}(\widetilde{S}_i \cdot \widetilde{S}_j) \tag{1.2}$$

The above form is the simplest model Hamiltonian used to describe magnetic systems and if the material is an insulator the range of the interactions is restricted to nearest or next nearest neighbor spins on the lattice of ions. Higher order terms in the spins can also be present but are generally much weaker (essentially a multipole expansion), so the general form of $\widehat{H}$ for a system of quantum spins each with spin S ($S = \frac{1}{2}, 1, \frac{3}{2}, \ldots$) is [3]

$$\widehat{H} = -\sum_{i,j} \sum_{n=1}^{2S} J_{ij}^{(n)}(\widetilde{S}_i \cdot \widetilde{S}_j)^n \tag{1.3}$$

There are $2S$ independent couplings $J_{ij}^{(n)}$ since the $(\widetilde{S}_i \cdot \widetilde{S}_j)^0$ term is absorbed into a shift in the zero of the energy. The strength of the $J_{ij}^{(n)}$ exchange integrals depend on the degree of overlap between the wavefunctions of the i^{th} and j^{th} electrons. Thus $J_{ij}^{(n)}$ decreases rapidly as r_{ij} (the distance between the i^{th} and j^{th} electrons) increases. Richard Lee [4] has previously studied in detail the excitation spectrum of (1.3) for the case of a one-dimensional lattice when the exchange integrals are nonzero, uniform and restricted to nearest neighbor spins. In this case, the Hamiltonian can be written as

$$\widehat{H} = -\sum_{i} \sum_{n=1}^{2S} J^{(n)}(\widetilde{S}_i \cdot \widetilde{S}_{i+1})^n \tag{1.4}$$

The eigenvalues of (1.4) can be labeled by the total z-component of the spin system, S_{tot}^z. The state of maximum or minimum $\mid S_{tot}^z \mid = NS$, which has all spins

parallel, is an exact eigenstate with energy

$$E = -N \sum_{n=1}^{2S} J^{(n)} S^{2n}$$

For arbitrary values of the $J^{(n)}$, this state may or may not be the lowest energy state. In the following discussion, we will assume that the values of the $J^{(n)}$ are restricted such that this "ferromagnetic" state is the ground state. Higher energy states correspond to reducing $\mid S^z_{tot} \mid = NS - m$ by m units and these states are called m-magnon states.

The other eigenvalues of (1.4) cannot be obtained in closed form except for special cases. In principal, the cases of $m = 1$ and $m = 2$ can be solved using elementary methods in any dimension. However, the general m-magnon problem is only soluble in special cases in $d = 1$. These special cases are known as completely integrable models and can be solved using a well known technique called the Bethe Ansatz [5]. Bethe first applied this approach to the $S = \frac{1}{2}$ Heisenberg Hamiltonian in 1931 and found that the Hamiltonian has an adequate number of symmetry properties, and thus conserved quantities, to completely diagonalize the Hamiltonian and solve the system. The Bethe Ansatz can be used to solve any completely integrable system but it cannot be used to solve systems of limited integrability. The excitation spectra of completely integrable systems have special properties which can be used to identify integrable models. Haldane [6] has conjectured that an m-magnon spectra has a bound state branch which in the extended zone scheme ranges over a minimum of $(m, 2S)$ consecutive Brillouin zones or which in the reduced zone scheme (which we will use) has several branches. In an integrable model the branches are both real and continuous, meet at the boundaries and are decoupled from the continuum. However, in a non-integrable model the branches will in general produce gaps at the boundaries and will become resonances upon entering the continuum.

In this thesis two distinct cases with additional interactions beyond nearest neighbor interactions will be considered. The first case includes a general form of two-spin interactions which extend to second neighbors.

$$\widehat{H} = -\sum_{i}\sum_{n=1}^{2S} J_1^{(n)}(\widetilde{S}_i \cdot \widetilde{S}_{i+1})^n - \sum_{i}\sum_{n=1}^{2S} J_2^{(n)}(\widetilde{S}_i \cdot \widetilde{S}_{i+2})^n \tag{1.5}$$

This Hamiltonian is restricted to a uniform, homogeneous, one-dimensional system, so all of the spins have the same magnitude S and the $J_{i,i+1}^{(n)}$ and the $J_{i,i+2}^{(n)}$ are independent of i. The second case that will be considered is the addition of a term involving interactions between three adjacent spins on the chain.

$$\widehat{H} \;=\; -J_1\sum_{i=1}^{N}(\widetilde{S}_i \cdot \widetilde{S}_{i+1}) - J_2\sum_{i=1}^{N}\widetilde{S}_{i-1}\cdot(\widetilde{S}_i \times \widetilde{S}_{i+1}) \tag{1.6}$$

This Hamiltonian is also restricted to a uniform, homogeneous, one-dimensional system. Thus all of the spins are equal in magnitude, and the J_1 and J_2 are independent of i.

Both of these Hamiltonians are integrable under certain conditions. For example, in equation (1.5) if the next nearest neighbor interactions are all set equal to zero, then the Hamiltonian reduces to the Hamiltonian studied by Lee [4], equation (1.4). In this case the model describes a family of integrable models for different values of S and the $J_1^{(n)}$ ([7], [8]) and reduces to the Heisenberg model when $S = \frac{1}{2}$. With the next nearest neighbor interactions nonzero and the nearest neighbor interactions zero, the Hamiltonian is also integrable for the above conditions since it describes the interactions between two decoupled chains. With both nearest neighbor and next nearest neighbor interactions present, the Hamiltonian is not integrable. We will study what happens to the excitation spectra as the Hamiltonian shifts from only nearest neighbor, to mixed, to only next nearest neighbor interactions.

The system in equation (1.6) was found by Tsvelik [9] to be integrable for $S = \frac{1}{2}$ for all values of $\frac{J_2}{J_1}$. For higher values of S the Hamiltonian is no longer integrable.

To study these systems in the limit of an infinite chain with an infinite number of quantum spins, we first consider the commutation relations of (1.5) and (1.6) with various operators. Periodic boundary conditions are used, so both of the Hamiltonians commute with the discrete translation operator $\widehat{T}_a$, where a is the lattice spacing.

$$\left[\widehat{T}_a, \widehat{H}\right] = 0 \tag{1.7}$$

This commutation relation indicates that the total momentum is a good quantum number. The Hamiltonians also commute with the total spin operator, $\widetilde{S}^2_{tot}$, and the total spin in the z-direction, S^z_{tot}.

$$\left[\widetilde{S}^2_{tot}, \widehat{H}\right] = 0 \tag{1.8}$$

$$\left[S^z_{tot}, \widehat{H}\right] = 0 \tag{1.9}$$

Only equations (1.7) and (1.9) are used in the formalism which follows and because equation (1.8) will not be used explicitly, anisotropic terms could be included in the Hamiltonian.

Since the Hamiltonians commute with S^z_{tot}, we can block diagonalize the Hamiltonian with respect to this quantum number. For each value of $\mid S^z_{tot} \mid = NS - m$, the simultaneous eigenkets of the local operators $\widetilde{S}^2_i$ and S^z_i are used to form basis states which in Dirac bra-ket notation are denoted by $\mid S, m_S\rangle_i$. Since we are dealing with the ferromagnetic ground state, the ground state has all spins parallel. We apply a very weak magnetic field in the -z direction to break the rotational symmetry of our Hamiltonian and we have a unique ground state given by the direct product of the single spin states.

$$\mid 0\rangle = \mid S, -S\rangle_1 \mid S, -S\rangle_2 \cdots \mid S, -S\rangle_N \tag{1.10}$$

The $\mid 0\rangle$ ket indicates the ground state and in an infinite chain $N \to \infty$. For the

Hamiltonian in (1.5) this state has the energy per site

$$E_0 = -\sum_{n=1}^{2S} J_1^{(n)} S^{2n} - \sum_{n=1}^{2S} J_2^{(n)} S^{2n}$$

and for the Hamiltonian in (1.6) this state has the energy per site

$$E_0 = -J_1 S^2$$

We will now consider excited states of these systems which correspond to $m \neq 0$. Consider a state with a single spin on site j raised by one unit from the ground state represented by

$$\mid j\rangle = \frac{1}{\sqrt{2S}} S_j^+ \mid 0\rangle \tag{1.11}$$

$$= \mid S,-S\rangle_1 \cdots \mid S,-S\rangle_{j-1} \mid S,-S+1\rangle_j \mid S,-S\rangle_{j+1} \cdots \mid S,-S\rangle_N \tag{1.12}$$

where $\frac{1}{\sqrt{2S}}$ is a normalization factor. This one site spin deviation state is not, however, an eigenstate of the Hamiltonian. We find that the deviation in spin must be shared by all spin sites in order for the state to be an eigenstate of the Hamiltonian. Due to (1.7) the state must also be an eigenstate of $\widehat{T}_a$ so using Bloch's theorem these eigenstates of the Hamiltonian are given by

$$\mid k\rangle = \sum_j \frac{e^{-ikr_j}}{\sqrt{N}} \mid j\rangle,\ r_j = ja \tag{1.13}$$

independent of the detailed form of $\widehat{H}$. The wavevector k can take on any of the values $k = \frac{2\pi n}{Na}$, $n = -\frac{N}{2}, -\frac{N}{2}+1, \ldots, \frac{N}{2}$. If N is infinite, k takes on any value between $-\frac{\pi}{a}$ and $\frac{\pi}{a}$. Then the conserved quantities, total spin in the z-direction $\mid S_{tot}^z \mid = NS - 1$ and total momentum k, diagonalize $\widehat{H}$ in the subspace of one-magnon excitations. When the spins are treated as classical vectors in the semiclassical limit, the excitations can be pictured as propagating waves or oscillations in the relative orientation of spins on a lattice. These propagating

waves are known as spin waves. Thus a one-magnon excitation is a quantized spin wave.

When we apply the Hamiltonian (1.5) to this one-magnon eigenstate, we get the following eigenvalue

$$E_1 = \alpha_1(S)(1-\cos ka) + \alpha_1'(S)(1-\cos 2ka) \tag{1.14}$$

where $\alpha_1(S)$ is a function of S and the $J_1^{(n)}$ and $\alpha_1'(S)$ is the same function of S and the $J_2^{(n)}$. These are convenient variables and will be defined in Chapter 2. We have restrictions on the allowed values of $\alpha_1(S)$ and $\alpha_1'(S)$ since the ferromagnetic ground state is stable only for $E_1 \geq 0$. For $\alpha_1(S) > 0$, we require that $\frac{\alpha_1'(S)}{\alpha_1(S)} \geq -\frac{1}{4}$.

The one-magnon excitation energy of the Hamiltonian of equation (1.6) is

$$E_1 = (2J_1S + 4J_2S^2 \sin ka)(1-\cos ka) \tag{1.15}$$

The ferromagnetic ground state is stable in this case for $J_1 > 0$ if $2S \mid J_2 \mid \leq J_1$.

These theoretical magnons have been observed in real materials. Methods such as inelastic magnetic neutron scattering, infrared absorption, and ESR are used to detect magnons. For example, Hoogerbeets et al. [10] used ESR experiments to observe the first 7 bound magnon levels in $(C_6H_{11}NH_3)CuCl_3$, a quasi-one-dimensional $S = \frac{1}{2}$ nearly Heisenberg ferromagnetic compound. Haines and Drumheller [11] also observed magnons in the same compound. As well, Torrace and Tinkham [12] observed bound magnons in the $S = \frac{1}{2}$ quasi-one-dimensional ferromagnet $CoCl_2 \cdot 2H_2O$ using far-infrared absorption. In all of these experiments interpretations involving magnons accounted for the qualitative behavior of the results. Recent experimental work on magnetic materials containing exchange-coupled rare earth ions and inorganic radicals have synthesized linear chain compounds. Magnetic susceptibility measurements indicate the presence of next nearest neighbor interactions [13], which provides motivation for our work.

Before we proceed, we should note that the Hamiltonians we are considering neglect many factors which are often important in real materials. These include alternating spins, anisotropic spin exchange, single-ion anisotropies, and the effects of an external magnetic field. These omissions, made to simplify the problem and the resulting Hamiltonian, would be straightforward to include in our formalism.

Now let us consider the subspace $\mid S^z_{tot} \mid = NS - 2$, where any eigenstate of the Hamiltonian can be written as a linear combination of states having two spin deviations. Such states can be regarded as a pair of interacting spin waves, and are called two-magnon excitations. The pair has conserved total momentum K but can scatter from each other. The total energy of the scattering states forms a continuum for any fixed value of K. In addition to the scattering states, there are also bound states which have complex wavevectors and correspond to the pair being localized in the neighborhood of each other due to an attractive interaction.

In general, the two-magnon problem is soluble in any dimension, since it reduces to essentially a defect problem on a d-dimensional lattice. In $d = 1$ Majumdar [14], Ono, Mikado and Oguchi [15], and Gochev [16] have studied the Hamiltonian (1.5) for $S = \frac{1}{2}$, and Bahurmuz and Loly [17] have studied (1.5) for general S in the Heisenberg case. We will extend these studies of the two-magnon problem to the general case for general S. We will also consider the two-magnon excitations of the Hamiltonian (1.6) for general S. For all of these cases the scattering state continuum edges will be found analytically. Analytic expressions for the bound state energies at certain values of K will be obtained using the one-dimensional scaling approach of Southern, Liu and Lavis [18]. This real space rescaling method constructs a transformation on the system of equations which leaves their form invariant but renormalizes the various parameters appearing in them. By iterating the transformation the spectral properties of the system can be determined. At

the values of K for which analytical solutions cannot be found, we can again use the scaling approach, but the method must be modified into a matrix form and the iterations are done numerically by computer [19]. We will refer to this procedure as the matrix rescaling method.

Finally, we will use the information from the one and two-magnon excitation spectra to study excitations involving three-magnons. Three or more magnon excitations can also be viewed as interacting spin waves. The eigenvalues are also composed of both scattering states and bound states. The solutions to the Schrödinger equation are not nearly so simple as in the one or two-magnon cases. In general, the problem is similar to an extended defect problem. The Heisenberg case of equation (1.5) has been studied by Millet and Kaplan [20] for $S = \frac{1}{2}, 1$ and $\frac{3}{2}$ with nearest neighbor interactions only, by Lee for general S with nearest neighbor interactions only, and by Kadolkar, Ghosh and Sarma [21] for $S = 1$ with nearest and next nearest neighbor interactions of varying strength. We will consider the general case for nearest neighbor and next nearest neighbor interactions of varying strength for general S. We will also consider the three-magnon excitations of the Hamiltonian of equation (1.6) for general S. Both the continuum edges and the bound state energies must now be found using numerical methods. The continuum edges are easily found by considering three free-magnons (solutions to the one-magnon problem) and two bound-magnons (solutions to the two-magnon problem) combined with one-free. To find the bound state energies we use a method known as the Recursion method. This method, first introduced by Haydock [22], reduces the Hamiltonian to a tridiagonal form, which can be used to calculate the Green's function and hence the density of states.

In the next chapter we will obtain the one and two-magnon equations for the Hamiltonian (1.5). The results of the one-magnon excitation energy will be exam-

ined and used to analytically predict the two-magnon scattering state continuum edges. The rescaling method used to predict the bound states of the two-magnon spectrum for special cases will be discussed and applied, as will be the matrix rescaling method. The results will be examined, and where possible comparisons will be made with previous literature. The three-magnon equations will be obtained in the first section of Chapter 3 and mapped to a convenient form for visualizing and programming. The three-magnon scattering state continuum edges will be found. Chapter 4 will begin with a description of the recursion method used to find the spectra of the three-magnon excitations. The results found for specific Hamiltonian cases and different values of S using this method will be given, discussed and, where possible, compared to previous literature. In Chapter 5 the Hamiltonian (1.6) will be considered. The one, two and three-magnon equations for this $S = \frac{1}{2}$ integrable Hamiltonian with competing interactions will be given, and the spectra will be found using the methods described in Chapters 2, 3 and 4. Chapter 6 will summarize the results of this thesis.

Chapter 2

One and Two-Magnon Excitations

In this chapter the one and two-magnon equations for the Hamiltonian (1.5),

$$\widehat{H} = -\sum_l \sum_{n=1}^{2S} J_1^{(n)} (\tilde{S}_l \cdot \tilde{S}_{l+1})^n - \sum_l \sum_{n=1}^{2S} J_2^{(n)} (\tilde{S}_l \cdot \tilde{S}_{l+2})^n$$

will be derived. It is convenient to express the Hamiltonian in terms of a sum over pair Hamiltonians $\widehat{H}_l^{nn}$ and $\widehat{H}_l^{nnn}$ [4]

$$\begin{aligned} \widehat{H} &= \sum_l \widehat{H}_l \\ &= \sum_l (\widehat{H}_l^{nn} + \widehat{H}_l^{nnn}) \end{aligned} \tag{2.1}$$

where

$$\begin{aligned} \widehat{H}_l^{nn} &= -\sum_{n=1}^{2S} J_1^{(n)} \tilde{P}_l^n \\ \widehat{H}_l^{nnn} &= -\sum_{n=1}^{2S} J_2^{(n)} \tilde{Q}_l^n \end{aligned} \tag{2.2}$$

and

$$\begin{aligned} \tilde{P}_l &= \tilde{S}_l \cdot \tilde{S}_{l+1} \\ \tilde{Q}_l &= \tilde{S}_l \cdot \tilde{S}_{l+2} \end{aligned} \tag{2.3}$$

One can express $\widetilde{P}_l$ and $\widetilde{Q}_l$ in terms of raising and lowering operators as follows

$$\begin{aligned}\widetilde{P}_l &= \frac{1}{2}(S_l^+ S_{l+1}^- + S_l^- S_{l+1}^+) + S_l^z S_{l+1}^z \\ \widetilde{Q}_l &= \frac{1}{2}(S_l^+ S_{l+2}^- + S_l^- S_{l+2}^+) + S_l^z S_{l+2}^z \end{aligned} \tag{2.4}$$

To find the ground state energy we let the pair Hamiltonians act on the ground state, equation (1.10).

$$\widehat{H}_l \mid 0\rangle \;=\; \left[-\sum_{n=1}^{2S}\left(J_1^{(n)}\widetilde{P}_l^n + J_2^{(n)}\widetilde{Q}_l^n\right)\right] \mid 0\rangle \tag{2.5}$$

Using

$$\begin{aligned}\widetilde{P}_l \mid 0\rangle &= S^2 \mid 0\rangle \\ \widetilde{Q}_l \mid 0\rangle &= S^2 \mid 0\rangle \end{aligned} \tag{2.6}$$

it is found that the ground state energy per site is

$$E_0 \;=\; -\sum_{n=1}^{2S}\left(J_1^{(n)}S^{2n} + J_2^{(n)}S^{2n}\right) \tag{2.7}$$

It is convenient to introduce the following variables by considering an isolated pair of nearest neighbor spins. The eigenvalues of the pair Hamiltonian $\widehat{H}_l^{nn}$ are given by λ_j, where j is the total angular momentum quantum number of any pair ($\widetilde{S}_l$ and $\widetilde{S}_{l+1}$).

$$\lambda_j \;=\; -\sum_{n=1}^{2S} J_1^{(n)}\left[\frac{j\,(j+1)}{2} - S(S+1)\right]^n,\; j = 0,1,2,\ldots,2S \tag{2.8}$$

The difference between these eigenvalues and the ground state eigenvalue λ_{2S} are given by

$$\alpha_m(S) \;=\; \lambda_{2S-m} - \lambda_{2S},\; m \in \{1,2,\ldots,2S\} \tag{2.9}$$

Similar variables ($\lambda'_{j'}(J_2^{(n)})$ and $\alpha'_{m'}(S, J_2^{(n)})$) are defined for the eigenvalues of the pair Hamiltonian $\widehat{H}_l^{nnn}$, where the j' is the total angular momentum quantum number of any pair ($\widetilde{S}_l$ and $\widetilde{S}_{l+2}$).

2.1 One-Magnon Excitations

To find the one-magnon excitation energy, let the Hamiltonian of equation (1.5) act on the one-magnon wavefunction (equation (1.13))

$$\mid k\rangle \;=\; \sum_j \frac{e^{-ikr_j}}{\sqrt{N}} \mid j\rangle,\; r_j = ja$$

where $-\frac{\pi}{a} < k \leq \frac{\pi}{a}$. We will break this process up into steps. First we will find the results of $\tilde{P}_l$ and $\tilde{Q}_l$ separately acting on the single spin deviation states. Second we will use equation (2.1) together with (2.2) to find the results of the Hamiltonian acting on these states and then we will use equation (1.13) to find the results of the Hamiltonian acting on an arbitrary state $\mid k\rangle$.

The normalized single spin deviation state is (equation (1.11))

$$\mid j\rangle \;=\; \frac{1}{\sqrt{2S}} S_j^+ \mid 0\rangle$$

Using the properties of the raising and lowering operators, $\tilde{P}_l$ and $\tilde{Q}_l$ acting on state $\mid j\rangle$ give

$$\left.\begin{array}{rcll} \tilde{P}_l \mid j\rangle &=& S^2 \mid j\rangle & ,j \neq l, l+1 \\ \tilde{P}_l \mid l\rangle &=& S(S-1) \mid l\rangle + S \mid l+1\rangle & ,j = l \\ \tilde{P}_l \mid l+1\rangle &=& S \mid l\rangle + S(S-1) \mid l+1\rangle & ,j = l+1 \end{array}\right\} \tag{2.10}$$

$$\left.\begin{array}{rcll} \tilde{Q}_l \mid j\rangle &=& S^2 \mid j\rangle & ,j \neq l, l+2 \\ \tilde{Q}_l \mid l\rangle &=& S(S-1) \mid l\rangle + S \mid l+2\rangle & ,j = l \\ \tilde{Q}_l \mid l+2\rangle &=& S \mid l\rangle + S(S-1) \mid l+2\rangle & ,j = l+2 \end{array}\right\} \tag{2.11}$$

These equations can be expressed in matrix form as

$$\tilde{P}_l \begin{pmatrix} \mid j\rangle \\ \mid l\rangle \\ \mid l+1\rangle \end{pmatrix} \;=\; \mathbf{A} \begin{pmatrix} \mid j\rangle \\ \mid l\rangle \\ \mid l+1\rangle \end{pmatrix} \tag{2.12}$$

with $j \neq l, l+1$ and

$$\tilde{Q}_l \begin{pmatrix} \mid j\rangle \\ \mid l\rangle \\ \mid l+2\rangle \end{pmatrix} \;=\; \mathbf{A} \begin{pmatrix} \mid j\rangle \\ \mid l\rangle \\ \mid l+2\rangle \end{pmatrix} \tag{2.13}$$

with $j \neq l, l+2$, where the matrix $\mathbf{A}$ is

$$\mathbf{A} = \begin{bmatrix} S^2 & 0 & 0 \\ 0 & S(S-1) & S \\ 0 & S & S(S-1) \end{bmatrix} \tag{2.14}$$

Notice that matrix $\mathbf{A}$ is in block diagonal form. From equation (2.2) we need to find $\widetilde{P}_l^n$ and $\widetilde{Q}_l^n$, or equivalently, $\mathbf{A}^n$

$$\mathbf{A}^n = \begin{bmatrix} S^{2n} & 0 & 0 \\ 0 & \theta+\chi & \theta-\chi \\ 0 & \theta-\chi & \theta+\chi \end{bmatrix} \tag{2.15}$$

where

$$\begin{aligned} \theta &= \frac{S^{2n}}{2} \\ \chi &= \frac{S^n (S-2)^n}{2} \end{aligned} \tag{2.16}$$

The variables θ and χ are related to α_1, α_1' and E_0 (equation (2.7)).

$$\begin{aligned} -\sum_n J_1^{(n)}\theta &= -\sum_n J_1^{(n)}\frac{S^{2n}}{2} \\ -\sum_n J_2^{(n)}\theta &= -\sum_n J_2^{(n)}\frac{S^{2n}}{2} \\ -\sum_n J_1^{(n)}\chi &= \frac{\alpha_1}{2} - \sum_n J_1^{(n)}\frac{S^{2n}}{2} \\ -\sum_n J_2^{(n)}\chi &= \frac{\alpha_1'}{2} - \sum_n J_2^{(n)}\frac{S^{2n}}{2} \end{aligned} \tag{2.17}$$

By substituting $\mathbf{A}^n$ into equation (2.2) we can find the effects of $\widehat{H}_l$ acting on an arbitrary state $\mid j\rangle$.

$$\widehat{H}_l \mid j\rangle = \begin{cases} E_0 \mid j\rangle & , j \neq l, l+1, l+2 \\ E_0 \mid l\rangle + \left(\frac{\alpha_1+\alpha_1'}{2}\right) \mid l\rangle - \frac{\alpha_1}{2} \mid l+1\rangle - \frac{\alpha_1'}{2} \mid l+2\rangle & , j = l \\ E_0 \mid l+1\rangle + \frac{\alpha_1}{2} \mid l+1\rangle - \frac{\alpha_1}{2} \mid l\rangle & , j = l+1 \\ E_0 \mid l+2\rangle + \frac{\alpha_1'}{2} \mid l+2\rangle - \frac{\alpha_1'}{2} \mid l\rangle & , j = l+2 \end{cases} \tag{2.18}$$

Therefore by summing over l for equation (2.1) we find

$$\widehat{H} \mid j\rangle = NE_0 \mid j\rangle + (\alpha_1+\alpha_1') \mid j\rangle - \frac{\alpha_1'}{2}[\mid j-2\rangle + \mid j+2\rangle] - \frac{\alpha_1}{2}[\mid j-1\rangle + \mid j+1\rangle] \tag{2.19}$$

Substitute the inverse of (1.13) into equation (2.19) to obtain

$$\hat{H} \mid k\rangle = N E_0 \mid k\rangle + \alpha_1(S)(1-\cos ka) \mid k\rangle + \alpha_1'(S)(1-\cos 2ka) \mid k\rangle \quad (2.20)$$

If we absorb the ground state energy into the zero of the energy, the one-magnon dispersion relation is

$$E_1(k) = \alpha_1(S)(1-\cos ka) + \alpha_1'(S)(1-\cos 2ka) \quad (2.21)$$

The ferromagnetic ground state is stable only for $E_1 \geq 0$, which places restrictions on the allowed values of $\frac{\alpha_1'(S)}{\alpha_1(S)}$. For $\alpha_1 > 0$

$$\beta = \frac{\alpha_1'(S)}{\alpha_1(S)} \geq -\frac{1-\cos ka}{1-\cos 2ka} \quad (2.22)$$

Over the range of k this restriction becomes $\beta = \frac{\alpha_1'(S)}{\alpha_1(S)} \geq -\frac{1}{4}$. If $\alpha_1' = 0$ then the restriction becomes $\alpha_1 \geq 0$ and if $\alpha_1 = 0$ then the restriction becomes $\alpha_1' \geq 0$. For $\alpha_1 > 0$ and $\beta < -\frac{1}{4}$, we find energies less than zero, which means that the ferromagnetic ground state is no longer the true ground state. The one-magnon excitation energy in units of α_1 for $\beta = -\frac{1}{4}, 0, \frac{1}{4}, \frac{1}{2}, \frac{3}{4}$ and 1 is shown in figure 2.1.

$$\frac{E_1(k)}{\alpha_1} = (1-\cos ka) + \beta(1-\cos 2ka) \quad (2.23)$$

Only the range $k = 0$ to π is shown since the excitation energy is symmetric about zero. The variable β is convenient for small ($\beta \leq 1$) next nearest neighbor interaction strength but for dominant next nearest neighbor interactions this variable is no longer convenient since the energy in units of α_1 tends to infinity as $\beta \to \infty$ (when only next nearest neighbor interactions are present). Over the entire range of β there is a more convenient variable for which the energy is in units of $(\alpha_1 + \alpha_1')$. This variable, $\tilde{\beta}$, is defined by

$$\tilde{\beta} = \frac{\beta}{1+\beta} \quad (2.24)$$

where $-\frac{1}{3} \leq \tilde{\beta} \leq 1$ (corresponding to the range $-\frac{1}{4} \leq \beta \leq \infty$). The energy remains finite and the relation between the energy in units of $(\alpha_1 + \alpha_1')$ and the energy in units of α_1 is $\frac{E_1}{\alpha_1+\alpha_1'} = \frac{E_1}{\alpha_1(1+\beta)}$. The one-magnon excitation energy in units of $(\alpha_1 + \alpha_1')$ in shown in figure 2.2 for $\tilde{\beta} = -\frac{1}{3}, 0, \frac{1}{4}, \frac{1}{2}, \frac{3}{4}$ and 1.

$$\frac{E_1(k)}{\alpha_1 + \alpha_1'} = (1-\tilde{\beta})(1-\cos ka) + \tilde{\beta}(1-\cos 2ka) \tag{2.25}$$

The symmetry of the one-magnon excitation energy about $\frac{ka}{\pi} = \frac{1}{2}$ at $\tilde{\beta} = 1$ occurs because the chain reduces to two decoupled chains each with a lattice spacing of $2a$. Note that when $E_1(k)$ is measured in units of $\alpha_1 + \alpha_1'$, the value at $\frac{ka}{\pi} = \frac{2}{3}$ is independent of $\tilde{\beta}$.

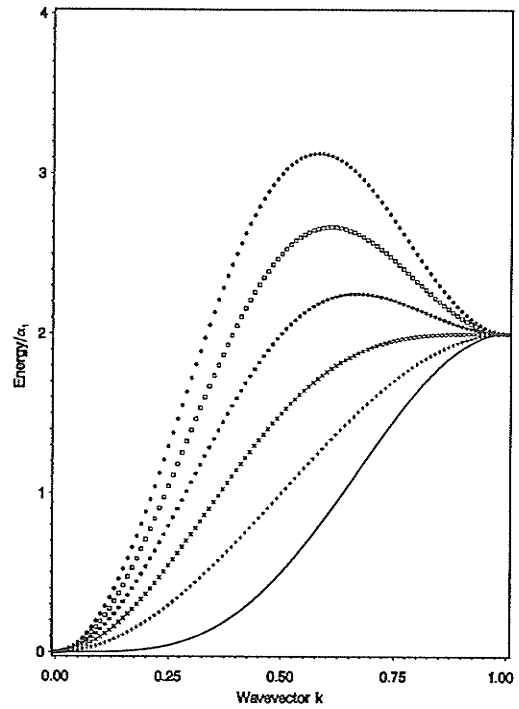

Figure 2.1: One-magnon excitation energy in units of $\alpha_1(S)$ for a uniform Heisenberg chain. The wavevector k is in units of $\frac{\pi}{a}$. The solid line corresponds to $\beta = -0.25$; $+$ to $\beta = 0.0$; $\times$ to $\beta = 0.25$; $*$ to $\beta = 0.5$; $\square$ to $\beta = 0.75$; $\diamond$ to $\beta = 1.0$.

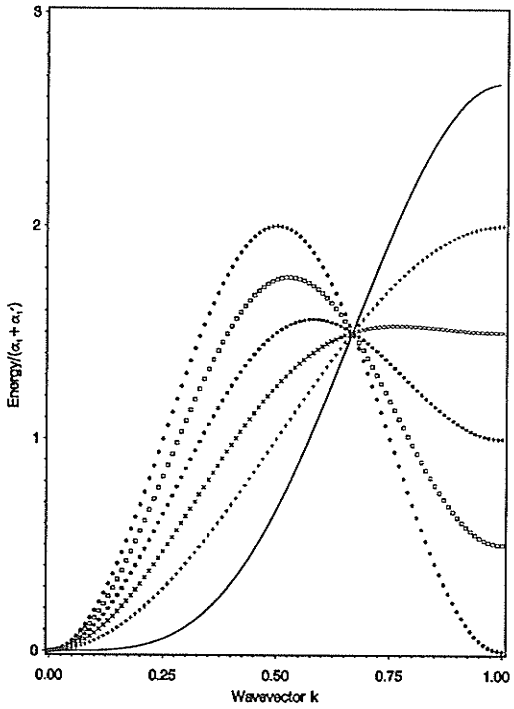

Figure 2.2: One-magnon excitation energy in units of $\alpha_1(S) + \alpha_1'(S)$ for a uniform Heisenberg chain. The wavevector k is in units of $\frac{\pi}{a}$. The solid line corresponds to $\tilde{\beta} = -\frac{1}{3}$; $+$ to $\tilde{\beta} = 0.0$; $\times$ to $\tilde{\beta} = 0.25$; $*$ to $\tilde{\beta} = 0.5$; $\square$ to $\tilde{\beta} = 0.75$; $\diamond$ to $\tilde{\beta} = 1.0$.

2.2 Two-Magnon Excitations

The development of the two-magnon excitation equations follows the method used in section 2.1. The orthonormal base kets are defined as before, but now with two raising operators on sites i and j acting on the ground state ket

$$\mid i,j\rangle = C_{ij} S_i^+ S_j^+ \mid 0\rangle \tag{2.26}$$

$$C_{ij} = \begin{cases} \frac{1}{\sqrt{2S}} & ,\text{if } i \neq j \\ \frac{1}{2\sqrt{S(2S-1)}} & ,\text{if } i = j \end{cases}$$

where the C_{ij} are normalization constants and the kets are labeled by sites i and j such that $i \leq j$.

The effects of $\tilde{P}_l$ (and $\tilde{Q}_l$) acting on the base kets with two deviations separated by more that nearest neighbors (next nearest neighbors) are given below. For the following $i \neq l, l+1$.

$$\left.\begin{array}{rcll} \tilde{P}_l \mid i,j\rangle & = & S^2 \mid i,j\rangle & ,j \neq l, l+1 \\ \tilde{P}_l \mid i,l\rangle & = & S(S-1) \mid i,l\rangle + S \mid i,l+1\rangle & ,j = l \\ \tilde{P}_l \mid i,l+1\rangle & = & S \mid i,l\rangle + S(S-1) \mid i,l+1\rangle & ,j = l+1 \end{array}\right\} \tag{2.27}$$

For the following $i \neq l, l+2$.

$$\left.\begin{array}{rcll} \tilde{Q}_l \mid i,j\rangle & = & S^2 \mid i,j\rangle & ,j \neq l, l+2 \\ \tilde{Q}_l \mid i,l\rangle & = & S(S-1) \mid i,l\rangle + S \mid i,l+2\rangle & ,j = l \\ \tilde{Q}_l \mid i,l+2\rangle & = & S \mid i,l\rangle + S(S-1) \mid i,l+2\rangle & ,j = l+2 \end{array}\right\} \tag{2.28}$$

Expressing these in matrix form we find

$$\begin{aligned} \tilde{P}_l \begin{pmatrix} \mid i,j\rangle \\ \mid i,l\rangle \\ \mid i,l+1\rangle \end{pmatrix} &= \mathbf{A} \begin{pmatrix} \mid i,j\rangle \\ \mid i,l\rangle \\ \mid i,l+1\rangle \end{pmatrix} \\ \tilde{Q}_l \begin{pmatrix} \mid i,j\rangle \\ \mid i,l\rangle \\ \mid i,l+2\rangle \end{pmatrix} &= \mathbf{A} \begin{pmatrix} \mid i,j\rangle \\ \mid i,l\rangle \\ \mid i,l+2\rangle \end{pmatrix} \end{aligned} \tag{2.29}$$

where $\mathbf{A}$ is the matrix defined in equation (2.14).

The matrix $\mathbf{A}^n$ is given in equation (2.15). Thus $\widehat{H}_l$ acting on these base kets gives

$$\widehat{H}_l \mid i,j\rangle = \begin{cases} E_0 \mid i,j\rangle & ,j \neq l, l+1, l+2 \\ E_0 \mid i,l\rangle + \frac{\alpha_1+\alpha_1'}{2} \mid i,l\rangle - \frac{\alpha_1}{2} \mid i,l+1\rangle - & \\ \quad \frac{\alpha_1'}{2} \mid i,l+2\rangle & ,j = l \\ E_0 \mid i,l+1\rangle + \frac{\alpha_1}{2} \mid i,l+1\rangle - \frac{\alpha_1}{2} \mid i,l\rangle & ,j = l+1 \\ E_0 \mid i,l+2\rangle + \frac{\alpha_1'}{2} \mid i,l+2\rangle - \frac{\alpha_1'}{2} \mid i,l\rangle & ,j = l+2 \end{cases} \tag{2.30}$$

where $i \neq l, l+1$, or $l+2$. Similar results are found for the pair Hamiltonian acting on the base kets with $j \neq l, l+1$ and $l+2$, but with $i = l, l+1$ or $l+2$. Therefore for i and j separated by more than two sites,

$$\begin{aligned} \widehat{H} \mid i,j\rangle = {} & NE_0 \mid i,j\rangle + 2(\alpha_1+\alpha_1') \mid i,j\rangle - \frac{\alpha_1'}{2} \mid i-2,j\rangle - \frac{\alpha_1}{2} \mid i-1,j\rangle - \\ & \frac{\alpha_1}{2} \mid i+1,j\rangle - \frac{\alpha_1'}{2} \mid i+2,j\rangle - \frac{\alpha_1'}{2} \mid i,j-2\rangle - \frac{\alpha_1}{2} \mid i,j-1\rangle - \\ & \frac{\alpha_1}{2} \mid i,j+1\rangle - \frac{\alpha_1'}{2} \mid i,j+2\rangle \end{aligned} \tag{2.31}$$

Since we will absorb the ground state energy into a shift in the zero of the energy, we can neglect the NE_0 term.

Next we must determine the effects of the pair Hamiltonians acting on base kets with spin deviations on the same site, nearest neighbor sites or next nearest neighbor sites.

$$\left.\begin{aligned} \widetilde{P}_l \mid l,l\rangle &= S(S-2) \mid l,l\rangle + \sqrt{S(2S-1)} \mid l,l+1\rangle \\ \widetilde{P}_l \mid l,l+1\rangle &= \sqrt{S(2S-1)}[\mid l,l\rangle + \mid l+1,l+1\rangle] + (1-S)^2 \mid l,l+1\rangle \\ \widetilde{P}_l \mid l+1,l+1\rangle &= \sqrt{S(2S-1)} \mid l,l+1\rangle + S(S-2) \mid l+1,l+1\rangle \end{aligned}\right\} \tag{2.32}$$

$$\left.\begin{aligned} \widetilde{Q}_l \mid l,l\rangle &= S(S-2) \mid l,l\rangle + \sqrt{S(2S-1)} \mid l,l+2\rangle \\ \widetilde{Q}_l \mid l,l+2\rangle &= \sqrt{S(2S-1)}[\mid l,l\rangle + \mid l+2,l+2\rangle] + (1-S)^2 \mid l,l+2\rangle \\ \widetilde{Q}_l \mid l+2,l+2\rangle &= \sqrt{S(2S-1)} \mid l,l+2\rangle + S(S-2) \mid l+2,l+2\rangle \end{aligned}\right\} \tag{2.33}$$

From these equations we can find the matrix elements of $\widetilde{P}_l$ and $\widetilde{Q}_l$ acting on these states.

$$\widetilde{P}_l \begin{pmatrix} \mid l,l\rangle \\ \mid l,l+1\rangle \\ \mid l+1,l+1\rangle \end{pmatrix} = \mathbf{B} \begin{pmatrix} \mid l,l\rangle \\ \mid l,l+1\rangle \\ \mid l+1,l+1\rangle \end{pmatrix} \tag{2.34}$$

Similarly,

$$\tilde{Q}_l \begin{pmatrix} |\, l, l\rangle \\ |\, l, l+2\rangle \\ |\, l+2, l+2\rangle \end{pmatrix} = \mathbf{B} \begin{pmatrix} |\, l, l\rangle \\ |\, l, l+2\rangle \\ |\, l+2, l+2\rangle \end{pmatrix} \tag{2.35}$$

where the matrix $\mathbf{B}$ is

$$\mathbf{B} = \begin{bmatrix} S(S-2) & \sqrt{S(2S-1)} & 0 \\ \sqrt{S(2S-1)} & (1-S)^2 & \sqrt{S(2S-1)} \\ 0 & \sqrt{S(2S-1)} & S(S-2) \end{bmatrix} \tag{2.36}$$

The matrix $\mathbf{B}^n$ is

$$\mathbf{B}^n = \begin{bmatrix} \phi+\chi & \rho & \phi-\chi \\ \rho & 2\phi + \frac{\rho}{\sqrt{S(2S-1)}} & \rho \\ \phi-\chi & \rho & \phi+\chi \end{bmatrix} \tag{2.37}$$

where

$$\begin{aligned} \chi &= \frac{(S-2)^n S^n}{2} \\ \phi &= \frac{(2S-1)S^{2n}}{2(4S-1)} + \frac{S\left(1-4S+S^2\right)^n}{4S-1} \\ \rho &= \frac{\sqrt{S(2S-1)}\left[S^{2n} - \left(1-4S+S^2\right)^n\right]}{4S-1} \end{aligned} \tag{2.38}$$

From the matrices $\mathbf{A}^n$ and $\mathbf{B}^n$ we can find the effects of the pair Hamiltonian acting on base kets with two deviations of the same site, nearest neighbor sites, or next nearest neighbor sites. Once again we will use the convenient variables of equation (2.9). The variable χ is related to α_1, α_1' and E_0 through equations (2.17). As well,

$$\begin{aligned} -\sum_n J_1^{(n)}\phi &= \frac{S\alpha_2}{4S-1} - \sum_n J_1^{(n)}\frac{S^{2n}}{2} \\ -\sum_n J_2^{(n)}\phi &= \frac{S\alpha_2'}{4S-1} - \sum_n J_2^{(n)}\frac{S^{2n}}{2} \\ -\sum_n J_1^{(n)}\rho &= -\frac{\sqrt{S(2S-1)}}{4S-1}\alpha_2 \\ -\sum_n J_2^{(n)}\rho &= -\frac{\sqrt{S(2S-1)}}{4S-1}\alpha_2' \end{aligned} \tag{2.39}$$

Since we will absorb the ground state energy into the zero of the energy, we can neglect all E_0 terms.

$$\hat{H}_l \mid j, j+2\rangle = \begin{cases} 0 \mid j, j+2\rangle & j \neq l-2, l-1, l, l+1, l+2 \\ \frac{\alpha_1+\alpha_1'}{2} \mid l-2, l\rangle - \frac{\alpha_1}{2} \mid l-2, l+1\rangle - \frac{\alpha_1'}{2} \mid l-2, l+2\rangle & , j = l-2 \\ \frac{\alpha_1}{2} \mid l-1, l+1\rangle - \frac{\alpha_1}{2} \mid l-1, l\rangle & , j = l-1 \\ \left(\frac{\alpha_1}{2} + \frac{2S-1}{4S-1}\alpha_2'\right) \mid l, l+2\rangle - \frac{\sqrt{S(2S-1)}}{4S-1}\alpha_2' [\mid l, l\rangle + & \\ \quad \mid l+2, l+2\rangle] - \frac{\alpha_1}{2} \mid l+1, l+2\rangle & , j = l \\ \frac{\alpha_1}{2} \mid l+1, l+3\rangle - \frac{\alpha_1}{2} \mid l, l+3\rangle & , j = l+1 \\ \frac{\alpha_1'}{2} \mid l+2, l+4\rangle - \frac{\alpha_1'}{2} \mid l, l+4\rangle & , j = l+2 \end{cases} \tag{2.40}$$

$$\hat{H}_l \mid j, j+1\rangle = \begin{cases} 0 \mid j, j+1\rangle & j \neq l-1, l, l+1, l+2 \\ \frac{\alpha_1+\alpha_1'}{2} \mid l-1, l\rangle - \frac{\alpha_1}{2} \mid l-1, l+1\rangle - \frac{\alpha_1'}{2} \mid l-1, l+1\rangle & , j = l-1 \\ \left(\frac{\alpha_1'}{2} + \frac{2S-1}{4S-1}\alpha_2\right) \mid l, l+1\rangle - \frac{\sqrt{S(2S-1)}}{4S-1}\alpha_2 [\mid l, l\rangle + & \\ \quad \mid l+1, l+1\rangle] - \frac{\alpha_1'}{2} \mid l+1, l+2\rangle & , j = l \\ \frac{\alpha_1+\alpha_1'}{2} \mid l+1, l+2\rangle - \frac{\alpha_1}{2} \mid l, l+2\rangle - \frac{\alpha_1'}{2} \mid l, l+1\rangle & , j = l+1 \\ \frac{\alpha_1'}{2} \mid l+2, l+3\rangle - \frac{\alpha_1'}{2} \mid l, l+3\rangle & , j = l+2 \end{cases} \tag{2.41}$$

$$\widehat{H}_l \mid j,j\rangle = \begin{cases} 0 \mid j,j\rangle & ,j \neq l,l+1,l+2 \\ \left(\frac{\alpha_1+\alpha_1'}{2}+\frac{S}{4S-1}(\alpha_2+\alpha_2')\right) \mid l,l\rangle - \frac{\sqrt{S(2S-1)}}{4S-1}[\alpha_2 \mid l,l+1\rangle + \\ \qquad \alpha_2' \mid l,l+2\rangle] - \left(\frac{\alpha_1}{2}-\frac{S\alpha_2}{4S-1}\right) \mid l+1,l+1\rangle - \left(\frac{\alpha_1'}{2}- \\ \qquad \frac{S\alpha_2'}{4S-1}\right) \mid l+2,l+2\rangle & ,j=l \\ \left(\frac{\alpha_1}{2}+\frac{S\alpha_2}{4S-1}\right) \mid l+1,l+1\rangle - \left(\frac{\alpha_1}{2}-\frac{S\alpha_2}{4S-1}\right) \mid l,l\rangle - \\ \qquad \frac{\sqrt{S(2S-1)}}{4S-1}\alpha_2 \mid l,l+1\rangle & ,j=l+1 \\ \left(\frac{\alpha_1'}{2}+\frac{S\alpha_2'}{4S-1}\right) \mid l+2,l+2\rangle - \left(\frac{\alpha_1'}{2}-\frac{S\alpha_2'}{4S-1}\right) \mid l,l\rangle - \\ \qquad \frac{\sqrt{S(2S-1)}}{4S-1}\alpha_2' \mid l,l+2\rangle & ,j=l+2 \end{cases} \tag{2.42}$$

Therefore the effect of the full Hamiltonian on these states is

$$\begin{aligned} \widehat{H} \mid j,j+2\rangle = & \left(2\alpha_1+\alpha_1'+\frac{2S-1}{4S-1}\alpha_2'\right) \mid j,j+2\rangle - \frac{\alpha_1'}{2} \mid j,j+4\rangle - \frac{\alpha_1}{2} \mid j,j+3\rangle \\ & - \frac{\alpha_1}{2} \mid j,j+1\rangle - \frac{\alpha_1}{2} \mid j+1,j+2\rangle - \frac{\alpha_1}{2} \mid j-1,j+2\rangle - \\ & \frac{\alpha_1'}{2} \mid j-2,j+2\rangle - \frac{\sqrt{S(2S-1)}}{4S-1}\alpha_2'[\mid j,j\rangle + \mid j+2,j+2\rangle] \end{aligned} \tag{2.43}$$

$$\begin{aligned} \widehat{H} \mid j,j+1\rangle = & \left(\alpha_1+\frac{2S-1}{4S-1}\alpha_2+2\alpha_1'\right) \mid j,j+1\rangle - \frac{\alpha_1'}{2} \mid j,j+3\rangle - \frac{\alpha_1}{2} \mid j,j+2\rangle \\ & - \frac{\alpha_1}{2} \mid j-1,j+1\rangle - \frac{\alpha_1'}{2} \mid j-1,j\rangle - \frac{\alpha_1'}{2} \mid j-2,j+1\rangle - \\ & \frac{\alpha_1'}{2} \mid j+1,j+2\rangle - \frac{\sqrt{S(2S-1)}}{4S-1}\alpha_2[\mid j,j\rangle + \mid j+1,j+1\rangle] \end{aligned} \tag{2.44}$$

$$\begin{aligned} \widehat{H} \mid j,j\rangle = & \left(\alpha_1+\frac{2S\alpha_2}{4S-1}+\alpha_1'+\frac{2S\alpha_2'}{4S-1}\right) \mid j,j\rangle - \frac{\sqrt{S(2S-1)}}{4S-1}[\alpha_2' \mid j-2,j\rangle + \\ & \alpha_2 \mid j-1,j\rangle + \alpha_2 \mid j,j+1\rangle + \alpha_2' \mid j,j+2\rangle] - \\ & \left(\frac{\alpha_1'}{2}-\frac{S\alpha_2'}{4S-1}\right)[\mid j-2,j-2\rangle + \mid j+2,j+2\rangle] - \\ & \left(\frac{\alpha_1}{2}-\frac{S\alpha_2}{4S-1}\right)[\mid j-1,j-1\rangle + \mid j+1,j+1\rangle] \end{aligned} \tag{2.45}$$

Each state is denoted by a ket containing the labels of the sites which have spins flipped (i and j), but due to the property of translational invariance the Hamiltonian only depends on the relative position of the flipped spins. Therefore we may perform a change of variables to states labeled by the relative coordinate $r = j - i$ and the center of mass coordinate $R = \frac{i+j}{2}$. As well, Bloch's theorem allows us to perform a Fourier transform with respect to the center of mass coordinate to states labeled by the total momentum K and the relative coordinate r.

$$\mid K;r\rangle \;=\; \frac{1}{\sqrt{N}}\sum_{R} e^{-iKaR} \mid i,j\rangle \tag{2.46}$$

The inverse transformation is

$$\mid i,j\rangle \;=\; \frac{1}{\sqrt{N}}\sum_{\{K\}} e^{iKaR} \mid K;r\rangle \tag{2.47}$$

Perform this transformation on equations (2.31), (2.43), (2.44) and (2.45). The full Hamiltonian acting on the states $\{\mid K;r\rangle\}$ gives:

$$\begin{aligned}
\widehat{H} \mid K;0\rangle &= (\varepsilon_0+\varepsilon_0')\mid K;0\rangle + V_0 \mid K;1\rangle + V_0' \mid K;2\rangle && (2.48)\\
\widehat{H} \mid K;1\rangle &= (\varepsilon_1+\varepsilon_1')\mid K;1\rangle + V \mid K;2\rangle + V' \mid K;3\rangle + V_0 \mid K;0\rangle && (2.49)\\
\widehat{H} \mid K;2\rangle &= (\varepsilon+\varepsilon_2')\mid K;2\rangle + V \mid K;1\rangle + V \mid K;3\rangle + V' \mid K;4\rangle + V_0' \mid K;0\rangle && (2.50)\\
\widehat{H} \mid K,r\rangle &= (\varepsilon+\varepsilon')\mid K;r\rangle + V[\mid K;r-1\rangle + \mid K;r+1\rangle] \\
&\quad + V'[\mid K;r-2\rangle + \mid K;r+2\rangle] \qquad ,r>2 && (2.51)
\end{aligned}$$

where all parameters are measured in units of $\alpha_1 + \alpha_1'$ and are given by

$$\begin{aligned}
\varepsilon_0 &= (1-\tilde{\beta})(1-\cos K) + \tfrac{2Sr_2}{4S-1}(1+\cos K)\\
\varepsilon_0' &= \tilde{\beta}(1-\cos 2K) + \tfrac{2Sr_2'}{4S-1}(1+\cos 2K)\\
\varepsilon_1 &= (1-\tilde{\beta}) + \tfrac{2S-1}{4S-1}r_2\\
\varepsilon_1' &= 2\tilde{\beta} + V'\\
\varepsilon_2' &= \tilde{\beta} + \tfrac{2S-1}{4S-1}r_2'\\
\varepsilon &= 2(1-\tilde{\beta})\\
\varepsilon' &= 2\tilde{\beta}\\
V_0 &= -\tfrac{2\sqrt{S(2S-1)}}{4S-1}r_2\cos\tfrac{K}{2}\\
V_0' &= -\tfrac{2\sqrt{S(2S-1)}}{4S-1}r_2'\cos K\\
V &= -(1-\tilde{\beta})\cos\tfrac{K}{2}\\
V' &= -\tilde{\beta}\cos K
\end{aligned} \tag{2.52}$$

where we have set $a = 1$ and where

$$\begin{aligned} r_2 &= \frac{\alpha_2}{\alpha_1 + \alpha_1'} \\ r_2' &= \frac{\alpha_2'}{\alpha_1 + \alpha_1'} \end{aligned} \tag{2.53}$$

This set of equations is equivalent to a semi-infinite mass-spring system where the springs couple both nearest neighbor sites and next nearest neighbor sites. The mapping is

$$\left.\begin{array}{rcl} m_0 & \Rightarrow & \varepsilon_0 + \varepsilon_0' \\ m_1 & \Rightarrow & \varepsilon_1 + \varepsilon_1' \\ m_2 & \Rightarrow & \varepsilon + \varepsilon_2' \\ m & \Rightarrow & \varepsilon + \varepsilon' \\ k_0 & = & V_0 \\ k_0' & = & V_0' \\ k & = & V \\ k' & = & V' \end{array}\right\} \tag{2.54}$$

In order to visualize the interactions on the one-dimensional semi-infinite chain, the nearest neighbor springs and the next nearest neighbor springs between the masses are shown separately in figures 2.3 a) to c).

There are two categories of two-magnon equations: equation (2.51) which involves only kets with spin deviations separated by more than two sites, and equations (2.48) to (2.50) which involve kets with spin deviations on the same, nearest neighbor or next nearest neighbor sites. The first set has solutions corresponding to two-free magnons with total energy $E(K) = E_1(k_1) + E_1(k_2)$ and total momentum $K = k_1 + k_2$. However, the other set of equations provide boundary conditions which can be satisfied for both real and complex values of k_1 and k_2. This leads to two different types of solutions, scattering state solutions and bound state solutions. The scattering state solutions correspond to both real and complex values of k_1 and k_2 and will be examined in the next section, and the bound state solutions have $Im(k_1) = -Im(k_2)$ and will be examined in section 2.4.

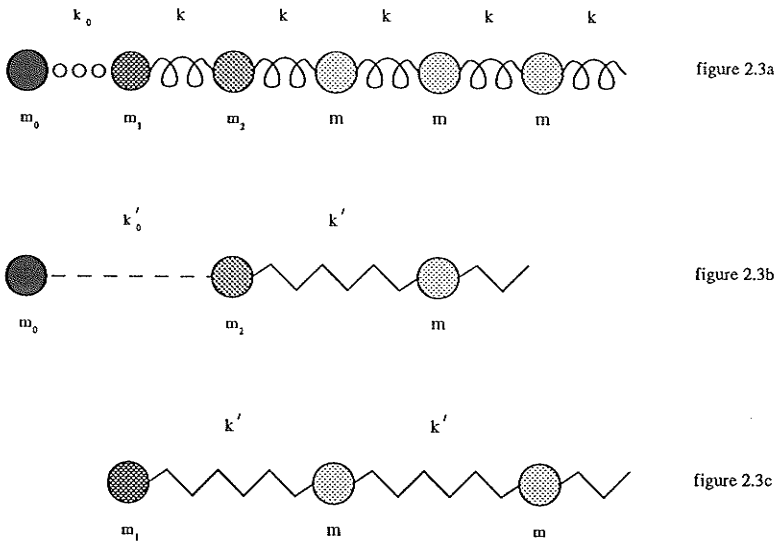

Figure 2.3: Graphical representation of equations (2.48) to (2.51). a) depicts the interactions between the nearest neighbors, b) depicts the interactions between the next nearest neighbor even sites, and c) depicts the interactions between the next nearest neighbor odd sites.

2.3 Two-Magnon Scattering State Continuum

Equation (2.51) by itself describes two free-magnons and consequently the scattering state energy with total momentum K is equal to the sum of the energies of the two free-magnons with momenta k_1 and k_2. For convenience, let a, the lattice distance, be set equal to unity and let the energies be in units of $(\alpha_1 + \alpha_1')$.

$$\begin{aligned} E^{ss}(K) &= E_1(k_1) + E_1(k_2) \qquad , k_1 + k_2 = K \\ &= 2 - 2(1-\tilde{\beta})\cos q \cos\left(\frac{K}{2}\right) - 2\tilde{\beta}\cos 2q \cos K \end{aligned} \tag{2.55}$$

where $q = \frac{k_1 - k_2}{2}$. In general there are four possible values of q ($\pm q_1$ and $\pm q_2$) for each choice of E and K. Two situations can occur in the scattering state continuum: both q_1 and q_2 can be real, or only one is real [16]. However, the minima and maxima of the scattering state continua are determined by real values of q. The solutions to $\frac{\partial E^{ss}}{\partial q} = 0$ give the following extrema:

$$\begin{aligned} E^{(1)}(q=0) &= 2 - 2(1-\tilde{\beta})\cos\frac{K}{2} - 2\tilde{\beta}\cos K \qquad \text{,for all } \tilde{\beta} \\ E^{(2)}(q=\pi) &= 2 + 2(1-\tilde{\beta})\cos\frac{K}{2} - 2\tilde{\beta}\cos K \qquad \text{,for all } \tilde{\beta} \\ E^{(3)}\left(\cos q = \frac{-\left(1-\tilde{\beta}\right)\cos\frac{K}{2}}{4\tilde{\beta}\cos K}\right) &= 2 + 2\tilde{\beta}\cos K + \frac{\left(1-\tilde{\beta}\right)^2}{4\tilde{\beta}}\frac{\cos^2\left(\frac{K}{2}\right)}{\cos K}, \\ &\qquad \text{provided } -1 \le \frac{-\left(1-\tilde{\beta}\right)\cos\frac{K}{2}}{4\tilde{\beta}\cos K} \le 1 \end{aligned} \tag{2.56}$$

Therefore the scattering state continuum is a single band which extends from the $E^{(i)}$ which attains the minimum energy to the $E^{(i)}$ which attains the maximum energy for given K. A summary of the conditions which determine whether $E^{(i)}$ is a minimum or a maximum are given in table 2.1.

The condition $-1 \le \frac{-\left(1-\tilde{\beta}\right)\cos\frac{K}{2}}{4\tilde{\beta}\cos K} = \cos q \le 1$ associated with $E^{(3)}$ ensures that q is real. Note that $\cos q = 1$ corresponds to an inflection point of $E^{(1)}$ and $\cos q = -1$ corresponds to an inflection point of $E^{(2)}$. At $K = 0$ and $K = \pi$ the

Table 2.1: Minimum and maximum scattering state energy in units of $\alpha_1 + \alpha_1'$.

Energy		Condition	
$E^{(1)}$	is a local maximum if	$\frac{\partial^2 E^{ss}}{\partial q^2} = 2(1-\tilde{\beta})\cos\frac{K}{2} + 8\tilde{\beta}\cos K$	< 0
	is a local minimum if		> 0
	is an inflection point if		$= 0$
$E^{(2)}$	is a local maximum if	$\frac{\partial^2 E^{ss}}{\partial q^2} = -2(1-\tilde{\beta})\cos\frac{K}{2} + 8\tilde{\beta}\cos K$	< 0
	is a local minimum if		> 0
	is an inflection point if		$= 0$
$E^{(3)}$	is a maximum if	$\frac{\partial^2 E^{ss}}{\partial q^2} = \frac{(1-\tilde{\beta})^2\cos^2\left(\frac{K}{2}\right)}{2\tilde{\beta}\cos K} - 8\tilde{\beta}\cos K$ and $-1 \leq \frac{-\left(1-\tilde{\beta}\right)\cos\frac{K}{2}}{4\tilde{\beta}\cos K} \leq 1$	< 0
	is a minimum if		> 0
	is an inflection point if		$= 0$

Table 2.2: Minimum and maximum scattering state energy

K	range of $\tilde{\beta}$	$\frac{E_{min}}{\alpha_1+\alpha_1'}$	$\frac{E_{max}}{\alpha_1+\alpha_1'}$
0	$-\frac{1}{3} \leq \tilde{\beta} \leq \frac{1}{5}$	0	$4(1-\tilde{\beta})$
0	$\frac{1}{5} \leq \tilde{\beta} \leq 1$	0	$2 + 2\tilde{\beta} + \frac{\left(1-\tilde{\beta}\right)^2}{4\tilde{\beta}}$
π	$-\frac{1}{3} \leq \tilde{\beta} \leq 1$	$2(1-\tilde{\beta})$	$2(1+\tilde{\beta})$

information in table 2.1 reduces to the information in table 2.2. If $\tilde{\beta} < 0$ at $K = \pi$ then E_{min} and E_{max} are interchanged.

The scattering state continua with energies measured in units of $\alpha_1 + \alpha_1'$ are shown in figures 2.4 to 2.8 for $\tilde{\beta} = -\frac{1}{3}, 0, \frac{1}{5}, \frac{1}{2}$ and 1. These plots are density plots, bounded by the minimum and maximum energy of the scattering state continua. Where either $E^{(1)}$ or $E^{(2)}$ are not an absolute extrema, they can still be seen in the density plots as a line separating a region of higher density from a region of lower density. These lines are called van Hove singularities and occur whenever the group velocity $v_q = \frac{\partial E^{ss}}{\partial q} = 0$ inside the scattering state continuum.

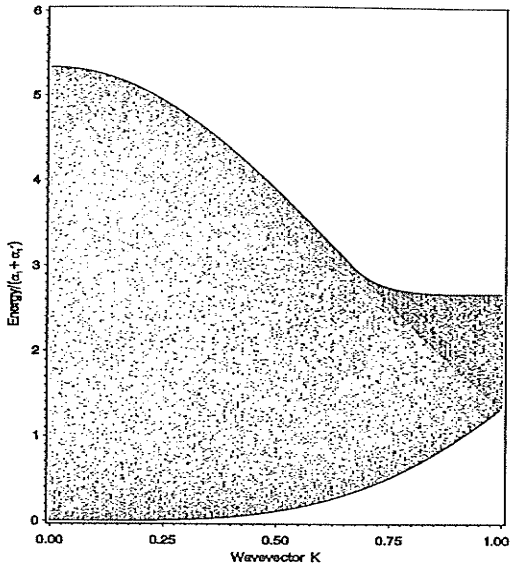

Figure 2.4: Two-magnon scattering state continuum density plot with energy in units of $\alpha_1 + \alpha_1'$. The wavevector K is in units of π and $\tilde{\beta} = -\frac{1}{3}$.

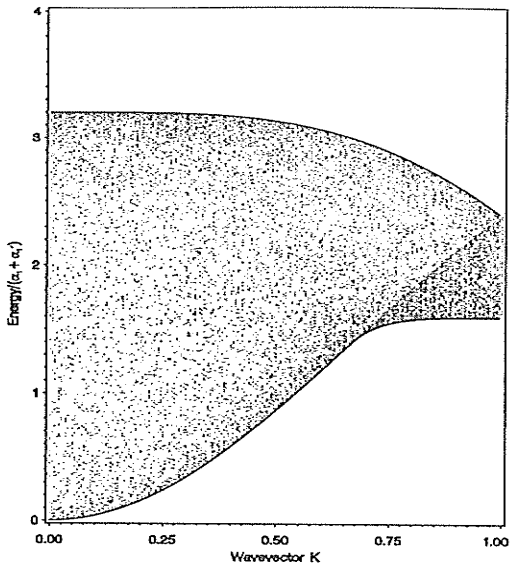

Figure 2.6: Two-magnon scattering state continuum density plot with energy in units of $\alpha_1 + \alpha_1'$. The wavevector K is in units of π and $\tilde{\beta} = \frac{1}{5}$.

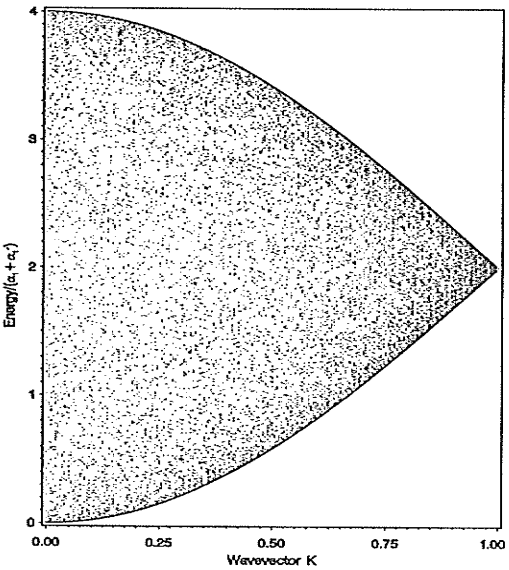

Figure 2.5: Two-magnon scattering state continuum density plot with energy in units of $\alpha_1 + \alpha_1'$. The wavevector K is in units of π and $\tilde{\beta} = 0$.

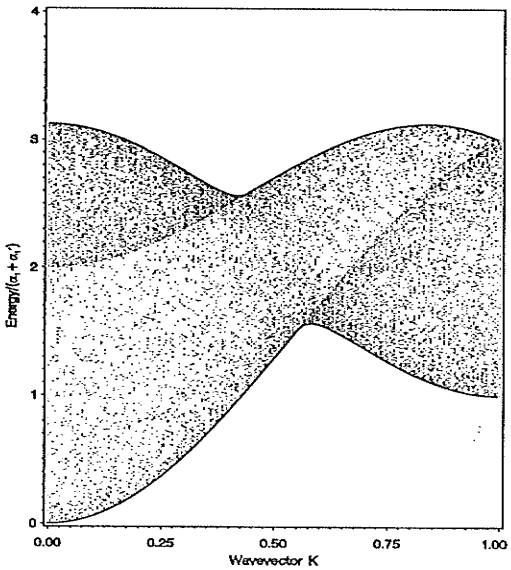

Figure 2.7: Two-magnon scattering state continuum density plot with energy in units of $\alpha_1 + \alpha_1'$. The wavevector K is in units of π and $\tilde{\beta} = \frac{1}{2}$.

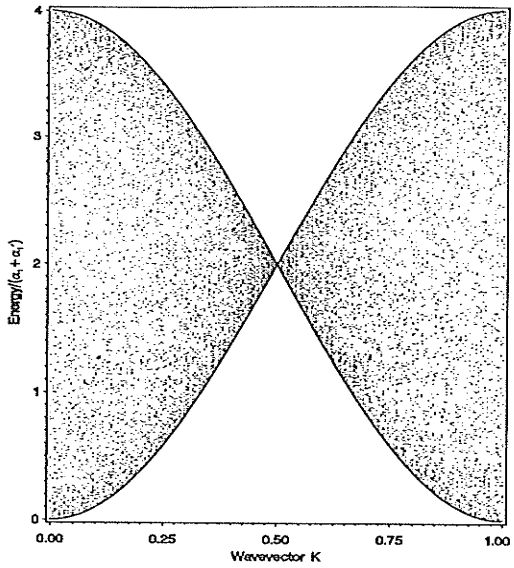

Figure 2.8: Two-magnon scattering state continuum density plot with energy in units of $\alpha_1 + \alpha_1'$. The wavevector K is in units of π and $\tilde{\beta} = 1$.

In figures 2.4, 2.6 and 2.7 the regions of higher density (darker) correspond to both q_1 and q_2 being real and the regions of lower density correspond to only one of q_1 or q_2 being real. As $\tilde{\beta} \to 0$ (figure 2.5), the higher density region is compressed to a point at $K = \pi$ and only one real value of q survives with the other having and infinite imaginary part. As $\tilde{\beta}$ increases towards 1 (figure 2.8), the region of lower density collapses into a line ($E = E^{(1)} = E^{(2)}$) and only real wavevectors remain [16].

These scattering state continua results agree with those obtained by Majumdar [14],Ono, Mikado and Takehiko [15], Gochev [16] and Bahurmuz and Loly [17] and are important for identifying the regions where the bound state solutions can occur. These will be discussed in the next section.

2.4 Two-Magnon Bound States

Equations (2.48) to (2.51) describe interactions between two magnons and can be solved for the bound state solutions using the real-space rescaling method([18], [23]). In general the method can be used to find the spectral properties of any system of linear equations with a large number (N) of degrees of freedom. The basic concept of the method is to perform a transformation on the equations which eliminates a fraction of the degrees of freedom but leaves the equations invariant in form with renormalized parameters. The spectral properties of the system can be determined by iterating the transformation. The main steps in the renormalization process are:

1. eliminate a fraction of the states.

2. renormalize the parameters so that the new equations have the same form as the original equations.

3. rescale the state indices and relabel the states.

This process is iterated so that at each step the renormalized parameters describe the effective interactions between the remaining states.

At certain values of $\tilde{\beta}$, S and K the system of equations (2.48) to (2.51) reduce to a simpler form so that the rescaling method can be applied analytically. Cases with values of $\tilde{\beta}$, S and K for which this is not true can be solved numerically using a matrix rescaling method.

2.4.1 Analytical Real-Space Rescaling Method

The solutions of equations (2.48) to (2.51) are linear combinations of the kets $\mid K;r\rangle$

$$\mid K\rangle \;=\; \sum_r c_r^* \mid K;r\rangle \tag{2.57}$$

where c_r are complex amplitudes. The equations for the amplitudes take the form:

$$\left.\begin{array}{rcl}(E-\varepsilon_0-\varepsilon_0')c_0 &=& V_0c_1+V_0'c_2\\ (E-\varepsilon_1-\varepsilon_1')c_1 &=& V_0c_0+Vc_2+V'c_3\\ (E-\varepsilon-\varepsilon_2')c_2 &=& V_0'c_0+Vc_1+Vc_3+V'c_4\\ (E-\varepsilon-\varepsilon')c_r &=& V'c_{r-2}+Vc_{r-1}+Vc_{r+1}+V'c_{r+2}\end{array}\right\} \tag{2.58}$$

The allowed values of E are thus the eigenvalues of a banded matrix. We will first consider cases for which this banded matrix reduces to a tridiagonal form.

Case (a): $\tilde{\beta}=0$, $r_2'=0$, but general S, r_2 and K.

Let us first consider the case $\tilde{\beta}=0$, so that all second nearest neighbor interactions are zero. In this limit our equations reduce to

$$\left.\begin{array}{rcl}(E-\varepsilon_0)c_0 &=& V_0c_1\\ (E-\varepsilon_1)c_1 &=& V_0c_0+Vc_2\\ (E-\varepsilon)c_r &=& Vc_{r-1}+Vc_{r+1}\end{array}\right\} \tag{2.59}$$

The energies E can be determined by a variety of techniques. The solutions of these equations for $S=\frac{1}{2}$ have the general form

$$c_r = Ae^{iqr}+Be^{-iqr} \qquad \text{for } r\geq 1 \tag{2.60}$$

where q is real or complex. The solutions for any real q have eigenvalues $E=\varepsilon+2V\cos q$ but the relationship between the amplitudes B and A depends on q. Hence these solutions are called scattering state solutions and form a continuum bounded by $\varepsilon\pm 2V$. For complex values of q, $B=0$ since $r>0$ and there are solutions only for certain energies. These solutions describe bound states of the interacting magnons and the eigenvalues lie outside the bounds of the scattering state continuum.

Southern, Liu and Lavis [18] have used real space rescaling methods for such a system to obtain analytic expressions for the eigenvalues without having to solve for the amplitudes. If we choose the amplitude c_0 as a reference point, and eliminate all amplitudes $c_1,\ldots c_{b-1}$, then a new effective interaction is generated between c_0 and c_b and the parameter ε_0 is renormalized. Figure 2.9 illustrates the method

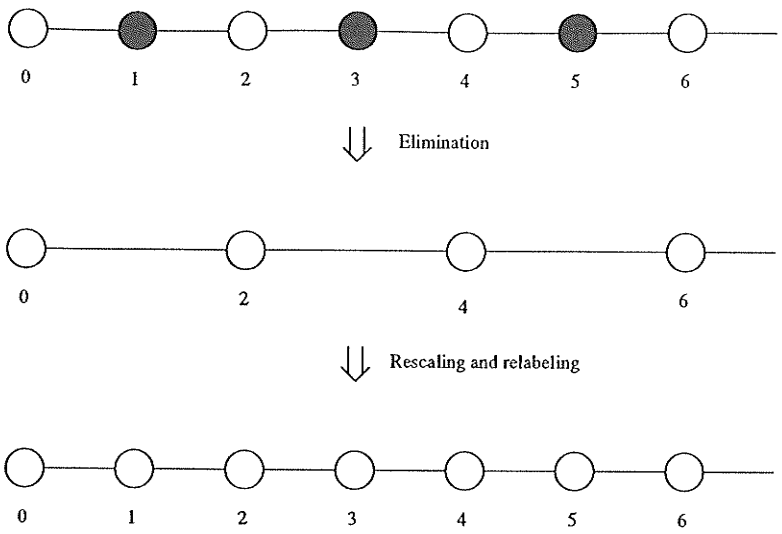

Figure 2.9: Schematic illustration of the rescaling procedure. The first step eliminates the odd sites. The second step rescales the distances by a factor of $\frac{1}{2}$ and relabels the sites.

for $b = 2$, but it can be carried out for any b. In the limit $b \to \infty$, the effective interaction between c_0 and c_b approaches a value which depends upon E. For values of E outside the scattering state continuum, it approaches zero and a non-trivial solution ($c_0 \neq 0$) is obtained from

$$E = \varepsilon_0^{(\infty)} \tag{2.61}$$

These solutions are the bound states. For values of E inside the scattering state continuum, a small imaginary part must be added to the energy E for the procedure to converge. However, $\varepsilon_0^{(\infty)}$ approaches a limiting complex value as the imaginary part tends to zero.

The solution for the bound state is given by [18]

$$E = \varepsilon_0^{(\infty)} = \varepsilon_0 + \frac{V_0^2}{E - \varepsilon_1 - VQ} \tag{2.62}$$

where

$$\left.\begin{array}{lll} Q = \Delta + (\Delta^2 - 1)^{\frac{1}{2}} & & \Delta < -1; \\ Q = \Delta - (\Delta^2 - 1)^{\frac{1}{2}} & & \Delta > 1; \\ Q = \Delta + i(1 - \Delta^2)^{\frac{1}{2}} & & \mid \Delta \mid < 1 \end{array}\right\} \tag{2.63}$$

and

$$\Delta = \frac{E - \varepsilon}{2V} \tag{2.64}$$

where $\mid \Delta \mid > 1$ corresponds to energies outside the scattering state continua. In general this leads to a cubic equation for E.

$$\left[(E - \varepsilon_1)(E - \varepsilon_0) - V_0^2\right]\left[(\varepsilon_1 - \varepsilon)(E - \varepsilon_0) + V_0^2\right] - (E - \varepsilon_0)^2 V^2 = 0 \tag{2.65}$$

Complex solutions to the cubic equation are unphysical. Occasionally (for $\tilde{\beta} < 0$) the real solutions may be unphysical. To determine which solutions are physical and which are unphysical, the solution must be put back into equation (2.62), the original equations, to see if the equality holds. This problem arises due to the squaring of both sides of an equation in the process of arriving at the cubic equation. Thus the bound state solutions can be found for all cases with interactions between nearest neighbor sites only.

Case (b): $\tilde{\beta} = 1$, $r_2 = 0$, but general S, r_2' and K.

With the nearest neighbor interactions zero and the next nearest neighbor interactions nonzero, the equations (2.58) reduce to

$$\left.\begin{array}{lll} (E - \varepsilon_0')c_0 &=& V_0' c_2 \\ (E - \varepsilon_1')c_1 &=& V' c_3 \\ (E - \varepsilon_2')c_2 &=& V_0' c_0 + V' c_4 \\ (E - \varepsilon')c_r &=& V' c_{r-2} + V' c_{r+2} \end{array}\right\} \tag{2.66}$$

Notice that the equations for even r couple only to each other and the equations for odd r couple only to each other. Thus we have two independent tridiagonal

forms. The form of the even r equations is identical to equation (2.59). The bound state energies E are again the solutions to a cubic equation, with the appropriate substitution for unprimed with primed variables. The odd r equations also have the same form as equations (2.59), but with some of the parameters equal. In this latter case, the bound state equation is linear with the solution

$$E = 2\tilde{\beta}(1-\cos K) \tag{2.67}$$

which is equal to the scattering state continuum edge and thus it is a bound state with zero binding energy.

Case (c): general $\tilde{\beta}$, S, r_2 and r_2', but $K=\pi$.

For this value of K, the parameters are

$$\begin{array}{ll} \varepsilon=\varepsilon_0=2(1-\tilde{\beta}) & \varepsilon_0'=\frac{4S}{4S-1}r_2' \\ \varepsilon_1=(1-\tilde{\beta})+\frac{2S-1}{4S-1}r_2 & \varepsilon_1'=3\tilde{\beta} \\ \varepsilon_2'=\tilde{\beta}+\frac{2S-1}{4S-1}r_2' & \varepsilon'=2\tilde{\beta} \\ V_0=0 & V_0'=\frac{2\sqrt{S(2S-1)}}{4S-1}r_2' \\ V=0 & V'=\tilde{\beta} \end{array} \tag{2.68}$$

and hence the equations reduce to

$$\left.\begin{array}{rcl} (E-\varepsilon_0-\varepsilon_0')c_0 &=& V_0'c_2 \\ (E-\varepsilon_1-\varepsilon_1')c_1 &=& V'c_3 \\ (E-\varepsilon-\varepsilon_2')c_2 &=& V_0'c_0+V'c_4 \\ (E-\varepsilon-\varepsilon')c_r &=& V'c_{r-2}+V'c_{r+2} \end{array}\right\} \tag{2.69}$$

Again we have two decoupled tridiagonal forms. For the even r amplitudes, the eigenvalue equation for the bound states at $K=\pi$ is in the form of a cubic equation.

$$\left[(E-\varepsilon-\varepsilon_2')(E-\varepsilon_0-\varepsilon_0')-V_0'^2\right]\left[(\varepsilon_2'-\varepsilon')(E-\varepsilon_0-\varepsilon_0')+V_0'^2\right]-(E-\varepsilon_0-\varepsilon_0')^2V'^2=0 \tag{2.70}$$

The odd r amplitude equations lead to a linear eigenvalue equation with the solution

$$E(K=\pi) = \frac{1-5\tilde{\beta}^2-4\tilde{\beta}\frac{2S-1}{4S-1}r_2-\left(\frac{2S-1}{4S-1}r_2\right)^2}{1-2\tilde{\beta}-\frac{2S-1}{4S-1}r_2} \tag{2.71}$$

The result for $S = \frac{1}{2}$ agrees with Majumdar [14].

Case (d): general $\tilde{\beta}$, $S > \frac{1}{2}$, but $r_2 = \frac{4S-1}{2S-1}(1-\tilde{\beta})$, $r_2' = \frac{4S-1}{2S-1}\tilde{\beta}$ and $K = \pi$.

In this case the cubic equation (2.70) for the bound states reduces to a quadratic. This corresponds to the integrable model of Takhtajan and Babujian ([7], [8]) if $\tilde{\beta} = 0$. Under these conditions, the variables reduce to

$$\begin{array}{ll} \varepsilon = \varepsilon_1 = \varepsilon_0 = 2(1-\tilde{\beta}) & \varepsilon_0' = \frac{4S}{2S-1}\tilde{\beta} \\ \varepsilon_1' = 3\tilde{\beta} & \varepsilon' = \varepsilon_2' = 2\tilde{\beta} \\ V_0 = 0 & V_0' = \frac{2\sqrt{S(2S-1)}}{2S-1}\tilde{\beta} \\ V = 0 & V' = \tilde{\beta} \end{array} \tag{2.72}$$

and the equations are equivalent to (2.69). Since $\varepsilon' = \varepsilon_2'$, the cubic equation reduces to a quadratic equation and the solutions are

$$E(K=\pi) \;=\; 2(1-\tilde{\beta})\;,\; 2(1-\tilde{\beta}) + \frac{16S^2\tilde{\beta}}{4S^2-1} \tag{2.73}$$

The first solution, $E = 2(1-\tilde{\beta})$, corresponds to the lower edge of the scattering state continuum, and is not a bound state. The other solution is a bound state for all values of $\tilde{\beta}$ except $\tilde{\beta} = 0$, where the energy is equal to the continuum energy. For $\tilde{\beta} < 0$ the bound state is below the continuum, and for $\tilde{\beta} > 0$ the bound state is above the continuum at $K = \pi$. The odd amplitude equations can be solved to find the bound state solutions and yield equation (2.71) with r_2 and r_2' related to $\tilde{\beta}$ as above. This gives $E = 2(1+\tilde{\beta})$, which is the upper edge of the scattering state continuum.

Case (e): general $\tilde{\beta}$, S, but $r_2 = \frac{4S-1}{2S}(1-\tilde{\beta})$, $r_2' = \frac{4S-1}{2S}\tilde{\beta}$ and $K = \pi$.

This case describes the spin S Heisenberg model, and the parameters become

$$\begin{array}{ll} \varepsilon = \varepsilon_0 = 2(1-\tilde{\beta}) & \varepsilon' = \varepsilon_0' = 2\tilde{\beta} \\ \varepsilon_1 = \frac{4S-1}{2S}(1-\tilde{\beta}) & \varepsilon_1' = 3\tilde{\beta} \\ \varepsilon_2' = \frac{4S-1}{2S}\tilde{\beta} & \\ V_0 = 0 & V_0' = \frac{\sqrt{S(2S-1)}}{S}\tilde{\beta} \\ V = 0 & V' = \tilde{\beta} \end{array} \tag{2.74}$$

and the form of the equations are equivalent to (2.69). The even amplitude equations have a bound state solution given by the cubic equation

$$\frac{\tilde{\beta}}{2S}(E-2)^3+\frac{\tilde{\beta}^2\left(1+4S-4S^2\right)}{(2S)^2}(E-2)^2-\tilde{\beta}^3\frac{2S-1}{S^2}(E-2)+\tilde{\beta}^4\frac{(2S-1)^2}{S^2}=0 \quad (2.75)$$

which always gives a physical solution equal to the energy of the lower edge of the continuum. The odd r equations lead to a bound state at

$$E(K=\pi) \;=\; \frac{1-5\tilde{\beta}^2-4\tilde{\beta}\frac{2S-1}{2S}\left(1-\tilde{\beta}\right)-\left(\frac{2S-1}{2S}\left(1-\tilde{\beta}\right)\right)^2}{1-2\tilde{\beta}-\frac{2S-1}{2S}\left(1-\tilde{\beta}\right)} \qquad (2.76)$$

Case (f): general $\tilde{\beta}$, $S>\frac{1}{2}$, but $r_2=\frac{4S-1}{2S-1}(1-\tilde{\beta})$, $r_2'=\frac{4S-1}{2S-1}\tilde{\beta}$ and $K=\frac{\pi}{2}$.

At $K=\frac{\pi}{2}$ and general r_2 and r_2', the equations for bound states lead to a quintic equation, which must be studied numerically.

The restrictions above correspond to the Takhtajan and Babujian model. Under these conditions, the variables reduce to

$$\begin{array}{ll}
\varepsilon_0=(1-\tilde{\beta})+\frac{2S}{2S-1}(1-\tilde{\beta}) & \varepsilon'=\varepsilon_2'=\varepsilon_1'=\varepsilon_0'=2\tilde{\beta} \\
\varepsilon=\varepsilon_1=2(1-\tilde{\beta}) & \\
V_0=-\frac{\sqrt{2S}}{\sqrt{2S-1}}(1-\tilde{\beta}) & V_0'=0 \\
V=-\frac{1}{\sqrt{2}}(1-\tilde{\beta}) & V'=0
\end{array} \qquad (2.77)$$

and the equations reduce to

$$\left.\begin{array}{rcl}
(E-\varepsilon_0-\varepsilon_0')c_0 &=& V_0c_1 \\
(E-\varepsilon_1-\varepsilon_1')c_1 &=& V_0c_0+Vc_2 \\
(E-\varepsilon-\varepsilon')c_r &=& Vc_{r-1}+Vc_{r+1}
\end{array}\right\} \qquad (2.78)$$

These equations are in the form of (2.59) and the quintic equation becomes a quadratic with solutions

$$E\left(K=\frac{\pi}{2}\right) \;=\; 2+\frac{1-\tilde{\beta}}{(2S+1)(2S-1)}\mp\frac{S\sqrt{32S^2-4}}{(2S+1)(2S-1)}(1-\tilde{\beta}) \quad (2.79)$$

Case (g): general $\tilde{\beta}$, $S = \frac{1}{2}$, and $K = \frac{\pi}{2}$.

In the Heisenberg model at $K = \frac{\pi}{2}$ and $S = \frac{1}{2}$ the parameters and equations reduce to

$$\begin{array}{ll} \varepsilon_1 = (1-\tilde{\beta}) & \varepsilon' = \varepsilon'_1 = 2\tilde{\beta} \\ \varepsilon'_2 = \tilde{\beta} & \varepsilon = 2(1-\tilde{\beta}) \\ V_0 = 0 & V'_0 = 0 \\ V = -\frac{1-\tilde{\beta}}{\sqrt{2}} & V' = 0 \end{array} \tag{2.80}$$

$$\left.\begin{array}{rcl} (E-\varepsilon_0-\varepsilon'_0)c_0 &=& 0 \\ (E-\varepsilon_1-\varepsilon'_1)c_1 &=& Vc_2 \\ (E-\varepsilon-\varepsilon'_2)c_2 &=& Vc_1 + Vc_3 \\ (E-\varepsilon-\varepsilon')c_r &=& Vc_{r-1} + Vc_{r+1} \end{array}\right\} \tag{2.81}$$

The amplitude c_0 decouples and is unphysical. These equations are in the form of (2.59) and the bound state solutions are the solutions of the cubic equation

$$\begin{aligned} \tilde{\beta}(E-2)^3 + (2\tilde{\beta}-\tilde{\beta}^2)(E-2)^2 + (1-\tilde{\beta})\left(\tfrac{1}{2}-\tilde{\beta}+\tfrac{5}{2}\tilde{\beta}^2\right)(E-2) + \\ (1-\tilde{\beta})^2\left(\tfrac{3}{4}-\tfrac{5}{2}\tilde{\beta}+\tfrac{11}{4}\tilde{\beta}^2\right) = 0 \end{aligned} \tag{2.82}$$

in agreement with Ono, Mikado and Oguchi [15] and with Gochev [16].

At all other values of r_2, r'_2, K and S the equations (2.58) retain their pentadiagonal form and the real space rescaling method discussed above must be generalized. Gochev [16] has considered the $S = \frac{1}{2}$ general K and $\tilde{\beta}$ case by assuming a solution with the general form

$$c_r = Ae^{iq_1 r} + Be^{-iq_1 r} + Ce^{iq_2 r} + De^{-iq_2 r} \tag{2.83}$$

and obtained a quartic equation for the eigenvalues of the bound states. The two-magnon equations can be solved for any case, however, using the scalar renormalization group method of Southern, Kumar and Ashraff [23] or the matrix rescaling method described in the next section. In the latter approach, no assumption about the form of the solution is necessary.

2.4.2 Matrix Rescaling Method

Write the equations (2.58) in matrix form by expressing the amplitudes in column vectors, or unit cells [19]

$$\mathbf{c}_0 = \begin{pmatrix} c_0 \\ c_1 \end{pmatrix} \qquad \mathbf{c}_1 = \begin{pmatrix} c_2 \\ c_3 \end{pmatrix} \qquad \mathbf{c}_r = \begin{pmatrix} c_{2r} \\ c_{2r+1} \end{pmatrix} \tag{2.84}$$

and let

$$\begin{aligned} \mathbf{M}_0 &= \begin{pmatrix} E-\varepsilon_0-\varepsilon_0' & -V_0 \\ -V_0 & E-\varepsilon_1-\varepsilon_1' \end{pmatrix} \\ \mathbf{M}_1 &= \begin{pmatrix} E-\varepsilon-\varepsilon_2' & -V \\ -V & E-\varepsilon-\varepsilon' \end{pmatrix} \\ \mathbf{M} &= \begin{pmatrix} E-\varepsilon-\varepsilon' & -V \\ -V & E-\varepsilon-\varepsilon' \end{pmatrix} \\ \mathbf{V}_0 &= \begin{pmatrix} V_0' & 0 \\ V & V' \end{pmatrix} \\ \mathbf{V} &= \begin{pmatrix} V' & 0 \\ V & V' \end{pmatrix} \end{aligned} \tag{2.85}$$

The two-magnon equations can be expressed as

$$\left.\begin{aligned} \mathbf{M}_0\mathbf{c}_0 &= \mathbf{V}_0\mathbf{c}_1 \\ \mathbf{M}_1\mathbf{c}_1 &= \mathbf{V}_0^T\mathbf{c}_0 + \mathbf{V}\mathbf{c}_2 \\ \mathbf{M}\mathbf{c}_r &= \mathbf{V}^T\mathbf{c}_{r-1} + \mathbf{V}\mathbf{c}_{r+1} \qquad r \geq 2 \end{aligned}\right\} \tag{2.86}$$

where ^{T} is the symbol for transpose. Using the rescaling method we eliminate every other unit cell except the reference cell (cell of interest) which corresponds to a scaling factor of $b = 2$. The equations for the remaining cells have the same form as the original set, but the matrices are renormalized. Using the cell $r = 0$ as our reference cell, the renormalized parameters are expressed in terms of the previous parameters as follows

$$\left.\begin{aligned} \mathbf{M}_0' &= \mathbf{M}_0 - \mathbf{V}_0\mathbf{M}_1^{-1}\mathbf{V}_0^T \\ \mathbf{M}_1' &= \mathbf{M} - \mathbf{V}^T\mathbf{M}_1^{-1}\mathbf{V} - \mathbf{V}\mathbf{M}^{-1}\mathbf{V}^T \\ \mathbf{M}' &= \mathbf{M} - \mathbf{V}^T\mathbf{M}^{-1}\mathbf{V} - \mathbf{V}\mathbf{M}^{-1}\mathbf{V}^T \\ \mathbf{V}_0' &= \mathbf{V}_0\mathbf{M}_1^{-1}\mathbf{V} \\ \mathbf{V}' &= \mathbf{V}\mathbf{M}^{-1}\mathbf{V} \end{aligned}\right\} \tag{2.87}$$

The spectral properties of the system can be obtained by adding a small imaginary part to the energy for convergence and iterating the transformation numerically until $\mathbf{V}_0'$ and $\mathbf{V}'$ approach zero. In this limit, $\mathbf{M}_0^{(\infty)}\mathbf{c}_0 = 0$ and non-trivial solutions correspond to $det\ \mathbf{M}_0^{(\infty)} = 0$. For energies outside the continuum, no imaginary part is needed and the bound states are located using $det\ \mathbf{M}_0^{(\infty)} = 0$. For energies inside the continuum, $\mathbf{M}_0^{(\infty)}$ has complex elements and the local density of states is proportional to the imaginary part of the diagonal elements of the inverse of $\mathbf{M}_0^{(\infty)}$. By fixing K and plotting the density of states versus the real part of the energy, the continuum, the bound states and any resonances can be identified. The continuum appears as a band of finite density, the bound states appear as delta functions outside the continua, and the resonances appear as sharp peaks inside the continua. Additional internal (van Hove) singularities can appear at special energies inside the continuum. The real part of $\mathbf{M}_0^{(\infty)-1}$, which diverges at the bound state energy, can also be used to identify bound states. The real and the imaginary parts of $M_0^{(\infty)-1}(1,1)$ are shown for the Takhtajan and Babujian model at $\tilde{\beta} = \frac{1}{2}$, $S = 1$ and $K = \pi$ in figures 2.10 and 2.11 respectively. Both the scattering state continuum and a bound state above the continuum are visible.

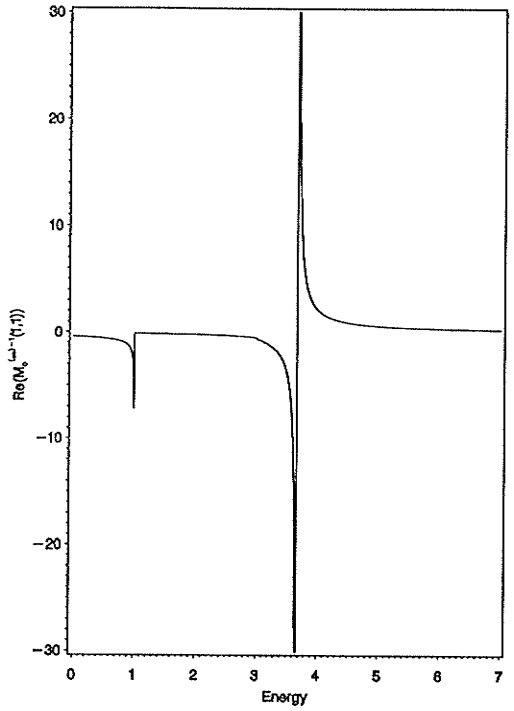

Figure 2.10: Real part of the density of states for two-magnon excitations on an $S = 1$ spin chain at $K = \pi$ for the Takhtajan and Babujian model with $\tilde{\beta} = \frac{1}{2}$.

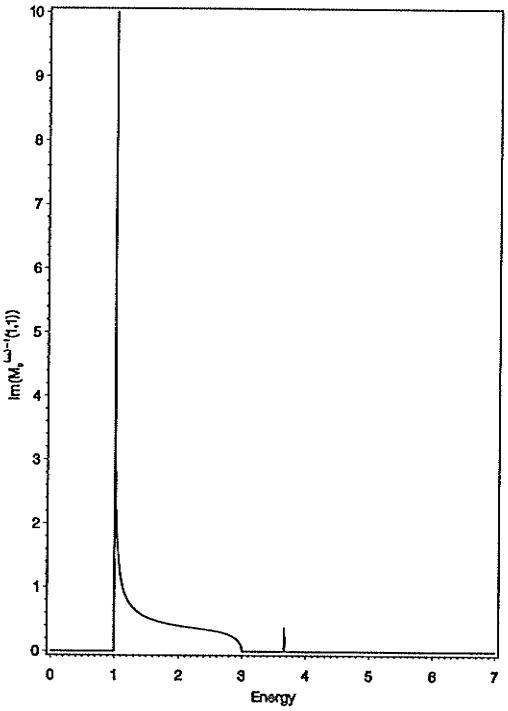

Figure 2.11: Imaginary part of the density of states for two-magnon excitations on an $S = 1$ spin chain at $K = \pi$ for the Takhtajan and Babujian model with $\tilde{\beta} = \frac{1}{2}$.

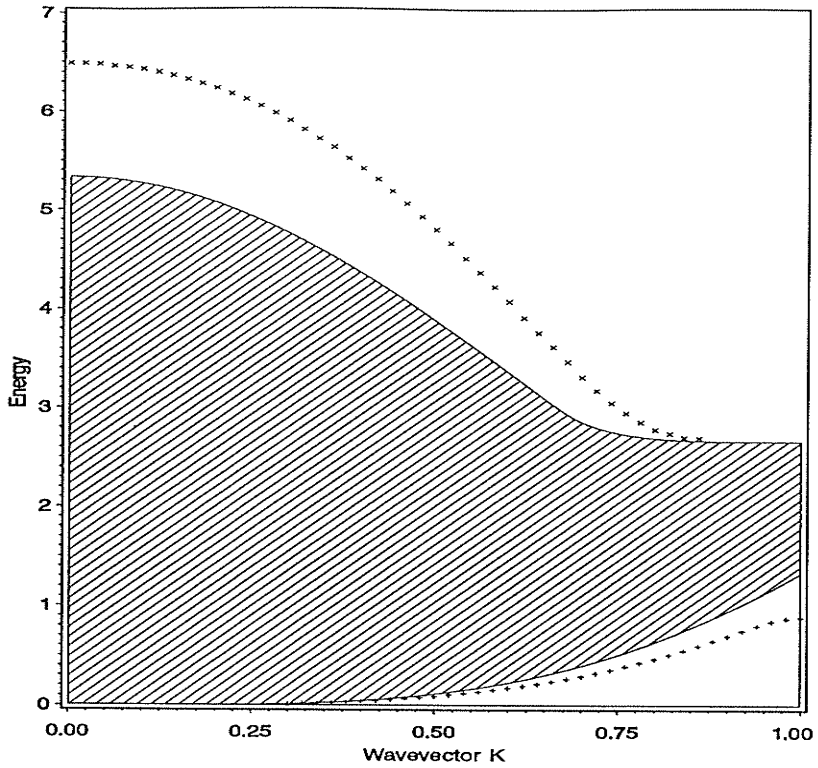

Figure 2.12: Two-magnon excitation dispersion diagram showing the lower and upper bound state branches (+ and × respectively) and the scattering state continuum (shaded region) for the $S = 1$ Takhtajan and Babujian model with $\tilde{\beta} = -\frac{1}{3}$.

The spectra can be found for all values of $K = 0$ to π and combined to show the complete dispersion diagram for a given S, r_2 and r_2'. Figures 2.12 to 2.15 show the dispersion diagrams for the Takhtajan and Babujian model with $S = 1$ and $\tilde{\beta} = -\frac{1}{3}, 0, \frac{1}{5}$ and 1. The scattering state continua are the shaded areas in the diagrams. The numerical results agree with the analytical predictions (cases (d) and (f)) at $K = \pi$ and $\frac{\pi}{2}$. At $\tilde{\beta} = 0$ the bound state branches meet at the Brillouin zone boundary since at this value of $\tilde{\beta}$ the model is integrable. If $\tilde{\beta} \neq 0$, the bound states no longer meet each other at the Brillouin zone boundary and the gap increases as $\tilde{\beta}$ increases or decreases from zero. For $\tilde{\beta} = 1$, the model is again integrable but the unit cell is doubled and hence the no gap occurs at $K = \frac{\pi}{2}$.

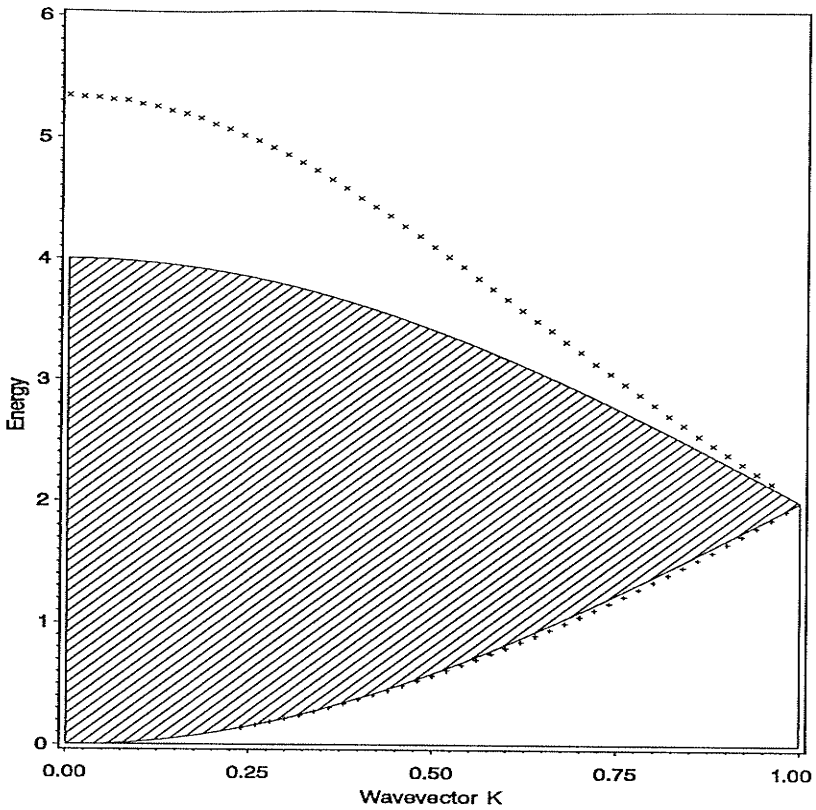

Figure 2.13: Two-magnon excitation dispersion diagram showing the lower and upper bound state branches (+ and × respectively) and the scattering state continuum (shaded region) for the $S = 1$ Takhtajan and Babujian model with $\tilde{\beta} = 0$.

At $\tilde{\beta} = 0$ both the lower and upper bound state branches touch the continuum edge at $K = \pi$. For $\tilde{\beta} < 0$, the upper bound state branch touches the upper continuum edge at $K = \pi$, and exists for all other values of K. For $\tilde{\beta} > 0$, the lower bound state branch sticks to the continuum edge at $K = 0$ and $K = \pi$ but exists for all intermediate values of K. From case (d) at $K = \pi$, the bound state solution (2.73) is below the continuum for $\tilde{\beta} < 0$, equals the continuum edge value at $\tilde{\beta} = 0$, and passes above the continuum for $\tilde{\beta} > 0$.

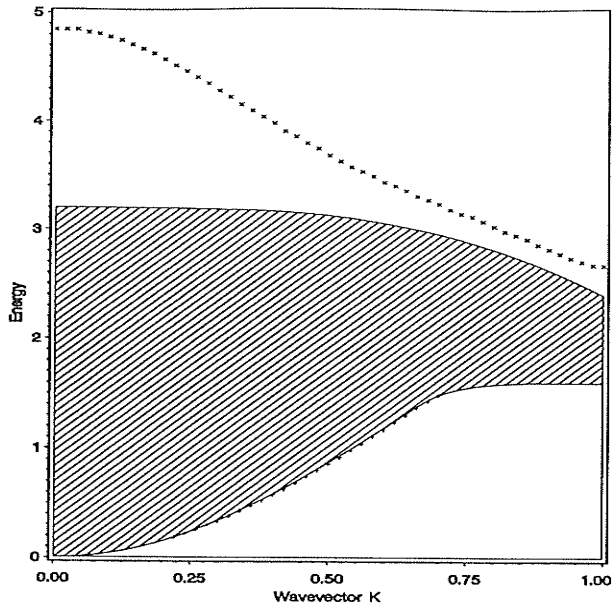

Figure 2.14: Two-magnon excitation dispersion diagram showing the lower and upper bound state branches (+ and × respectively) and the scattering state continuum (shaded region) for the $S = 1$ Takhtajan and Babujian model with $\tilde{\beta} = \frac{1}{5}$.

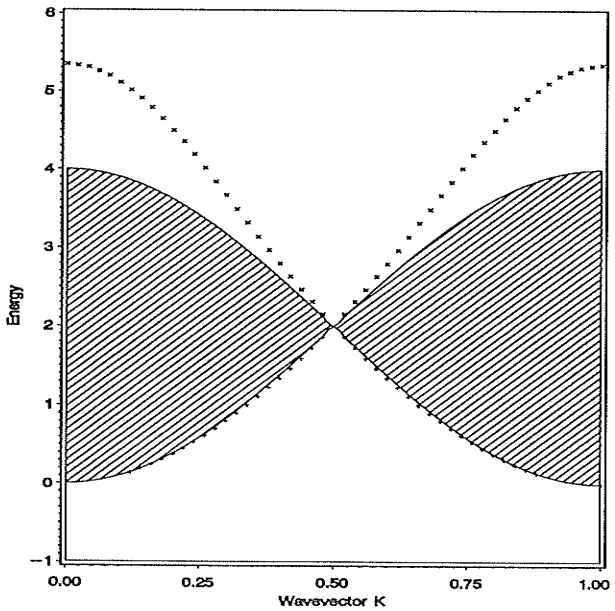

Figure 2.15: Two-magnon excitation dispersion diagram showing the lower and upper bound state branches (+ and × respectively) and the scattering state continuum (shaded region) for the $S = 1$ Takhtajan and Babujian model with $\tilde{\beta} = 1$.

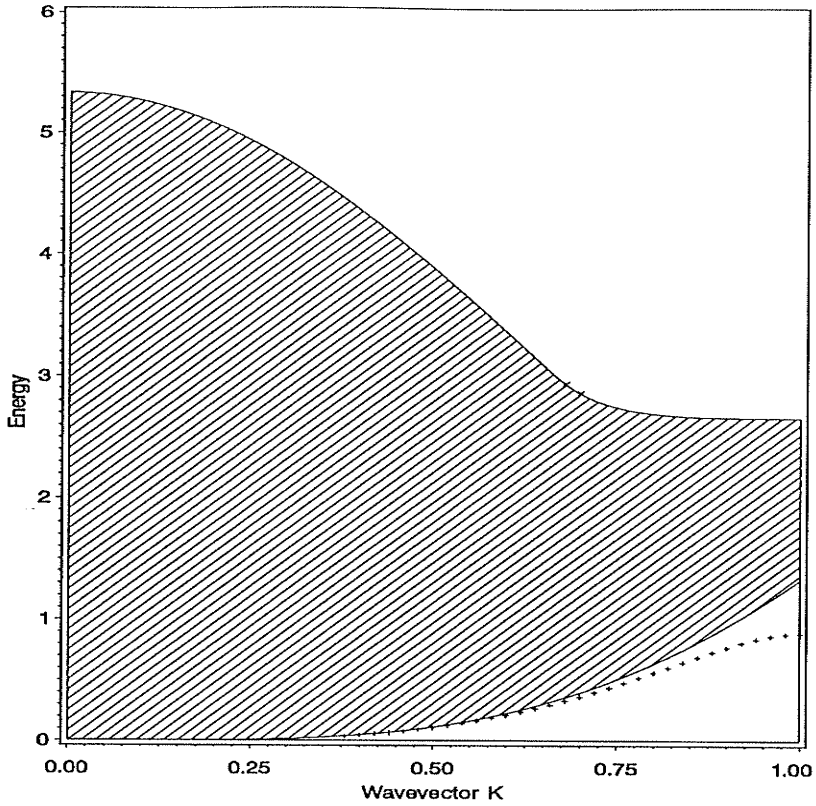

Figure 2.16: Two-magnon excitation dispersion diagram showing the lower and upper bound state branches (+ and × respectively) and the scattering state continuum (shaded region) for the $S = 1$ Heisenberg model with $\tilde{\beta} = -\frac{1}{3}$.

Figures 2.16 to 2.19 show the dispersion diagrams for the $S = 1$ Heisenberg case with nearest neighbor interactions and next nearest neighbor interactions of strength $\tilde{\beta} = -\frac{1}{3}, 0, \frac{1}{5}$ and 1. The analytical results (case (e)) agree with the numerical results. For $\tilde{\beta} > 0$ the upper bound state of the Takhtajan and Babujian model has moved into the continuum, becoming a resonance, and only the lower branch remains. However, for $\tilde{\beta} < 0$ a second bound state is found weakly separated above the continuum for a small range of K intermediate between $K = 0$ and π, in agreement with Bahurmuz and Loly [17]. This bound state is only found for a small range of $\tilde{\beta}$ above $-\frac{1}{3}$.

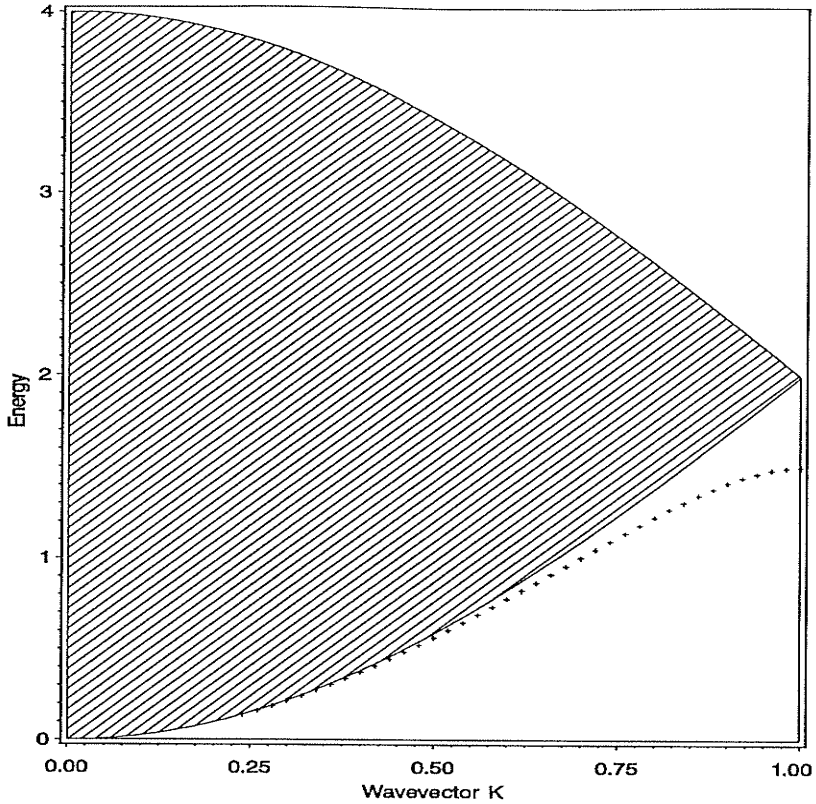

Figure 2.17: Two-magnon excitation dispersion diagram showing the lower bound state branch (+) and the scattering state continuum (shaded region) for the $S = 1$ Heisenberg model with $\tilde{\beta} = 0$.

For $\tilde{\beta} > 0$, the lower bound state moves up to the continuum at $K = \pi$ when $\tilde{\beta} = \frac{1}{4S+1} = \frac{1}{5}$. As $\tilde{\beta}$ increases above this value, the bound state sticks to the continuum edge $K = 0$ and $K = \pi$ but exists for all intermediate values of K.

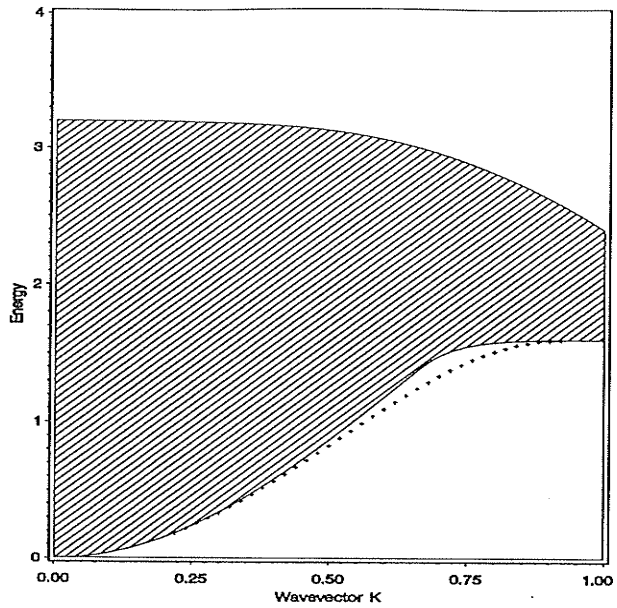

Figure 2.18: Two-magnon excitation dispersion diagram showing the lower bound state branch (+) and the scattering state continuum (shaded region) for the $S = 1$ Heisenberg model with $\tilde{\beta} = \frac{1}{5}$.

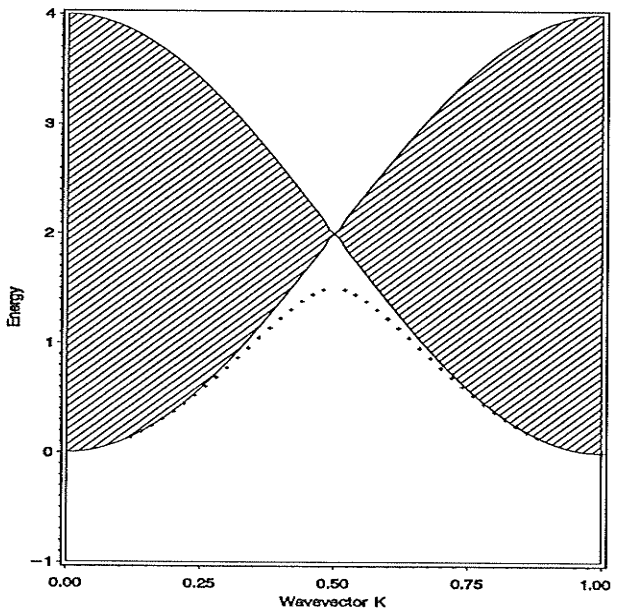

Figure 2.19: Two-magnon excitation dispersion diagram showing the lower bound state branch (+) and the scattering state continuum (shaded region) for the $S = 1$ Heisenberg model with $\tilde{\beta} = 1$.

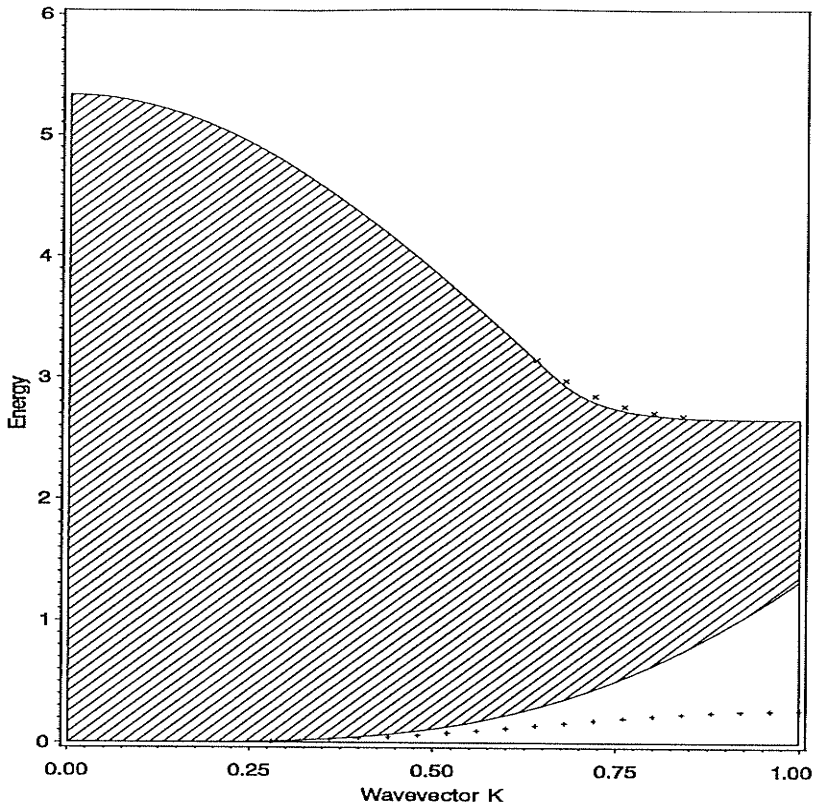

Figure 2.20: Two-magnon excitation dispersion diagram showing the lower and upper bound state branches (+ and × respectively) and the scattering state continuum (shaded region) for the $S = \frac{1}{2}$ Heisenberg model with $\tilde{\beta} = -\frac{1}{3}$.

For $S = \frac{1}{2}$ the site c_0 (two spin deviations on the same site) is not physical. The physically interesting components are the real and imaginary parts of $M_0^{(\infty)-1}(2,2)$ (spins flipped on nearest neighbor sites). The dispersion relation for the $S = \frac{1}{2}$ Heisenberg case with $\tilde{\beta} = -\frac{1}{3}, 0, \frac{1}{5}$ and 1 are shown in figures 2.20 to 2.23 and are in agreement with Ono, Mikado and Oguchi [15]. Analytical solutions at $K = \pi$ and $\frac{\pi}{2}$ were obtained in cases (c) and (g). The bound state branch above the continuum has less restricted ranges of K and $\tilde{\beta} < 0$ than for $S = 1$, in agreement with Bahurmuz and Loly.

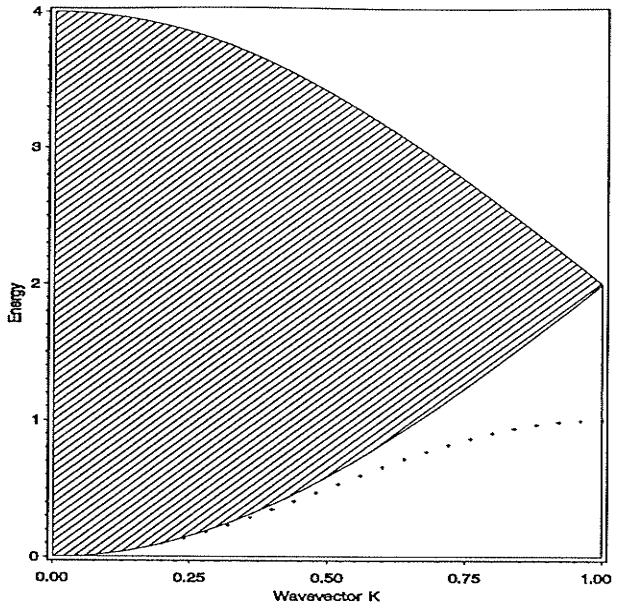

Figure 2.21: Two-magnon excitation dispersion diagram showing the lower bound state branch (+) and the scattering state continuum (shaded region) for the $S = \frac{1}{2}$ Heisenberg model with $\tilde{\beta} = 0$.

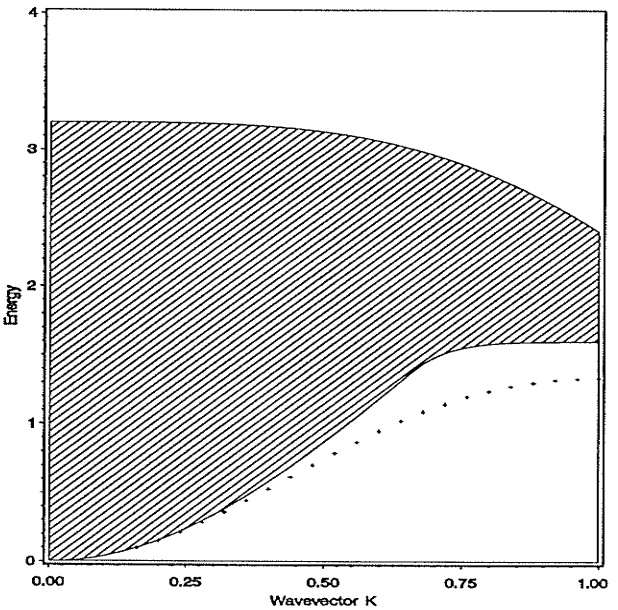

Figure 2.22: Two-magnon excitation dispersion diagram showing the lower bound state branch (+) and the scattering state continuum (shaded region) for the $S = \frac{1}{2}$ Heisenberg model with $\tilde{\beta} = \frac{1}{5}$.

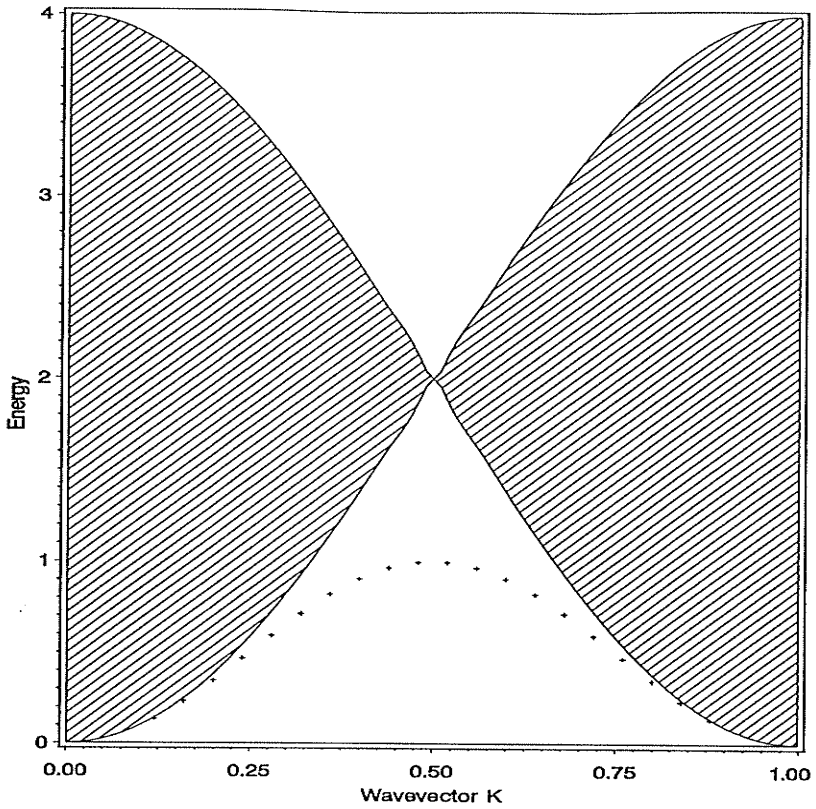

Figure 2.23: Two-magnon excitation dispersion diagram showing the lower bound state branch (+) and the scattering state continuum (shaded region) for the $S = \frac{1}{2}$ Heisenberg model with $\tilde{\beta} = 1$.

The lower branch moves up to the continuum at $K = \pi$ when $\tilde{\beta} = \frac{1}{4S+1} = \frac{1}{3}$. As $\tilde{\beta}$ increases above this value, the bound state sticks to the continuum edge at $K = 0$ and $K = \pi$ but exists for all intermediate values of K, in agreement with Gochev [16].

Using this numerical procedure the dispersion relations for any given values of $\tilde{\beta}, S, r_2$ and r_2' can be found. This information is needed to describe the scattering state solutions of the three-magnon excitations. These excitations are considered in the next chapter.

Chapter 3

Three-Magnon Excitations

The development of the three-magnon equations follows the method used to find the one and two-magnon equations. The three spin deviation state is

$$| i,j,k\rangle = C_{ijk} S_i^+ S_j^+ S_k^+ \mid 0\rangle \tag{3.1}$$

$$C_{ijk} = \begin{cases} \frac{1}{\sqrt{8S^3}} & \text{if } i \neq j \neq k \\ \frac{1}{\sqrt{8S^2(2S-1)}} & \text{if 2 of } \{i,j,k\} \text{ are equal} \\ \frac{1}{\sqrt{24S(2S-1)(S-1)}} & \text{if } i = j = k \end{cases}$$

where the C_{ijk} are normalization constants and the kets are labeled such that $i \leq j \leq k$. The derivation of the effect of the Hamiltonian on these orthonormal base kets is straight-forward but somewhat lengthy and is included in Appendix A. The final set of equations in Appendix A, equations (A.12), (A.16) to (A.18), (A.22) to (A.24) and (A.29) to (A.31), involve kets in coordinate space (i,j,k) and due to the translational invariance of the Hamiltonian a transformation can be made from coordinate space to a center of mass coordinate (R) and two relative coordinates (x,y). Specifically the transformation is

$$| i,j,k\rangle \Rightarrow | R,x,y\rangle, \begin{cases} R = \frac{1}{3}(i+j+k) \\ x = j - i \\ y = k - j \end{cases} \tag{3.2}$$

and since $i \leq j \leq k$, then $x, y \geq 0$. Using Bloch's theorem, a Fourier transform can be made to the center of mass wavevector K and relative coordinates x and y

as follows:

$$| K; x, y\rangle = \frac{1}{\sqrt{N}} \sum_R e^{-iRK} | R, x, y\rangle \tag{3.3}$$

where the wavevector K can take on the values $K = \frac{2\pi n}{N}$, $n \in \mathcal{Z}$. Having performed these transformations on the final equations from Appendix A, the resulting Hamiltonian is best expressed using the following variables:

$$\begin{aligned}
\varepsilon &= 3\alpha_1(S) \\
\varepsilon_0 &= 3S(S-1)\left[\frac{1-\cos K}{S(4S-3)}\alpha_1(S) + \frac{1+\cos K}{(S-1)(4S-1)}\alpha_2(S) + \frac{1-\cos K}{3(S-1)(4S-3)}\alpha_3(S)\right] \\
\varepsilon_1 &= \frac{1}{2}\left[\frac{3(3S-2)}{4S-3}\alpha_1(S) + \frac{3S-1}{4S-1}\alpha_2(S) - \frac{3(1-S)}{4S-3}\alpha_3(S)\right] \\
\varepsilon_2 &= \alpha_1(S) + 2\left(\frac{2S-1}{4S-1}\right)\alpha_2(S) \\
\varepsilon_3 &= 2\left[\alpha_1(S) + \frac{S}{4S-1}\alpha_2(S)\right] \\
\varepsilon_4 &= 2\alpha_1(S) + \frac{2S-1}{4S-1}\alpha_2(S) \\
u &= -\frac{\zeta}{2}\left[\frac{S}{4S-3}\alpha_1(S) + \frac{1-S}{4S-1}\alpha_2(S) - \frac{3(1-S)}{4S-3}\alpha_3(S)\right] \\
v &= -\frac{\zeta}{2}\alpha_1(S) \\
v_0 &= \frac{\zeta}{2}\sqrt{3S(S-1)}\left[\frac{1-\zeta^{*3}}{4S-3}\alpha_1(S) - \frac{1+\zeta^{*3}}{4S-1}\alpha_2(S) - \frac{1-\zeta^{*3}}{4S-3}\alpha_3(S)\right] \\
v_1 &= -\frac{\zeta}{2}\left[(1+\zeta^{*3})\alpha_1(S) - \frac{2S\zeta^{*3}}{4S-1}\alpha_2(S)\right] \\
w &= -\frac{\zeta\sqrt{S(2S-1)}}{4S-1}\alpha_2(S)
\end{aligned} \tag{3.4}$$

In these equations the * represents complex conjugation and $\zeta = e^{\frac{iK}{3}}$. In addition to these variables we also have primed variables which are equal to the above definitions, but with the following changes:

$$\begin{aligned}
\zeta &\rightarrow \zeta^2 \\
\cos K &\rightarrow \cos 2K \\
\alpha_1(S) &\rightarrow \alpha_1'(S)
\end{aligned} \tag{3.5}$$

$$\alpha_2(S) \rightarrow \alpha_2'(S)$$
$$\alpha_3(S) \rightarrow \alpha_3'(S)$$

For example,

$$\begin{aligned} \varepsilon' &= 3\alpha_1'(S) \\ v' &= -\frac{\zeta^2}{2}\alpha_1'(S) \end{aligned} \tag{3.6}$$

The resulting three-magnon equations are:

$$\begin{aligned}
\widehat{H} \mid K;0,0\rangle &= (\varepsilon_0+\varepsilon_0') \mid K;0,0\rangle + v_0 \mid K;0,1\rangle + v_0^* \mid K;1,0\rangle + v_0' \mid K;0,2\rangle \\
&\quad + v_0'^* \mid K;2,0\rangle && (3.7)\\
\widehat{H} \mid K;0,1\rangle &= (\varepsilon_1+\varepsilon_3') \mid K;0,1\rangle + v_0^* \mid K;0,0\rangle + (u+v_1'^*) \mid K;1,0\rangle + v_1 \mid K;0,2\rangle \\
&\quad + v_1' \mid K;0,3\rangle + (w^*+w') \mid K;1,1\rangle + w'^* \mid K;2,1\rangle && (3.8)\\
\widehat{H} \mid K;1,0\rangle &= (\varepsilon_1+\varepsilon_3') \mid K;1,0\rangle + v_0 \mid K;0,0\rangle + (u^*+v_1') \mid K;0,1\rangle + v_1^* \mid K;2,0\rangle \\
&\quad + v_1'^* \mid K;3,0\rangle + (w+w'^*) \mid K;1,1\rangle + w' \mid K;1,2\rangle && (3.9)\\
\widehat{H} \mid K;1,1\rangle &= (\varepsilon_2+\varepsilon_4') \mid K;1,1\rangle + (w+w'^*) \mid K;0,1\rangle + (w^*+w') \mid K;1,0\rangle \\
&\quad + w^* \mid K;0,2\rangle + w \mid K;2,0\rangle + (v+v'^*) \mid K;1,2\rangle + (v^*+v') \mid K;2,1\rangle \\
&\quad + v' \mid K;1,3\rangle + v'^* \mid K;3,1\rangle && (3.10)\\
\widehat{H} \mid K;0,2\rangle &= (\varepsilon_3+\varepsilon_1') \mid K;0,2\rangle + v_0'^* \mid K;0,0\rangle + v_1^* \mid K;0,1\rangle + v_1 \mid K;0,3\rangle \\
&\quad + v_1' \mid K;0,4\rangle + u'^* \mid K;2,0\rangle + w \mid K;1,1\rangle + w^* \mid K;1,2\rangle \\
&\quad + w'^* \mid K;2,2\rangle && (3.11)\\
\widehat{H} \mid K;2,0\rangle &= (\varepsilon_3+\varepsilon_1') \mid K;2,0\rangle + v_0' \mid K;0,0\rangle + v_1 \mid K;1,0\rangle + v_1^* \mid K;3,0\rangle \\
&\quad + v_1'^* \mid K;4,0\rangle + u' \mid K;0,2\rangle + w^* \mid K;1,1\rangle + w \mid K;2,1\rangle \\
&\quad + w' \mid K;2,2\rangle && (3.12)\\
\widehat{H} \mid K;1,2\rangle &= (\varepsilon_4+\varepsilon_4') \mid K;1,2\rangle + w'^* \mid K;1,0\rangle + w \mid K;0,2\rangle + w^* \mid K;0,3\rangle \\
&\quad + w' \mid K;3,0\rangle + (v^*+v') \mid K;1,1\rangle + v \mid K;2,1\rangle + (v \\
&\quad + v'^*) \mid K;1,3\rangle + v' \mid K;1,4\rangle + v^* \mid K;2,2\rangle + v'^* \mid K;3,2\rangle && (3.13)\\
\widehat{H} \mid K;2,1\rangle &= (\varepsilon_4+\varepsilon_4') \mid K;2,1\rangle + w' \mid K;0,1\rangle + w^* \mid K;2,0\rangle + w \mid K;3,0\rangle \\
&\quad + w'^* \mid K;0,3\rangle + (v+v'^*) \mid K;1,1\rangle + v^* \mid K;1,2\rangle + (v^* \\
&\quad + v') \mid K;3,1\rangle + v'^* \mid K;4,1\rangle + v \mid K;2,2\rangle + v' \mid K;2,3\rangle && (3.14)\\
\widehat{H} \mid K;2,2\rangle &= (\varepsilon+\varepsilon_2') \mid K;2,2\rangle + w' \mid K;0,2\rangle + w'^* \mid K;2,0\rangle + w'^* \mid K;0,4\rangle \\
&\quad + w' \mid K;4,0\rangle + v \mid K;1,2\rangle + v^* \mid K;2,1\rangle + v^* \mid K;1,3\rangle + v \mid K;3,1\rangle \\
&\quad + v \mid K;2,3\rangle + v^* \mid K;3,2\rangle + v' \mid K;2,4\rangle + v'^* \mid K;4,2\rangle && (3.15)\\
\widehat{H} \mid K;0,y\rangle &= (\varepsilon_3+\varepsilon_3') \mid K;0,y\rangle + v_1'^* \mid K;0,y-2\rangle + v_1^* \mid K;0,y-1\rangle \\
&\quad + v_1 \mid K;0,y+1\rangle + v_1' \mid K;0,y+2\rangle + w \mid K;1,y-1\rangle + w^* \mid K;1,y\rangle
\end{aligned}$$

$$+ w' \mid K; 2, y-2\rangle + w'^{*} \mid K; 2, y\rangle \tag{3.16}$$

$$\begin{aligned}\widehat{H} \mid K; x, 0\rangle &= (\varepsilon_3 + \varepsilon_3') \mid K; x, 0\rangle + v_1' \mid K; x-2, 0\rangle + v_1 \mid K; x-1, 0\rangle \\ &+ v_1^* \mid K; x+1, 0\rangle + v_1'^{*} \mid K; x+2, 0\rangle + w^* \mid K; x-1, 1\rangle + w \mid K; x, 1\rangle \\ &+ w'^{*} \mid K; x-2, 2\rangle + w' \mid K; x, 2\rangle \end{aligned} \tag{3.17}$$

$$\begin{aligned}\widehat{H} \mid K; 1, y\rangle &= (\varepsilon_4 + \varepsilon') \mid K; 1, y\rangle + (v + v'^{*}) \mid K; 1, y+1\rangle + (v^* + v') \mid K; 1, y-1\rangle \\ &+ v \mid K; 2, y-1\rangle + v^* \mid K; 2, y\rangle + v' \mid K; 1, y+2\rangle + v'^{*} \mid K; 1, y-2\rangle \\ &+ v'^{*} \mid K; 3, y\rangle + v' \mid K; 3, y-2\rangle + w \mid K; 0, y\rangle + w^* \mid K; 0, y+1\rangle \end{aligned} \tag{3.18}$$

$$\begin{aligned}\widehat{H} \mid K; x, 1\rangle &= (\varepsilon_4 + \varepsilon') \mid K; x, 1\rangle + (v + v'^{*}) \mid K; x-1, 1\rangle + (v^* + v') \mid K; x+1, 1\rangle \\ &+ v \mid K; x, 2\rangle + v^* \mid K; x-1, 2\rangle + v' \mid K; x-2, 1\rangle + v'^{*} \mid K; x+2, 1\rangle \\ &+ v'^{*} \mid K; x-2, 3\rangle + v' \mid K; x, 3\rangle + w \mid K; x+1, 0\rangle + w^* \mid K; x, 0\rangle \end{aligned} \tag{3.19}$$

$$\begin{aligned}\widehat{H} \mid K; 2, y\rangle &= (\varepsilon + \varepsilon_4') \mid K; 2, y\rangle + v \mid K; 1, y\rangle + v^* \mid K; 1, y+1\rangle + v \mid K; 2, y+1\rangle \\ &+ v^* \mid K; 2, y-1\rangle + v \mid K; 3, y-1\rangle + v^* \mid K; 3, y\rangle + v' \mid K; 2, y+2\rangle \\ &+ v'^{*} \mid K; 2, y-2\rangle + v' \mid K; 4, y-2\rangle + v'^{*} \mid K; 4, y\rangle + w' \mid K; 0, y\rangle \\ &+ w'^{*} \mid K; 0, y+2\rangle \end{aligned} \tag{3.20}$$

$$\begin{aligned}\widehat{H} \mid K; x, 2\rangle &= (\varepsilon + \varepsilon_4') \mid K; x, 2\rangle + v \mid K; x+1, 1\rangle + v^* \mid K; x, 1\rangle + v \mid K; x-1, 2\rangle \\ &+ v^* \mid K; x+1, 2\rangle + v \mid K; x, 3\rangle + v^* \mid K; x-1, 3\rangle + v' \mid K; x-2, 2\rangle \\ &+ v'^{*} \mid K; x+2, 2\rangle + v' \mid K; x, 4\rangle + v'^{*} \mid K; x-2, 4\rangle + w' \mid K; x+2, 0\rangle \\ &+ w'^{*} \mid K; x, 0\rangle \end{aligned} \tag{3.21}$$

$$\begin{aligned}\widehat{H} \mid K; x, y\rangle &= (\varepsilon + \varepsilon') \mid K; x, y\rangle + v \mid K; x-1, y\rangle + v^* \mid K; x+1, y\rangle \\ &+ v^* \mid K; x, y-1\rangle + v \mid K; x, y+1\rangle + v^* \mid K; x-1, y+1\rangle \\ &+ v \mid K; x+1, y-1\rangle + v'^{*} \mid K; x+2, y\rangle + v' \mid K; x-2, y\rangle \\ &+ v' \mid K; x; y+2\rangle + v'^{*} \mid K; x, y-2\rangle + v'^{*} \mid K; x-2, y+2\rangle \\ &+ v' \mid K; x+2, y-2\rangle \end{aligned} \tag{3.22}$$

where both $x, y > 2$.

In order to visualize the interactions between the various kets, the equations can be represented graphically. As in the two-magnon graphical representation, the interactions between nearest neighbors and next nearest neighbors are shown separately. In addition, the next nearest interactions will be broken up into four categories: interactions between even/even kets (x = an even number, y = an even number), even/odd kets, odd/even kets, and odd/odd kets. For nearest neighbor interactions only, each ket in general has interactions between itself and six other kets. Therefore the proper underlying lattice of the graphical representation would be triangular. However, for clarity of labeling the sites, we have deformed the

underlying lattice to a square lattice. A result of this deformation is that some of the nearest neighbor sites appear to be $\sqrt{2}$ of the distance of the other nearest neighbor sites. A ket $\mid K; x, y\rangle$ can only have an interaction with kets $\mid K; x-1, y+1\rangle, \mid K; x+1, y-1\rangle, \mid K; x, y+1\rangle, \mid K; x, y-1\rangle, \mid K; x+1, y\rangle$ and $\mid K; x-1, y\rangle$. It can not interact with kets $\mid K; x-1, y-1\rangle$ and $\mid K; x+1, y+1\rangle$. For the next nearest neighbor graphical representations, a similar restriction applies.

The axis labels x and y are the ket indices ($\mid K; x, y\rangle$) and the shapes at each site represent the $(\varepsilon_i + \varepsilon'_j)$ that result when the Hamiltonian acts on that ket. The various types of lines between the kets correspond to the different interactions and the arrows indicate whether or not the complex conjugate of the interaction is to be taken. For example, if the Hamiltonian is acting on a ket and the diagram shows an arrow pointing away from that ket, then the interaction between that ket and the ket towards which the arrow point is as shown. However, if the arrow is pointing towards the ket that the Hamiltonian is acting on, then the interaction is the complex conjugate of the interaction shown.

An example best explains the details of the diagram. Let us find the effects of $\widehat{H}$ acting on the ket $\mid K; 0, 0\rangle$. At the site $(x = 0, y = 0)$, there is a shape which represents $(\varepsilon_0 + \varepsilon'_0)$ so the first term is $(\varepsilon_0 + \varepsilon'_0) \mid K; 0, 0\rangle$. The nearest neighbor diagram shows an interaction v_0 between site $(x = 0, y = 0)$ and site $(x = 0, y = 1)$, and the arrow points away from site $(x = 0, y = 0)$ so the complex conjugate is not taken and the term is $v_0 \mid K; 0, 1\rangle$. Similarly an interaction is shown between site $(x = 0, y = 0)$ and site $(x = 1, y = 0)$, but the arrow points towards site $(x = 0, y = 0)$, so the term is $v_0^* \mid K; 1, 0\rangle$. On the nearest neighbor diagram there are no more lines from site $(x = 0, y = 0)$ to any other site, so we look at the next nearest neighbor even/even diagram which shows an interaction v'_0 between sites $(x = 0, y = 0)$ and $(x = 0, y = 2)$ and v'^*_0 between sites $(x = 0, y = 0)$ and

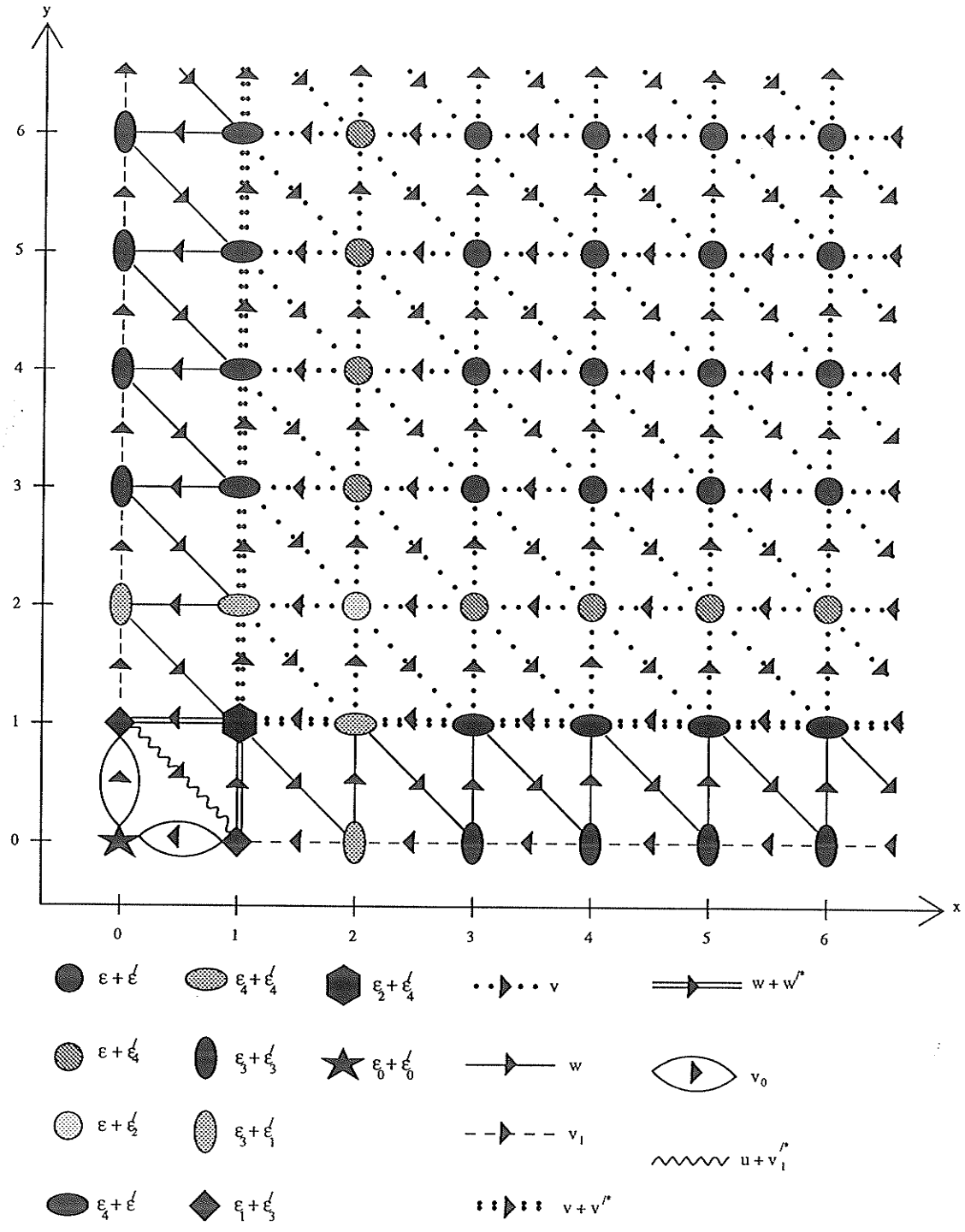

Figure 3.1: Graphical representation of the interactions between the nearest neighbor kets in the three-magnon equations.

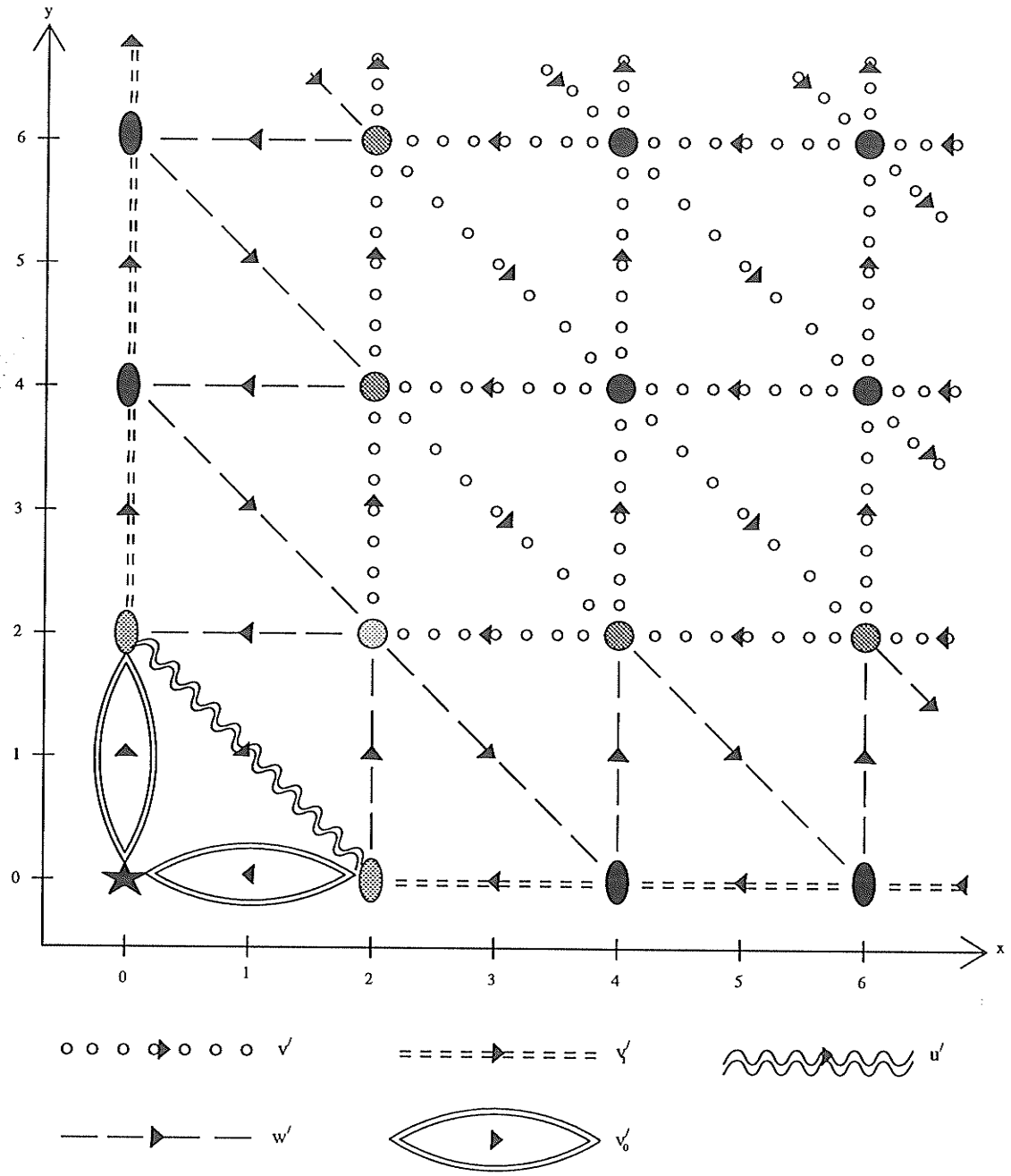

Figure 3.2: Graphical representation of the interactions between the next nearest neighbor even/even kets in the three-magnon equations.

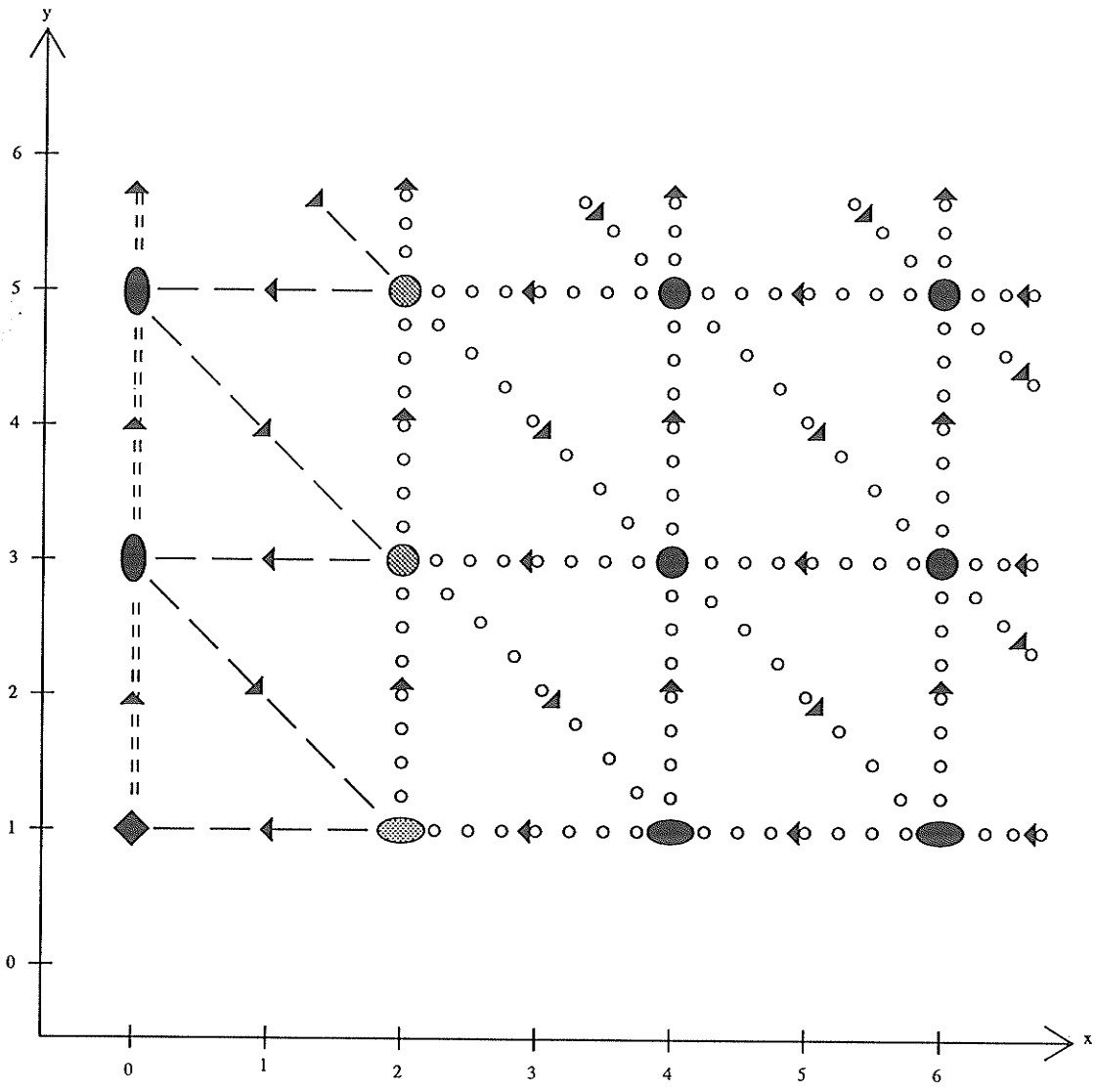

Figure 3.3: Graphical representation of the interactions between the next nearest neighbor even/odd kets in the three-magnon equations.

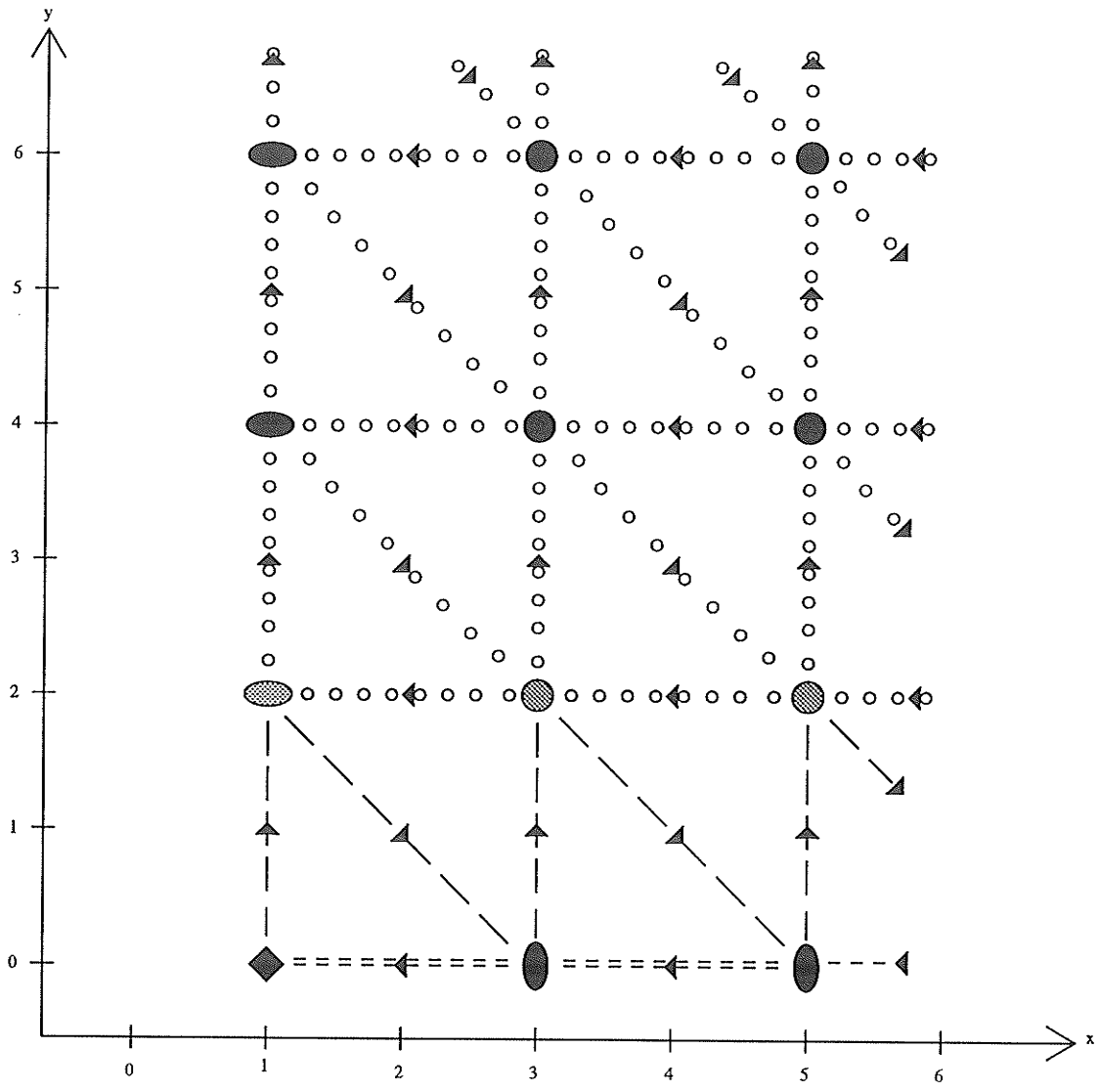

Figure 3.4: Graphical representation of the interactions between the next nearest neighbor odd/even kets in the three-magnon equations.

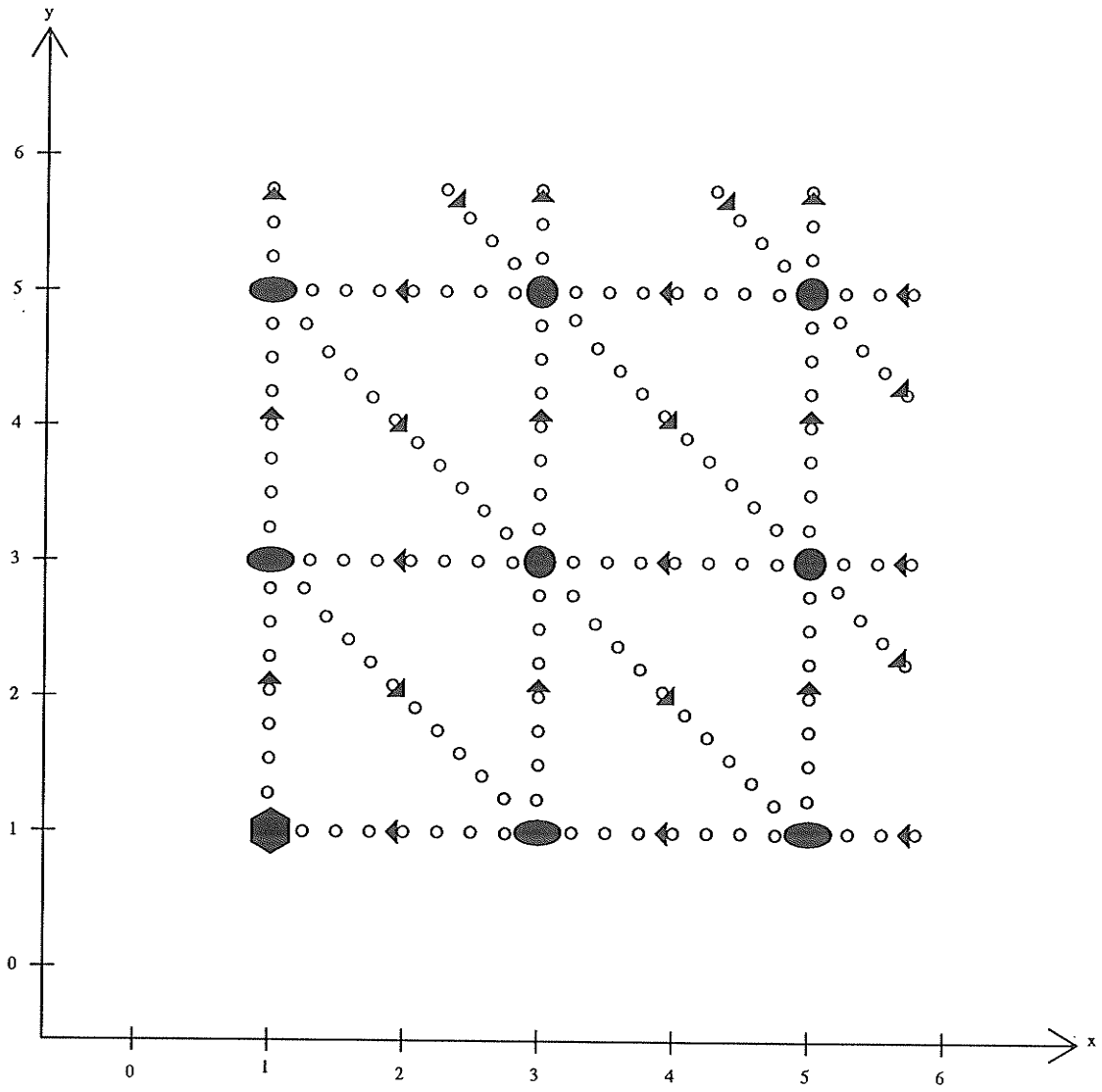

Figure 3.5: Graphical representation of the interactions between the next nearest neighbor odd/odd kets in the three-magnon equations.

$(x = 2, y = 0)$. Therefore we add on the terms $v_0' \mid K; 0, 2\rangle$ and $v_0'^* \mid K; 2, 0\rangle$. The next nearest neighbor even/odd, odd/even and odd/odd diagrams do not give any contributions, so the entire effect is

$$\widehat{H} \mid K; 0, 0\rangle = (\varepsilon_0 + \varepsilon_0') \mid K; 0, 0\rangle + v_0 \mid K; 0, 1\rangle + v_0^* \mid K; 1, 0\rangle + v_0' \mid K; 0, 2\rangle + v_0'^* \mid K; 2, 0\rangle$$

as in (3.7). In general the Hamiltonian can generate thirteen terms when acting on kets of the form $\mid K; x, y\rangle$.

The graphical representation of the three-magnon equations corresponds to a lattice which is semi-infinite in the x and y directions and are useful in determining what type of solutions can occur. The equations have three basic components involving kets far from the $x = 0$ and $y = 0$ surfaces (bulk states), kets near either surface but far away from the intersection of the two surfaces (surface states) and kets near to the intersection of the two surfaces (defect states). The bulk is described by equation (3.22), the surface layers by equations (3.16) to (3.21), and the defect states by equations (3.7) to (3.15). Equation (3.22), by itself, has a solution

$$E(K) = E_1(k_1) + E_1(k_2) + E_1(k_3) \qquad , K = k_1 + k_2 + k_3 \tag{3.23}$$

and since K must be real, there are two possibilities: all k_1, k_2 and k_3 are real, or $Im(k_1) = -Im(k_2)$ and k_3 is real.

However, as in the two-magnon case, the other equations (3.7) to (3.21) provide boundary conditions. For all k_i real, these equations provide no restrictions on energy and the solution is

$$E(K) = E_1(k_1) + E_1(k_2) + E_1(K - k_1 - k_2) \tag{3.24}$$

which is the sum of three free magnon energies and since both k_1 and k_2 can range

between $-\pi$ and π the solution is called the three-free continuum. These solutions are scattering states and the range of energies is the same for all S.

There are also solutions with complex values of the k_i which divide into two kinds. This can be shown explicitly in the case of the nearest neighbor $S = \frac{1}{2}$ (Heisenberg) model [24] which is integrable using the Bethe Ansatz. In general, $k_1 = k_2^*$ and k_3 is real, but the relationship of k_3 to the real parts of k_1 and k_2 can take two forms. The first possibility has $k_1 = k_2^*$, as in the two-magnon bound case, and $k_3 \in (-\pi, \pi)$ so that the energy is the sum of a two-magnon bound state energy ($E_2(k_b)$) and a one-magnon free energy ($E_1(k_3)$):

$$E(K) = E_2(K - k_3) + E_1(k_3) \tag{3.25}$$

where $K = k_b + k_3$ and k_b is the momentum of the two-magnon bound state ($k_b = k_1 + k_2$). Since k_3 can range between $-\pi$ and π for any given K, the energy can take on a continuous range of values. This continuum is called the two-bound one-free continuum. These solutions are localized near the surface $x = 0$ or $y = 0$ but can extend to infinity along the edge. The second possibility is $k_1 = k_2^* = k_R - ik_I$ and

$$k_3 = -\arctan\left[\frac{4\sin k_R \sinh k_I}{4\sin^2 k_R - \sinh^2 k_I}\right] \tag{3.26}$$

It can be shown that this case leads to three-magnon bound states which are localized near the intersection of the two edges and exist only for certain discrete energies [24].

Since there are two continua (three-free continuum and two-bound one-free continuum), the entire three-magnon continuum is taken as the union of the two continua. Thus the three-magnon continuum extends from the continuum which attains the lowest energy to the continuum which attains the highest energy at any value of K. No gaps are present in the final three-magnon continuum since

the two continua overlap. The continua edges which are internal to the three-magnon continuum generate van Hove singularities in the combined continuum (other internal singularities may be present).

Examples of the three-magnon continua for $S = \frac{1}{2}$ are shown in figures 3.6 to 3.9. The region with the shading leaning to the left is the two-bound one-free continuum, and the region with the shading leaning to the right is the three-free continuum. The crosshatching shows the area of overlap. Figure 3.6 shows the three-magnon continuum for $\tilde{\beta} = -\frac{1}{3}$ where there are two two-bound one-free continua since there is an upper and a lower two-magnon bound state branch (figure 2.20). Figure 3.7 shows the $\tilde{\beta} = 0$ (integrable) continuum, figure 3.8 shows the $\tilde{\beta} = \frac{1}{5}$ case and figure 3.9 shows the $\tilde{\beta} = 1$ case where the model is again integrable and the lattice spacing is $2a$. The lower bound of the $\tilde{\beta} = 0$ continuum is in agreement with Bethe [5] and at $K = \pi$ it is in agreement with Millet and Kaplan [20]. The $S = 1$ Heisenberg continua are similar to the $S = \frac{1}{2}$ continua and are in agreement with Millet and Kaplan for $\tilde{\beta} = 0$ at $K = \pi$, and with Kadolkar, Ghosh and Sarma [21] for $\tilde{\beta} \neq 0$.

Figures 3.10 to 3.13 show the continua for the integrable ($\tilde{\beta} = 0$) spin-1 model of Takhtajan and Babujian with $\tilde{\beta} = -\frac{1}{3}, 0, \frac{1}{5}$ and 1. The three-free continua are seen to be the same as in the $S = \frac{1}{2}$ case, but the two-bound one-free continua are different and determine both the maxima and the minima of the three-magnon continua. The three-free minima are close to or equal to the two-bound one-free minima. There are two two-bound one-free continua, one for each two-magnon bound state branch. The $\tilde{\beta} = 0$ continuum is in agreement with Lee [4][1].

[1]The figure shown here is the corrected version of the continuum in figure 5.1 in the thesis by Lee [4].

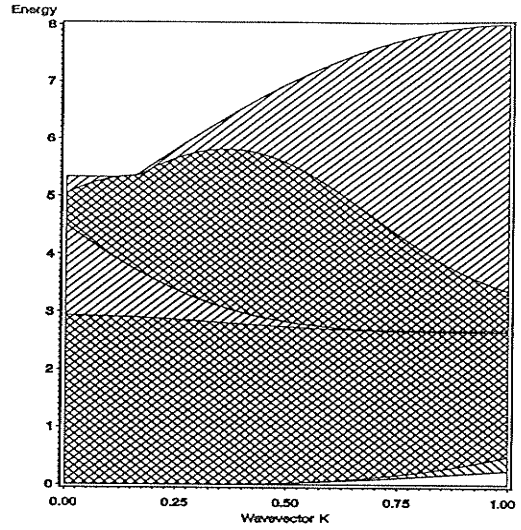

Figure 3.6: Three-magnon scattering state continuum for the $S = \frac{1}{2}$ Heisenberg model with energy in units of $\alpha_1 + \alpha_1'$. The wavevector K is in units of π and $\tilde{\beta} = -\frac{1}{3}$.

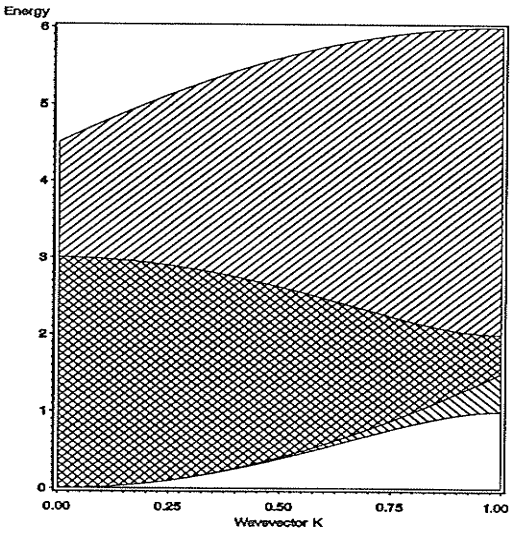

Figure 3.7: Three-magnon scattering state continuum for the $S = \frac{1}{2}$ Heisenberg model with energy in units of $\alpha_1 + \alpha_1'$. The wavevector K is in units of π and $\tilde{\beta} = 0$.

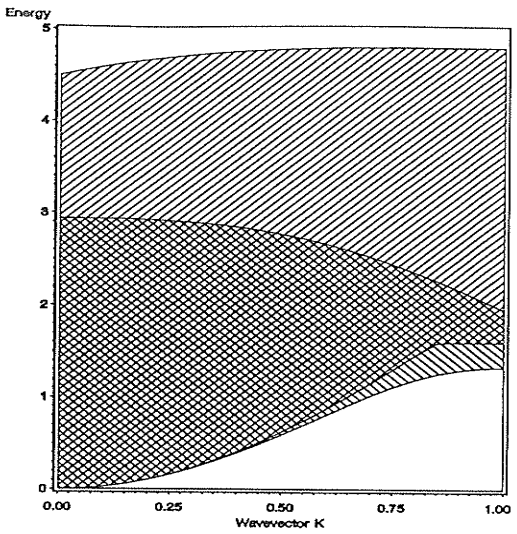

Figure 3.8: Three-magnon scattering state continuum for the $S = \frac{1}{2}$ Heisenberg model with energy in units of $\alpha_1 + \alpha_1'$. The wavevector K is in units of π and $\tilde{\beta} = \frac{1}{5}$.

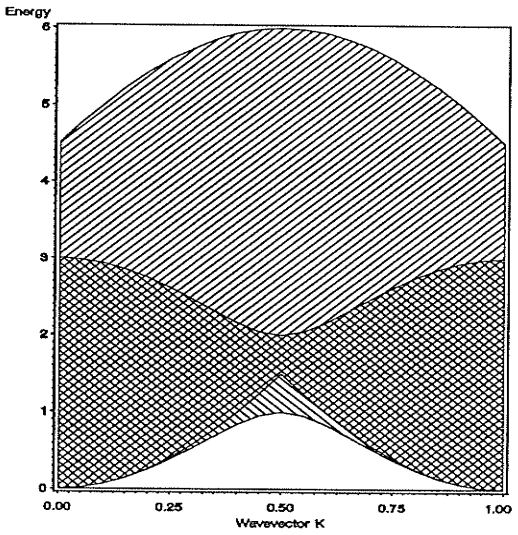

Figure 3.9: Three-magnon scattering state continuum for the $S = \frac{1}{2}$ Heisenberg model with energy in units of $\alpha_1 + \alpha_1'$. The wavevector K is in units of π and $\tilde{\beta} = 1$.

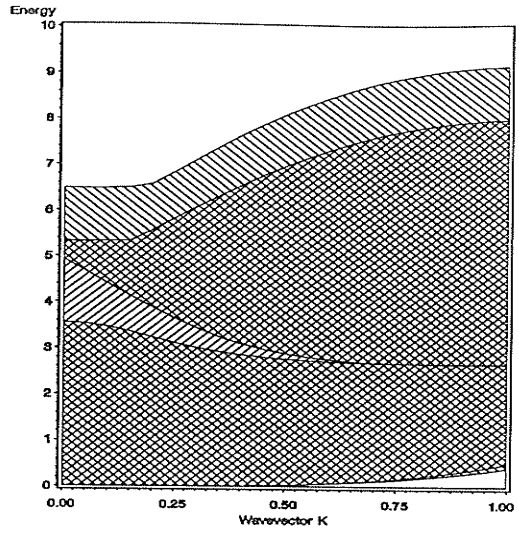

Figure 3.10: Three-magnon scattering state continuum for the $S = 1$ Takhtajan and Babujian model with energy in units of $\alpha_1 + \alpha_1'$. The wavevector K is in units of π and $\tilde{\beta} = -\frac{1}{3}$.

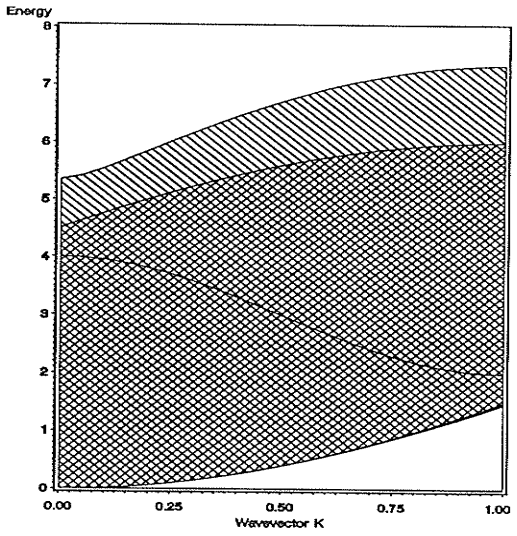

Figure 3.11: Three-magnon scattering state continuum for the $S = 1$ Takhtajan and Babujian model with energy in units of $\alpha_1 + \alpha_1'$. The wavevector K is in units of π and $\tilde{\beta} = 0$.

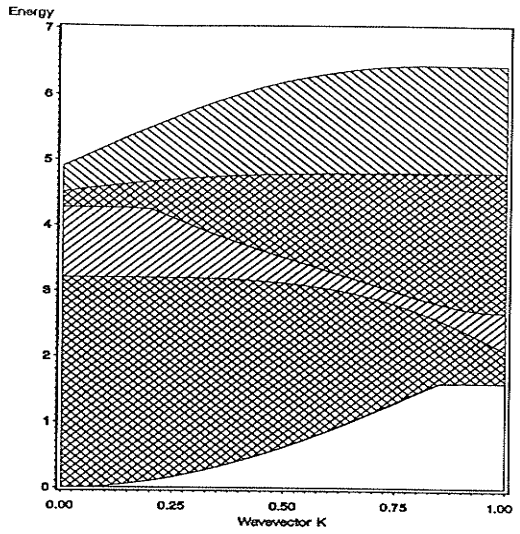

Figure 3.12: Three-magnon scattering state continuum for the $S = 1$ Takhtajan and Babujian model with energy in units of $\alpha_1 + \alpha_1'$. The wavevector K is in units of π and $\tilde{\beta} = \frac{1}{5}$.

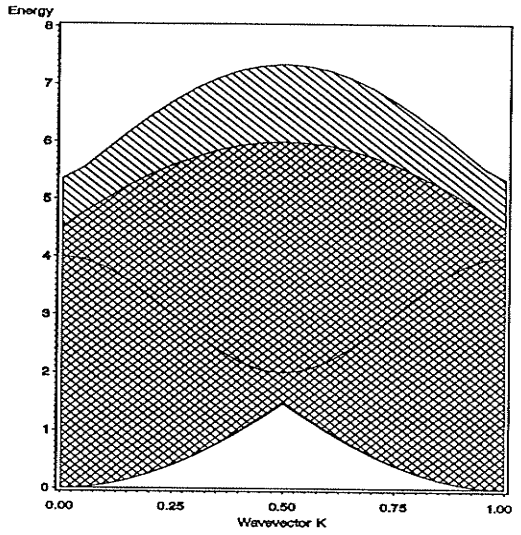

Figure 3.13: Three-magnon scattering state continuum for the $S = 1$ Takhtajan and Babujian model with energy in units of $\alpha_1 + \alpha_1'$. The wavevector K is in units of π and $\tilde{\beta} = 1$.

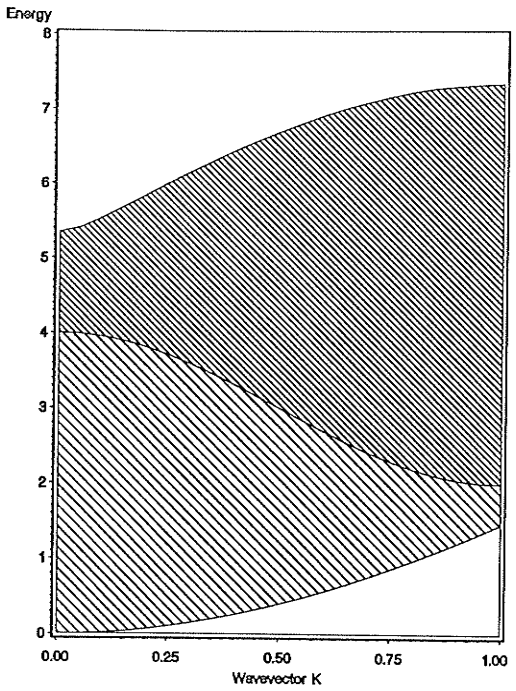

Figure 3.14: The upper and lower two-bound one-free scattering state continua with energy in units of $\alpha_1 + \alpha_1'$ of the $S = 1$, $\tilde{\beta} = 0$ integrable model. The wavevector K is in units of π.

For the Takhtajan and Babujian integrable models with $S \geq 1$, there are two two-magnon bound state branches as shown in figure 2.13. In these cases, the three-magnon scattering state solutions have three components: the three-free continua, and a two-bound one-free continuum for each branch which meet over the whole Brillouin zone (figure 3.14). The three-magnon bound state solution has two branches for $S = 1$ and three branches for $S \geq \frac{3}{2}$. These branches meet at $K = \pi$ with no gaps and cross through the continuum without interacting with it (figure 3.15) [4]. As the model deviates from these integrable cases, the two-bound one-free continua do not meet over the whole Brillouin zone (figure 3.12) since the two-magnon bound states do not meet at $K = \pi$ (figure 2.14). For non-integrable models the three-magnon bound states can not cross through the continuum without interacting with it. In these cases if a three-magnon bound

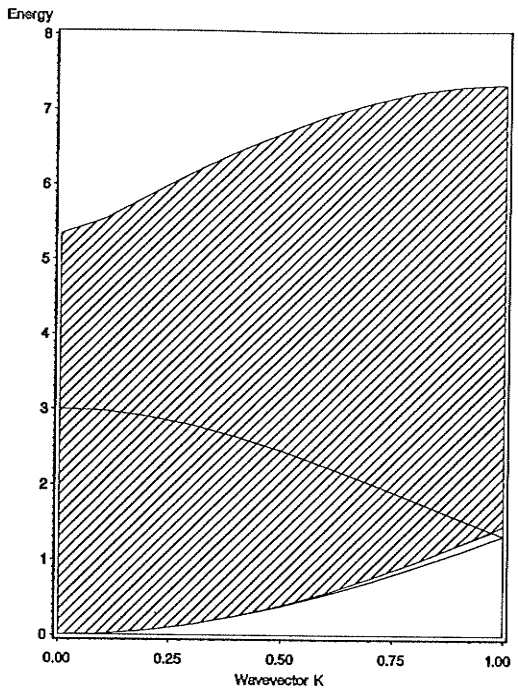

Figure 3.15: Three-magnon scattering state continuum with energy in units of $\alpha_1 + \alpha_1'$ and the two three-magnon bound state branches of the $S = 1$, $\tilde{\beta} = 0$ integrable model. The wavevector K is in units of π.

state enters the continuum, it interacts with the two-bound one-free continuum to produce a resonance [4].

The scattering state continua are important for identifying the regions where the three-magnon bound state solutions can exist. The bound state solutions must appear outside the scattering state continuum bounds, except for the special integrable models where the bound states can exist inside these bounds.

Chapter 4

Three-Magnon Bound States

The eigenvalues and eigenvectors of equations (3.7) to (3.22) provide the complete solution to the three-magnon problem. However, the calculation of the eigenvalues and eigenvectors of this system is very complicated. As well, the rescaling method used to find the two-magnon bound state solutions is not applicable for this system since applying the rescaling method on the three-magnon equations leads to a proliferation of the range of interaction and the parameter space does not close. For these reasons we will use a different method to find the three-magnon bound states. We will find the density of states using the Recursion method [22] and from the density of states we can identify bound states, continua, resonances and singularities, as we could from the two-magnon density of states. First we will discuss the relationship of the density of states to the Green's function, then how to find the Green's function from a tridiagonal, symmetric matrix. The Recursion method, which transforms matrices to a tridiagonal, symmetric form, will then be described.

4.1 Green's Function

The local Green's function is defined as

$$G_j(E+i\epsilon) \;=\; \langle j \mid (E-\widehat{H}+i\epsilon)^{-1} \mid j \rangle \qquad \mid \epsilon \mid \ll 1 \tag{4.1}$$

where $\mid j\rangle$ is an arbitrary ket in the three-magnon basis and can be written as a linear combination of the eigenstates of $\widehat{H}$ ($\widehat{H} \mid \lambda\rangle = E_\lambda \mid \lambda\rangle$)

$$\mid j\rangle = \sum_\lambda c_\lambda \mid \lambda\rangle \tag{4.2}$$

The local Green's function becomes

$$\begin{aligned} G_j(E+i\epsilon) &= \sum_\lambda \frac{\mid c_\lambda \mid^2}{E - E_\lambda + i\epsilon} \\ &= \sum_\lambda \mid c_\lambda \mid^2 \left[\frac{E - E_\lambda}{(E-E_\lambda)^2 + \epsilon^2} - i \frac{\epsilon}{(E-E_\lambda)^2 + \epsilon^2} \right] \end{aligned} \tag{4.3}$$

and the imaginary part of $G_j(E+i\epsilon)$, in the limit $\epsilon \to 0$, is seen to be proportional to a sum of delta functions

$$\lim_{\epsilon \to 0}[Im(G_j(E+i\epsilon))] = -\pi \sum_\lambda \mid c_\lambda \mid^2 \delta(E - E_\lambda) \tag{4.4}$$

In fact, the density of states of a system is the sum of delta functions of the exact eigenvalues. Therefore the density of states local to $\mid j\rangle$ can be written as

$$\eta_j(E) = \lim_{\epsilon \to 0} \frac{-1}{\pi} Im[G_j(E+i\epsilon)] \tag{4.5}$$

and the total density of states is obtained by summing over all the kets in the basis

$$\eta(E) = \lim_{\epsilon \to 0} \frac{-1}{\pi} \sum_{\{\mid j\rangle\}} Im[G_j(E+i\epsilon)] \tag{4.6}$$

(See, for example, White [25] or Economou [26]). The real part of the Green's function has the physical interpretation of describing the resistance of the system to excitation at an energy E [22].

To calculate the Green's function, we use the matrix representation of $[E - \widehat{H}]$. Using the standard formula for the inverse element of a matrix, the G_0 element can be written as

$$G_0(E) = \frac{D_1([E - \widehat{H}])}{D_0([E - \widehat{H}])} \tag{4.7}$$

where $D_n([E-\widehat{H}])$ is the determinant of the matrix $[E-\widehat{H}]$ with the first n rows and n columns deleted.

The Hamiltonian should be transformed to a basis where the calculation of the Green's function is simple, such as the basis where the Hamiltonian is diagonal. This is often very difficult or impossible, but it is always possible to find a set of kets which transform a hermitian Hamiltonian to a tridiagonal, symmetric form:

$$\widehat{H} = \begin{pmatrix} h_{00} & h_{01} & & 0 & \\ h_{01} & h_{11} & h_{12} & & \\ & h_{12} & h_{22} & h_{23} & \\ & 0 & & \ddots & \\ & & & h_{n-1n} & h_{nn} \end{pmatrix} \tag{4.8}$$

Using this form of $\widehat{H}$ and expanding the determinants in (4.7), we find that the local Green's function can be expressed in the form:

$$\begin{aligned} G_0(E) &= \frac{D_1([E-\widehat{H}])}{(E-h_{00})D_1([E-\widehat{H}]) - h_{01}^2 D_2([E-\widehat{H}])} \\ &= \frac{1}{E-h_{00}-h_{01}^2\frac{D_2([E-\widehat{H}])}{D_1([E-\widehat{H}])}} \end{aligned} \tag{4.9}$$

The term $\frac{D_2([E-\widehat{H}])}{D_1([E-\widehat{H}])}$ has the same form as (4.7). We can continue this procedure, producing a continued fraction for the local Green's function:

$$G_0(E) = \cfrac{1}{E-h_{00}-\cfrac{h_{01}^2}{E-h_{11}-\cfrac{h_{12}^2}{E-h_{22}-\cfrac{h_{23}^2}{\ddots}}}} \tag{4.10}$$

Thus for any tridiagonal, symmetric Hamiltonian matrix, the local Green's function and thus the density of states can be found. Before we can apply this method, however, we need to transform our Hamiltonian into a tridiagonal, symmetric matrix. A procedure which can do this is the Recursion method, described in the next section.

4.2 The Recursion Method

The Recursion method as described below is easily adapted for use on a computer since the quantities used are discrete, and the implementation can be made finite.

We wish to transform our Hamiltonian matrix, which is not tridiagonal in the present basis $\{|\, K; x, y\rangle\}$, to a tridiagonal form in the basis $\{\mathbf{u}_n\}$. The Recursion method, as given by Haydock [22], describes the action of the Hamiltonian $\widehat{H}$ on a complete set of orthonormal states $\{\mathbf{u}_n\}$ by a symmetric three-term recurrence relation of the form

$$\widehat{H}\mathbf{u}_n = a_n\mathbf{u}_n + b_{n+1}\mathbf{u}_{n+1} + b_n\mathbf{u}_{n-1} \tag{4.11}$$

where $\{a_0, a_1, \ldots\}$ and $\{b_1, b_2, \ldots\}$ are real parameters. For the first step $\mathbf{u}_{-1}$ is taken as zero and $\mathbf{u}_0$ is some arbitrary state.

$$\widehat{H}\mathbf{u}_0 = a_0\mathbf{u}_0 + b_1\mathbf{u}_1 \tag{4.12}$$

The left hand side is known and a_0, b_1 and $\mathbf{u}_1$ are to be determined. Since the $\{\mathbf{u}_i\}$ are orthonormal we can determine a_0 by

$$a_0 = \mathbf{u}_0^\dagger\widehat{H}\mathbf{u}_0 \tag{4.13}$$

so $b_1\mathbf{u}_1$ can be found by

$$b_1\mathbf{u}_1 = \widehat{H}\mathbf{u}_0 - a_0\mathbf{u}_0 \tag{4.14}$$

Orthonormality fixes b_1^2 to be

$$b_1^2 = [\widehat{H}\mathbf{u}_0 - a_0\mathbf{u}_0][\widehat{H}\mathbf{u}_0 - a_0\mathbf{u}_0] \tag{4.15}$$

and if we take b_1 as the positive root of b_1^2, we find

$$\mathbf{u}_1 = \frac{\widehat{H}\mathbf{u}_0 - a_0\mathbf{u}_0}{b_1} \tag{4.16}$$

which is orthogonal to $\mathbf{u}_0$ and normalized to one. For the general step of the transformation we have already found the orthonormal states $\{\mathbf{u}_0, \mathbf{u}_1, \ldots, \mathbf{u}_n\}$ and the real parameters $\{a_0, a_1, \ldots, a_{n-1}\}$ and $\{b_1, b_2, \ldots, b_n\}$ so that

$$\begin{aligned}
\widehat{H}\mathbf{u}_n &= a_n\mathbf{u}_n + b_{n+1}\mathbf{u}_{n+1} + b_n\mathbf{u}_{n-1} \\
a_n &= \mathbf{u}_n^\dagger \widehat{H}\mathbf{u}_n \\
b_{n+1}\mathbf{u}_{n+1} &= \widehat{H}\mathbf{u}_n - a_n\mathbf{u}_n - b_n\mathbf{u}_{n-1} \\
b_{n+1}^2 &= [\widehat{H}\mathbf{u}_n - a_n\mathbf{u}_n - b_n\mathbf{u}_{n-1}][\widehat{H}\mathbf{u}_n - a_n\mathbf{u}_n - b_n\mathbf{u}_{n-1}] \\
\mathbf{u}_{n+1} &= \frac{\widehat{H}\mathbf{u}_n - a_n\mathbf{u}_n - b_n\mathbf{u}_{n-1}}{b_{n+1}}
\end{aligned} \tag{4.17}$$

where $\mathbf{u}_{n+1}$ is orthogonal to all $\{\mathbf{u}_0, \mathbf{u}_1, \ldots, \mathbf{u}_n\}$. The Hamiltonian is thus transformed to the desired tridiagonal, symmetric form.

$$\widehat{H}\begin{pmatrix} \mathbf{u}_0 \\ \mathbf{u}_1 \\ \mathbf{u}_2 \\ \vdots \\ \end{pmatrix} = \begin{bmatrix} a_0 & b_1 & & & \\ b_1 & a_1 & b_2 & & 0 \\ & b_2 & a_2 & b_3 & \\ & 0 & & \ddots & \end{bmatrix} \begin{pmatrix} \mathbf{u}_0 \\ \mathbf{u}_1 \\ \mathbf{u}_2 \\ \vdots \\ \end{pmatrix} \tag{4.18}$$

The original choice of the state $\mathbf{u}_0$ is arbitrary. However, for certain choices of the state $\mathbf{u}_0$ some properties of the system may not be present in the resulting density of states. For example, for spin-$\frac{1}{2}$ the kets $|\ K;0,0\rangle$, $|\ K;0,y\rangle$ $(y>0)$ and $|\ K;x,0\rangle$ $(x>0)$ are unphysical since they involve more than one spin deviation on each site. Therefore if $\mathbf{u}_0$ is set equal to any of these kets, only unphysical solutions are found. In the $S=1$ cases, the $|\ K;0,0\rangle$ ket is unphysical. Another example is in the next nearest neighbor interactions only case where the even/even kets are decoupled from the other kets. If in the $S=1, K=\frac{\pi}{2}$ Heisenberg case $\mathbf{u}_0 =|\ K;2,0\rangle$, the spectra in figure 4.1 result and two bound states below the continuum can clearly be seen. However, if $\mathbf{u}_0 =|\ K;1,0\rangle$ or $|\ K;0,1\rangle$ (the initial choices of $|\ K;1,0\rangle$ and $|\ K;0,1\rangle$ are identical, which can clearly be seen in the diagrams 3.1 to 3.5), the spectra in figure 4.2 result and if $\mathbf{u}_0 =|\ K;1,1\rangle$ the spectra

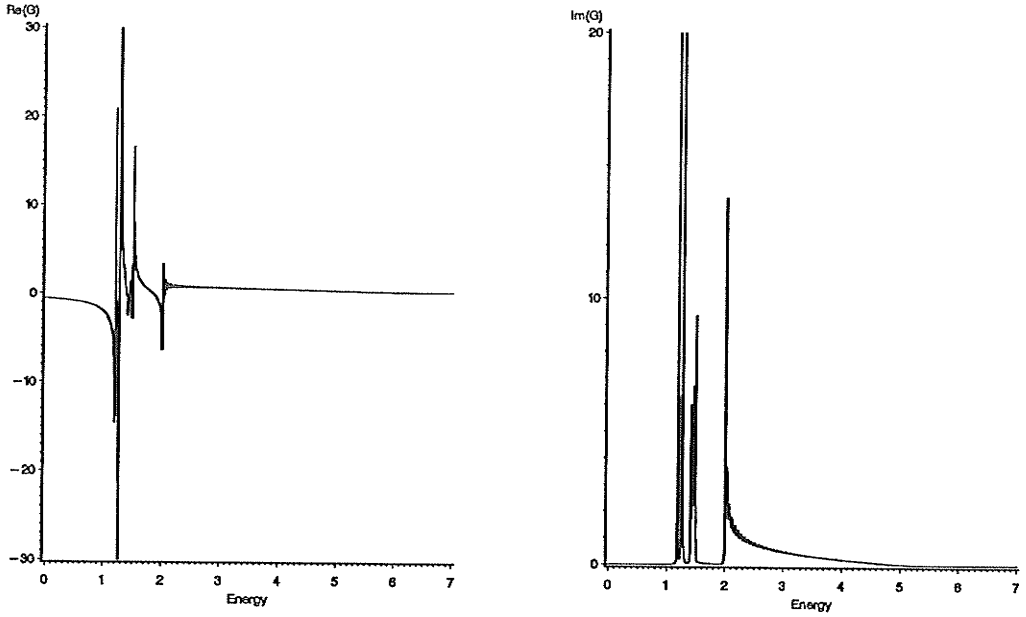

Figure 4.1: Real and Imaginary parts of the Green's function found for the $S = 1, \tilde{\beta} = 1$ Heisenberg case at $K = \frac{\pi}{2}$ with an initial even/even ket $\mid K; 2, 0\rangle$. Energy is in units of $\alpha_1 + \alpha_1'$.

of figure 4.3 result. In these last two cases the bound states are not seen below the scattering state continuum. Thus, in order not to miss components in the spectra, more than one spectrum with different $\mathbf{u_0}$ should be calculated.

4.3 Termination of the Continued Fraction

Once we have transformed our Hamiltonian to this tridiagonal form, we can calculate the Green's function from the continued fraction (4.10). But the problem of how to terminate the continued fraction arises. We will discuss two situations which can occur in the sequence of $\{a_0, a_1, \ldots\}$ and $\{b_1, b_2, \ldots\}$. The first situation occurs if there are no gaps in the scattering state continuum so the coefficients (a_n, b_n) of the continued fraction converge as $n \to \infty$. If gaps are present, they exhibit undamped oscillations [27]. Internal singularities within a continuum in the density of states induce damped oscillations in the coefficients, but since this

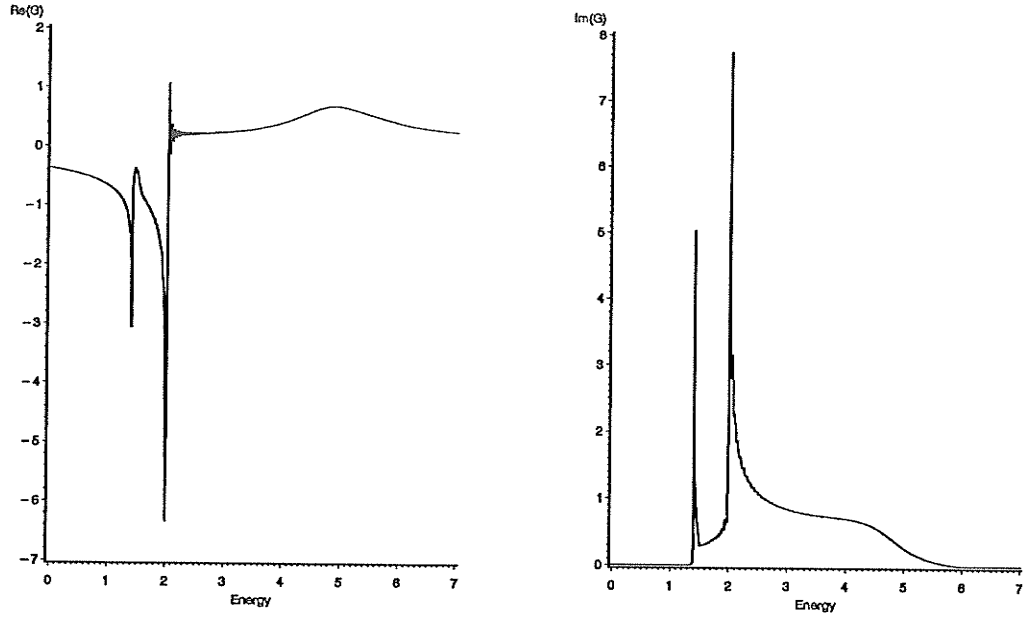

Figure 4.2: Real and Imaginary parts of the Green's function found for the $S = 1, \tilde{\beta} = 1$ Heisenberg case at $K = \frac{\pi}{2}$ with an initial odd/even ket $\mid K; 1, 0\rangle$ or even/odd ket $\mid K; 0, 1\rangle$. Energy is in units of $\alpha_1 + \alpha_1'$.

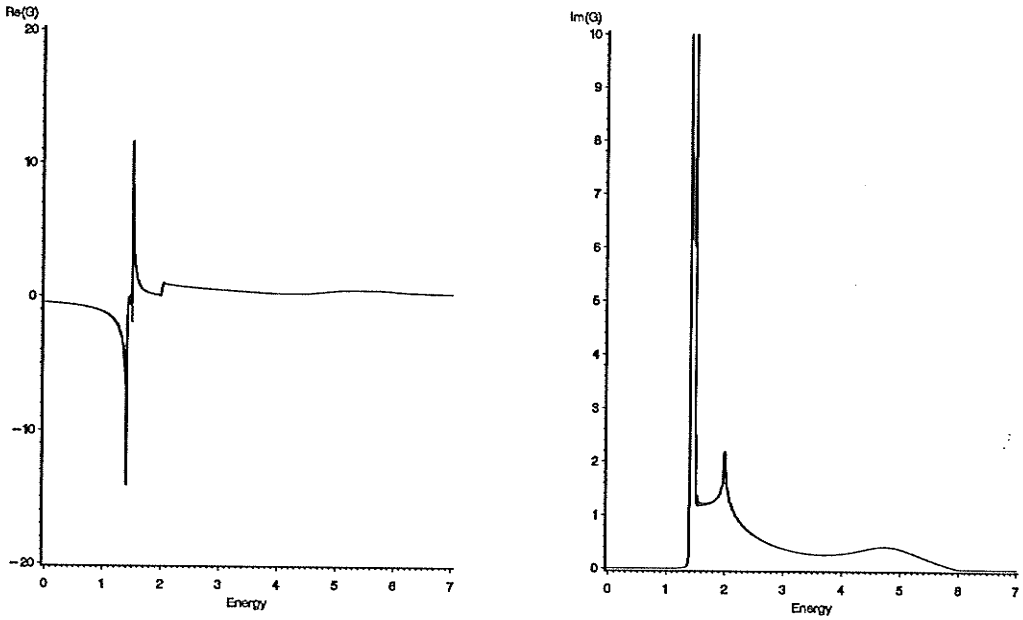

Figure 4.3: Real and Imaginary parts of the Green's function found for the $S = 1, \tilde{\beta} = 1$ Heisenberg case at $K = \frac{\pi}{2}$ with an initial odd/odd ket $\mid K; 1, 1\rangle$. Energy is in units of $\alpha_1 + \alpha_1'$.

behavior dies out, we will not discuss it in detail.

4.3.1 Constant Coefficients

If there are no gaps in the scattering state continuum, the coefficients (a_n and b_n) converge to constant values which are related to the minimum (E_{min}) and maximum (E_{max}) energies of the continuum. Consider the case when a_n and b_n converge to constant coefficients such that

$$\left.\begin{array}{l} a_n = a \\ b_n = b \end{array}\right\} \quad \text{for } n > n_{max} \tag{4.19}$$

The Green's function is

$$G_0(E_c) = \cfrac{1}{E_c - a_0 - \cfrac{b_1^2}{E_c - a_1 - \cfrac{b_2^2}{\ddots \cfrac{}{E_c - a_{n_{max}} - b_{n_{max}}^2 G_\infty}}}} \tag{4.20}$$

where $E_c = E + i\epsilon$, $\mid \epsilon \mid \ll 1$ and G_∞ is the terminator of the continued fraction and is equal to

$$\begin{aligned} G_\infty(E_c) &= \cfrac{1}{E_c - a - \cfrac{b^2}{E_c - a - \cfrac{b^2}{\ddots}}} \\ &= \frac{1}{E_c - a - b^2 G_\infty} \\ &= \frac{E_c - a}{2b^2} \pm \frac{1}{2b^2}\sqrt{(E_c - a)^2 - 4b^2} \end{aligned} \tag{4.21}$$

One of these roots is spurious, and the choice of positive or negative square root depends on whether E is less than or greater than a.

The minimum and maximum of the continuum (E_{min} and E_{max}) can be found by calculating the energies where $G_0(E)$ is complex. $G_0(E)$ is complex when

$$\begin{aligned} (E - a)^2 - 4b^2 &< 0 \\ a - 2b < E &< a + 2b \end{aligned} \tag{4.22}$$

The continuum extends from $E_{min} = a - 2b$ to $E_{max} = a + 2b$. We can express a and b in terms of the minimum and maximum energies of the continuum by

$$\begin{aligned} a &= \frac{1}{2}(E_{min} + E_{max}) \\ b &= \frac{1}{4}(E_{max} - E_{min}) \end{aligned} \tag{4.23}$$

Therefore, knowing E_{min} and E_{max} (from the three-magnon continuum - see Chapter 3) we can terminate the continued fraction using equations (4.23) and (4.21). The tail of the continued fraction is found using the coefficients $\{a_0,a_1,\ldots,a_n\}$ and $\{b_1, b_2, \ldots, b_n\}$ ($n \sim 100$) generated using the Recursion Method.

4.3.2 Oscillating Coefficients

If there are gaps in the scattering state continuum, then the coefficients (a_n, b_n) of the continued fraction exhibit undamped oscillations [27]. In the case of a single gap, let $E_1 < E_2 < E_3 < E_4$ where the gap extends from E_2 to E_3 and the continuum extends from E_1 to E_2 and from E_3 to E_4. Turchi, Ducastelle and Tréglia [27] have described a phase space representation of the coefficients. Any pair of neighboring coefficients $(A, B) = (a_n, b_{n-1}^2)$ or (a_n, b_n^2) should satisfy the equation

$$(A^2 + E'A + E'' + 2B)^2 = X(-E' - A) \tag{4.24}$$

where

$$\begin{aligned} E' &= -\frac{1}{2}\sum_{i=1}^{4} E_i \\ E'' &= \frac{1}{2}\sum_{i<j} E_i E_j - \frac{E'^2}{2} \\ X(x) &= \prod_{i=1}^{4}(x - E_i) \end{aligned} \tag{4.25}$$

Defining $\alpha_n = -(E' + a_n)$, the solution of (4.24) for B can be written as

$$b^2 = -(\alpha_n^2 + E'\alpha_n + E'') \mp \sqrt{X(\alpha_n)} \tag{4.26}$$

where the negative sign is for b_{n-1}^2 and the positive sign is for b_n^2. In the phase space (a_n, b_{n-1}^2) or (a_n, b_n^2) there is a closed loop. The coefficients satisfy the relations:

$$\begin{aligned}\left[\frac{(E_1+E_4)-(E_3-E_2)}{2}\right] &\leq a_n \leq \left[\frac{(E_1+E_4)+(E_3-E_2)}{2}\right] \\ \left[\frac{(E_4-E_1)-(E_3-E_2)}{4}\right]^2 &\leq b^2 \leq \left[\frac{(E_4-E_1)+(E_3-E_2)}{4}\right]^2 \end{aligned} \quad (4.27)$$

Thus from the phase space diagram of b_n^2 and b_{n-1}^2 vs a_n we can determine the energies E_1, E_2, E_3 and E_4. Note that the range of a_n is proportional to the width of the gap.

A similar relationship is found by Turchi, Ducastelle and Tréglia for the coefficients in the case of two gaps in the continuum. Let $E_1 < E_2 < E_3 < E_4 < E_5 < E_6$ with the gaps extending from E_2 to E_3 and from E_4 to E_5. Defining α_n^1 and α_n^2 by

$$\begin{aligned}\alpha_n^1 + \alpha_n^2 &= -(E' + a_n) \\ \alpha_n^1 \alpha_n^2 &= a_n^2 + b_{n-1}^2 + b_n^2 + E' a_n + E'' \end{aligned} \quad (4.28)$$

where $E_2 < \alpha_n^1 < E_3$ and $E_4 < \alpha_n^2 < E_5$, B can be written as

$$\begin{aligned} Y &= -[(\alpha_n^1)^2 + \alpha_n^1\alpha_n^2 + (\alpha_n^2)^2] - E'' - E'(\alpha_n^1 + \alpha_n^2) \\ b^2 &= \frac{1}{2}\left[Y \pm \frac{\sqrt{X(\alpha_n^1)} + \sqrt{X(\alpha_n^2)}}{\alpha_n^1 - \alpha_n^2}\right] \end{aligned} \quad (4.29)$$

where b_{n-1}^2 is given by the positive sign and b_n^2 by the negative sign and where $X(x), E'$ and E'' are defined as in equation (4.25), but the indices range from one to six. In this case in the phase space of (a_n, b_{n-1}^2) or (a_n, b_n^2) there is a double loop. Once again the range of values of a_n will be proportional to the widths of the gaps. Conversely, if we find the coefficients using the Recursion method, we could determine whether there is one gap or two in the scattering state continuum depending on which of the above equations fits the data.

In the cases we consider, the scattering state continua do not have gaps. However, the theory behind the oscillating coefficients is useful in understanding a

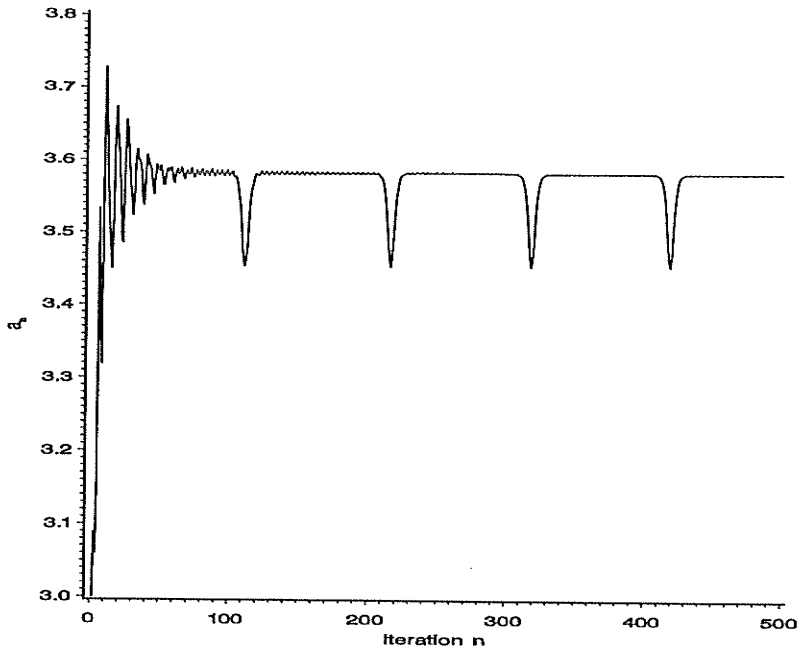

Figure 4.4: The coefficients a_n plotted versus the iteration number n for the $S = 1, \tilde{\beta} = 0$ Heisenberg case at $K = \frac{9\pi}{10}$.

numerical effect which is observed in the sequence of coefficients (a_n, b_n). Due to computer limitation, there is a loss of orthogonality of the $\{\mathbf{u}_i\}$. The $\mathbf{u}_{n+1}$ will be orthogonal to $\mathbf{u}_n$ and $\mathbf{u}_{n-1}$, but may have a component from one or more of $\{\mathbf{u}_0, \mathbf{u}_1, \ldots, \mathbf{u}_{n-2}\}$. This computer limitation has a significant effect on the coefficients in the form of large deviations from the values to which the coefficients converge. An example for the $S = 1$, $\tilde{\beta} = 0$ Heisenberg case at $K = \frac{9\pi}{10}$ is shown in figure 4.4. Lee [4] has shown that the behavior of the coefficients suggests the presence of a 'gap' between the continuum and a bound state that has a very narrow but finite width equal to machine precision. The period of the deviations is proportional to the log of the width of the narrow band and the height of the deviations is proportional to the width of the gap. Although these oscillations are numerical in origin, they can be used to identify the presence of bound states.

The phase space diagrams can also be used to identify the presence of one or two bound states, depending of whether there is a single or a double loop in the diagram. Consider the $S = 1$ Heisenberg case with $\tilde{\beta} = 0$ at $K = \frac{9\pi}{10}$, which has one bound state. The sequence of coefficients b_n^2 and b_{n-1}^2 vs a_n are shown on the left hand side of figure 4.5, with the first 80 iterations deleted. The asymptotic value of a_n is 3.58 and can be read off of the diagram. The asymptotic value of b_n is 1.20 . From these values we can calculate the minimum and maximum of the continuum to be $E_{min} = a - 2b = 1.18$, and $E_{max} = a + 2b = 5.98$, in agreement with the predicted values. The amplitude of the major deviations in a_n is 0.13, so that the bound state is at $E_{min} - 0.13 = 1.05$, in agreement with Lee [4]. The second picture in figure 4.5 is the predicted curve found using equation (4.26) and the known values of the continuum edges and the bound state. This loop agrees well with the calculated coefficients. The first picture in figure 4.6 shows the phase space diagram for the $S = 1$ Heisenberg $\tilde{\beta} = 0$ case at $K = \pi$ with the first 80 iterations deleted. Here there are two bound states, so a double loop is present. Reading from the figure we find $E_{min} = a - 2b = 3.705 - 2(1.15) = 1.41$, $E_{max} = a + 2b = 3.70 + 2(1.15) = 6.0$, $E_{b_1} = E_{min} - 0.22 = 1.19$ and $E_{b_2} = E_{min} - 0.14 = 1.27$. These values are also in agreement with Lee. The second picture in figure 4.6 is the predicted curve found using equation (4.29) and the known values of the continuum edges and the bound states.

In the next sections we will look at the three-magnon results for two models, the Heisenberg model and the Takhtajan and Babujian model. The results for the Heisenberg model are found for both $S = \frac{1}{2}$ and $S = 1$. The $S = \frac{1}{2}$ Heisenberg model has the parameters $\frac{\alpha_1}{\alpha_1+\alpha_1'} = 1 - \tilde{\beta}$, $\frac{\alpha_1'}{\alpha_1+\alpha_1'} = \tilde{\beta}$, $r_2 = \frac{\alpha_2}{\alpha_1+\alpha_1'} = 0$, $r_2' = \frac{\alpha_2'}{\alpha_1+\alpha_1'} = 0$, $r_3 = \frac{\alpha_3}{\alpha_1+\alpha_1'} = 0$ and $r_3' = \frac{\alpha_3'}{\alpha_1+\alpha_1'} = 0$. For $S > 1$ the parameters are the same except $r_2 = \frac{4S-1}{2S}(1 - \tilde{\beta})$ and $r_2' = \frac{4S-1}{2S}\tilde{\beta}$.

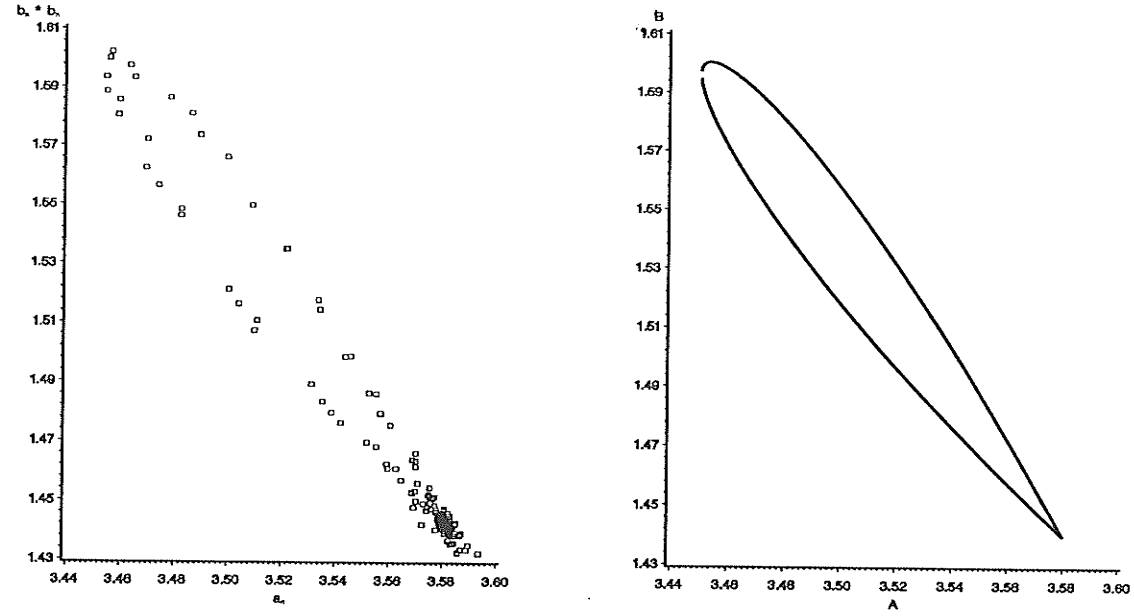

Figure 4.5: The figure on the left shows the coefficients b_{n-1}^2 and b_n^2 plotted versus a_n for the $S = 1, \tilde{\beta} = 0$ Heisenberg case at $K = \frac{9\pi}{10}$. The first 80 iterations are deleted. The figure on the right shows the predicted curve for this case.

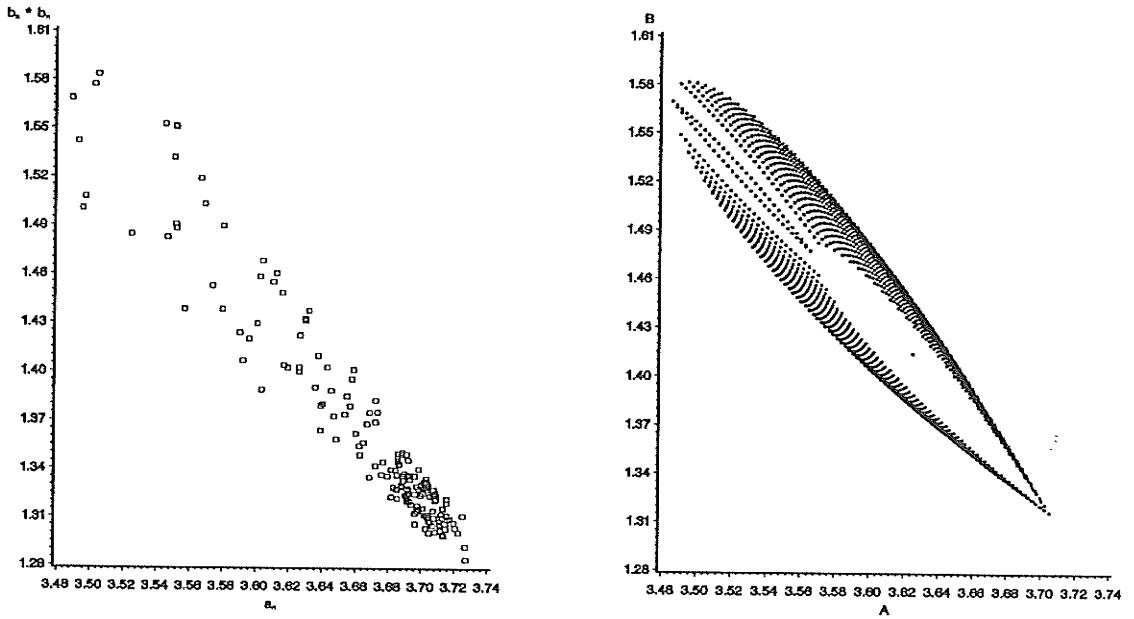

Figure 4.6: The figure on the left shows the coefficients b_{n-1}^2 and b_n^2 plotted versus a_n for the $S = 1, \tilde{\beta} = 0$ Heisenberg case at $K = \pi$. The first 80 iterations are deleted. The figure on the right shows the predicted curve for this case.

For $S = \frac{1}{2}$, the Takhtajan and Babujian model is identical to the Heisenberg model. The results for the Takhtajan and Babujian model are found for both $S = 1$ and $S = \frac{3}{2}$. The parameters for the $S = 1$ model are $\frac{\alpha_1}{\alpha_1+\alpha_1'} = 1 - \tilde{\beta}$, $\frac{\alpha_1'}{\alpha_1+\alpha_1'} = \tilde{\beta}$, $r_2 = \frac{4S-1}{2S-1}(1 - \tilde{\beta})$ and $r_2' = \frac{4S-1}{2S-1}\tilde{\beta}$. The $S > \frac{3}{2}$ models have these parameters as well as $r_3 = \frac{6S^2-6S+1}{2S^2-3S+1}(1 - \tilde{\beta})$ and $r_3' = \frac{6S^2-6S+1}{2S^2-3S+1}\tilde{\beta}$. The results for each model are found for specific $\tilde{\beta}$ values in the range $-\frac{1}{3} \leq \tilde{\beta} \leq 1$.

4.4 The $S = \frac{1}{2}$ Heisenberg Case

The three-magnon results of the integrable $S = \frac{1}{2}$, $\tilde{\beta} = 0$ Heisenberg case are shown in figure 4.7, where the shading slanted to the left is the two-bound one-free continuum, the shading to the right is the three-free continuum and the solid line below the continuum is the bound state. These results completely agree with those obtained by Bethe [5] using an ansatz for the three-particle wavefunction. As $\tilde{\beta}$ decreases from zero, the lower continuum edge and the bound state decrease in energy. The $\tilde{\beta} = -\frac{1}{3}$ case is shown in figure 4.8.

As $\tilde{\beta}$ increases from zero, a resonance appears inside the continuum, and emerges as a bound state below the continuum for a small range of $\tilde{\beta}$ at intermediate values of K. The $\tilde{\beta} = \frac{1}{2}$ case is shown in figure 4.9, where the second bound state is present around $K = 0.65\pi$. As $\tilde{\beta}$ increases further the resonance no longer emerges as a bound state and at $\tilde{\beta} = 1$ it no longer exists. The $\tilde{\beta} = 1$ integrable case is shown in figure 4.10. These results indicate that the spin-$\frac{1}{2}$ Heisenberg case is not integrable for $\tilde{\beta} \neq 0$, in disagreement with Tsvelik [28], who suggests that this case is integrable by the Bethe ansatz but does not give explicit results.

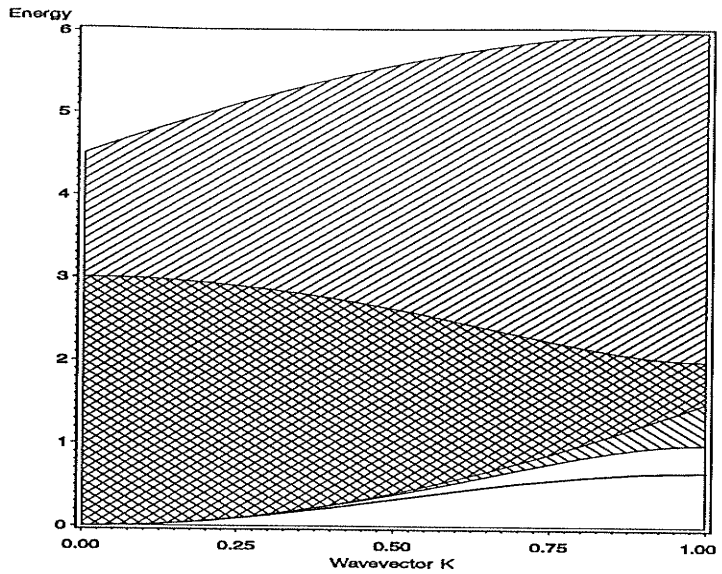

Figure 4.7: The dispersion diagram for the $S = \frac{1}{2}, \tilde{\beta} = 0$ Heisenberg case with energy in units of $\alpha_1 + \alpha_1'$ and K in units of π. The shaded area is the scattering state continuum and the solid line below the continuum is the bound state.

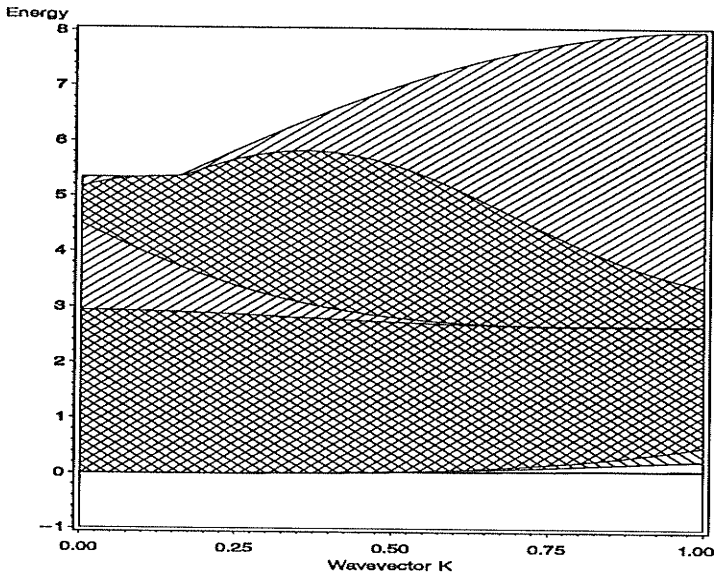

Figure 4.8: The dispersion diagram for the $S = \frac{1}{2}, \tilde{\beta} = -\frac{1}{3}$ Heisenberg case with energy in units of $\alpha_1 + \alpha_1'$ and K in units of π. The shaded area is the scattering state continuum and the solid line below the continuum is the bound state.

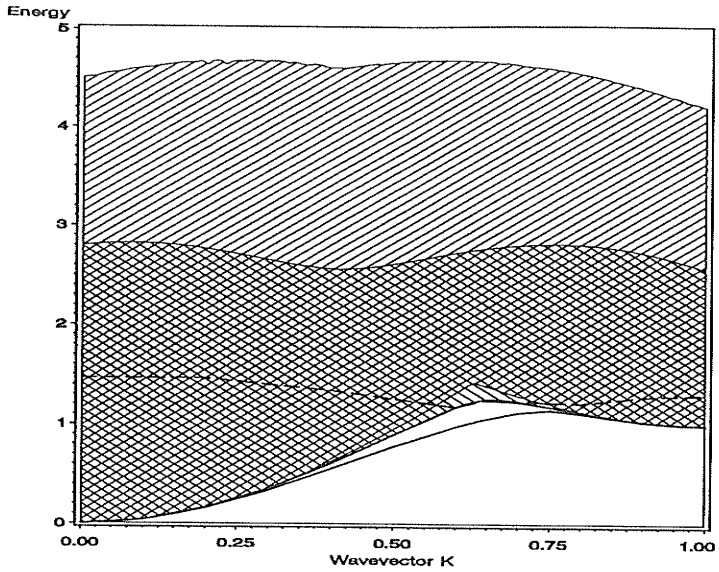

Figure 4.9: The dispersion diagram for the $S = \frac{1}{2}, \tilde{\beta} = \frac{1}{2}$ Heisenberg case with energy in units of $\alpha_1 + \alpha_1'$ and K in units of π. The shaded area is the scattering state continuum, the solid lines below the continuum are the bound states and the dashed line is the resonance.

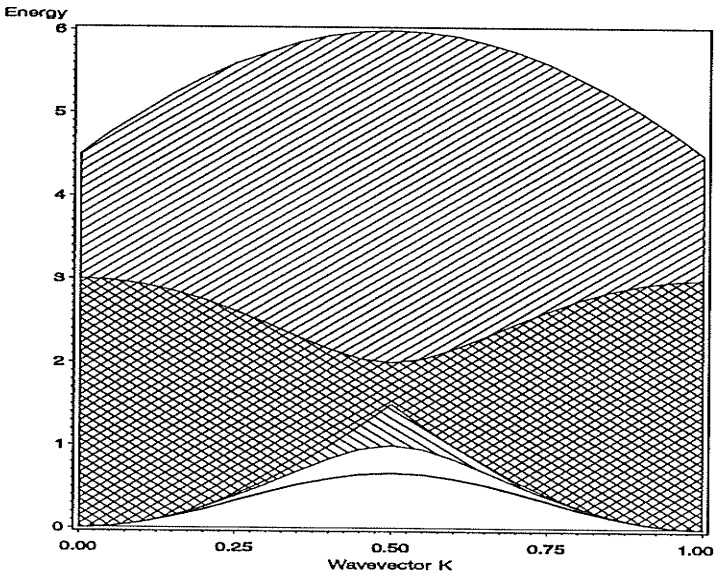

Figure 4.10: The dispersion diagram for the $S = \frac{1}{2}, \tilde{\beta} = 1$ Heisenberg case with energy in units of $\alpha_1 + \alpha_1'$ and K in units of π. The shaded area is the scattering state continuum and the solid line below the continuum is the bound state.

4.5 The $S = 1$ Heisenberg Case

The three-magnon results of the $S = 1$ Heisenberg case are shown in figure 4.11 for $\tilde{\beta} = 0$. The shaded region is the scattering state continuum (shading slanted to the left is the two-bound one-free continuum, and shading slanted to the right is the three-free continuum), the solid lines below the continuum are the bound states, and the dashed line is a resonance. The energies of the bound states at $K = \pi$ do not agree well with the energies found by Millet and Kaplan [20] and our results only partially agree with those of Kadolkar, Ghosh and Sarma [21]. We find two bound states below the continuum: the lower exists across the entire Brillouin zone but the upper enters the continuum near $K = \pi$ and becomes a resonance. The energies of our lower bound state branch agree with Kadolkar, Ghosh and Sarma, but they find that the upper bound state is present for all K values, which disagrees with our results.

As $\tilde{\beta}$ decreases from zero the lower continuum edge and the bound state energies decrease. The $S = 1$ Heisenberg case for $\tilde{\beta} = -\frac{1}{3}$ is shown in figure 4.12. Kadolkar, Ghosh and Sarma did not consider $\tilde{\beta} < 0$.

As $\tilde{\beta}$ increases from zero the upper bound state's range decreases further and the lower bound state moves up to touch the continuum at $K = \pi$ at $\tilde{\beta} = 0.21$. For $\tilde{\beta} > 0.21$, the lower bound state exists for all $0 < K < \pi$. The bound states and lower continuum edges are plotted in figure 4.13. For the larger values of $\tilde{\beta}$ there is an upper bound state located where the continuum edge curves down, but it is so close to the continuum edge that it is not visible in the diagram. Kadolkar, Ghosh and Sarma claim that the lower bound state disappears for values of K near π when $\tilde{\beta} > 0.21$, in disagreement with our results. This disagreement may occur due to their method of discretizing the integral equation.

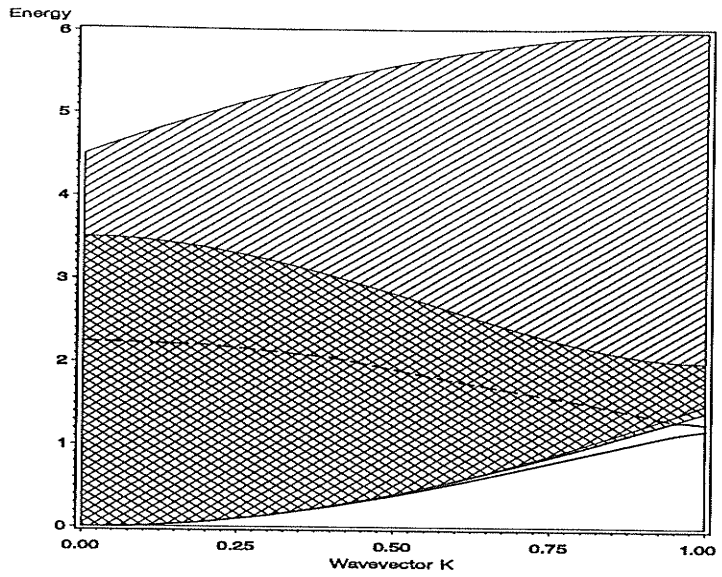

Figure 4.11: The dispersion diagram for the $S = 1, \tilde{\beta} = 0$ Heisenberg case with energy in units of $\alpha_1 + \alpha_1'$ and K in units of π. The shaded area is the scattering state continuum, the solid lines below the continuum are the bound states, and the dashed line is the resonance.

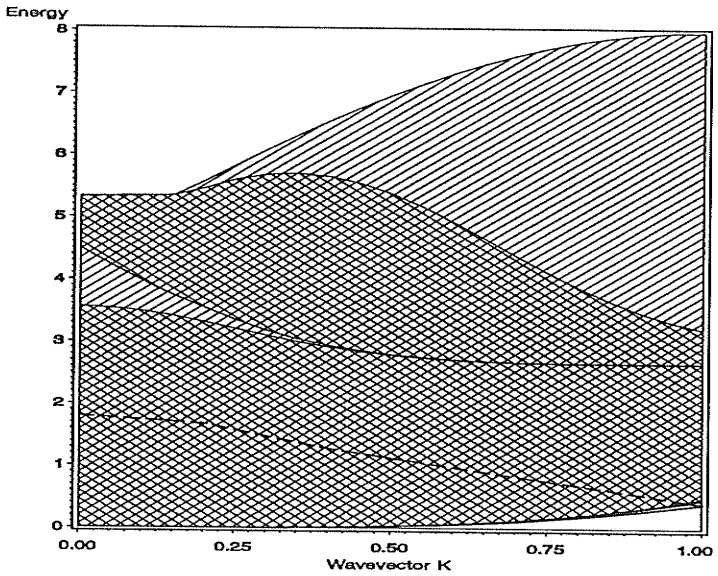

Figure 4.12: The dispersion diagram for the $S = 1, \tilde{\beta} = -\frac{1}{3}$ Heisenberg case with energy in units of $\alpha_1 + \alpha_1'$ and K in units of π. The shaded area is the scattering state continuum, the solid lines below the continuum are the bound states, and the dashed line is the resonance.

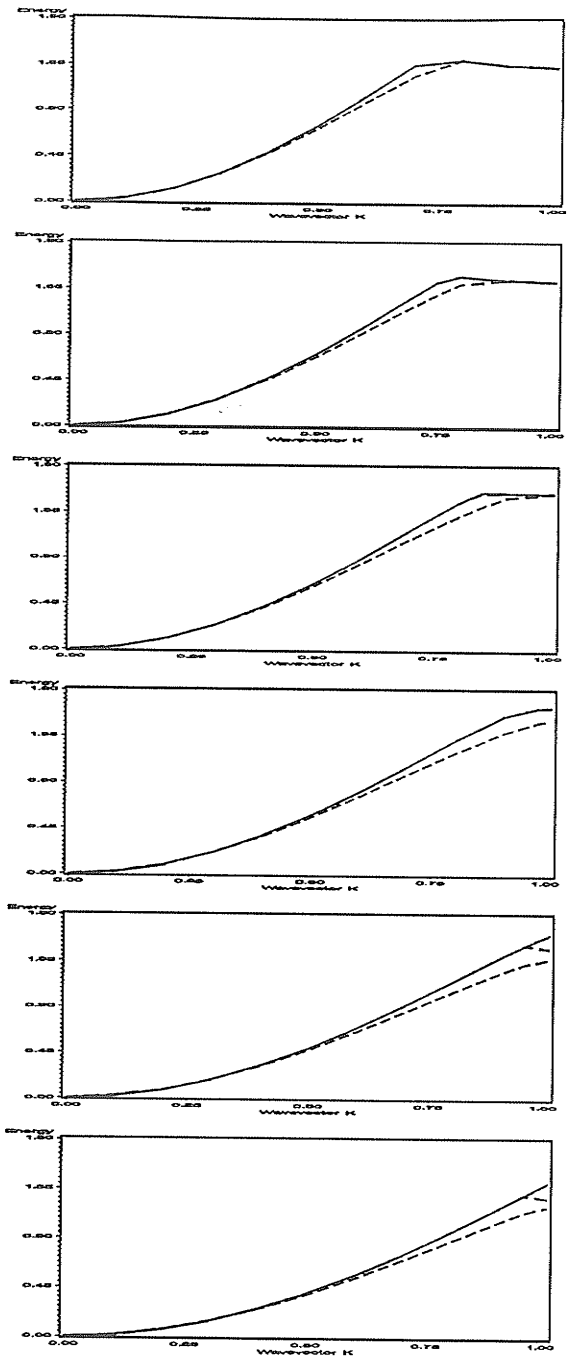

Figure 4.13: The lower continuum edges and the bound states for the $S = 1, \beta = 0, 0.1, 0.2, 0.3, 0.4$ and 0.5 ($\tilde{\beta} = 0, 0.0909, 0.17, 0.23, 0.29$ and 0.33) Heisenberg cases with energy in units of $\alpha_1 + \alpha_1'$ and K in units of π. The solid lines are the lower edge of the scattering state continua and the dashed lines are the bound states. The bottom diagram corresponds to $\beta = 0$ and the top to $\beta = 0.5$.

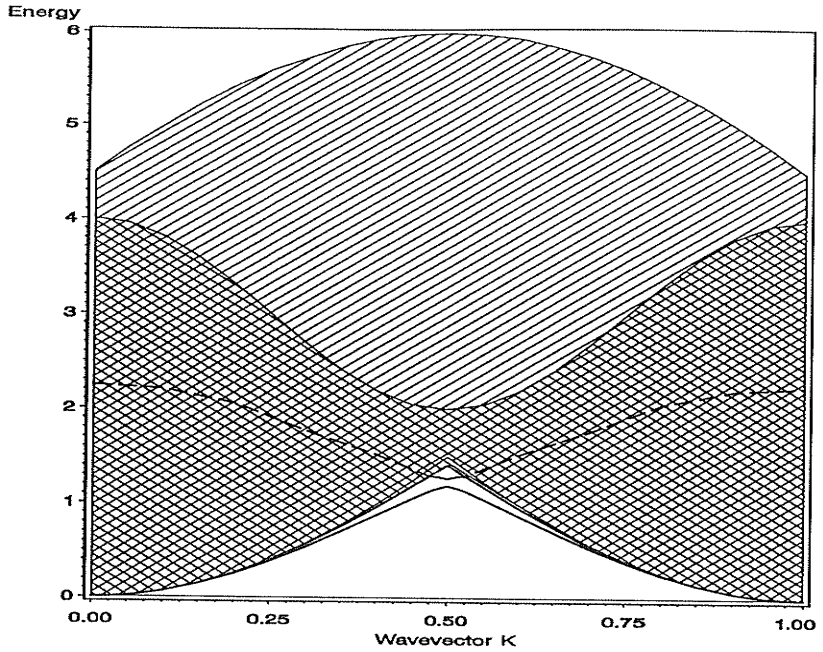

Figure 4.14: The dispersion diagram for the $S = 1, \tilde{\beta} = 1$ Heisenberg case with energy in units of $\alpha_1 + \alpha_1'$ and K in units of π. The shaded area is the scattering state continuum, the solid lines below the continuum are the bound states, and the dashed line is the resonance.

As $\tilde{\beta} \to 1$, the upper bound state emerges from the continuum at values of K closer to $K = \frac{\pi}{2}$ so that at $\tilde{\beta} = 1$ (figure 4.14) we have the $\tilde{\beta} = 0$ case with the lattice distance doubled.

4.6 The $S = 1$ Takhtajan and Babujian Model

The $S = 1, \tilde{\beta} = 0$ integrable model of Takhtajan and Babujian ([7], [8]) has already been discussed at the end of Chapter 3. It is shown again in figure 4.15 with the three-free (shading to right) and the upper and lower two-bound one-free (shading to left) continua shown. The two-bound one-free continua meet over the whole Brillouin zone and the two solid lines are the bound states.

As $\tilde{\beta}$ decreases from zero, the lower continuum and the two bound states below

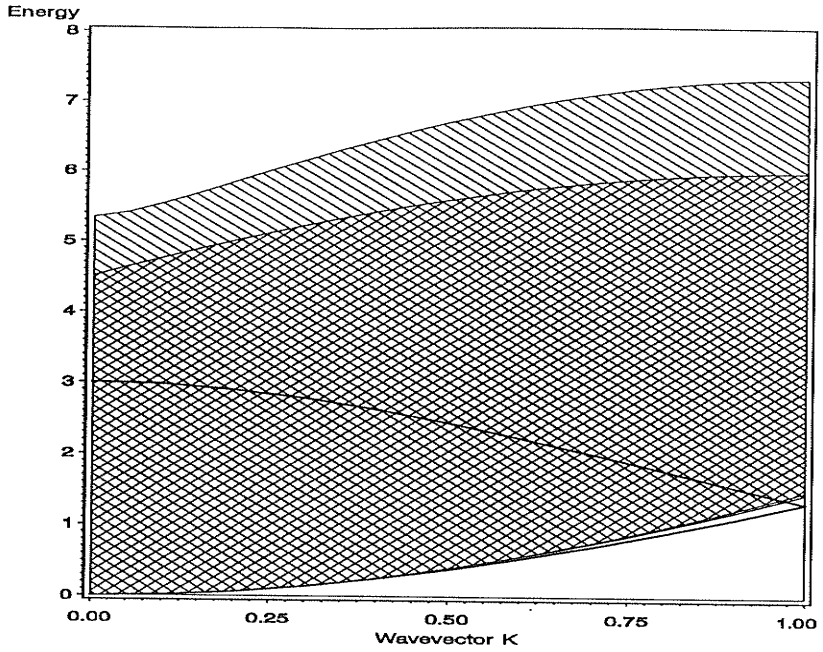

Figure 4.15: The dispersion diagram for the $S = 1, \tilde{\beta} = 0$ Takhtajan and Babujian model with energy in units of $\alpha_1 + \alpha_1'$ and K in units of π. The shaded area is the scattering state continuum and the solid lines are the bound states.

the continuum decrease in energy, as shown for $\tilde{\beta} = -\frac{1}{3}$ in figure 4.16. A gap appears at $K = \pi$ between the two bound states below the continuum and the higher of the two bound states enters the continuum and becomes a resonance near $K = \pi$. There is also a bound state above the continuum which appears first at $K = \pi$ as $\tilde{\beta}$ decreases from zero. These results were obtained by calculating the local density of states at each value of K. However, the presence of the bound states can also be read off directly from the recursion coefficients. The sequence of coefficients a_n versus n at $K = \pi$ and $\tilde{\beta} = -\frac{1}{3}$ are shown in figure 4.17, where there are two deviations below and one above the value to which a_n converges.

Figure 4.18 shows the $\tilde{\beta} = \frac{1}{5}$, $S = 1$ case of the Takhtajan and Babujian model. The upper bound state below the continuum of figure 4.15 has entered the continuum completely and is now a resonance. There is also a bound state

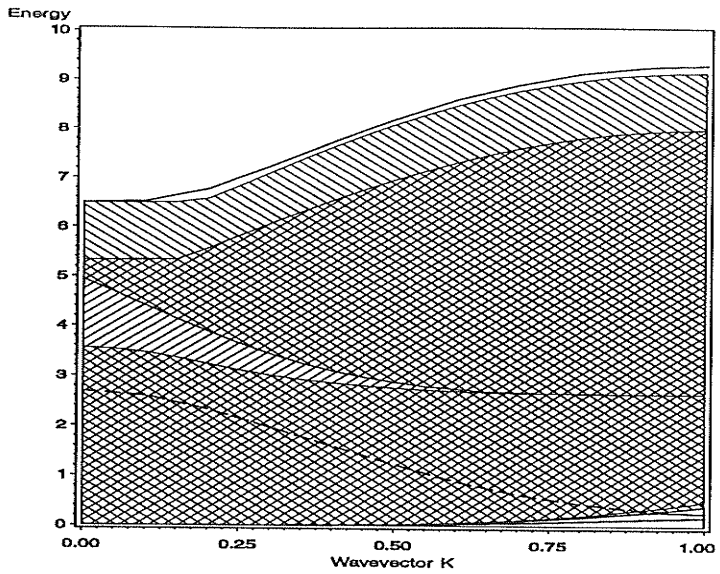

Figure 4.16: The dispersion diagram for the $S = 1, \tilde{\beta} = -\frac{1}{3}$ Takhtajan and Babujian model with energy in units of $\alpha_1 + \alpha_1'$ and K in units of π. The shaded area is the scattering state continuum, the solid lines outside of the continuum are the bound states and the dashed line is the resonance.

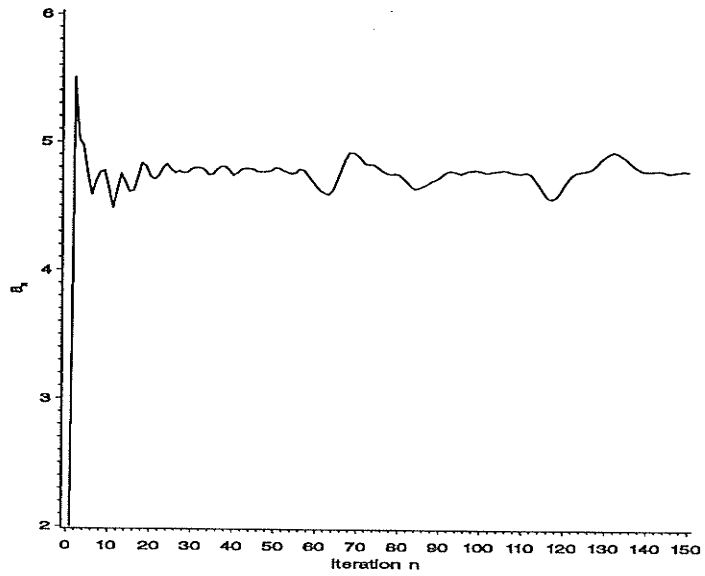

Figure 4.17: The sequence of coefficients a_n versus the iteration number n for the $S = 1, \tilde{\beta} = -\frac{1}{3}$ Takhtajan and Babujian model at $K = \pi$.

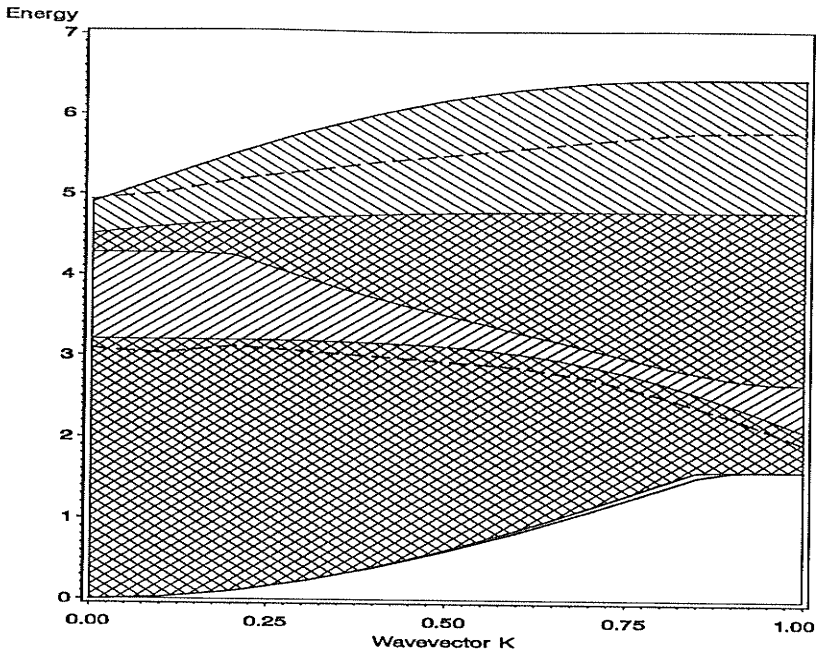

Figure 4.18: The dispersion diagram for the $S = 1, \tilde{\beta} = \frac{1}{5}$ Takhtajan and Babujian model with energy in units of $\alpha_1 + \alpha_1'$ and K in units of π. The shaded area is the scattering state continuum, the solid lines outside of the continuum are the bound states and the dashed lines are the resonances.

above the continuum for a small range near $K = 0$ which enters the continuum and becomes a resonance for larger values of K. This bound state first appears at $K = 0$ as $\tilde{\beta}$ increases from zero. Figure 4.19 shows the dispersion diagram for $\tilde{\beta} = \frac{1}{2}$, where the resonance in the lower part of the continuum can be seen to be lowering towards the maximum value of the lower continuum. As $\tilde{\beta}$ increases this resonance emerges as a bound state for a small range of K, as shown in figure 4.20 for $\tilde{\beta} = 1$.

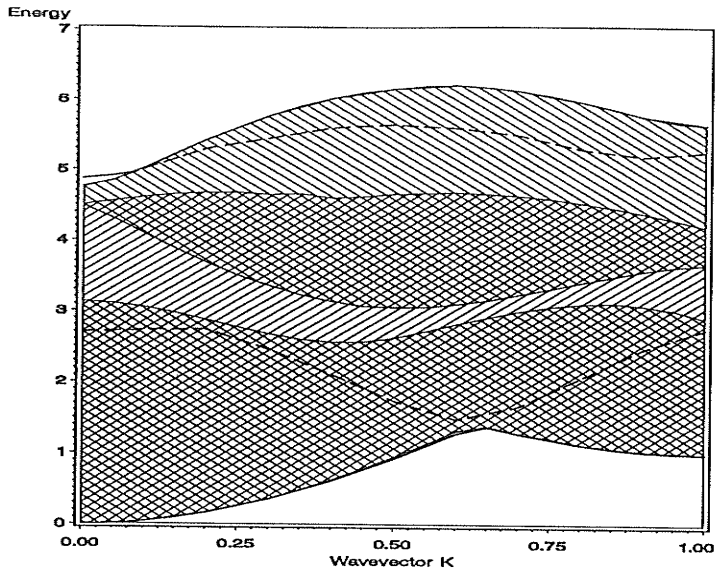

Figure 4.19: The dispersion diagram for the $S = 1, \tilde{\beta} = \frac{1}{2}$ Takhtajan and Babujian model with energy in units of $\alpha_1 + \alpha_1'$ and K in units of π. The shaded area is the scattering state continuum, the solid lines outside of the continuum are the bound states and the dashed lines are the resonances.

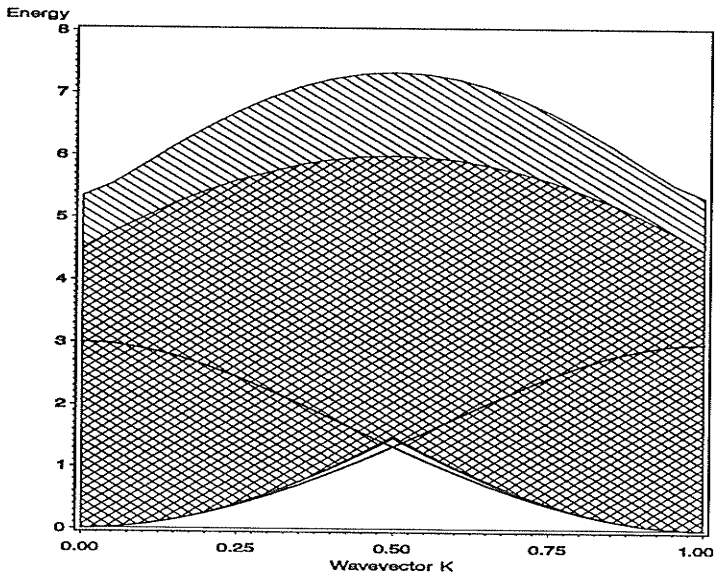

Figure 4.20: The dispersion diagram for the $S = 1, \tilde{\beta} = 1$ Takhtajan and Babujian model with energy in units of $\alpha_1 + \alpha_1'$ and K in units of π. The shaded area is the scattering state continuum and the solid lines are the bound states.

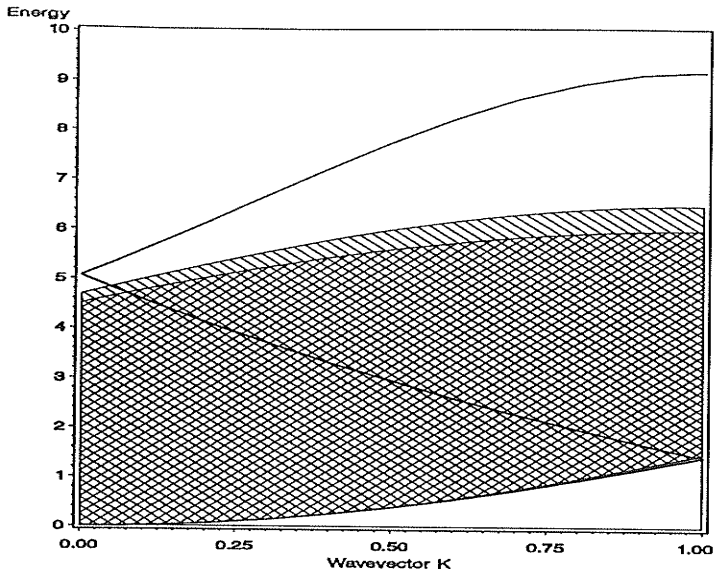

Figure 4.21: The dispersion diagram for the $S = \frac{3}{2}, \tilde{\beta} = 0$ Takhtajan and Babujian model with energy in units of $\alpha_1 + \alpha_1'$ and K in units of π. The shaded area is the scattering state continuum and the solid lines are the bound states.

4.7 The $S = \frac{3}{2}$ Takhtajan and Babujian Model

Figure 4.21 shows the dispersion diagram for the $S = \frac{3}{2}$, $\tilde{\beta} = 0$ Takhtajan and Babujian integrable model. As in the $S = 1$, $\tilde{\beta} = 0$ case, the bound state passes through the scattering state continuum without interacting with it. As $\tilde{\beta}$ decreases from zero another bound state is found above the continuum at $K = \pi$, and as $\tilde{\beta}$ decreases further the bound state extends to lower and lower values of K. In figure 4.22 the $\tilde{\beta} = -\frac{1}{3}$ case is shown, but the lower bound state above the continuum is so close to the continuum that it can not be seen on this scale. The upper bound state above the continuum enters the continuum near $K = 0$ and becomes a resonance. There is a gap between this resonance and the lower resonance which emerges from the continuum near $K = \pi$ to become a bound state. There is a gap between this bound state and the lowest bound state, which exists for all values of $K > 0$.

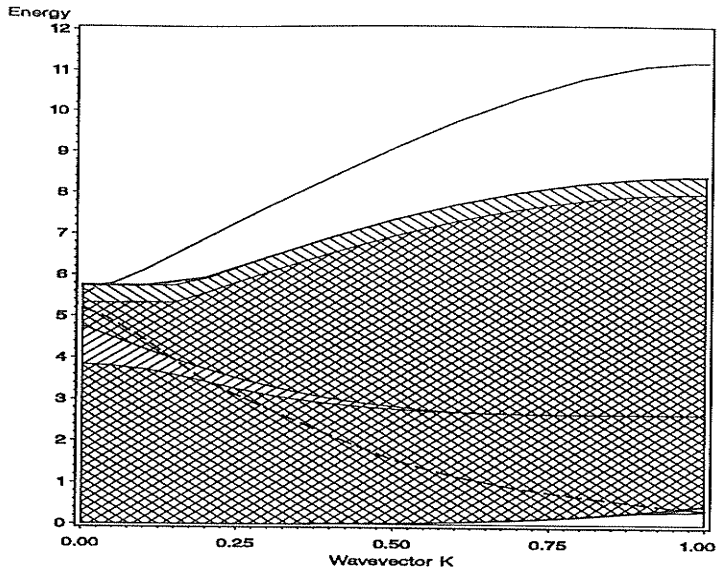

Figure 4.22: The dispersion diagram for the $S = \frac{3}{2}, \tilde{\beta} = -\frac{1}{3}$ Takhtajan and Babujian model with energy in units of $\alpha_1 + \alpha_1'$ and K in units of π. The shaded area is the scattering state continuum, the solid lines outside of the continuum are the bound states and the dashed lines are the resonances.

As $\tilde{\beta}$ increases from zero a gap occurs between the two bound states above the continuum at $K = 0$ and a third bound state appears above the continuum near $K = 0$. This third bound state enters the continuum and becomes a resonance. The $\tilde{\beta} = \frac{1}{5}$ case is shown in figure 4.23, but the third bound state above is close to the continuum and can not be seen on this scale. There is also a bound state below which is difficult to see on this scale. The integrable $\tilde{\beta} = 1$ case is shown in figure 4.24.

This concludes the discussion of the Hamiltonian (1.5). We have only studied two second neighbor models: the Heisenberg model and the Takhtajan and Babujian model. However, the method can be applied to any case. In the next chapter we will consider the Hamiltonian (1.6). The one, two and three- magnon equations and the spectra will be found using the methods described in chapters 2, 3 and 4. Both the integrable $S = \frac{1}{2}$ case and the $S = 1$ case will be discussed.

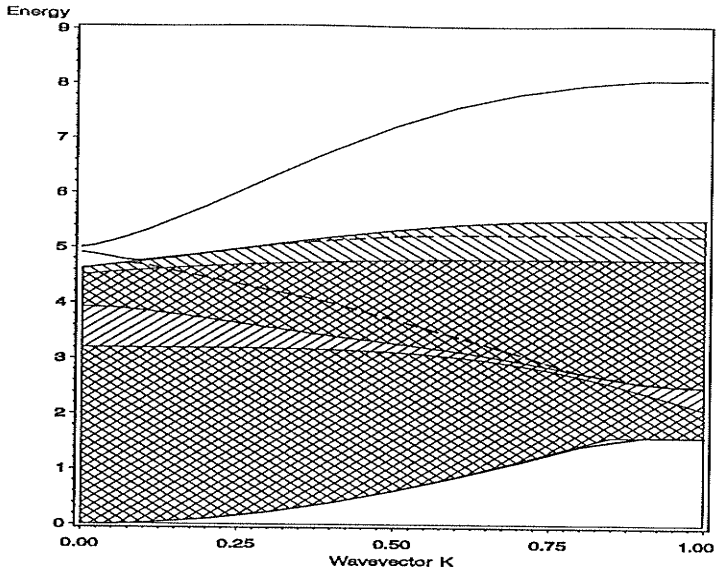

Figure 4.23: The dispersion diagram for the $S = \frac{3}{2}, \tilde{\beta} = \frac{1}{5}$ Takhtajan and Babujian model with energy in units of $\alpha_1 + \alpha_1'$ and K in units of π. The shaded area is the scattering state continuum, the solid lines outside of the continuum are the bound states and the dashed lines are the resonances.

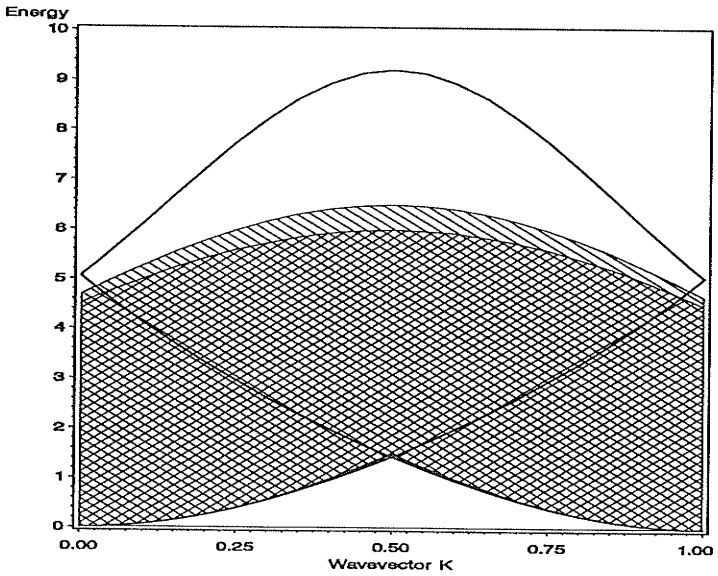

Figure 4.24: The dispersion diagram for the $S = \frac{3}{2}, \tilde{\beta} = 1$ Takhtajan and Babujian model with energy in units of $\alpha_1 + \alpha_1'$ and K in units of π. The shaded area is the scattering state continuum and the solid lines are the bound states.

Chapter 5

Heisenberg Chain with Competing Interactions

In this chapter we consider the nearest neighbor Heisenberg Hamiltonian plus a term involving interactions between three adjacent spins on the chain (equation 1.6)(Tsvelik [9], [29], [30])

$$\widehat{H} = -J_1 \sum_{l=1}^{N} (\widetilde{S}_l \cdot \widetilde{S}_{l+1}) - J_2 \sum_{l=1}^{N} \widetilde{S}_{l-1} \cdot (\widetilde{S}_l \times \widetilde{S}_{l+1})$$

The three-spin term favours the state with three adjacent spins along the chain all at 90° to each other. Thus, the term involving J_2 competes with the Heisenberg term J_1, which favours parallel alignment. If $S = \frac{1}{2}$ this Hamiltonian is integrable and solvable by the Bethe ansatz for arbitrary values of $\frac{J_2}{J_1}$ but for higher values of S this Hamiltonian is no longer integrable. We will derive the one, two and three-magnon equations for general S, and present the resulting spectra for both $S = \frac{1}{2}$ and $S = 1$.

The Hamiltonian above can be expressed as the sum of two separate terms:

$$\widehat{H} = J_1 I_1 + J_2 I_2 \tag{5.1}$$

where

$$I_1 = -\sum_{l=1}^{N} (\widetilde{S}_l \cdot \widetilde{S}_{l+1})$$

$$I_2 = -\sum_{l=1}^{N} \widetilde{S}_{l-1} \cdot (\widetilde{S}_l \times \widetilde{S}_{l+1}) \tag{5.2}$$

The first term, I_1, is the nearest neighbor only Heisenberg case which we studied in the last chapters. It can be expressed as a sum over $\widetilde{P}_l$ (equation (2.3)).

$$\begin{aligned} \widetilde{P}_l &= \widetilde{S}_l \cdot \widetilde{S}_{l+1} \\ I_1 &= -\sum_{l=1}^{N} \widetilde{P}_l \end{aligned} \tag{5.3}$$

The derivations of the one, two and three-magnon equations for this term have been discussed in Chapters 2 and 3 and Appendix A and thus we concentrate on the second term, I_2. The term I_2 can be written as a sum over $\widetilde{O}_l$

$$I_2 = -\sum_{l=1}^{N} \widetilde{O}_l \tag{5.4}$$

where

$$\widetilde{O}_l = \widetilde{S}_{l-1} \cdot (\widetilde{S}_l \times \widetilde{S}_{l+1}) \tag{5.5}$$

One can express $\widetilde{O}_l$ in terms of raising and lowering operators

$$\begin{aligned} \widetilde{O}_l = \frac{1}{2i} \Big\{ & -S^+_{l-1} S^-_l S^z_{l+1} + S^-_{l-1} S^+_l S^z_{l+1} + S^+_{l-1} S^z_l S^-_{l+1} - S^-_{l-1} S^z_l S^+_{l+1} - S^z_{l-1} S^+_l S^-_{l+1} \\ & + S^z_{l-1} S^-_l S^+_{l+1} \Big\} \end{aligned} \tag{5.6}$$

To find the ground state energy we let the Hamiltonian act on the ground state, equation (1.10).

$$\widehat{H} = J_1 I_1 \mid 0\rangle + J_2 I_2 \mid 0\rangle \tag{5.7}$$

From the form of $\widetilde{O}_l$ we can see that the second term does not contribute. The first term gives a contribution and the ground state energy per site is

$$E_0 = -J_1 S^2 \tag{5.8}$$

5.1 One-Magnon Excitations

Following the method used in chapter 2.1, the normalized spin deviation state is (equation (1.11))

$$| j\rangle = \frac{1}{\sqrt{2S}} S_j^+ | 0\rangle$$

The operator $\tilde{O}_l$ acting on state $| j\rangle$ gives

$$\hat{O}_l | j\rangle = \begin{cases} 0 | j\rangle & , j \neq l-1, l, l+1 \\ \frac{1}{2i}(-2S^2 | l\rangle + 2S^2 | l+1\rangle) & , j = l-1 \\ \frac{1}{2i}(2S^2 | l-1\rangle - 2S^2 | l+1\rangle) & , j = l \\ \frac{1}{2i}(-2S^2 | l-1\rangle + 2S^2 | l\rangle) & , j = l+1 \end{cases} \tag{5.9}$$

Summing over l we can find the effects of I_2 acting on an arbitrary state $| j\rangle$

$$I_2 | j\rangle = -\frac{1}{2i} 2S^2 \{| j+2\rangle - | j-2\rangle - 2 | j+1\rangle + 2 | j-1\rangle\} \tag{5.10}$$

The one-magnon wavefunction is (equation (1.13))

$$| k\rangle = \sum_j \frac{e^{-ikr_j}}{\sqrt{N}} | j\rangle, \; r_j = ja$$

where for convenience we will set $a = 1$. Substituting the inverse of (1.13) into (5.10) we find

$$I_2 | k\rangle = -2S^2(\sin 2k - 2\sin k) | k\rangle \tag{5.11}$$

From (2.20), I_1 gives a contribution of

$$I_1 | k\rangle = -NJ_1S^2 | k\rangle + 2SJ_1(1 - \cos k) | k\rangle \tag{5.12}$$

Combining these terms and absorbing the ground state energy into the zero of the energy, the one-magnon dispersion relation is

$$\frac{E_1(k)}{2SJ_1} = (1 + \alpha \sin k)(1 - \cos k) \tag{5.13}$$

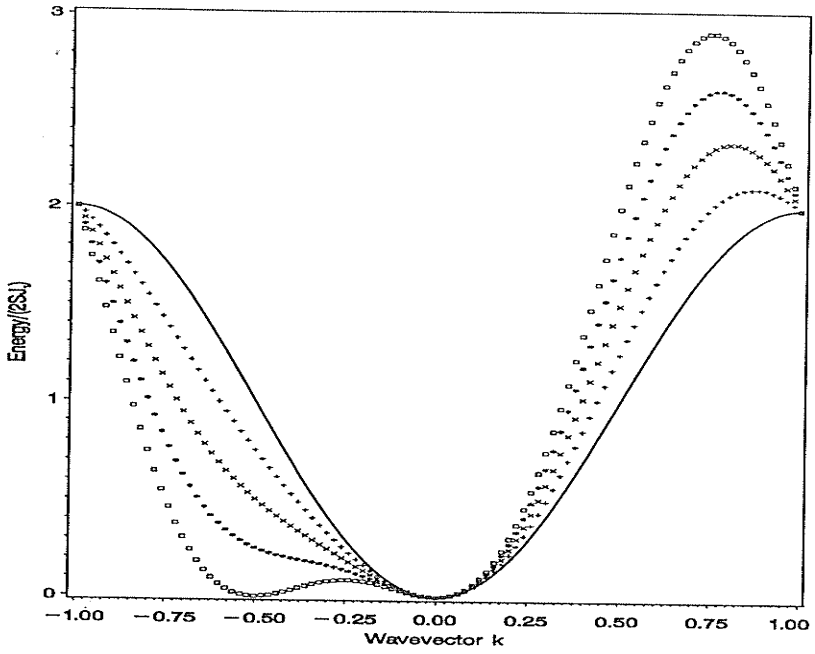

Figure 5.1: One-magnon excitation energy in units of $2SJ_1$ for the general S Tsvelik Hamiltonian. The wavevector k is in units of π. The solid line corresponds to $\alpha = 0$; $+$ to $\alpha = \frac{1}{4}$; $\times$ to $\alpha = \frac{1}{2}$; $*$ to $\alpha = \frac{3}{4}$ and $\Box$ to $\alpha = 1$.

where the energy is expressed in units of $2SJ_1$ and $\alpha = \frac{2SJ_2}{J_1}$. The ferromagnetic ground state is stable for $J_1 > 0$ if $\mid \alpha \mid \leq 1$.

The one-magnon excitation energy in units of $2SJ_1$ for $\alpha = 0, \frac{1}{4}, \frac{1}{2}, \frac{3}{4}$ and 1 is shown in figure 5.1. The entire range of $k = -\pi$ to π must be plotted since the energy is not symmetric about $k = 0$ (as opposed to the Hamiltonian (1.5)). That is, this Hamiltonian is not parity invariant [9]. For $\alpha < 0$ the spectra is just the mirror image of that for $\mid \alpha \mid$.

5.2 Two-Magnon Excitations

The orthonormal base kets for two spin deviations are

$$\mid i,j\rangle = C_{ij} S_i^+ S_j^+ \mid 0\rangle \tag{5.14}$$

$$C_{ij} = \begin{cases} \frac{1}{\sqrt{2S}} & ,\text{if } i \neq j \\ \frac{1}{2\sqrt{S(2S-1)}} & ,\text{if } i = j \end{cases}$$

where the C_{ij} are normalization constants and the kets are labeled by sites i and j such that $i \leq j$. The derivation of the effect of I_2 on these base kets is straight forward and is included in Appendix B. The final set of equations in Appendix B (equations (B.3), (B.7), (B.8) and (B.9)) involve kets containing the labels of the sites which have spins flipped (i and j), but due to the property of translational invariance the Hamiltonian only depends on the relative position of the flipped spins. Therefore we may perform a change of variables to states labeled by the relative coordinate $r = j - i$ and the center of mass coordinate $R = \frac{i+j}{2}$. As well, Bloch's theorem allows us to perform a Fourier transform with respect to the center of mass coordinate to states labeled by the total momentum K and the relative coordinate r (equation (2.46)).

$$\mid K; r\rangle \;=\; \frac{1}{\sqrt{N}} \sum_R e^{-iKaR} \mid i, j\rangle$$

For convenience we have let $a = 1$. Performing the inverse of this transformation on equations (B.3) and (B.7) to (B.9), we find the effect of I_2 acting on the states $\{\mid K; r\rangle\}$.

$$\begin{aligned}
J_2 I_2 \mid K;0\rangle &= U_0 \mid K;1\rangle + U_0' \mid K;2\rangle \\
J_2 I_2 \mid K;1\rangle &= U_0 \mid K;0\rangle + Y \mid K;1\rangle + U_1 \mid K;2\rangle + U' \mid K;3\rangle \\
J_2 I_2 \mid K;3\rangle &= U_0' \mid K;0\rangle + U_1 \mid K;1\rangle + U \mid K;3\rangle + U' \mid K;4\rangle \\
J_2 I_2 \mid K;r\rangle &= U'(\mid K;r+2\rangle + \mid K;r-2\rangle) + U(\mid K;r+1\rangle + \mid K;r-1\rangle) \qquad (5.15)
\end{aligned}$$

where $r > 2$ and the parameters are:

$$\left.\begin{aligned}
U_0 &= 4SJ_2\sqrt{S(2S-1)}\sin\tfrac{K}{2} \\
U_0' &= -2SJ_2\sqrt{S(2S-1)}\sin K \\
Y &= 2S(1-S)J_2 \sin K \\
U_1 &= (4S^2 - 2S)J_2 \sin\tfrac{K}{2} \\
U &= 4S^2 J_2 \sin\tfrac{K}{2} \\
U' &= -2S^2 J_2 \sin K
\end{aligned}\right\} \qquad (5.16)$$

The Heisenberg term contributions are found from equations (2.48) to (2.51) and involve the parameters

$$\left.\begin{array}{rcl} \varepsilon_0 & = & 4SJ_1 \\ \varepsilon_1 & = & (4S-1)J_1 \\ \varepsilon & = & 4SJ_1 \\ V_0 & = & -2\sqrt{S(2S-1)}J_1\cos\frac{K}{2} \\ V & = & -2SJ_1\cos\frac{K}{2} \end{array}\right\} \tag{5.17}$$

Therefore the effect of the full Hamiltonian on the states $\{\mid K;r\rangle\}$ is

$$\widehat{H}\mid K;0\rangle = \varepsilon_0\mid K;0\rangle + (V_0+U_0)\mid K;1\rangle + U_0'\mid K;2\rangle \tag{5.18}$$

$$\widehat{H}\mid K;1\rangle = (\varepsilon_1+Y)\mid K;1\rangle + (V_0+U_0)\mid K;0\rangle + (V+U_1)\mid K;2\rangle + U'\mid K;3\rangle \tag{5.19}$$

$$\widehat{H}\mid K;2\rangle = \varepsilon\mid K;2\rangle + U_0'\mid K;0\rangle + (V+U_1)\mid K;1\rangle + (V+U)\mid K;3\rangle + U'\mid K;4\rangle \tag{5.20}$$

$$\widehat{H}\mid K,r\rangle = \varepsilon\mid K;r\rangle + (V+U)[\mid K;r-1\rangle + \mid K;r+1\rangle] + U'[\mid K;r-2\rangle + \mid K;r+2\rangle] \qquad ,r>2 \tag{5.21}$$

This set of equations is equivalent to a semi-infinite mass spring system where the springs couple to both nearest neighbor sites and next nearest neighbor sites, as for the two-magnon equations of the Hamiltonian (1.5). The mapping is

$$\left.\begin{array}{rcl} m_0 & \Rightarrow & \varepsilon_0 \\ m_1 & \Rightarrow & \varepsilon_1+Y \\ m,m_2 & \Rightarrow & \varepsilon \\ k_0 & = & V_0+U_0 \\ k_0' & = & U_0' \\ k_1 & = & V+U_1 \\ k & = & V+U \\ k' & = & U' \end{array}\right\} \tag{5.22}$$

The visualization is the same as that of figure 2.3, with the exceptions that the nearest neighbor coupling between m_1 and m_2 is k_1 and that m_2 is the same as m.

The set of equations (5.18) to (5.21) leads to two different types of solutions, scattering state solutions and bound state solutions. The scattering state solutions will be examined in the next section, and the bound state solutions will be examined in section 5.2.2.

5.2.1 The Two-Magnon Scattering State Continuum

Equation (5.21) by itself describes two free-magnons and consequently the scattering state energy with total momentum K is equal to the sum of the energies of the two free-magnons with momenta k_1 and k_2. Let energy be in units of $(2SJ_1)$.

$$\begin{aligned} E^{ss}(K) &= E_1(k_1) + E_1(k_2) \qquad , k_1 + k_2 = K \\ &= 2\left(1 - \cos\frac{K}{2}\cos q\right) + 2\alpha \sin\frac{K}{2}\left[\cos q + \cos\frac{K}{2}\left(1 - 2\cos^2 q\right)\right] \end{aligned} \tag{5.23}$$

where $q = \frac{k_1 - k_2}{2}$. In general there are four possible values of q ($\pm q_1$ and $\pm q_2$) for each choice of E and K. Two situations can occur in the scattering state continuum: both q_1 and q_2 can be real, or only one is real. However, the minima and maxima of the scattering state continua are determined by real values of q. The solutions to $\frac{\partial E^{ss}}{\partial q} = 0$ give the following extrema:

$$\begin{aligned} E^{(1)}(q = 0) &= 2\left(1 + \alpha \sin\frac{K}{2}\right)\left(1 - \cos\frac{K}{2}\right) \\ E^{(2)}(q = \pi) &= 2\left(1 - \alpha \sin\frac{K}{2}\right)\left(1 + \cos\frac{K}{2}\right) \\ E^{(3)}\left(\cos q = \frac{1}{4\cos\frac{K}{2}} - \frac{1}{4\alpha \sin\frac{K}{2}}\right) &= \frac{3}{2} + \frac{1}{2\sin K}\left(\alpha \sin^2\frac{K}{2} + \frac{1}{\alpha}\cos^2\frac{K}{2}\right) + \alpha \sin K, \\ &\qquad \text{provided } -1 \le \frac{1}{4\cos\frac{K}{2}} - \frac{1}{4\alpha\sin\frac{K}{2}} \le 1 \end{aligned} \tag{5.24}$$

Therefore the scattering state continuum is a single band which extends from the $E^{(i)}$ which attains the minimum energy to the $E^{(i)}$ which attains the maximum energy for given K. A summary of the conditions which determine whether $E^{(i)}$ is a minimum or a maximum are given in table 5.1.

The condition $-1 \le \frac{1}{4\cos\frac{K}{2}} - \frac{1}{4\alpha\sin\frac{K}{2}} = \cos q \le 1$ associated with $E^{(3)}$ ensures that q is real. Note that $\cos q = 1$ corresponds to an inflection point of $E^{(1)}$ and $\cos q = -1$ corresponds to an inflection point of $E^{(2)}$. At $K = 0, \pi$ and $-\pi$ the information in table 5.1 reduces to the information in table 5.2.

Table 5.1: Minimum and maximum scattering state energy in units of $2SJ_1$.

Energy		Condition	
$E^{(1)}$	is a local maximum if	$\frac{\partial^2 E^{ss}}{\partial q^2} = 2\cos\frac{K}{2} - 2\alpha\sin\frac{K}{2}\left(1 - 4\cos\frac{K}{2}\right)$	< 0
	is a local minimum if		> 0
	is an inflection point if		$= 0$
$E^{(2)}$	is a local maximum if	$\frac{\partial^2 E^{ss}}{\partial q^2} = -2\cos\frac{K}{2} + 2\alpha\sin\frac{K}{2}\left(1 + 4\cos\frac{K}{2}\right)$	< 0
	is a local minimum if		> 0
	is an inflection point if		$= 0$
$E^{(3)}$	is a maximum if	$\frac{\partial^2 E^{ss}}{\partial q^2} = \frac{\cos\frac{K}{2}}{2\alpha\sin\frac{K}{2}} - \frac{3}{8} - 4\alpha\sin K$ and $-1 \leq \frac{1}{4\cos\frac{K}{2}} - \frac{1}{4\alpha\sin\frac{K}{2}} \leq 1$	< 0
	is a minimum if		> 0
	is an inflection point if		$= 0$

Table 5.2: Minimum and maximum scattering state energy

K	E_{min}	E_{max}
0	0	4
π and $-\pi$	$2(1-\alpha)$	$2(1+\alpha)$

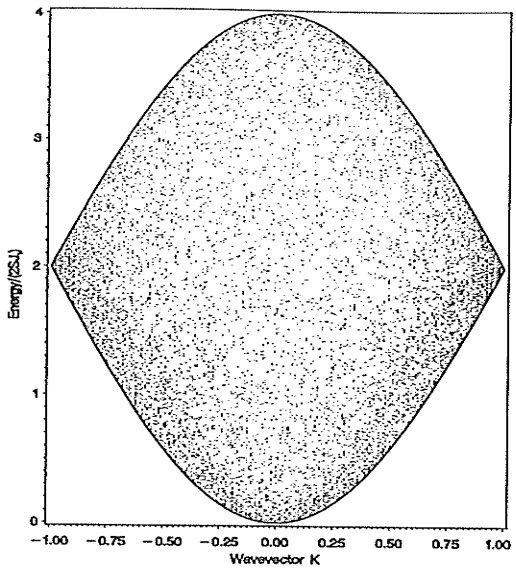

Figure 5.2: Two-magnon scattering state continuum density plot with energy in units of $2SJ_1$. The wavevector K is in units of π and $\alpha = 0$.

The scattering state continua (density plots - as in section 2.3) with energies measured in units of $2SJ_1$ are shown in figures 5.2 to 5.6 for $\alpha = 0, \frac{1}{4}, \frac{1}{2}, \frac{3}{4}$ and 1. In figures 5.3 to 5.6 the regions of higher density (darker) correspond to both q_1 and q_2 being real and the regions of lower density correspond to only one of q_1 or q_2 being real. As $\alpha \to 0$ (figure 5.2), the higher density region is compressed to a point at $K = \pi$ and only one real value of q survives with the other having and infinite imaginary part.

Note that the continua extend to zero energy at $K = 0, \pm\pi$ and $-\frac{\pi}{2}$ when $\alpha = 1$. For $\alpha > 1$ the ferromagnetic state is no longer the lowest energy state and the continuum energies first go negative at $K = \pm\pi$ and $-\frac{\pi}{2}$ as α increases above one.

These scattering state continua are important for identifying the regions where the two-magnon bound state solutions can occur. These will be discussed in the next section.

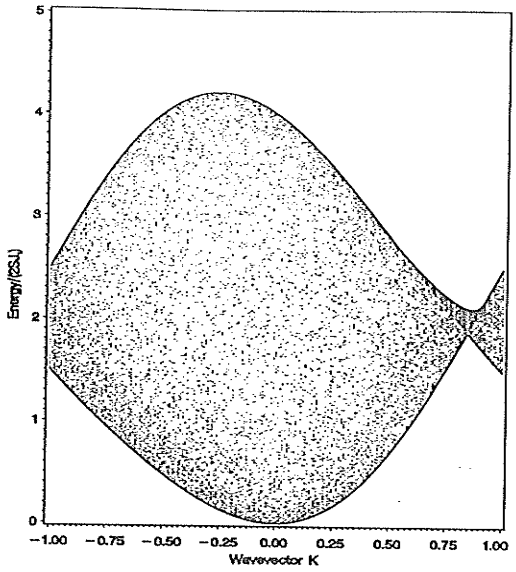

Figure 5.3: Two-magnon scattering state continuum density plot with energy in units of $2SJ_1$. The wavevector K is in units of π and $\alpha = \frac{1}{4}$.

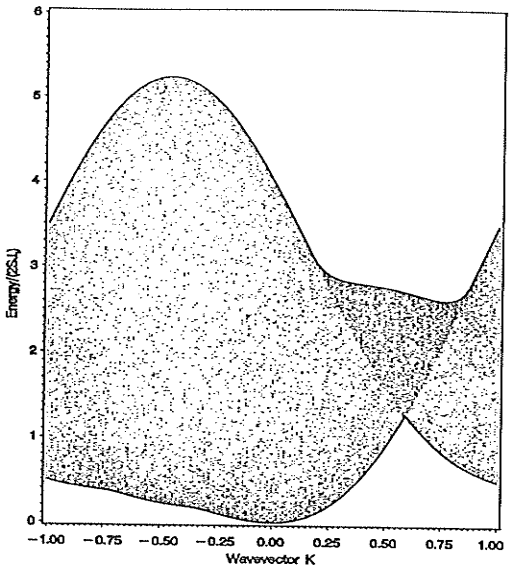

Figure 5.5: Two-magnon scattering state continuum density plot with energy in units of $2SJ_1$. The wavevector K is in units of π and $\alpha = \frac{3}{4}$.

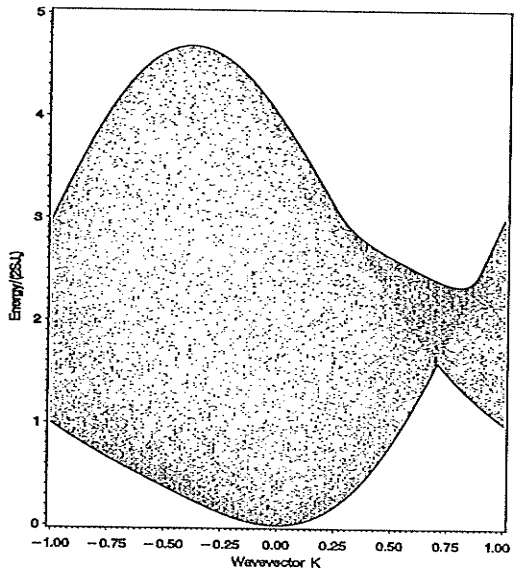

Figure 5.4: Two-magnon scattering state continuum density plot with energy in units of $2SJ_1$. The wavevector K is in units of π and $\alpha = \frac{1}{2}$.

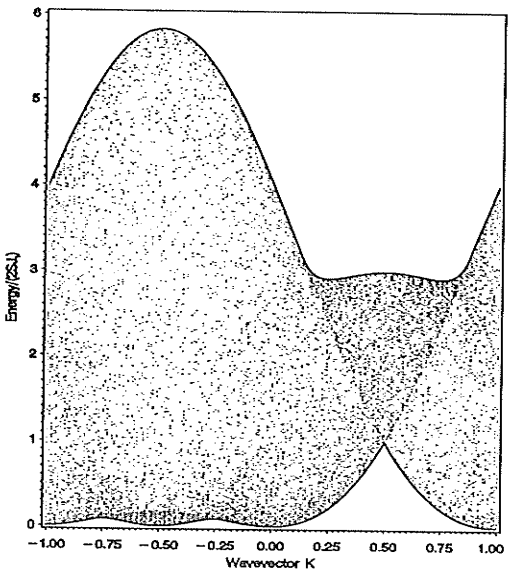

Figure 5.6: Two-magnon scattering state continuum density plot with energy in units of $2SJ_1$. The wavevector K is in units of π and $\alpha = 1$.

5.2.2 Two-Magnon Bound States

Using the real-space rescaling method [18] described in section 2.4, we can analytically solve the equations (5.19) to (5.22) for the bound state solutions. We will first rewrite these equations in terms of the complex amplitudes c_r (equation (2.57))

$$| K\rangle = \sum_r c_r^* | K; r\rangle$$

The equations for the amplitudes take the form:

$$\left.\begin{array}{rcl} (E-\varepsilon_0)c_0 &=& (V_0+U_0)c_1 + U_0'c_2 \\ (E-\varepsilon_1-Y)c_1 &=& (V_0+U_0)c_0 + (V+U_1)c_2 + U'c_3 \\ (E-\varepsilon)c_2 &=& U_0'c_0 + (V+U_1)c_1 + (V+U)c_3 + U'c_4 \\ (E-\varepsilon)c_r &=& U'(c_{r-2}+c_{r+2}) + (V+U)(c_{r-1}+c_{r+1}) \end{array}\right\} \quad (5.25)$$

In matrix form, these equations involve a pentadiagonal matrix, but we will first consider cases for which the matrix reduces to tridiagonal form.

Case a: $\alpha = 0$, but general K and S.

The equations (5.26) reduce to

$$\left.\begin{array}{rcl} (E-\varepsilon_0)c_0 &=& V_0c_1 \\ (E-\varepsilon_1)c_1 &=& V_0c_0 + Vc_2 \\ (E-\varepsilon)c_r &=& Vc_{r-1} + Vc_{r+1} \end{array}\right\} \quad (5.26)$$

This is the case considered in section 2.4, Case a, and leads to the following cubic equation (2.65) for the energy E of the bound states

$$\left[(E-\varepsilon_1)(E-\varepsilon_0) - V_0^2\right]\left[(\varepsilon_1-\varepsilon)(E-\varepsilon_0) + V_0^2\right] - (E-\varepsilon_0)^2V^2 = 0$$

If $S = \frac{1}{2}$ the c_0 site is unphysical and the solution for the bound state reduces to $E = 1 - \cos^2\frac{K}{2}$.

Case b: $\alpha \neq 0$ but $K = \pm\pi$ and general S.

Under these conditions the equations reduce to

$$\left.\begin{array}{rcl} (E-\varepsilon_0)c_0 &=& U_0c_1 \\ (E-\varepsilon_1)c_1 &=& U_0c_0 + U_1c_2 \\ (E-\varepsilon)c_2 &=& U_1c_1 + Uc_3 \\ (E-\varepsilon)c_r &=& Uc_{r-1} + Uc_{r+1} \end{array}\right\} \quad (5.27)$$

This leads to a quartic equation for the energy E of the bound states

$$U_1^2(E-\varepsilon)^3(E-\varepsilon_1)-(E-\varepsilon)(E-\varepsilon_0)U_0^2U_1^2-U_1^4(E-\varepsilon_0)^2 - \left[(E-\varepsilon_1)(E-\varepsilon_0)-U_0^2\right]^2U^2=0 \tag{5.28}$$

If $S=\frac{1}{2}$, both $U_1, U_0 = 0$ and the bound state solution is $E=\varepsilon_1$.

Case c: $\alpha \neq 0$ but $K=0$ and general S.

Under these conditions the equations reduce to (5.27) and there are no bound state solutions.

At other values of α, K and S the equations (2.56) retain their pentadiagonal form. We solve these equations for the bound states using the matrix rescaling method described in section 2.4.2.

Figures 5.7 to 5.11 show the dispersion diagrams for the spin-$\frac{1}{2}$ model with $\alpha = 0, \frac{1}{4}, \frac{1}{2}, \frac{3}{4}$ and 1. The scattering state continua are the shaded areas in the diagrams and the bound states are the solid lines. Since this model is integrable, the bound states can enter the continuum without interacting with it. At $\alpha = 0$ there is one bound state below the continuum for all values of $K \neq 0$. As α increases from zero, the continuum moves down in energy and the bound state touches it at $K = \pm\pi$ when $\alpha = \frac{1}{2}$ and as α increases further, the bound state enters the continuum near these values. The bound state energy at $K = \pm\pi$ is $E = 1$ and at $K = 0$ there is no bound state solution, in agreement with the predictions (Cases b and c). Note that the bound state branch inside the scattering state continuum remains completely decoupled from it. This seems to be a general feature of integrable models.

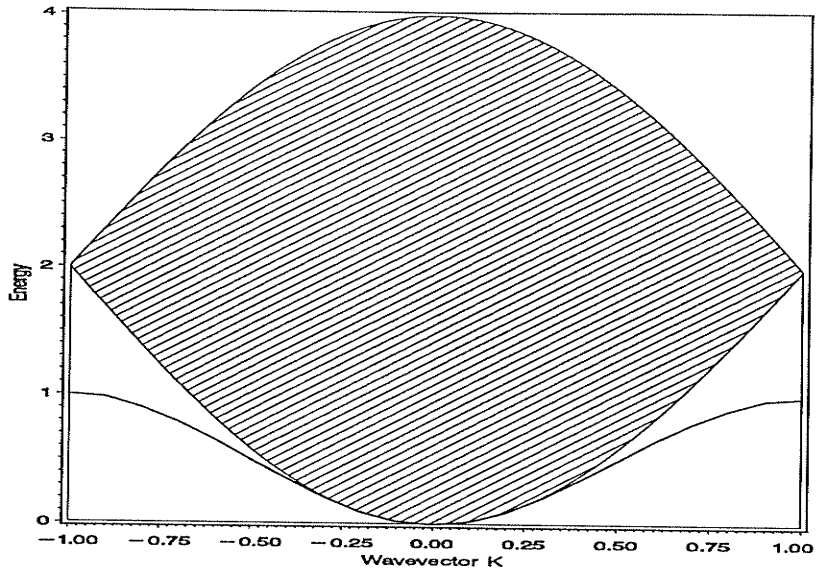

Figure 5.7: Two-magnon excitation dispersion diagram showing the bound state branch (solid line) and the scattering state continuum (shaded region) for the $S = \frac{1}{2}$ Tsvelik model with $\alpha = 0$.

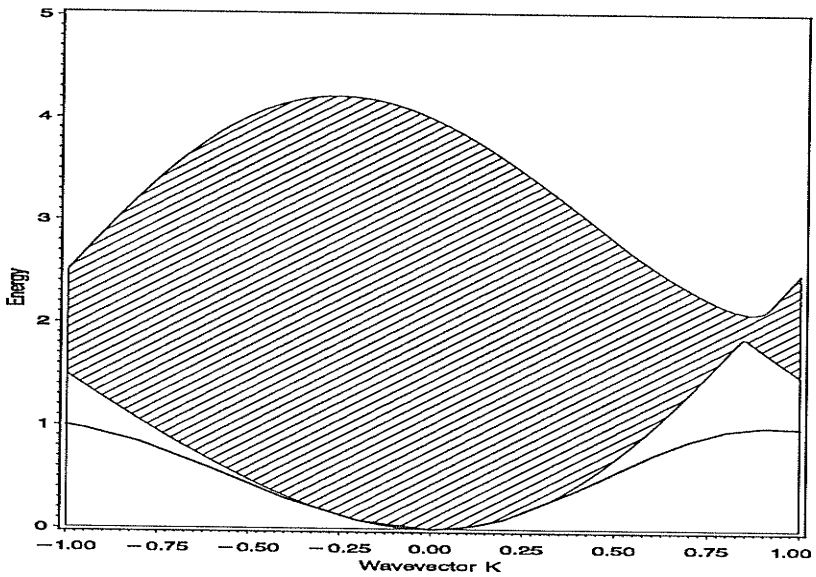

Figure 5.8: Two-magnon excitation dispersion diagram showing the bound state branch (solid line) and the scattering state continuum (shaded region) for the $S = \frac{1}{2}$ Tsvelik model with $\alpha = \frac{1}{4}$.

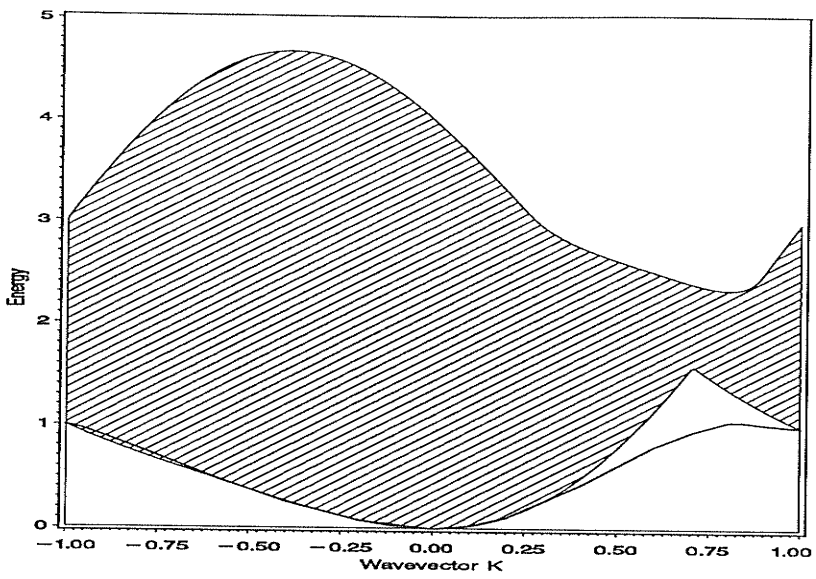

Figure 5.9: Two-magnon excitation dispersion diagram showing the bound state branch (solid line) and the scattering state continuum (shaded region) for the $S = \frac{1}{2}$ Tsvelik model with $\alpha = \frac{1}{2}$.

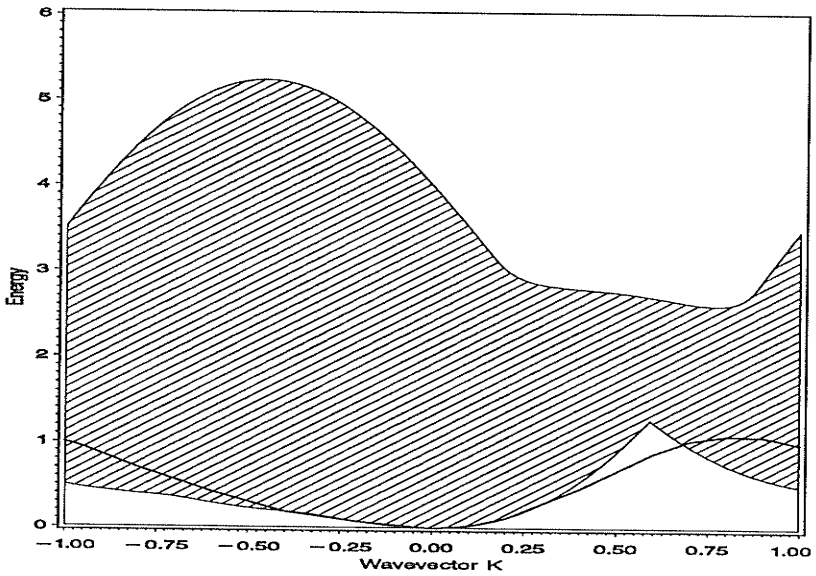

Figure 5.10: Two-magnon excitation dispersion diagram showing the bound state branch (solid line) and the scattering state continuum (shaded region) for the $S = \frac{1}{2}$ Tsvelik model with $\alpha = \frac{3}{4}$.

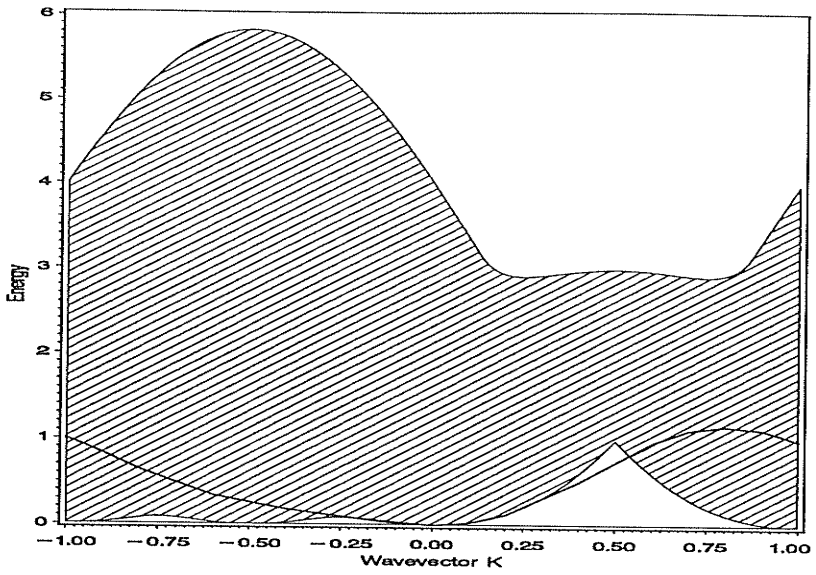

Figure 5.11: Two-magnon excitation dispersion diagram showing the bound state branch (solid line) and the scattering state continuum (shaded region) for the $S = \frac{1}{2}$ Tsvelik model with $\alpha = 1$.

Figures 5.12, 5.13 and 5.14 show the dispersion diagrams for the $S = 1$ model with $\alpha = 0, \frac{1}{2}$ and 1 respectively. At $\alpha = 0$ there is a bound state below the continuum for all values of $K \neq 0$ and this is the usual Heisenberg case. As α increases from zero the bound state touches the continuum edge at $K = \pm\pi$ when $\alpha = \frac{2}{5}$ and enters the continuum and becomes a resonance near $K = \pm\pi$. The range of the resonance increases as α increases further. The bound states are not decoupled from the continuum since the spin-1 case is non-integrable.

The dispersion relation for any given value of α can be found using this numerical procedure. This information is needed to describe the scattering state solutions of the three-magnon excitations. These excitations will be considered in the next section.

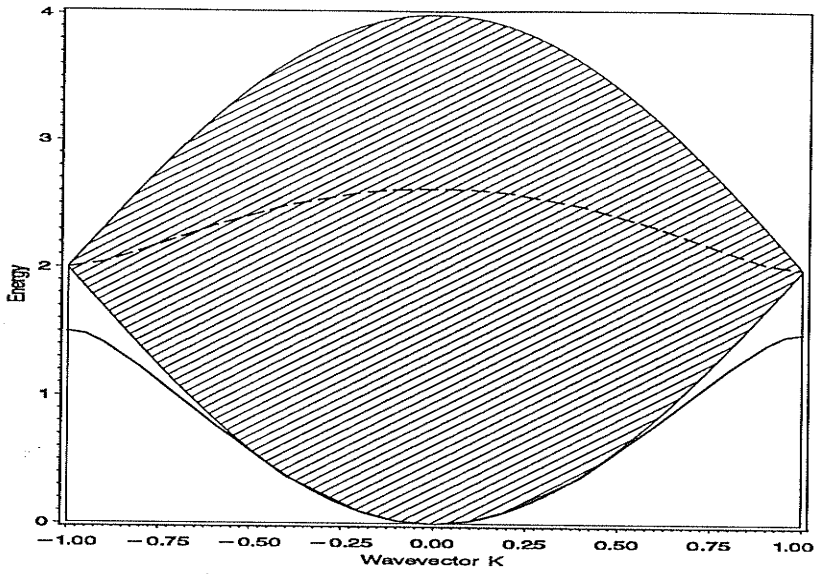

Figure 5.12: Two-magnon excitation dispersion diagram showing the bound state branch (solid line), the scattering state continuum (shaded region) and the resonance (dashed line) for the $S = 1$ Tsvelik model with $\alpha = 0$.

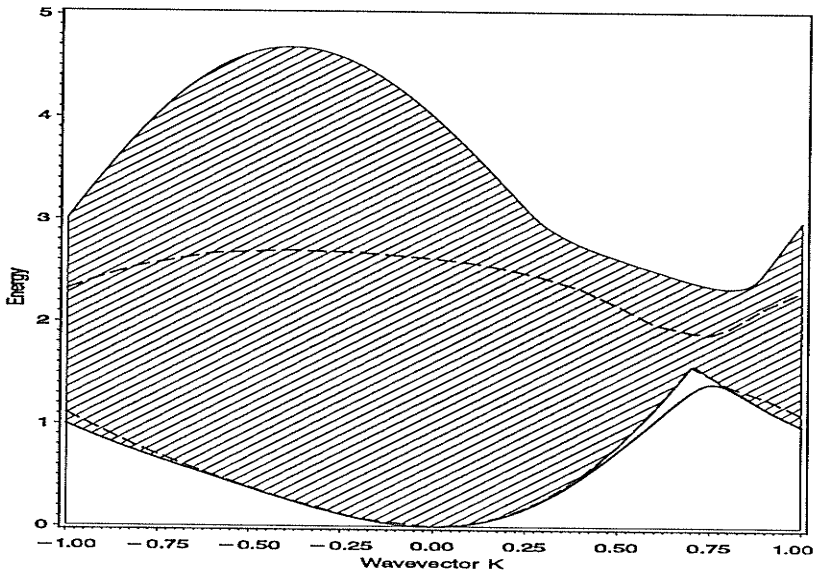

Figure 5.13: Two-magnon excitation dispersion diagram showing the bound state branch (solid line), the scattering state continuum (shaded region) and the resonances (dashed lines) for the $S = 1$ Tsvelik model with $\alpha = \frac{1}{2}$.

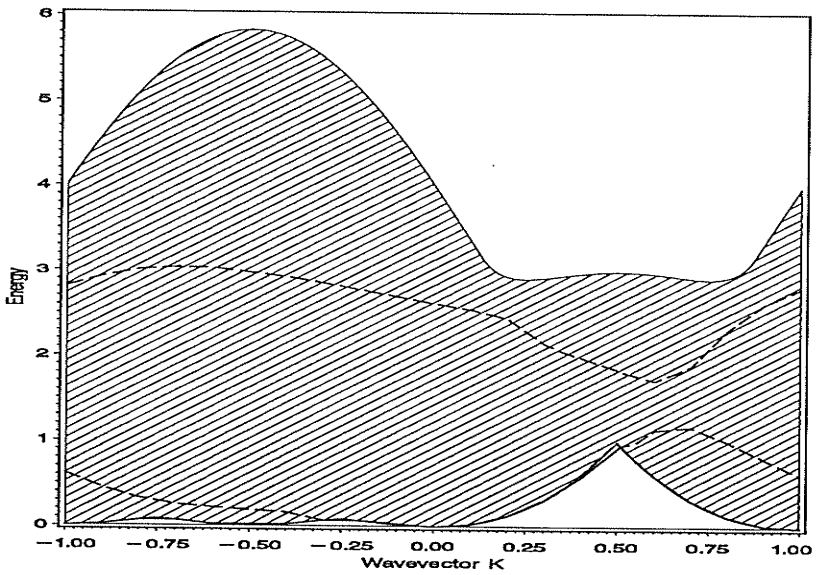

Figure 5.14: Two-magnon excitation dispersion diagram showing the bound state branch (solid line), the scattering state continuum (shaded region) and the resonances (dashed lines) for the $S = 1$ Tsvelik model with $\alpha = 1$.

5.3 Three-Magnon Excitations

The derivation of the three-magnon equations follows the method used to find the three-magnon equations of the Hamiltonian (1.5) and is included in Appendix C. The final set of equations in Appendix C, equations (C.2), (C.6) to (C.8), (C.12) to (C.14) and (C.18) to (C.20), involve kets in coordinate space (i, j, k) and can be transformed using equations (3.2) and (3.3) to kets involving the wavevector K and two relative coordinates x and y. Performing these transformations on the final equations of Appendix C, the effect of I_2 on the base kets is best expressed using the following variables:

$$\begin{aligned} t &= -iS^2\zeta J_2 \\ s &= -iS\sqrt{S(2S-1)}\zeta J_2 \\ r &= -iS\sqrt{3S(S-1)}\zeta J_2 \\ q &= iS(2-S)\zeta J_2 \\ p &= -iS(2S-1)\zeta J_2 \\ s_1 &= \left(\frac{S-1}{S}\right)s \\ t_1 &= \left(\frac{S-1}{S}\right)t \end{aligned} \tag{5.29}$$

where $\zeta = e^{i\frac{K}{3}}$. In addition to these variables we also have primed variables which are equal to the above definitions, but with the change $\zeta \to \zeta^2$. For example, $t' = -iS^2\zeta^2 J_2$. The term I_1 acting on the base kets also gives a contribution which can be found from equations (3.7) to (3.22), involving the variables (equation (3.4)):

$$\begin{aligned} \varepsilon &= 3\alpha_1(S) \\ \varepsilon_0 &= 3S(S-1)\left[\frac{1-\cos K}{S\,(4S-3)}\alpha_1(S) + \frac{1+\cos K}{(S-1)\,(4S-1)}\alpha_2(S) + \frac{1-\cos K}{3\,(S-1)\,(4S-3)}\alpha_3(S)\right] \\ \varepsilon_1 &= \frac{1}{2}\left[\frac{3\,(3S-2)}{4S-3}\alpha_1(S) + \frac{3S-1}{4S-1}\alpha_2(S) - \frac{3\,(1-S)}{4S-3}\alpha_3(S)\right] \end{aligned}$$

$$
\begin{aligned}
\varepsilon_2 &= \alpha_1(S) + 2\left(\frac{2S-1}{4S-1}\right)\alpha_2(S) \\
\varepsilon_3 &= 2\left[\alpha_1(S) + \frac{S}{4S-1}\alpha_2(S)\right] \\
\varepsilon_4 &= 2\alpha_1(S) + \frac{2S-1}{4S-1}\alpha_2(S) \\
u &= -\frac{\zeta}{2}\left[\frac{S}{4S-3}\alpha_1(S) + \frac{1-S}{4S-1}\alpha_2(S) - \frac{3(1-S)}{4S-3}\alpha_3(S)\right] \\
v &= -\frac{\zeta}{2}\alpha_1(S) \\
v_0 &= \frac{\zeta}{2}\sqrt{3S(S-1)}\left[\frac{1-\zeta^{*3}}{4S-3}\alpha_1(S) - \frac{1+\zeta^{*3}}{4S-1}\alpha_2(S) - \frac{1-\zeta^{*3}}{4S-3}\alpha_3(S)\right] \\
v_1 &= -\frac{\zeta}{2}\left[(1+\zeta^{*3})\alpha_1(S) - \frac{2S\zeta^{*3}}{4S-1}\alpha_2(S)\right] \\
w &= -\frac{\zeta\sqrt{S(2S-1)}}{4S-1}\alpha_2(S)
\end{aligned}
$$

where $\alpha_1 = 2SJ_1$, $\alpha_2 = 0$ for $S = \frac{1}{2}$, $\alpha_2 = (4S-1)J_1$ for $S \geq 1$, $\alpha_3 = 0$ for $S \leq 1$ and $\alpha_3 = (6S-3)J_1$ for $S \geq \frac{3}{2}$. The resulting three-magnon equations are:

$$
\begin{aligned}
\widehat{H} \mid K;0,0\rangle &= \varepsilon_0 \mid K;0,0\rangle + (v_0 + 2r) \mid K;0,1\rangle + (v_0^* + 2r^*) \mid K;1,0\rangle - r' \mid K;0,2\rangle \\
&\quad - r'^* \mid K;2,0\rangle \qquad (5.30) \\
\widehat{H} \mid K;0,1\rangle &= \varepsilon_1 \mid K;0,1\rangle + (v_0^* + 2r^*) \mid K;0,0\rangle + (u + 2p - q'^*) \mid K;1,0\rangle + (v_1 \\
&\quad + t + q) \mid K;0,2\rangle - t' \mid K;0,3\rangle + (w^* + s^* + s_1^* - s_1') \mid K;1,1\rangle \\
&\quad - s'^* \mid K;2,1\rangle \qquad (5.31) \\
\widehat{H} \mid K;1,0\rangle &= \varepsilon_1 \mid K;1,0\rangle + (v_0 + 2r) \mid K;0,0\rangle + (u^* + 2p^* - q') \mid K;0,1\rangle + (v_1^* \\
&\quad + t^* + q^*) \mid K;2,0\rangle - t'^* \mid K;3,0\rangle + (w + s + s_1 - s_1'^*) \mid K;1,1\rangle \\
&\quad - s' \mid K;1,2\rangle \qquad (5.32) \\
\widehat{H} \mid K;1,1\rangle &= \varepsilon_2 \mid K;1,1\rangle + (w + s + s_1 - s_1'^*) \mid K;0,1\rangle + (w^* + s^* + s_1^* \\
&\quad - s_1') \mid K;1,0\rangle + (w^* + s^* + s_1^*) \mid K;0,2\rangle + (w + s + s_1) \mid K;2,0\rangle \\
&\quad + (v + t + t_1 - t_1'^*) \mid K;1,2\rangle + (v^* + t^* + t_1^* - t_1') \mid K;2,1\rangle \\
&\quad - t' \mid K;1,3\rangle - t'^* \mid K;3,1\rangle \qquad (5.33) \\
\widehat{H} \mid K;0,2\rangle &= \varepsilon_3 \mid K;0,2\rangle - r'^* \mid K;0,0\rangle + (v_1^* + t^* + q^*) \mid K;0,1\rangle + (v_1 \\
&\quad + 2t) \mid K;0,3\rangle - t' \mid K;0,4\rangle - p' \mid K;2,0\rangle + (w + s + s_1) \mid K;1,1\rangle \\
&\quad + (w^* + 2s^*) \mid K;1,2\rangle - s'^* \mid K;2,2\rangle \qquad (5.34) \\
\widehat{H} \mid K;2,0\rangle &= \varepsilon_3 \mid K;2,0\rangle - r' \mid K;0,0\rangle + (v_1 + t + q) \mid K;1,0\rangle + (v_1^* \\
&\quad + 2t^*) \mid K;3,0\rangle - t'^* \mid K;4,0\rangle - p'^* \mid K;0,2\rangle + (w^* + s^* + s_1^*) \mid K;1,1\rangle \\
&\quad + (w + 2s) \mid K;2,1\rangle - s' \mid K;2,2\rangle \qquad (5.35) \\
\widehat{H} \mid K;1,2\rangle &= \varepsilon_4 \mid K;1,2\rangle - s'^* \mid K;1,0\rangle + (w + 2s) \mid K;0,2\rangle + (w^* + 2s^*) \mid K;0,3\rangle
\end{aligned}
$$

$$
\begin{aligned}
& - s' \mid K;3,0\rangle + (v^* + t^* + t_1^* - t_1') \mid K;1,1\rangle + (v + 2t_1) \mid K;2,1\rangle \\
& + (v + 2t - t_1'^*) \mid K;1,3\rangle - t' \mid K;1,4\rangle + (v^* + t^* + t_1^*) \mid K;2,2\rangle \\
& - t'^* \mid K;3,2\rangle \qquad (5.36)
\end{aligned}
$$

$$
\begin{aligned}
\widehat{H} \mid K;2,1\rangle \;=\; & \varepsilon_4 \mid K;2,1\rangle - s' \mid K;0,1\rangle + (w^* + 2s^*) \mid K;2,0\rangle + (w + 2s) \mid K;3,0\rangle \\
& - s'^* \mid K;0,3\rangle + (v + t + t_1 - t_1'^*) \mid K;1,1\rangle + (v^* + 2t_1^*) \mid K;1,2\rangle \\
& + (v^* + 2t^* - t_1') \mid K;3,1\rangle - t'^* \mid K;4,1\rangle + (v + t + t_1) \mid K;2,2\rangle \\
& - t' \mid K;2,3\rangle \qquad (5.37)
\end{aligned}
$$

$$
\begin{aligned}
\widehat{H} \mid K;2,2\rangle \;=\; & \varepsilon \mid K;2,2\rangle - s' \mid K;0,2\rangle - s'^* \mid K;2,0\rangle - s'^* \mid K;0,4\rangle - s' \mid K;4,0\rangle \\
& + (v+t+t_1) \mid K;1,2\rangle + (v^*+t^*+t_1^*) \mid K;2,1\rangle + (v^*+t^*+t_1^*) \mid K;1,3\rangle \\
& + (v + t + t_1) \mid K;3,1\rangle + (v + 2t) \mid K;2,3\rangle + (v^* + 2t^*) \mid K;3,2\rangle \\
& - t' \mid K;2,4\rangle - t'^* \mid K;4,2\rangle \qquad (5.38)
\end{aligned}
$$

$$
\begin{aligned}
\widehat{H} \mid K;0,y\rangle \;=\; & \varepsilon_3 \mid K;0,y\rangle - t'^* \mid K;0,y-2\rangle + (v_1^* + 2t^*) \mid K;0,y-1\rangle + (v_1 \\
& + 2t) \mid K;0,y+1\rangle - t' \mid K;0,y+2\rangle + (w + 2s) \mid K;1,y-1\rangle \\
& + (w^* + 2s^*) \mid K;1,y\rangle - s' \mid K;2,y-2\rangle - s'^* \mid K;2,y\rangle \qquad (5.39)
\end{aligned}
$$

$$
\begin{aligned}
\widehat{H} \mid K;x,0\rangle \;=\; & \varepsilon_3 \mid K;x,0\rangle - t' \mid K;x-2,0\rangle + (v_1 + 2t) \mid K;x-1,0\rangle + (v_1^* \\
& + 2t^*) \mid K;x+1,0\rangle - t'^* \mid K;x+2,0\rangle + (w^* + 2s^*) \mid K;x-1,1\rangle \\
& + (w + 2s) \mid K;x,1\rangle - s'^* \mid K;x-2,2\rangle - s' \mid K;x,2\rangle \qquad (5.40)
\end{aligned}
$$

$$
\begin{aligned}
\widehat{H} \mid K;1,y\rangle \;=\; & \varepsilon_4 \mid K;1,y\rangle + (v + 2t - t_1'^*) \mid K;1,y+1\rangle + (v^* + 2t^* - t_1') \mid K;1,y-1\rangle \\
& + (v + t + t_1) \mid K;2,y-1\rangle + (v^* + t^* + t_1^*) \mid K;2,y\rangle - t' \mid K;1,y+2\rangle \\
& - t'^* \mid K;1,y-2\rangle - t'^* \mid K;3,y\rangle - t' \mid K;3,y-2\rangle + (w + 2s) \mid K;0,y\rangle \\
& + (w^* + 2s^*) \mid K;0,y+1\rangle \qquad (5.41)
\end{aligned}
$$

$$
\begin{aligned}
\widehat{H} \mid K;x,1\rangle \;=\; & \varepsilon_4 \mid K;x,1\rangle + (v + 2t - t_1'^*) \mid K;x-1,1\rangle + (v^* + 2t^* - t_1') \mid K;x+1,1\rangle \\
& + (v + t + t_1) \mid K;x,2\rangle + (v^* + t^* + t_1^*) \mid K;x-1,2\rangle - t' \mid K;x-2,1\rangle \\
& - t'^* \mid K;x+2,1\rangle - t'^* \mid K;x-2,3\rangle - t' \mid K;x,3\rangle \\
& + (w + 2s) \mid K;x+1,0\rangle + (w^* + 2s^*) \mid K;x,0\rangle \qquad (5.42)
\end{aligned}
$$

$$
\begin{aligned}
\widehat{H} \mid K;2,y\rangle \;=\; & \varepsilon \mid K;2,y\rangle + (v + t + t_1) \mid K;1,y\rangle + (v^* + t^* + t_1^*) \mid K;1,y+1\rangle \\
& + (v + 2t) \mid K;2,y+1\rangle + (v^* + 2t^*) \mid K;2,y-1\rangle \\
& + (v + 2t) \mid K;3,y-1\rangle + (v^* + 2t^*) \mid K;3,y\rangle - t' \mid K;2,y+2\rangle \\
& - t'^* \mid K;2,y-2\rangle - t' \mid K;4,y-2\rangle + t'^* \mid K;4,y\rangle - s' \mid K;0,y\rangle \\
& - s'^* \mid K;0,y+2\rangle \qquad (5.43)
\end{aligned}
$$

$$
\begin{aligned}
\widehat{H} \mid K;x,2\rangle \;=\; & \varepsilon \mid K;x,2\rangle + (v + t + t_1) \mid K;x+1,1\rangle + (v^* + t^* + t_1^*) \mid K;x,1\rangle \\
& + (v + 2t) \mid K;x-1,2\rangle + (v^* + 2t^*) \mid K;x+1,2\rangle + (v + 2t) \mid K;x,3\rangle \\
& + (v^* + 2t^*) \mid K;x-1,3\rangle - t' \mid K;x-2,2\rangle - t'^* \mid K;x+2,2\rangle \\
& - t' \mid K;x,4\rangle - t'^* \mid K;x-2,4\rangle - s' \mid K;x+2,0\rangle \\
& - s'^* \mid K;x,0\rangle \qquad (5.44)
\end{aligned}
$$

$$
\begin{aligned}
\widehat{H} \mid K;x,y\rangle \;=\; & \varepsilon \mid K;x,y\rangle + (v + 2t) \mid K;x-1,y\rangle + (v^* + 2t^*) \mid K;x+1,y\rangle \\
& + (v^* + 2t^*) \mid K;x,y-1\rangle + (v + 2t) \mid K;x,y+1\rangle + (v^*
\end{aligned}
$$

$$+ 2t^*) \mid K; x-1, y+1\rangle + (v+2t) \mid K; x+1, y-1\rangle - t'^* \mid K; x+2, y\rangle$$
$$- t' \mid K; x-2, y\rangle - t' \mid K; x; y+2\rangle - t'^* \mid K; x, y-2\rangle$$
$$- t'^* \mid K; x-2, y+2\rangle - t' \mid K; x+2, y-2\rangle \qquad (5.45)$$

where both $x, y > 2$.

In order to visualize the interactions between the various kets, the equations can be represented graphically. Figure 5.15 shows the interactions between the nearest neighbor kets. The interactions between the next nearest neighbor even/even, even/odd, odd/even and odd/odd kets are as shown in figures 3.2 to 3.5, with the identification of the interaction symbols and site symbols as shown in figure 5.16.

As in Chapter 3, these equations lead to three different types of solutions, the three-free scattering state continuum, the two-bound one-free scattering state continuum and the three-magnon bound states. Examples of the three-magnon continua for the integrable spin-$\frac{1}{2}$ model are shown in figures 5.17 to 5.19 with $\alpha = 0, \frac{1}{2}$ and 1. The regions with the shading leaning to the left are the two-bound one-free continua and to the right are the three-free continua. The crosshatching shows the area of overlap. Figures 5.20 and 5.21 show the continua for the spin-1 model with $\alpha = 0$ and 1. These scattering state continua are important for identifying the regions where the three-magnon bound state solutions can exist. The bound state solutions must appear outside the scattering state continuum bounds for the spin-1 model, but for the spin-$\frac{1}{2}$ integrable model the bound states can exist inside these bounds. Note that the continua extend to $E = 0$ when $\alpha = 1$ at $K = 0, -\frac{\pi}{2}$ and $\pm\pi$. This indicates that the ferromagnetic state is becoming unstable to another state.

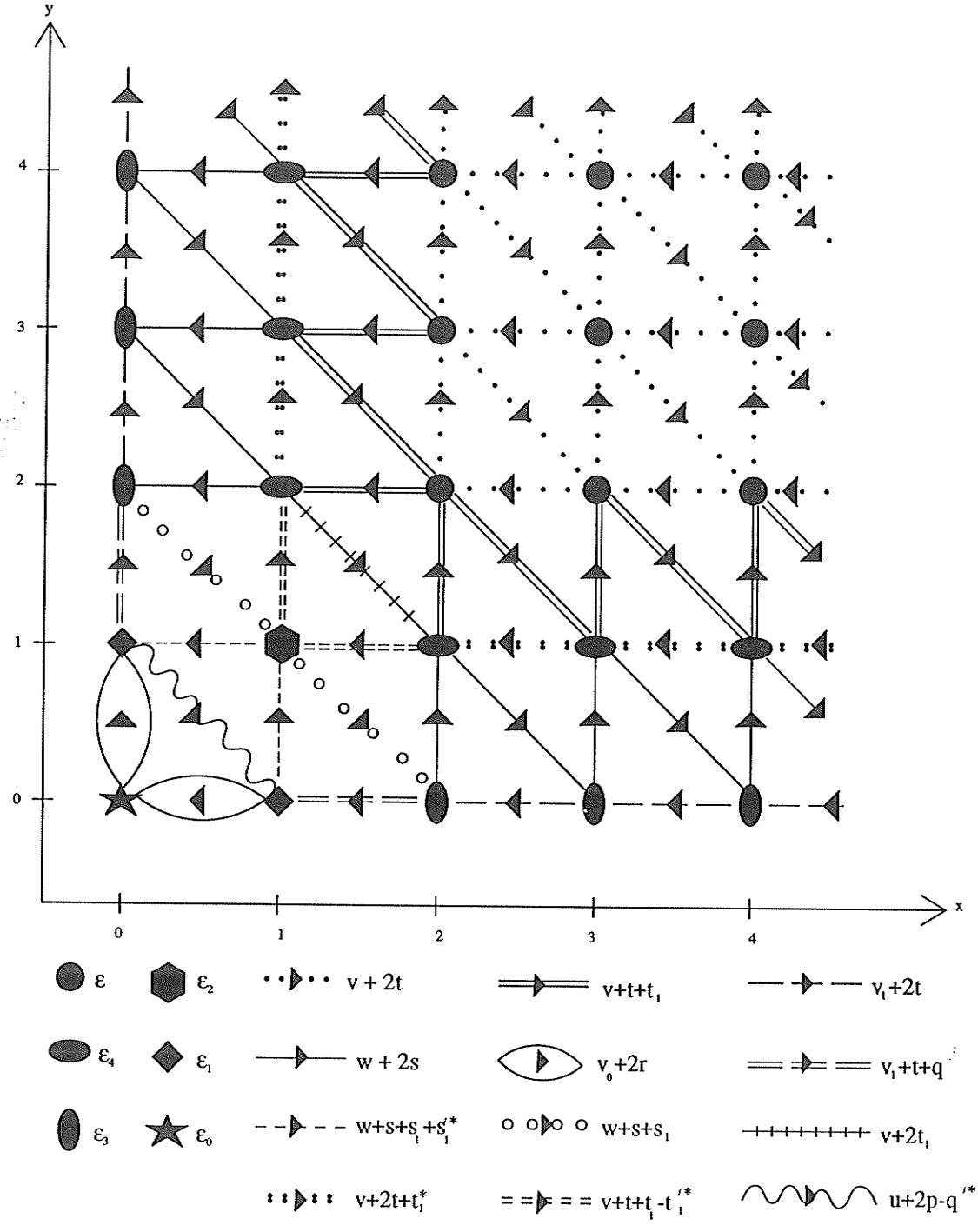

Figure 5.15: Graphical representation of the interactions between the nearest neighbor kets in the three-magnon equations.

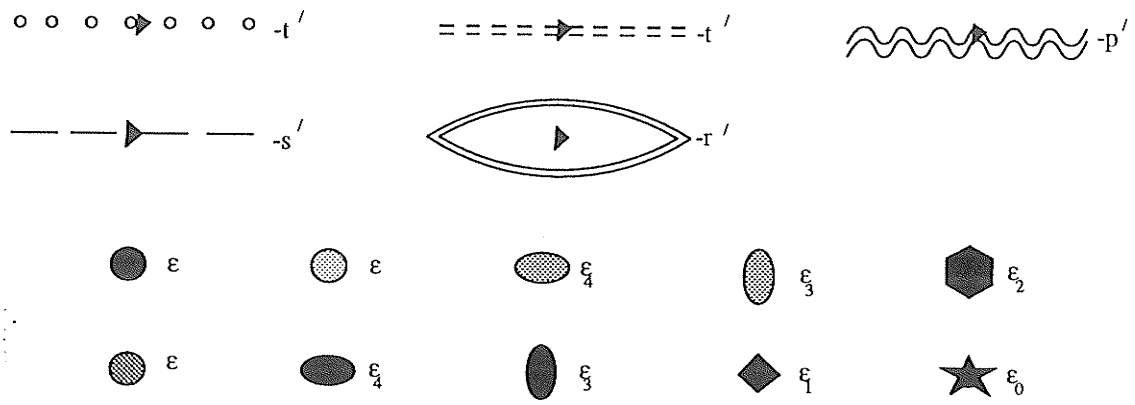

Figure 5.16: Identification of the interaction symbols between the next nearest neighbor kets and the site symbols.

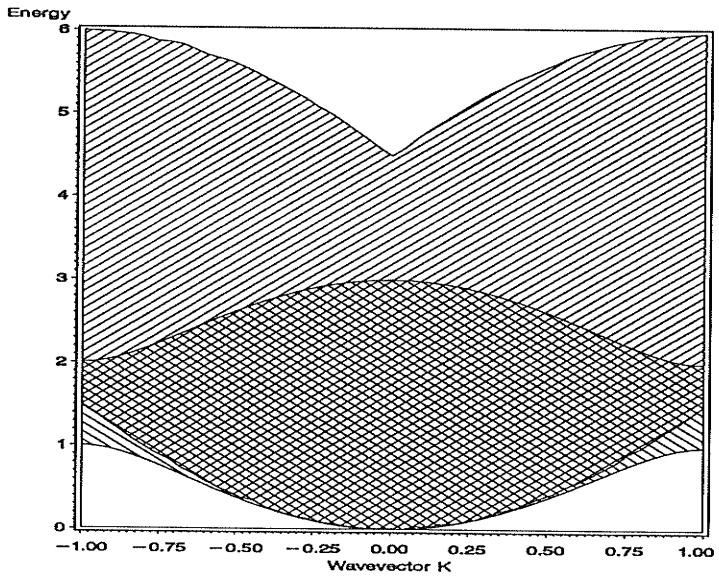

Figure 5.17: The three-magnon scattering state continuum for the $S = \frac{1}{2}$, $\alpha = 0$ Tsvelik model with energy in units of $2SJ_1$ and K in units of π.

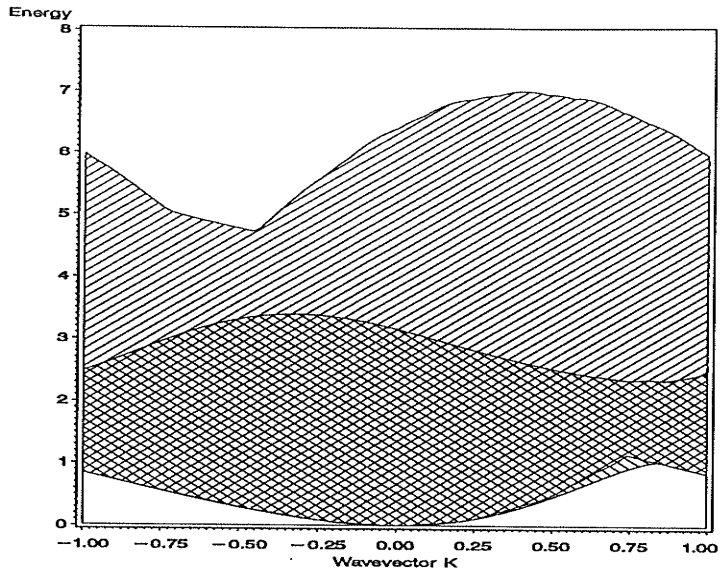

Figure 5.18: The three-magnon scattering state continuum for the $S = \frac{1}{2}$, $\alpha = \frac{1}{2}$ Tsvelik model with energy in units of $2SJ_1$ and K in units of π.

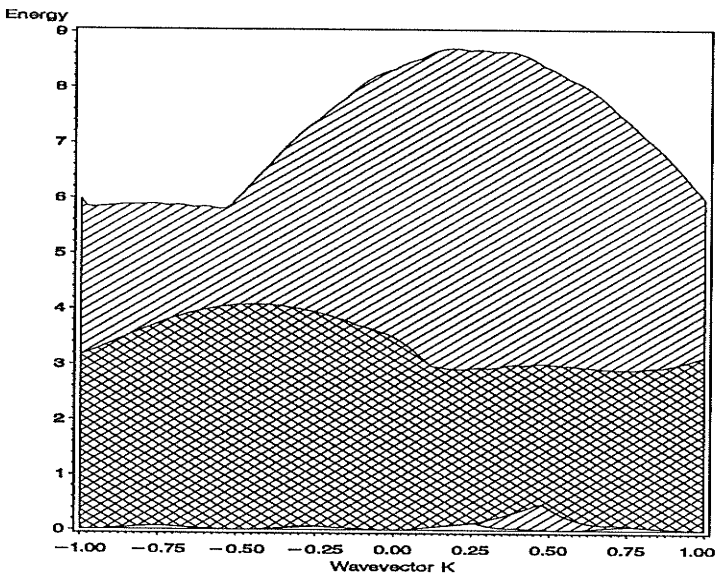

Figure 5.19: The three-magnon scattering state continuum for the $S = \frac{1}{2}$, $\alpha = 1$ Tsvelik model with energy in units of $2SJ_1$ and K in units of π.

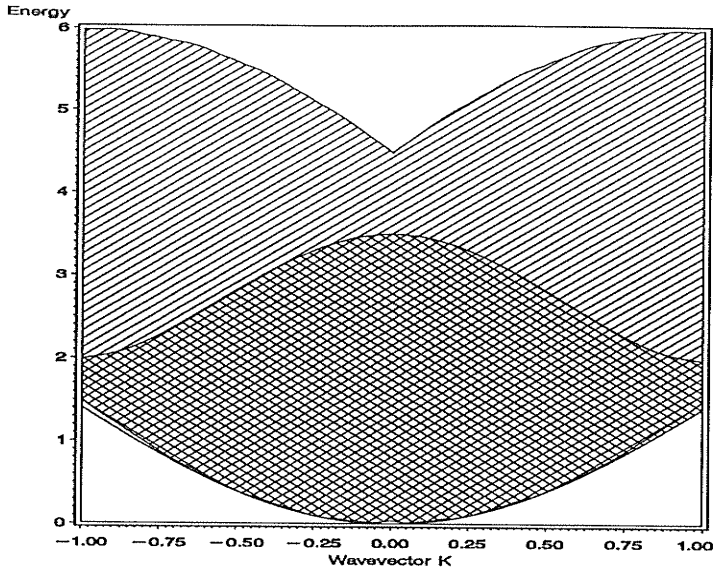

Figure 5.20: The three-magnon scattering state continuum for the $S = 1$, $\alpha = 0$ Tsvelik model with energy in units of $2SJ_1$ and K in units of π.

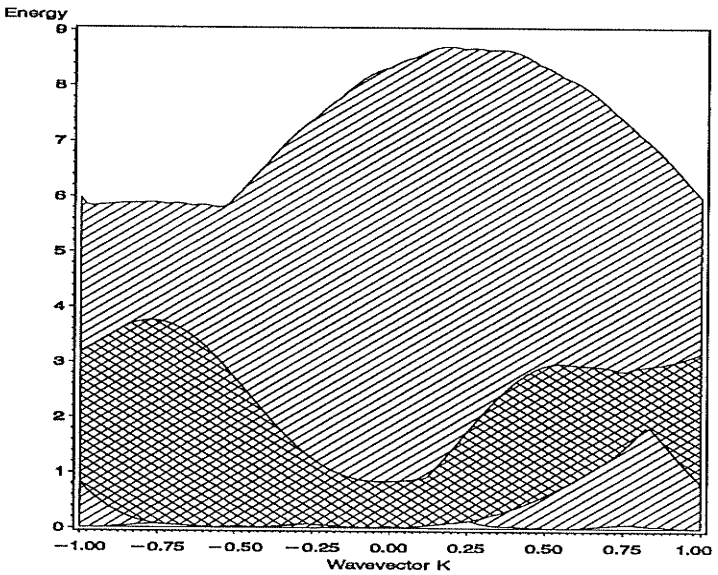

Figure 5.21: The three-magnon scattering state continuum for the $S = 1$, $\alpha = 1$ Tsvelik model with energy in units of $2SJ_1$ and K in units of π.

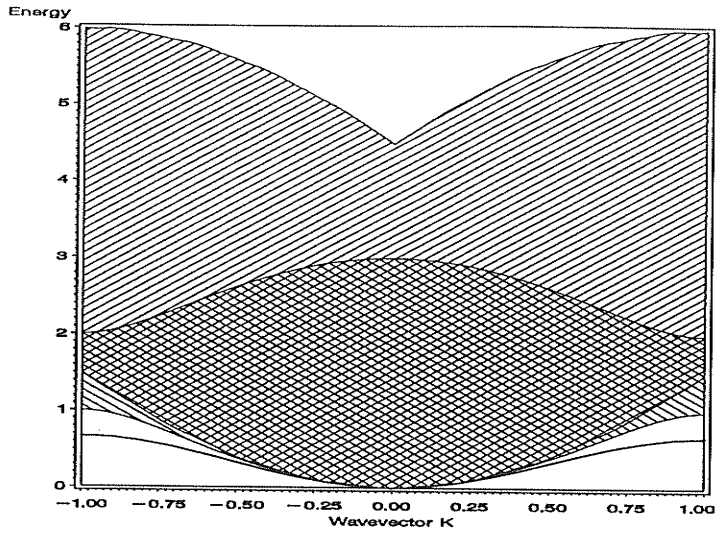

Figure 5.22: The dispersion diagram for the $S = \frac{1}{2}$, $\alpha = 0$ Tsvelik model with energy in units of $2SJ_1$ and K in units of π. The shaded area is the scattering state continuum and the solid line is the bound state.

5.4 Three-Magnon Bound States

As in Chapter 4, we will find the density of states and hence the dispersion diagrams using the Recursion Method [22].

5.4.1 The Spin-$\frac{1}{2}$ Case

The $S = \frac{1}{2}$, $\alpha = 0$ case is shown in figure 5.22, and is the nearest neighbor Heisenberg case which we have previously discussed in section 4.4. As α increases above zero the lower continuum edge decreases in energy (figure 5.24, $\alpha = \frac{1}{2}$) and as α increases further the bound state enters the continuum first near $K = \pm\pi$ and then for intermediate values of K (figure 5.24, $\alpha = 1$). These results confirm the general features of integrable models: bound states and scattering states can exist at the same energy but are completely decoupled. As one moves away from integrability, the bound states inside the continuum should broaden into resonances.

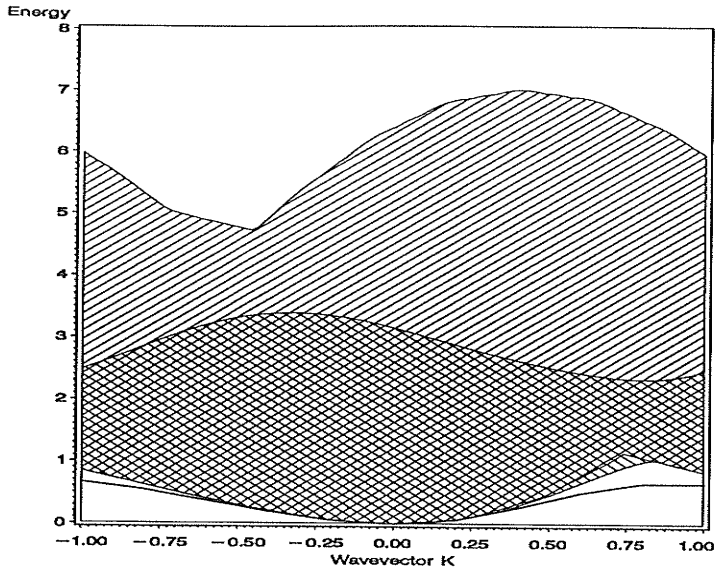

Figure 5.23: The dispersion diagram for the $S = \frac{1}{2}$, $\alpha = \frac{1}{2}$ Tsvelik model with energy in units of $2SJ_1$ and K in units of π. The shaded area is the scattering state continuum and the solid line is the bound state.

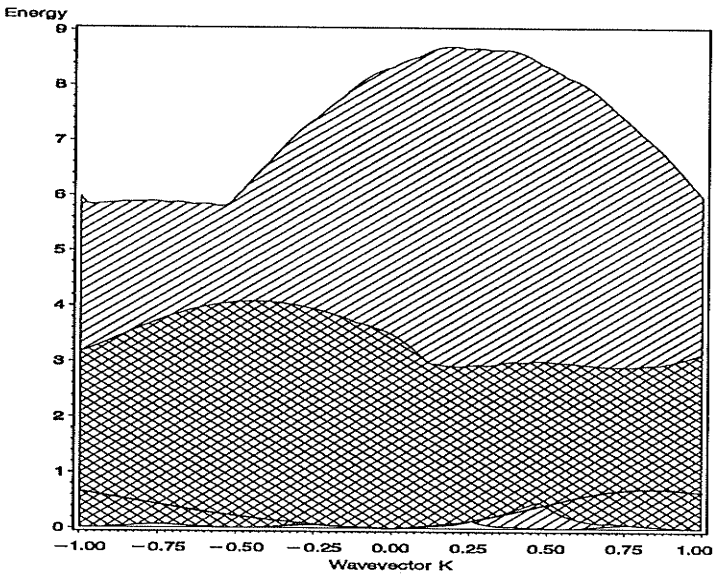

Figure 5.24: The dispersion diagram for the $S = \frac{1}{2}$, $\alpha = 1$ Tsvelik model with energy in units of $2SJ_1$ and K in units of π. The shaded area is the scattering state continuum and the solid line is the bound state.

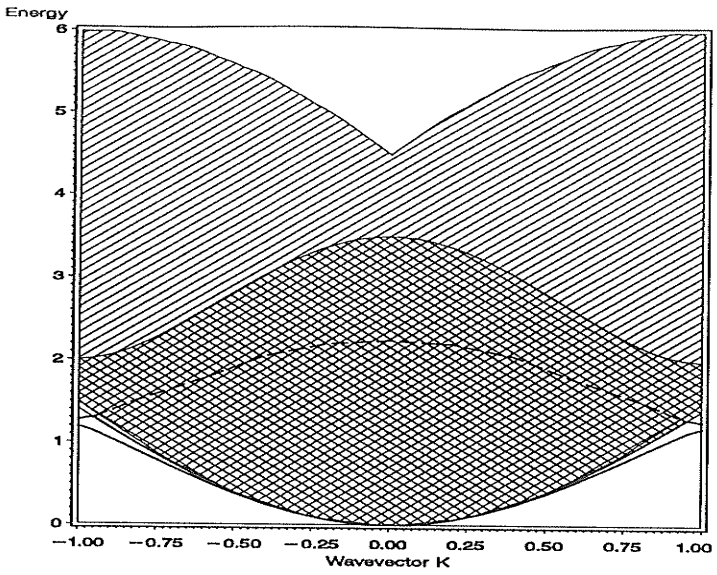

Figure 5.25: The dispersion diagram for the $S = 1$, $\alpha = 0$ Tsvelik model with energy in units of $2SJ_1$ and K in units of π. The shaded area is the scattering state continuum, the solid lines are the bound states and the dashed line is the resonance.

5.4.2 The Spin-1 Case

The $S = 1$, $\alpha = 0$ Heisenberg case, shown in figure 5.25 and previously discussed in section 4.5, has two bound states near $K = \pm\pi$. The upper bound state enters the continuum near $K = \pm\pi$ and becomes a resonance, and the lower bound state exists for all values of $K \neq 0$. At $\alpha = \frac{1}{2}$ (figure 5.26), the upper state has completely entered the continuum and is a resonance for all values of K. The lower bound state is on or near the continuum edge for values around $K \leq \frac{\pi}{2}$ (and is hard to see on the figure) and near $K = \pm\pi$ it has entered the continuum and become a resonance. When α is increased to one (figure 5.27), the lower bound state has completely entered the continuum so that there are two resonances inside the continuum. As the I_2 term drives the ferromagnetic state towards instability, the bound states disappear.

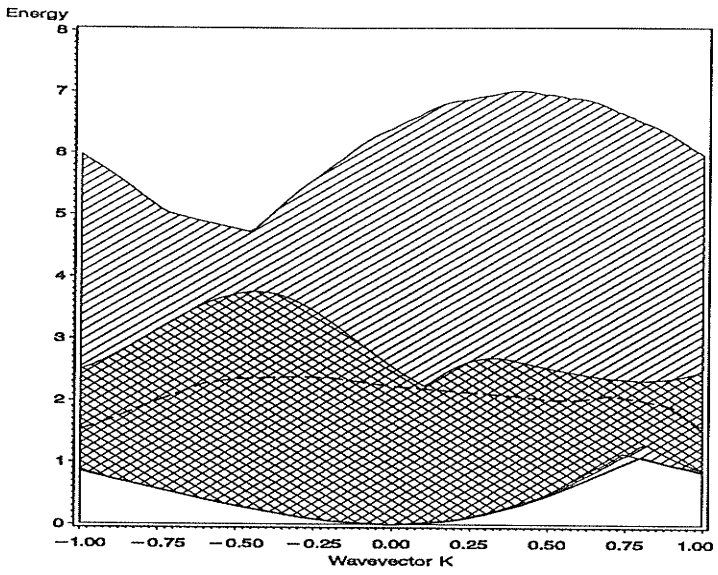

Figure 5.26: The dispersion diagram for the $S = 1$, $\alpha = \frac{1}{2}$ Tsvelik model with energy in units of $2SJ_1$ and K in units of π. The shaded area is the scattering state continuum, the solid line is the bound state and the dashed lines are the resonances.

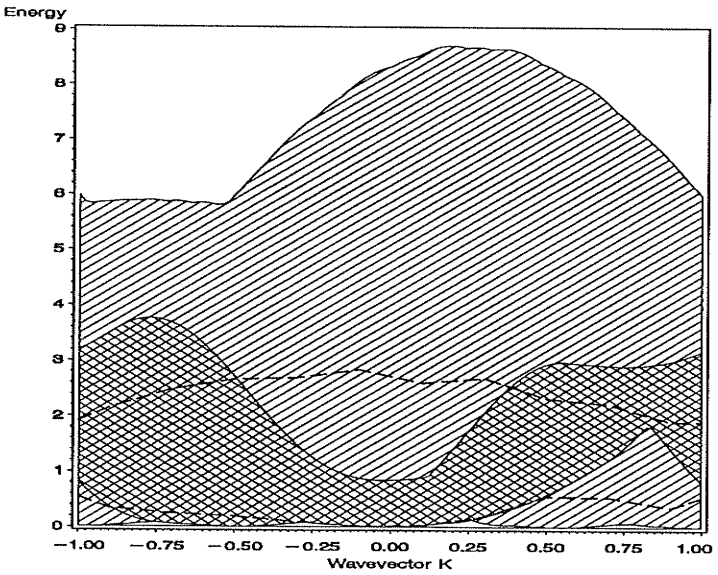

Figure 5.27: The dispersion diagram for the $S = 1$, $\alpha = 1$ Tsvelik model with energy in units of $2SJ_1$ and K in units of π. The shaded area is the scattering state continuum, the solid line is the bound state and the dashed lines are the resonances.

This concludes the discussion of the Hamiltonian (1.6). We have only studied two cases of this Hamiltonian, the $S = \frac{1}{2}$ integrable case and the $S = 1$ nonintegrable case. However, the equations have been obtained for all values of S and the method can be applied to any spin value.

Chapter 6

Summary

In this thesis we studied the one, two and three-magnon excitations of two distinct cases of nearest neighbor two-spin interactions with additional interactions beyond nearest neighbors. We only considered systems in which the ground state was ferromagnetic and in which the Hamiltonian was restricted to a uniform, homogeneous, one-dimensional lattice. The cases we studied were the Heisenberg model, the Takhtajan and Babujian model and the Tsvelik model. In all three cases we allowed for varying strengths of the next nearest neighbor interactions and changes in the spin value.

Two different types of methods were used to find solutions of the two-magnon problem. The first methods were analytic approaches which allowed us to solve for the continua boundaries and for the bound state solutions at certain values of the wavevector K (the analytic real-space rescaling method). The second method, the matrix rescaling method, found the density of states from which we could identify both bound states and resonances. Combined, these two methods allowed us to find the complete dispersion diagrams for all the cases which we considered. The methods could, of course, be used to find the dispersion diagrams of other cases which we did not consider.

For the spin-$\frac{1}{2}$ and spin-1 Heisenberg cases with the general two spin interaction

extending to second neighbors, the results were as expected. For positive values of the second neighbor interaction ($0 \leq \tilde{\beta} \leq 1$), there is one bound state below the continuum which exists for all values of $K \neq 0$ and $K \neq \pi$ for $\tilde{\beta} \geq \frac{1}{4S+1}$. For some negative values of $\tilde{\beta}$ a second bound state is found weakly separated above the continuum for a small range of K values.

For the spin-1 Takhtajan and Babujian model two bound state branches exist for all values of $\tilde{\beta}$, one below the continuum and one above. At $\tilde{\beta} = 0$ the bound state branches meet at $K = \pi$, but as $\tilde{\beta}$ increases or decreases from zero a gap appeared and grew at $K = \pi$, which is consistent with the model moving away from integrability.

For the spin-$\frac{1}{2}$ Tsvelik model there is one bound state for all values of the second neighbor interaction strength α ($-1 \leq \alpha \leq 1$), which remains a bound state even when it enters the continuum ($\alpha \geq \frac{1}{2}$). This is a general feature of integrable models. For the spin-1 Tsvelik model there is one bound state below the continuum for all values of K for $\alpha < \frac{2}{5}$, but above $\alpha = \frac{2}{5}$ the bound state enters the continuum near $K = \pm\pi$ and becomes a resonance, in agreement with this model being non-integrable.

The two-bound one-free continua and the three-free continua were found numerically and combined to find the three-magnon continua. The recursion method was used to find the three-magnon density of states and thus the bound states and the resonances. For the spin-$\frac{1}{2}$ Heisenberg case we find one bound state present below the continuum for all values of $\tilde{\beta}$, with the addition of another bound state close to the lower continuum edge for intermediate values of K and $\tilde{\beta}$, which enters the continuum and becomes a resonance. For the spin-1 Heisenberg case there are two bound states below the continuum for $\tilde{\beta} \leq 0$. The upper of these two bound states enters the continuum near $K = \pi$ and becomes a resonance. As $\tilde{\beta}$ increases

above zero the upper bound state is present for a shorter range of K and emerges from the continuum at lower values of K. As $\tilde{\beta} \to 1$ this resonance emerges as a bound state near $K = \frac{\pi}{2}$. The lower bound state is present for all values of $\tilde{\beta}$ and K.

We also studied the $S = 1$ and $S = \frac{3}{2}$ Takhtajan and Babujian model, in which we find that as $\tilde{\beta}$ moves away from zero and integrability, gaps open up between the bound states and any bound states which enter the continuum becomes resonances. In addition for non-integrable values of $\tilde{\beta}$ we find a bound state weakly separated from the upper continuum which is present for a short range of $K \approx 0$ for $\tilde{\beta} > 0$ and for a larger range of $K \leq \pi$ for $\tilde{\beta} < 0$.

The spin-$\frac{1}{2}$ and spin-1 Tsvelik cases were also studied. For $\alpha = 0$ and $S = \frac{1}{2}$ there is one bound state below the continuum and for the $S = 1$ there are two, the upper of which enters the continuum and becomes a resonance near $K = \pi$. For both cases as $\alpha \to 1$ the lower continuum edge decreases towards zero, causing the bound states to enter the continuum. For the spin-$\frac{1}{2}$ case the bound state remains decoupled from the continuum and for the spin-1 case the bound states become resonances. This confirms the integrability of the spin-$\frac{1}{2}$ case and the non-integrability of the spin-1 case.

Although we have restricted our study to relatively simple systems, it would not be difficult to include (for example) alternating spins, anisotropic spin exchange, single-ion anisotropies and the effects of an external field. The methods we have used would still be applicable after such additions.

Appendix A

Derivation of Three-Magnon Excitation Equations

This appendix includes the main steps and equations in the derivation of the three-magnon excitation equations of the Hamiltonian (1.5). The method followed is that of the derivation of the one and two-magnon excitation equations.

The orthonormal base kets are defined as before, with three raising operators on sites i, j and k acting on the ground state ket

$$\mid i,j,k\rangle = C_{ijk} S_i^+ S_j^+ S_k^+ \mid 0\rangle \tag{A.1}$$

$$C_{ijk} = \begin{cases} \frac{1}{\sqrt{8S^3}} & \text{if } i \neq j \neq k \\ \frac{1}{\sqrt{8S^2(2S-1)}} & \text{if 2 of } \{ijk\} \text{ are equal} \\ \frac{1}{\sqrt{24S(2S-1)(S-1)}} & \text{if } i = j = k \end{cases}$$

where the C_{ijk} are normalization constants.

Let $\tilde{P}_l$ and $\tilde{Q}_l$ act on the above states. First consider the case of $\tilde{P}_l$ acting on kets with three spin deviations separated by more than nearest neighbors ($i+1 < j, j+1 < k$) and then consider $\tilde{Q}_l$ acting on kets with three spin deviations separated by more than second nearest neighbors ($i+2 < j, j+2 < k$).

$$\left.\begin{array}{rcll} \tilde{P}_l \mid i,j,k\rangle &=& S^2 \mid i,j,k\rangle & ,i,j,k \neq l, l+1 \\ \tilde{P}_l \mid i,j,l\rangle &=& S(S-1) \mid i,j,l\rangle + S \mid i,j,l+1\rangle & ,k = l \\ \tilde{P}_l \mid i,j,l+1\rangle &=& S \mid i,j,l\rangle + S(S-1) \mid i,j,l+1\rangle & ,k = l+1 \end{array}\right\}$$

$$\left.\begin{array}{rcll} \widetilde{Q}_l \mid i,j,k\rangle &=& S^2 \mid i,j,k\rangle & ,i,j,k \neq l,l+2 \\ \widetilde{Q}_l \mid i,j,l\rangle &=& S(S-1) \mid i,j,l\rangle + S \mid i,j,l+2\rangle & ,k=l \\ \widetilde{Q}_l \mid i,j,l+2\rangle &=& S \mid i,j,l\rangle + S(S-1) \mid i,j,l+2\rangle & ,k=l+2 \end{array}\right\} \quad \text{(A.2)}$$

The matrix form of $\widetilde{P}_l$ (and $\widetilde{Q}_l$) acting on the base kets of three deviations separated by more than nearest neighbors (second nearest neighbors) are:

$$\begin{aligned} \widetilde{P}_l \begin{pmatrix} \mid i,j,k\rangle \\ \mid i,j,l\rangle \\ \mid i,j,l+1\rangle \end{pmatrix} &= \mathbf{A} \begin{pmatrix} \mid i,j,k\rangle \\ \mid i,j,l\rangle \\ \mid i,j,l+1\rangle \end{pmatrix} \\ \widetilde{Q}_l \begin{pmatrix} \mid i,j,l\rangle \\ \mid i,j,l+2\rangle \\ \mid i,j,l+1\rangle \end{pmatrix} &= \mathbf{A} \begin{pmatrix} \mid i,j,l\rangle \\ \mid i,j,l+2\rangle \\ \mid i,j,l+1\rangle \end{pmatrix} \end{aligned} \quad \text{(A.3)}$$

where matrix $\mathbf{A}$ is defined in equation (2.14). Following this method one can find the effects of $\widetilde{P}_l$ (and $\widetilde{Q}_l$) acting on kets with two deviations on the same site or nearest neighbor sites (or next nearest neighbor sites) and the other spin deviation farther than nearest neighbors (next nearest neighbors) from either of the other two deviations.

$$\left.\begin{array}{rcl} \widetilde{P}_l \mid i,l,l\rangle &=& S(S-2) \mid i,l,l\rangle + \sqrt{S(2S-1)} \mid i,l,l+1\rangle \\ \widetilde{P}_l \mid i,l,l+1\rangle &=& (S-1)^2 \mid i,l,l+1\rangle + \sqrt{S(2S-1)}[\mid i,l,l\rangle + \mid i,l+1,l+1\rangle] \\ \widetilde{P}_l \mid i,l+1,l+1\rangle &=& \sqrt{S(2S-1)} \mid i,l,l+1\rangle + S(S-2) \mid i,l+1,l+1\rangle \end{array}\right\}$$
$$\left.\begin{array}{rcl} \widetilde{Q}_l \mid i,l,l\rangle &=& S(S-2) \mid i,l,l\rangle + \sqrt{S(2S-1)} \mid i,l,l+2\rangle \\ \widetilde{Q}_l \mid i,l,l+2\rangle &=& (S-1)^2 \mid i,l,l+2\rangle + \sqrt{S(2S-1)}[\mid i,l,l\rangle + \mid i,l+2,l+2\rangle] \\ \widetilde{Q}_l \mid i,l+2,l+2\rangle &=& \sqrt{S(2S-1)} \mid i,l,l+2\rangle + S(S-2) \mid i,l+2,l+2\rangle \end{array}\right\} \quad \text{(A.4)}$$

From these equations we find the matrix form of $\widetilde{P}_l$ and $\widetilde{Q}_l$ acting on these states to be

$$\begin{aligned} \widetilde{P}_l \begin{pmatrix} \mid i,l,l\rangle \\ \mid i,l,l+1\rangle \\ \mid i,l+1,l+1\rangle \end{pmatrix} &= \mathbf{B} \begin{pmatrix} \mid i,l,l\rangle \\ \mid i,l,l+1\rangle \\ \mid i,l+1,l+1\rangle \end{pmatrix} \\ \widetilde{Q}_l \begin{pmatrix} \mid i,l,l\rangle \\ \mid i,l,l+2\rangle \\ \mid i,l+2,l+2\rangle \end{pmatrix} &= \mathbf{B} \begin{pmatrix} \mid i,l,l\rangle \\ \mid i,l,l+2\rangle \\ \mid i,l+2,l+2\rangle \end{pmatrix} \end{aligned} \quad \text{(A.5)}$$

where matrix $\mathbf{B}$ is the matrix defined in equation (2.36). One can also find the effects of $\widetilde{P}_l$ (and $\widetilde{Q}_l$) acting on kets with all three spin deviations on the same site, or kets with two spin deviations on the same site and the other deviation on a nearest neighbor site (next nearest neighbor site).

$$\left.\begin{aligned}
\widetilde{P}_l \mid l,l,l\rangle &= S(S-3) \mid l,l,l\rangle + \sqrt{3S(S-1)} \mid l,l,l+1\rangle \\
\widetilde{P}_l \mid l,l,l+1\rangle &= \sqrt{3S(S-1)} \mid l,l,l\rangle + (S^2-3S+2) \mid l,l,l+1\rangle \\
&\quad + (2S-1) \mid l,l+1,l+1\rangle \\
\widetilde{P}_l \mid l,l+1,l+1\rangle &= (2S-1) \mid l,l,l+1\rangle + (S^2-3S+2) \mid l,l+1,l+1\rangle \\
&\quad + \sqrt{3S(S-1)} \mid l+1,l+1,l+1\rangle \\
\widetilde{P}_l \mid l+1,l+1,l+1\rangle &= S(S-3) \mid l+1,l+1,l+1\rangle + \\
&\quad \sqrt{3S(S-1)} \mid l,l+1,l+1\rangle
\end{aligned}\right\}$$

$$\left.\begin{aligned}
\widetilde{Q}_l \mid l,l,l\rangle &= S(S-3) \mid l,l,l\rangle + \sqrt{3S(S-1)} \mid l,l,l+2\rangle \\
\widetilde{Q}_l \mid l,l,l+2\rangle &= \sqrt{3S(S-1)} \mid l,l,l\rangle + (S^2-3S+2) \mid l,l,l+2\rangle \\
&\quad + (2S-1) \mid l,l+2,l+2\rangle \\
\widetilde{Q}_l \mid l,l+2,l+2\rangle &= (2S-1) \mid l,l,l+2\rangle + (S^2-3S+2) \mid l,l+2,l+2\rangle \\
&\quad + \sqrt{3S(S-1)} \mid l+2,l+2,l+2\rangle \\
\widetilde{Q}_l \mid l+2,l+2,l+2\rangle &= S(S-3) \mid l+2,l+2,l+2\rangle + \\
&\quad \sqrt{3S(S-1)} \mid l,l+2,l+2\rangle
\end{aligned}\right\} \quad \text{(A.6)}$$

Thus the matrix forms of $\widetilde{P}_l$ and $\widetilde{Q}_l$ acting on these base kets are found to be

$$\begin{aligned}
\widetilde{P}_l \begin{pmatrix} \mid l,l,l\rangle \\ \mid l,l,l+1\rangle \\ \mid l,l+1,l+1\rangle \\ \mid l+1,l+1,l+1\rangle \end{pmatrix} &= \mathbf{C} \begin{pmatrix} \mid l,l,l\rangle \\ \mid l,l,l+1\rangle \\ \mid l,l+1,l+1\rangle \\ \mid l+1,l+1,l+1\rangle \end{pmatrix} \\
\widetilde{Q}_l \begin{pmatrix} \mid l,l,l\rangle \\ \mid l,l,l+2\rangle \\ \mid l,l+2,l+2\rangle \\ \mid l+2,l+2,l+2\rangle \end{pmatrix} &= \mathbf{C} \begin{pmatrix} \mid l,l,l\rangle \\ \mid l,l,l+2\rangle \\ \mid l,l+2,l+2\rangle \\ \mid l+2,l+2,l+2\rangle \end{pmatrix}
\end{aligned} \quad \text{(A.7)}$$

where matrix $\mathbf{C}$ is

$$\mathbf{C} = \begin{bmatrix} S(S-3) & \sqrt{3S(S-1)} & 0 & 0 \\ \sqrt{3S(S-1)} & (S^2-3S+2) & (2S-1) & 0 \\ 0 & (2S-1) & (S^2-3S+2) & \sqrt{3S(S-1)} \\ 0 & 0 & \sqrt{3S(S-1)} & S(S-3) \end{bmatrix} \quad \text{(A.8)}$$

The n^{th} power of the matrices are needed in order to substitute into equation (2.2) to find the effects of $\widehat{H}_l$ acting on the above kets. Matrix $\mathbf{A}^n$ is given in

equation (2.15) and matrix $\mathbf{B}^n$ is given in equation (2.36). Matrix $\mathbf{C}^n$ is:

$$\mathbf{C}^n = \begin{bmatrix} m_{11} - S^{2n} & m_{12} & m_{13} & m_{14} \\ m_{12} & m_{22} - S^{2n} & m_{23} & m_{13} \\ m_{13} & m_{23} & m_{22} - S^{2n} & m_{12} \\ m_{14} & m_{13} & m_{12} & m_{11} - S^{2n} \end{bmatrix} \tag{A.9}$$

where

$$\begin{aligned}
m_{11} &= \frac{-3}{2}(S-1)\left[\frac{S^{2n}-S^n(S-2)^n}{S(4S-3)}+\frac{S^{2n}-(S^2-4S+1)^n}{(S-1)(4S-1)}+\frac{S^{2n}-(S^2-6S+3)^n}{3(S-1)(4S-3)}\right] \\
m_{12} &= \frac{-1}{2}\sqrt{3S(S-1)}\left[\frac{S^{2n}-S^n(S-2)^n}{(4S-3)}-\frac{S^{2n}-(S^2-4S+1)^n}{(4S-1)}\right. \\
&\quad \left.-\frac{S^{2n}-(S^2-6S+3)^n}{(4S-3)}\right] \\
m_{13} &= \frac{-1}{2}\sqrt{3S(S-1)}\left[-\frac{S^{2n}-S^n(S-2)^n}{(4S-3)}-\frac{S^{2n}-(S^2-4S+1)^n}{(4S-1)}\right. \\
&\quad \left.+\frac{S^{2n}-(S^2-6S+3)^n}{(4S-3)}\right] \\
m_{14} &= \frac{3}{2}S(S-1)\left[\frac{S^{2n}-S^n(S-2)^n}{S(4S-3)}-\frac{S^{2n}-(S^2-4S+1)^n}{(S-1)(4S-1)}+\frac{S^{2n}-(S^2-6S+3)^n}{3(S-1)(4S-3)}\right] \\
m_{22} &= \frac{-1}{2}\left[S\frac{S^{2n}-S^n(S-2)^n}{(4S-3)}+(S-1)\frac{S^{2n}-(S^2-4S+1)^n}{(4S-1)}\right. \\
&\quad \left.+3(S-1)\frac{S^{2n}-(S^2-6S+3)^n}{(4S-3)}\right] \\
m_{23} &= \frac{-1}{2}\left[-S\frac{S^{2n}-S^n(S-2)^n}{(4S-3)}+(S-1)\frac{S^{2n}-(S^2-4S+1)^n}{(4S-1)}\right. \\
&\quad \left.-3(S-1)\frac{S^{2n}-(S^2-6S+3)^n}{(4S-3)}\right]
\end{aligned} \tag{A.10}$$

Once again absorb the ground state energy into a shift in the zero of the energy. From equation (2.2) and the matrix $\mathbf{A}^n$, one can obtain the following results for $\widehat{H}_l$ acting on base kets with i, j, and k separated by more than second nearest neighbors.

$$\widehat{H}_l \mid i,j,k\rangle \;=\; \begin{cases} 0 \mid i,j,k\rangle & i,j,k \neq l, l+1, l+2 \\ \frac{\alpha_1+\alpha_1'}{2} \mid i,j,l\rangle - \frac{\alpha_1}{2} \mid i,j,l+1\rangle - \frac{\alpha_1'}{2} \mid i,j,l+2\rangle & \\ \qquad , k = l & \\ \frac{\alpha_1}{2} \mid i,j,l+1\rangle - \frac{\alpha_1}{2} \mid i,j,l\rangle & , k = l+1 \\ \frac{\alpha_1'}{2} \mid i,j,l+2\rangle - \frac{\alpha_1'}{2} \mid i,j,l\rangle & , k = l+2 \end{cases} \tag{A.11}$$

Similar equations are found for $\widehat{H}_l$ acting on kets with $i = l, l+1, l+2$ or $j = l, l+1, l+2$. Therefore for three spin deviations separated by more that second nearest neighbors, the full Hamiltonian is:

$$\begin{aligned} \widehat{H} \mid i,j,k\rangle \;=\; & 3(\alpha_1+\alpha_1') \mid i,j,k\rangle - \frac{\alpha_1'}{2}[\mid i-2,j,k\rangle + \mid i+2,j,k\rangle + \mid i,j-2,k\rangle \\ & + \mid i,j+2,k\rangle + \mid i,j,k-2\rangle + \mid i,j,k+2\rangle] - \frac{\alpha_1}{2}[\mid i-1,j,k\rangle \\ & + \mid i+1,j,k\rangle + \mid i,j-1,k\rangle + \mid i,j+1,k\rangle + \mid i,j,k-1\rangle \\ & + \mid i,j,k+1\rangle] \end{aligned} \tag{A.12}$$

Similarly, from equation (2.1) and the matrices $\mathbf{A}^n$ and $\mathbf{B}^n$, one can obtain the equations for $\widehat{H}_l$ acting on the kets $\mid i,j,j\rangle, \mid i,j,j+1\rangle, \mid i,j,j+2\rangle, \mid i,i,j\rangle$, $\mid i-1,i,j\rangle$ and $\mid i-2,i,j\rangle$. Then the equations for the full Hamiltonian acting on kets with two spin deviations on the same site, nearest neighbor sites, or second nearest neighbor sites, and the other deviation farther than second nearest neighbors from either of the other two deviations can be found.

$$\widehat{H}_l \mid i,j,j+2\rangle =$$

$$\begin{cases} 0 \mid i,j,j+2\rangle & i \neq l,l+1,l+2, j \neq l-2,l-1,l,l+1,l+2 \\ \frac{\alpha_1+\alpha_1'}{2} \mid l,j,j+2\rangle - \frac{\alpha_1}{2} \mid l+1,j,j+2\rangle - \frac{\alpha_1'}{2} \mid l+2,j,j+2\rangle & ,i=l \\ \frac{\alpha_1}{2} \mid l+1,j,j+2\rangle - \frac{\alpha_1}{2} \mid l,j,j+2\rangle & ,i=l+1 \\ \frac{\alpha_1'}{2} \mid l+2,j,j+2\rangle - \frac{\alpha_1'}{2} \mid l,j,j+2\rangle & ,i=l+2 \\ \frac{\alpha_1+\alpha_1'}{2} \mid i,l-2,l\rangle - \frac{\alpha_1}{2} \mid i,l-2,l+1\rangle - \frac{\alpha_1'}{2} \mid i,l-2,l+2\rangle & ,j=l-2 \\ \frac{\alpha_1}{2} \mid i,l-1,l+1\rangle - \frac{\alpha_1}{2} \mid i,l-1,l\rangle & ,j=l-1 \\ \left(\frac{\alpha_1}{2}+\frac{2S-1}{4S-1}\alpha_2'\right) \mid i,l,l+2\rangle - \frac{\sqrt{S(2S-1)}}{4S-1}\alpha_2' [\mid i,l,l\rangle + \mid i,l+2,l+2\rangle] & \\ \quad -\frac{\alpha_1}{2} \mid i,l+1,l+2\rangle & ,j=l \\ \frac{\alpha_1}{2} \mid i,l+1,l+3\rangle - \frac{\alpha_1}{2} \mid i,l,l+3\rangle & ,j=l+1 \\ \frac{\alpha_1'}{2} \mid i,l+2,l+4\rangle - \frac{\alpha_1'}{2} \mid i,l,l+4\rangle & ,j=l+2 \end{cases} \tag{A.13}$$

$$\widehat{H}_l \mid i,j,j+1\rangle =$$

$$\begin{cases} 0 \mid i,j,j+1\rangle & i \neq l,l+1,l+2, j \neq l-1,l,l+1,l+2 \\ \frac{\alpha_1+\alpha_1'}{2} \mid l,j,j+1\rangle - \frac{\alpha_1}{2} \mid l+1,j,j+1\rangle - \frac{\alpha_1'}{2} \mid l+2,j,j+1\rangle & ,i=l \\ \frac{\alpha_1}{2} \mid l+1,j,j+1\rangle - \frac{\alpha_1}{2} \mid l,j,j+1\rangle & ,i=l+1 \\ \frac{\alpha_1'}{2} \mid l+2,j,j+1\rangle - \frac{\alpha_1'}{2} \mid l,j,j+1\rangle & ,i=l+2 \\ \frac{\alpha_1+\alpha_1'}{2} \mid i,l-1,l\rangle - \frac{\alpha_1}{2} \mid i,l-1,l+1\rangle - \frac{\alpha_1'}{2} \mid i,l-1,l+2\rangle & ,j=l-1 \\ \left(\frac{\alpha_1'}{2}+\frac{2S-1}{4S-1}\alpha_2\right) \mid i,l,l+1\rangle - \frac{\sqrt{S(2S-1)}}{4S-1}\alpha_2 [\mid i,l,l\rangle + \mid i,l+1,l+1\rangle] & \\ \quad -\frac{\alpha_1'}{2} \mid i,l+1,l+2\rangle & ,j=l \\ \frac{\alpha_1+\alpha_1'}{2} \mid i,l+1,l+2\rangle - \frac{\alpha_1}{2} \mid i,l,l+2\rangle - \frac{\alpha_1'}{2} \mid i,l,l+1\rangle & ,j=l+1 \\ \frac{\alpha_1'}{2} \mid i,l+2,l+3\rangle - \frac{\alpha_1'}{2} \mid i,l,l+3\rangle & ,j=l+2 \end{cases} \tag{A.14}$$

$$\widehat{H}_l \mid i,j,j\rangle =$$

$$\begin{cases} 0 \mid i,j,j\rangle & ,i,j \neq l,l+1,l+2 \\ \frac{\alpha_1+\alpha_1'}{2} \mid l,j,j\rangle - \frac{\alpha_1}{2} \mid l+1,j,j\rangle - \frac{\alpha_1'}{2} \mid l+2,j,j\rangle & ,i=l \\ \frac{\alpha_1}{2} \mid l+1,j,j\rangle - \frac{\alpha_1}{2} \mid l,j,j\rangle & ,i=l+1 \\ \frac{\alpha_1'}{2} \mid l+2,j,j\rangle - \frac{\alpha_1'}{2} \mid l,j,j\rangle & ,i=l+2 \\ \left(\frac{\alpha_1+\alpha_1'}{2} + \frac{S(\alpha_2+\alpha_2')}{4S-1}\right) \mid i,l,l\rangle - \frac{\sqrt{S(2S-1)}}{4S-1}[\alpha_2 \mid i,l,l+1\rangle + \alpha_2' \mid i,l,l+2\rangle] & \\ \quad - \left(\frac{\alpha_1}{2} - \frac{S\alpha_2}{4S-1}\right) \mid i,l+1,l+1\rangle - \left(\frac{\alpha_1'}{2} - \frac{S\alpha_2'}{4S-1}\right) \mid i,l+2,l+2\rangle & ,j=l \\ \left(\frac{\alpha_1}{2} + \frac{S\alpha_2}{4S-1}\right) \mid i,l+1,l+1\rangle - \left(\frac{\alpha_1}{2} - \frac{S\alpha_2}{4S-1}\right) \mid i,l,l\rangle - \frac{\sqrt{S(2S-1)}}{4S-1}\alpha_2 \mid i,l,l+1\rangle & \\ \quad ,j=l+1 & \\ \left(\frac{\alpha_1'}{2} + \frac{S\alpha_2'}{4S-1}\right) \mid i,l+2,l+2\rangle - \left(\frac{\alpha_1'}{2} - \frac{S\alpha_2'}{4S-1}\right) \mid i,l,l\rangle - \frac{\sqrt{S(2S-1)}}{4S-1}\alpha_2' \mid i,l,l+2\rangle & \\ \quad ,j=l+2 & \end{cases} \quad \text{(A.15)}$$

Equations for the Hamiltonian acting on the kets $\mid i,i,j\rangle, \mid i-1,i,j\rangle$ and $\mid i-2,i,j\rangle$ follow the forms of equations (A.15), (A.14) and (A.13) respectively. The equations for the full Hamiltonian acting on states with two spin deviations on the same site, nearest neighbor sites, or second nearest neighbor sites, and the other deviation farther than second nearest neighbor from either of the other two deviations are found to be

$$\begin{aligned} \widehat{H} \mid i,j,j+2\rangle &= \left(3\alpha_1 + 2\alpha_1' + \frac{2S-1}{4S-1}\alpha_2'\right) \mid i,j,j+2\rangle \\ &\quad - \frac{\alpha_1'}{2}[\mid i-2,j,j+2\rangle + \mid i+2,j,j+2\rangle + \mid i,j,j+4\rangle + \mid i,j-2,j+2\rangle] \\ &\quad - \frac{\alpha_1}{2}[\mid i-1,j,j+2\rangle + \mid i+1,j,j+2\rangle + \mid i,j,j+3\rangle + \mid i,j,j+1\rangle + \mid i,j+1,j+2\rangle \\ &\quad + \mid i,j-1,j+2\rangle] - \frac{\sqrt{S(2S-1)}}{4S-1}\alpha_2'[\mid i,j,j\rangle + \mid i,j+2,j+2\rangle] \end{aligned} \quad \text{(A.16)}$$

$$\begin{aligned} \widehat{H} \mid i,j,j+1\rangle &= \left(2\alpha_1 + \frac{2S-1}{4S-1}\alpha_2 + 3\alpha_1'\right) \mid i,j,j+1\rangle - \frac{\alpha_1'}{2}[\mid i-2,j,j+1\rangle \\ &\quad + \mid i+2,j,j+1\rangle + \mid i,j-1,j\rangle + \mid i,j-2,j+1\rangle + \mid i,j+1,j+2\rangle + \mid i,j,j+3\rangle] \end{aligned}$$

$$-\frac{\alpha_1}{2}[|\, i-1,j,j+1\rangle+|\, i+1,j,j+1\rangle+|\, i,j,j+2\rangle+|\, i,j-1,j+1\rangle]$$
$$-\frac{\sqrt{S\,(2S-1)}}{4S-1}\alpha_2\,[|\, i,j,j\rangle+|\, i,j+1,j+1\rangle] \tag{A.17}$$

$$\widehat{H}\,|\, i,j,j\rangle=\left(2(\alpha_1+\alpha_1')+\frac{2S\,(\alpha_2+\alpha_2')}{4S-1}\right)|\, i,j,j\rangle-\frac{\alpha_1'}{2}[|\, i-2,j,j\rangle+|\, i+2,j,j\rangle]$$
$$-\frac{\alpha_1}{2}[|\, i-1,j,j\rangle+|\, i+1,j,j\rangle]-\left(\frac{\alpha_1'}{2}-\frac{S\alpha_2'}{4S-1}\right)[|\, i,j-2,j-2\rangle+|\, i,j+2,j+2\rangle]$$
$$-\left(\frac{\alpha_1}{2}-\frac{S\alpha_2}{4S-1}\right)[|\, i,j-1,j-1\rangle+|\, i,j+1,j+1\rangle]-\frac{\sqrt{S\,(2S-1)}}{4S-1}\,[\alpha_2'\,|\, i,j-2,j\rangle$$
$$+\alpha_2'\,|\, i,j,j+2\rangle+\alpha_2\,|\, i,j-1,j\rangle+\alpha_2\,|\, i,j,j+1\rangle] \tag{A.18}$$

The full Hamiltonian acting on the states $|\, i-2,i,j\rangle, |\, i-1,i,j\rangle$ and $|\, i,i,j\rangle$ are similar to the above equations.

Using the matrices $\mathbf{A}^n$ and $\mathbf{B}^n$, we can find the effects of the full Hamiltonian acting on states with all three spin deviations on nearest neighbor or next nearest neighbor sites, or two spin deviations on nearest neighbor sites and the other deviation on a second nearest neighbor site. First find $\widehat{H}_l$ acting on these states.

$$\widehat{H}_l\,|\, j,j+2,j+4\rangle=$$
$$\begin{cases} 0\,|\, j,j+2,j+4\rangle & ,j\neq l-4,l-3,l-2,l-1,l,l+1,l+2 \\ \frac{\alpha_1+\alpha_1'}{2}\,|\, l-4,l-2,l\rangle-\frac{\alpha_1}{2}\,|\, l-4,l-2,l+1\rangle-\frac{\alpha_1'}{2}\,|\, l-4,l-2,l+2\rangle & \\ \qquad ,j=l-4 & \\ \frac{\alpha_1}{2}\,|\, l-3,l-1,l+1\rangle-\frac{\alpha_1}{2}\,|\, l-3,l-1,l\rangle & ,j=l-3 \\ \left(\frac{\alpha_1}{2}+\frac{2S-1}{4S-1}\alpha_2'\right)|\, l-2,l,l+2\rangle-\frac{\sqrt{S(2S-1)}}{4S-1}\alpha_2'\,[|\, l-2,l,l\rangle+|\, l-2,l+2,l+2\rangle] & \\ \qquad -\frac{\alpha_1}{2}\,|\, l-2,l+1,l+2\rangle & ,j=l-2 \\ \frac{\alpha_1}{2}\,|\, l-1,l+1,l+3\rangle-\frac{\alpha_1}{2}\,|\, l-1,l,l+3\rangle & ,j=l-1 \\ \left(\frac{\alpha_1}{2}+\frac{2S-1}{4S-1}\alpha_2'\right)|\, l,l+2,l+4\rangle-\frac{\sqrt{S(2S-1)}}{4S-1}\alpha_2'\,[|\, l,l,l+4\rangle+|\, l+2,l+2,l+4\rangle] & \\ \qquad -\frac{\alpha_1}{2}\,|\, l+1,l+2,l+4\rangle & ,j=l \\ \frac{\alpha_1}{2}\,|\, l+1,l+3,l+5\rangle-\frac{\alpha_1}{2}\,|\, l,l+3,l+5\rangle & ,j=l+1 \\ \frac{\alpha_1'}{2}\,|\, l+2,l+4,l+6\rangle-\frac{\alpha_1'}{2}\,|\, l,l+4,l+6\rangle & ,j=l+2 \end{cases} \tag{A.19}$$

$$\widehat{H}_l \mid j, j+1, j+3\rangle =$$

$$\begin{cases} 0 \mid j, j+1, j+3\rangle & , j \neq l-3, l-2, l-1, l, l+1, l+2 \\ \frac{\alpha_1+\alpha_1'}{2} \mid l-3, l-2, l\rangle - \frac{\alpha_1}{2} \mid l-3, l-2, l+1\rangle - \frac{\alpha_1'}{2} \mid l-3, l-2, l+2\rangle & \\ \qquad , j = l-3 & \\ \frac{\alpha_1}{2} \mid l-2, l-1, l+1\rangle - \frac{\alpha_1}{2} \mid l-2, l-1, l\rangle & , j = l-2 \\ \left(\frac{\alpha_1}{2} + \frac{2S-1}{4S-1}\alpha_2'\right) \mid l-1, l, l+2\rangle - \frac{\sqrt{S(2S-1)}}{4S-1}\alpha_2' [\mid l-1, l, l\rangle + \mid l-1, l+2, l+2\rangle] & \\ \qquad - \frac{\alpha_1}{2} \mid l-1, l+1, l+2\rangle & , j = l-1 \\ \left(\frac{\alpha_1'}{2} + \frac{2S-1}{4S-1}\alpha_2\right) \mid l, l+1, l+3\rangle - \frac{\sqrt{S(2S-1)}}{4S-1}\alpha_2 [\mid l, l, l+3\rangle + \mid l+1, l+1, l+3\rangle] & \\ \qquad - \frac{\alpha_1'}{2} \mid l+1, l+2, l+3\rangle & , j = l \\ \frac{\alpha_1+\alpha_1'}{2} \mid l+1, l+2, l+4\rangle - \frac{\alpha_1}{2} \mid l, l+2, l+4\rangle - \frac{\alpha_1'}{2} \mid l, l+1, l+4\rangle & , j = l+1 \\ \frac{\alpha_1'}{2} \mid l+2, l+3, l+5\rangle - \frac{\alpha_1'}{2} \mid l, l+3, l+5\rangle & , j = l+2 \end{cases} \tag{A.20}$$

$$\widehat{H}_l \mid j, j+1, j+2\rangle =$$

$$\begin{cases} 0 \mid j, j+1, j+2\rangle & , j \neq l-2, l-1, l, l+1, l+2 \\ \frac{\alpha_1+\alpha_1'}{2} \mid l-2, l-1, l\rangle - \frac{\alpha_1}{2} \mid l-2, l-1, l+1\rangle - \frac{\alpha_1'}{2} \mid l-2, l-1, l+2\rangle & \\ \qquad , j = l-2 & \\ \left(\frac{\alpha_1'}{2} + \frac{2S-1}{4S-1}\alpha_2\right) \mid l-1, l, l+1\rangle - \frac{\sqrt{S(2S-1)}}{4S-1}\alpha_2 [\mid l-1, l, l\rangle + \mid l-1, l+1, l+1\rangle] & \\ \qquad - \frac{\alpha_1'}{2} \mid l-1, l+1, l+2\rangle & , j = l-1 \\ \frac{2S-1}{4S-1}(\alpha_2 + \alpha_2') \mid l, l+1, l+2\rangle - \frac{\sqrt{S(2S-1)}}{4S-1} [\alpha_2' \mid l, l, l+1\rangle + \alpha_2 \mid l, l, l+2\rangle & \\ \qquad + \alpha_2 \mid l+1, l+1, l+2\rangle + \alpha_2' \mid l+1, l+2, l+2\rangle] & , j = l \\ \frac{\alpha_1+\alpha_1'}{2} \mid l+1, l+2, l+3\rangle - \frac{\alpha_1}{2} \mid l, l+2, l+3\rangle - \frac{\alpha_1'}{2} \mid l, l+1, l+3\rangle & , j = l+1 \\ \frac{\alpha_1'}{2} \mid l+2, l+3, l+4\rangle - \frac{\alpha_1'}{2} \mid l, l+3, l+4\rangle & , j = l+2 \end{cases} \tag{A.21}$$

The full Hamiltonian acting on these states are:

$$\widehat{H} \mid j, j+2, j+4\rangle = \left\{3\alpha_1 + \left(\alpha_1' + 2\frac{2S-1}{4S-1}\alpha_2'\right)\right\} \mid i, i+2, i+4\rangle$$
$$- \frac{\alpha_1'}{2}[\mid j, j+2, j+6\rangle + \mid j-2, j+2, j+4\rangle] - \frac{\alpha_1}{2}[\mid j, j+2, j+5\rangle + \mid j, j+2, j+3\rangle$$

$$+ \mid j,j+1,j+4\rangle + \mid j,j+3,j+4\rangle + \mid j+1,j+2,j+4\rangle + \mid j-1,j+2,j+4\rangle]$$
$$- \frac{\sqrt{S(2S-1)}}{4S-1}\alpha_2'[\mid j,j+2,j+2\rangle + \mid j,j+4,j+4\rangle + \mid j,j,j+4\rangle$$
$$+ \mid j+2,j+2,j+4\rangle] \tag{A.22}$$

$$\widehat{H} \mid j,j+1,j+3\rangle = \left\{2\alpha_1 + \frac{2S-1}{4S-1}\alpha_2 + 2\alpha_1' + \frac{2S-1}{4S-1}\alpha_2'\right\} \mid j,j+1,j+3\rangle -$$
$$\frac{\alpha_1'}{2}[\mid j,j+1,j+5\rangle + \mid j+1,j+2,j+3\rangle + \mid j-1,j,j+3\rangle + \mid j-2,j+1,j+3\rangle]$$
$$- \frac{\alpha_1}{2}[\mid j,j+1,j+4\rangle + \mid j,j+1,j+2\rangle + \mid j,j+2,j+3\rangle + \mid j-1,j+1,j+3\rangle]$$
$$- \frac{\sqrt{S(2S-1)}}{4S-1}[\alpha_2 \mid j,j,j+3\rangle + \alpha_2 \mid j+1,j+1,j+3\rangle$$
$$+ \alpha_2' \mid j,j+1,j+1\rangle + \alpha_2' \mid j,j+3,j+3\rangle] \tag{A.23}$$

$$\widehat{H} \mid j,j+1,j+2\rangle = \left\{\alpha_1 + 2\frac{2S-1}{4S-1}\alpha_2 + 2\alpha_1' + \frac{2S-1}{4S-1}\alpha_2'\right\} \mid j,j+1,j+2\rangle$$
$$- \frac{\alpha_1}{2}[\mid j,j+1,j+3\rangle + \mid j-1,j+1,j+2\rangle]$$
$$- \frac{\alpha_1'}{2}[\mid j,j+1,j+4\rangle + \mid j,j+2,j+3\rangle + \mid j-1,j,j+2\rangle + \mid j-2,j+1,j+2\rangle]$$
$$- \frac{\sqrt{S(2S-1)}}{4S-1}[\alpha_2 \mid j,j+1,j+1\rangle + \alpha_2 \mid j,j+2,j+2\rangle + \alpha_2' \mid j,j,j+1\rangle$$
$$+ \alpha_2 \mid j,j,j+2\rangle + \alpha_2 \mid j+1,j+1,j+2\rangle + \alpha_2' \mid j+1,j+2,j+2\rangle] \tag{A.24}$$

$\widehat{H} \mid j-2,j,j+1\rangle$ is similar to $\widehat{H} \mid j,j+1,j+3\rangle$.

From the matrices $\mathbf{A}^n$, $\mathbf{B}^n$ and $\mathbf{C}^n$ we can obtain the equations for $\widehat{H}_l$ acting on the kets $\mid j,j,j\rangle, \mid j,j,j+1\rangle$ and $\mid j,j,j+2\rangle$. Then the equations for the full Hamiltonian acting on states with all three spin deviations on the same site, or two deviations of the same site and the other deviation on a nearest neighbor or next nearest neighbor site can be found.

$$\widehat{H}_l \mid j,j,j+2\rangle =$$

$$\begin{cases} 0 \mid j,j,j+2\rangle & ,j \neq l-2,l-1,l,l+1,l+2 \\ \\ \frac{\alpha_1+\alpha_1'}{2} \mid l-2,l-2,l\rangle - \frac{\alpha_1}{2} \mid l-2,l-2,l+1\rangle - \frac{\alpha_1'}{2} \mid l-2,l-2,l+2\rangle & \\ \qquad ,j=l-2 & \\ \\ \frac{\alpha_1}{2} \mid l-1,l-1,l+1\rangle - \frac{\alpha_1}{2} \mid l-1,l-1,l\rangle & ,j=l-1 \\ \\ -\sum_n J_2^{(n)} m_{12} \mid l,l,l\rangle + \left(\frac{\alpha_1}{2} + \frac{S\alpha_2}{4S-1} - \sum_n J_2^{(n)} m_{22}\right) \mid l,l,l+2\rangle & \\ \qquad - \frac{\sqrt{S(2S-1)}}{4S-1}\alpha_2 \mid l,l+1,l+2\rangle + \left(\frac{\alpha_1}{2} - \frac{S\alpha_2}{4S-1}\right) \mid l+1,l+1,l+2\rangle & \\ \qquad - \sum_n J_2^{(n)} m_{23} \mid l,l+2,l+2\rangle - \sum_n J_2^{(n)} m_{13} \mid l+2,l+2,l+2\rangle & \\ \qquad ,j=l & \\ \\ \left(\frac{\alpha_1}{2} + \frac{S\alpha_2}{4S-1}\right) \mid l+1,l+1,l+3\rangle - \frac{\sqrt{S(2S-1)}}{4S-1}\alpha_2 \mid l,l+1,l+3\rangle & \\ \qquad - \left(\frac{\alpha_1}{2} - \frac{S\alpha_2}{4S-1}\right) \mid l,l,l+3\rangle & ,j=l+1 \\ \\ \left(\frac{\alpha_1'}{2} + \frac{S\alpha_2'}{4S-1}\right) \mid l+2,l+2,l+4\rangle - \frac{\sqrt{S(2S-1)}}{4S-1}\alpha_2' \mid l,l+2,l+4\rangle & \\ \qquad - \left(\frac{\alpha_1'}{2} - \frac{S\alpha_2'}{4S-1}\right) \mid l,l,l+4\rangle & ,j=l+2 \end{cases} \tag{A.25}$$

$$\widehat{H}_l \mid j,j,j+1\rangle =$$

$$\begin{cases} 0 \mid j,j,j+1\rangle & ,j \neq l-1,l,l+1,l+2 \\ \\ \frac{\alpha_1+\alpha_1'}{2} \mid l-1,l-1,l\rangle - \frac{\alpha_1}{2} \mid l-1,l-1,l+1\rangle - \frac{\alpha_1'}{2} \mid l-1,l-1,l+2\rangle & \\ \qquad ,j=l-1 & \\ \\ -\sum_n J_1^{(n)} m_{12} \mid l,l,l\rangle + \left(\frac{\alpha_1'}{2} + \frac{S\alpha_2'}{4S-1} - \sum_n J_1^{(n)} m_{22}\right) \mid l,l,l+1\rangle & \\ \qquad - \frac{\sqrt{S(2S-1)}}{4S-1}\alpha_2' \mid l,l+1,l+2\rangle - \left(\frac{\alpha_1'}{2} - \frac{S\alpha_2'}{4S-1}\right) \mid l+1,l+2,l+2\rangle & \\ \qquad - \sum_n J_1^{(n)} m_{23} \mid l,l+1,l+1\rangle - \sum_n J_1^{(n)} m_{13} \mid l+1,l+1,l+1\rangle & \\ \qquad ,j=l & \\ \\ \left(\frac{\alpha_1}{2} + \frac{S\alpha_2}{4S-1} + \frac{\alpha_1'}{2}\right) \mid l+1,l+1,l+2\rangle - \frac{\sqrt{S(2S-1)}}{4S-1}\alpha_2 \mid l,l+1,l+2\rangle & \\ \qquad - \left(\frac{\alpha_1}{2} - \frac{S\alpha_2}{4S-1}\right) \mid l,l,l+2\rangle - \frac{\alpha_1'}{2} \mid l,l+1,l+1\rangle & ,j=l+1 \\ \\ \left(\frac{\alpha_1'}{2} + \frac{S\alpha_2'}{4S-1}\right) \mid l+2,l+2,l+3\rangle - \frac{\sqrt{S(2S-1)}}{4S-1}\alpha_2' \mid l,l+2,l+3\rangle & \\ \qquad - \left(\frac{\alpha_1'}{2} - \frac{S\alpha_2'}{4S-1}\right) \mid l,l,l+3\rangle & ,j=l+2 \end{cases} \tag{A.26}$$

$$\widehat{H}_l \mid j,j,j\rangle =$$

$$\begin{cases} 0 \mid j,j,j\rangle & ,j \neq l,l+1,l+2 \\ \\ -\sum_n \left(J_1^{(n)} + J_2^{(n)}\right) m_{11} \mid l,l,l\rangle - \sum_n J_1^{(n)} m_{12} \mid l,l,l+1\rangle & \\ \quad -\sum_n J_1^{(n)} m_{13} \mid l,l+1,l+1\rangle - \sum_n J_1^{(n)} m_{14} \mid l+1,l+1,l+1\rangle & \\ \quad -\sum_n J_2^{(n)} m_{12} \mid l,l,l+2\rangle - \sum_n J_2^{(n)} m_{13} \mid l,l+2,l+2\rangle & \\ \quad -\sum_n J_2^{(n)} m_{14} \mid l+2,l+2,l+2\rangle & ,j = l \\ \\ -\sum_n J_1^{(n)} m_{14} \mid l,l,l\rangle - \sum_n J_1^{(n)} m_{13} \mid l,l,l+1\rangle - \sum_n J_1^{(n)} m_{12} \mid l,l+1,l+1\rangle & \\ \quad -\sum_n J_1^{(n)} m_{11} \mid l+1,l+1,l+1\rangle & ,j = l+1 \\ \\ -\sum_n J_2^{(n)} m_{14} \mid l,l,l\rangle - \sum_n J_2^{(n)} m_{13} \mid l,l,l+2\rangle - \sum_n J_2^{(n)} m_{12} \mid l,l+2,l+2\rangle & \\ \quad -\sum_n J_2^{(n)} m_{11} \mid l+2,l+2,l+2\rangle & ,j = l+2 \end{cases} \tag{A.27}$$

The matrix elements m_{ij} are related to the variables defined in equation (2.9) in the following way:

$$\begin{aligned} -\sum_n J_1^{(n)} m_{11} &= \frac{3}{2} S(S-1) \left[\frac{\alpha_1}{S(4S-3)} + \frac{\alpha_2}{(S-1)(4S-1)} + \frac{\alpha_3}{3(S-1)(4S-3)} \right] \\ -\sum_n J_1^{(n)} m_{12} &= \frac{1}{2} \sqrt{3S(S-1)} \left[\frac{\alpha_1}{4S-3} - \frac{\alpha_2}{4S-1} - \frac{\alpha_3}{4S-3} \right] \\ -\sum_n J_1^{(n)} m_{13} &= -\frac{1}{2} \sqrt{3S(S-1)} \left[\frac{\alpha_1}{4S-3} + \frac{\alpha_2}{4S-1} - \frac{\alpha_3}{4S-3} \right] \\ -\sum_n J_1^{(n)} m_{14} &= -\frac{3}{2} S(S-1) \left[\frac{\alpha_1}{S(4S-3)} - \frac{\alpha_2}{(S-1)(4S-1)} + \frac{\alpha_3}{3(S-1)(4S-3)} \right] \\ -\sum_n J_1^{(n)} m_{22} &= \frac{1}{2} \left[\frac{S\alpha_1}{4S-3} + \frac{S-1}{4S-1} \alpha_2 + \frac{3(S-1)}{4S-3} \alpha_3 \right] \\ -\sum_n J_1^{(n)} m_{23} &= -\frac{1}{2} \left[\frac{S\alpha_1}{4S-3} - \frac{S-1}{4S-1} \alpha_2 + \frac{3(S-1)}{4S-3} \alpha_3 \right] \end{aligned} \tag{A.28}$$

If the substitutions $J_1^{(n)} \rightarrow J_2^{(n)}$ are made in the above equations, then the equalities hold if the substitutions $\alpha_1 \rightarrow \alpha_1'$, $\alpha_2 \rightarrow \alpha_2'$ and $\alpha_3 \rightarrow \alpha_3'$ are also made. Therefore the effective Hamiltonian acting on states with all three spin deviations on the same site or two deviations on the same site and the other deviation on a nearest neighbor or a next nearest neighbor site are:

$$\widehat{H} \mid j,j,j+2\rangle = \left\{2\alpha_1 + \frac{2S\alpha_2}{4S-1} - \sum_n J_2^{(n)} m_{22} + \alpha_1' + \frac{S\alpha_2'}{4S-1}\right\} \mid j,j,j+2\rangle$$
$$- \frac{\alpha_1'}{2} \mid j,j,j+4\rangle - \frac{\alpha_1}{2}[\mid j,j,j+3\rangle + \mid j,j,j+1\rangle] - \frac{\sqrt{S(2S-1)}}{4S-1}[\alpha_2 \mid j,j+1,j+2\rangle$$
$$+\alpha_2 \mid j-1,j,j+2\rangle + \alpha_2' \mid j-2,j,j+2\rangle] - \left(\frac{\alpha_1}{2} - \frac{S\alpha_2}{4S-1}\right)[\mid j+1,j+1,j+2\rangle$$
$$+ \mid j-1,j-1,j+2\rangle] - \left(\frac{\alpha_1'}{2} - \frac{S\alpha_2'}{4S-1}\right) \mid j-2,j-2,j+2\rangle - \sum_n J_2^{(n)} m_{12} \mid j,j,j\rangle$$
$$- \sum_n J_2^{(n)} m_{23} \mid j,j+2,j+2\rangle - \sum_n J_2^{(n)} m_{13} \mid j+2,j+2,j+2\rangle \qquad \text{(A.29)}$$

$$\widehat{H} \mid j,j,j+1\rangle = \left\{\alpha_1 + \frac{S\alpha_2}{4S-1} - \sum_n J_1^{(n)} m_{22} + 2\alpha_1' + \frac{2S\alpha_2'}{4S-1}\right\} \mid j,j,j+1\rangle$$
$$- \frac{\alpha_1}{2} \mid j,j,j+2\rangle - \frac{\alpha_1'}{2}[\mid j,j,j+3\rangle + \mid j-1,j,j\rangle] - \frac{\sqrt{S(2S-1)}}{4S-1}[\alpha_2' \mid j,j+1,j+2\rangle$$
$$+ \alpha_2 \mid j-1,j,j+1\rangle + \alpha_2' \mid j-2,j,j+1\rangle] - \left(\frac{\alpha_1}{2} - \frac{S\alpha_2}{4S-1}\right) \mid j-1,j-1,j+1\rangle$$
$$- \left(\frac{\alpha_1'}{2} - \frac{S\alpha_2'}{4S-1}\right)[\mid j-2,j-2,j+1\rangle + \mid j+1,j+2,j+2\rangle] - \sum_n J_1^{(n)} m_{12} \mid j,j,j\rangle$$
$$- \sum_n J_1^{(n)} m_{23} \mid j,j+1,j+1\rangle - \sum_n J_1^{(n)} m_{13} \mid j+1,j+1,j+1\rangle \qquad \text{(A.30)}$$

$$\widehat{H} \mid j,j,j\rangle = -2\sum_n \left(J_1^{(n)} + J_2^{(n)}\right) m_{11} \mid j,j,j\rangle - \sum_n J_1^{(n)} m_{12}[\mid j,j,j+1\rangle + \mid j-1,j,j\rangle]$$
$$- \sum_n J_2^{(n)} m_{12}[\mid j,j,j+2\rangle + \mid j-2,j,j\rangle] - \sum_n J_1^{(n)} m_{13}[\mid j,j+1,j+1\rangle$$
$$+ \mid j-1,j-1,j\rangle] - \sum_n J_2^{(n)} m_{13}[\mid j,j+2,j+2\rangle + \mid j-2,j-2,j\rangle]$$
$$- \sum_n J_1^{(n)} m_{14}[\mid j+1,j+1,j+1\rangle + \mid j-1,j-1,j-1\rangle]$$
$$- \sum_n J_2^{(n)} m_{14}[\mid j+2,j+2,j+2\rangle + \mid j-2,j-2,j-2\rangle] \qquad \text{(A.31)}$$

$\widehat{H} \mid j-2,j,j\rangle$ is similar to $\widehat{H} \mid j,j,j+2\rangle$ and $\widehat{H} \mid j-1,j,j\rangle$ is similar to $\widehat{H} \mid j,j,j+1\rangle$.

The full set of equations specifying the effect of the Hamiltonian on the complete set of orthonormal states are equations (A.12), (A.16) to (A.18), (A.22) to (A.24) and (A.29) to (A.31). The conversion of these equations to a more understandable form is done in Chapter 3.

Appendix B

Derivation of the Two-Magnon Excitation Equations for the Heisenberg Chain with Competing Interactions

The development of the two-magnon excitation equations follows the method used in section 2.2. The orthonormal base kets are defined as before with two raising operators on sites i and j acting on the ground state ket

$$| i,j\rangle = C_{ij} S_i^+ S_j^+ \mid 0\rangle \tag{B.1}$$

$$C_{ij} = \begin{cases} \frac{1}{\sqrt{2S}} & ,\text{if } i \neq j \\ \frac{1}{2\sqrt{S(2S-1)}} & ,\text{if } i = j \end{cases}$$

where the C_{ij} are normalization constants and the kets are labeled by sites i and j such that $i \leq j$. The effect of $\tilde{O}_l$ acting on the base kets with two deviations separated by more than next nearest neighbors is

$$\hat{O}_l \mid i,j\rangle = \begin{cases} 0 \mid i,j\rangle & i,j \neq l-1,l,l+1 \\ \frac{1}{2i} 2S^2(-\mid l,j\rangle + \mid l+1,j\rangle) & ,i = l-1 \\ \frac{1}{2i} 2S^2(\mid l-1,j\rangle - \mid l+1,j\rangle) & ,i = l \\ \frac{1}{2i} 2S^2(-\mid l-1,j\rangle + \mid l,j\rangle) & ,i = l+1 \end{cases} \tag{B.2}$$

where $j \neq l-1, l$ or $l+1$. Similar results are found for $\tilde{O}_l$ acting on the base kets with $i \neq l-1, l$ and $l+1$, but with $j = l-1, l$ or $l+1$. Therefore, for i and j

separated by more than two sites,

$$I_2 \mid i,j\rangle = -\frac{1}{2i}2S^2\{-\mid i-2,j\rangle+\mid i+2,j\rangle+2\mid i-1,j\rangle-2\mid i+1,j\rangle-\mid i,j-2\rangle \\ +\mid i,j+2\rangle+2\mid i,j-1\rangle-2\mid i,j+1\rangle\} \tag{B.3}$$

Next we must determine the effects of $\tilde{O}_l$ acting on base kets with spin deviations on the same site, nearest neighbor sites or next nearest neighbor sites.

$$\hat{O}_l \mid j,j\rangle = \begin{cases} 0 \mid j,j\rangle & j \neq l-1,l,l+1 \\ \frac{1}{2i}2S\sqrt{S(2S-1)}(-\mid l-1,l\rangle+\mid l-1,l+1\rangle) & j=l-1 \\ \frac{1}{2i}2S\sqrt{S(2S-1)}(\mid l-1,l\rangle-\mid l,l+1\rangle) & j=l \\ \frac{1}{2i}2S\sqrt{S(2S-1)}(-\mid l-1,l+1\rangle+\mid l,l+1\rangle) & j=l+1 \end{cases} \tag{B.4}$$

$$\hat{O}_l \mid j,j+1\rangle = \begin{cases} 0 \mid j,j\rangle & j \neq l-2,l-1,l,l+1 \\ \frac{1}{2i}2S^2(-\mid l-2,l\rangle+\mid l-2,l+1\rangle) & j=l-2 \\ \frac{1}{2i}[2S\sqrt{S(2S-1)}(-\mid l,l\rangle+\mid l-1,l-1\rangle) \\ \quad +2S(1-S)(-\mid l,l+1\rangle+\mid l-1,l+1\rangle)] \\ \quad j=l-1 \\ \frac{1}{2i}[2S\sqrt{S(2S-1)}(\mid l,l\rangle-\mid l+1,l+1\rangle) \\ \quad +2S(1-S)(\mid l-1,l\rangle-\mid l-1,l+1\rangle)] & j=l \\ \frac{1}{2i}2S^2(-\mid l-1,l+2\rangle+\mid l,l+2\rangle) & j=l+1 \end{cases} \tag{B.5}$$

$$\hat{O}_l \mid j-1,j+1\rangle = \begin{cases} 0 \mid j,j\rangle & j \neq l-2,l-1,l,l+1,l+2 \\ \frac{1}{2i}2S^2(-\mid l-3,l\rangle+\mid l-3,l+1\rangle) & j=l-2 \\ \frac{1}{2i}2S^2(\mid l-2,l-1\rangle-\mid l-2,l+1\rangle) & j=l-1 \\ \frac{1}{2i}[2S\sqrt{S(2S-1)}(-\mid l-1,l-1\rangle+\mid l+1,l+1\rangle) \\ \quad +2S(1-S)(\mid l,l+1\rangle-\mid l-1,l\rangle)] & j=l \\ \frac{1}{2i}2S^2(\mid l-1,l+2\rangle-\mid l+1,l+2\rangle) & j=l+1 \\ \frac{1}{2i}2S^2(-\mid l-1,l+3\rangle+\mid l,l+3\rangle) & j=l+2 \end{cases} \tag{B.6}$$

Summing over l we find I_2 acting on $|\, j,j\rangle$, $|\, j,j+1\rangle$ and $|\, j-1,j+1\rangle$ to be

$$I_2\,|\, j,j\rangle = -\frac{1}{2i}2S\sqrt{S(2S-1)}\{-\,|\, j-2,j\rangle + |\, j,j+2\rangle + 2\,|\, j-1,j\rangle - 2\,|\, j,j+1\rangle\} \tag{B.7}$$

$$\begin{aligned} I_2\,|\, j,j+1\rangle = -\frac{1}{2i}\{&2S^2(-\,|\, j,j+2\rangle + |\, j-1,j+1\rangle + |\, j,j+3\rangle - |\, j-2,j+1\rangle) \\ &+ 2S\sqrt{S(2S-1)}(-2\,|\, j+1,j+1\rangle + 2\,|\, j,j\rangle) \\ &+ 2S(1-S)(-\,|\, j+1,j+2\rangle + |\, j-1,j\rangle + |\, j,j+2\rangle - |\, j-1,j+1\rangle)\} \end{aligned} \tag{B.8}$$

$$\begin{aligned} I_2\,|\, j-1,j+1\rangle = -\frac{1}{2i}\{&2S^2(-2\,|\, j-1,j+2\rangle + 2\,|\, j-2,j+1\rangle + |\, j-1,j+3\rangle \\ &- |\, j-3,j+1\rangle + |\, j-1,j\rangle - |\, j,j+1\rangle) \\ &+ 2S\sqrt{S(2S-1)}(|\, j+1,j+1\rangle - |\, j-1,j-1\rangle) \\ &+ 2S(1-S)(|\, j,j+1\rangle - |\, j-1,j\rangle)\} \end{aligned} \tag{B.9}$$

The full set of equations specifying the effect of the Hamiltonian on the complete set of orthonormal states are equations (B.3), (B.7), (B.8) and (B.9). The conversion of these equations to a more understandable form is done in section 5.2.

Appendix C

Derivation of the Three-Magnon Excitation Equations for the Heisenberg Chain with Competing Interactions

This appendix includes the main steps and equations in the derivation of the three-magnon excitation equations of the Hamiltonian (1.6). The method follows Appendix A.

The orthonormal base kets are defined as before, with three raising operators on sites i, j and k acting on the ground state ket (equation A.1)

$$\mid i,j,k\rangle = C_{ijk} S_i^+ S_j^+ S_k^+ \mid 0\rangle$$

$$C_{ijk} = \begin{cases} \frac{1}{\sqrt{8S^3}} & \text{if } i \neq j \neq k \\ \frac{1}{\sqrt{8S^2(2S-1)}} & \text{if 2 of } \{ijk\} \text{ are equal} \\ \frac{1}{\sqrt{24S(2S-1)(S-1)}} & \text{if } i = j = k \end{cases}$$

where the C_{ijk} are normalization constants.

Let $\tilde{O}_l$ act on the above states. First consider the case of $\tilde{O}_l$ acting on kets with three spin deviations separated by more than second nearest neighbors ($i + 2 <$

$j, j+2 < k$).

$$\tilde{O}_l \mid i,j,k\rangle = \begin{cases} 0 \mid i,j,k\rangle & i,j,k \neq l-1,l,l+1 \\ \frac{1}{2i}2S^2\{-\mid l,j,k\rangle + \mid l+1,j,k\rangle\} & ,i = l-1 \\ \frac{1}{2i}2S^2\{\mid l-1,j,k\rangle - \mid l+1,j,k\rangle\} & ,i = l \\ \frac{1}{2i}2S^2\{-\mid l-1,j,k\rangle + \mid l,j,k\rangle\} & ,i = l+1 \end{cases} \quad \text{(C.1)}$$

where $j,k \neq l-1,l,l+1$. Similar equations are found for kets with $i,j \neq l-1,l,l+1$ but $k = l-1,l$ or $l+1$ and for $i,k \neq l-1,l,l+1$ but $j = l-1,l$ or $l+1$. Therefore I_2 acting on three spin deviations separated by more that second nearest neighbors gives

$$\begin{aligned} I_2 \mid i,j,k\rangle = & -\frac{1}{2i}2S^2\{-\mid i-2,j,k\rangle + \mid i+2,j,k\rangle - \mid i,j-2,k\rangle + \mid i,j+2,k\rangle \\ & - \mid i,j,k-2\rangle + \mid i,j,k+2\rangle + 2\mid i-1,j,k\rangle - 2\mid i+1,j,k\rangle \\ & +2\mid i,j-1,k\rangle - 2\mid i,j+1,k\rangle + 2\mid i,j,k-1\rangle - 2\mid i,j,k+1\rangle\} \quad \text{(C.2)} \end{aligned}$$

One can also find the effects of $\tilde{O}_l$ acting on kets with two spin deviations on the same site, nearest neighbor sites, or second nearest neighbor sites, and the other deviation farther than second nearest neighbors from either of the other two deviations.

$$\widetilde{O}_l \mid i,j,j+2\rangle =$$

$$\frac{1}{2i}\begin{cases} 0 \mid i,j,j+2\rangle & i \neq l-1,l,l+1,\ j \neq l-3,l-2,l-1,l,l+1 \\ 2S^2\{-\mid l,j,j+2\rangle + \mid l+1,j,j+2\rangle\} & ,i=l-1 \\ 2S^2\{\mid l-1,j,j+2\rangle - \mid l+1,j,j+2\rangle\} & ,i=l \\ 2S^2\{-\mid l-1,j,j+2\rangle + \mid l,j,j+2\rangle\} & ,i=l+1 \\ 2S^2\{-\mid i,l-3,l\rangle + \mid i,l-3,l+1\rangle\} & ,j=l-3 \\ 2S^2\{\mid i,l-2,l-1\rangle - \mid i,l-2,l+1\rangle\} & ,j=l-2 \\ 2S(1-S)\{\mid i,l,l+1\rangle - \mid i,l-1,l\rangle\} & \\ \quad +2S\sqrt{S(2S-1)}\{\mid i,l+1,l+1\rangle - \mid i,l-1,l-1\rangle\} & ,j=l-1 \\ 2S^2\{\mid i,l-1,l+2\rangle - \mid i,l+1,l+2\rangle\} & ,j=l \\ 2S^2\{-\mid i,l-1,l+3\rangle + \mid i,l,l+3\rangle\} & ,j=l+1 \end{cases} \tag{C.3}$$

$$\widetilde{O}_l \mid i,j,j+1\rangle =$$

$$\frac{1}{2i}\begin{cases} 0 \mid i,j,j+1\rangle & i \neq l-1,l,l+1,\ j \neq l-2,l-1,l,l+1 \\ 2S^2\{-\mid l,j,j+1\rangle + \mid l+1,j,j+1\rangle\} & ,i=l-1 \\ 2S^2\{\mid l-1,j,j+1\rangle - \mid l+1,j,j+1\rangle\} & ,i=l \\ 2S^2\{-\mid l-1,j,j+1\rangle + \mid l,j,j+1\rangle\} & ,i=l+1 \\ 2S^2\{-\mid i,l-2,l\rangle + \mid i,l-2,l+1\rangle\} & ,j=l-2 \\ 2S\sqrt{S(2S-1)}\{-\mid i,l,l\rangle + \mid i,l-1,l-1\rangle\} & \\ \quad +2S(1-S)\{\mid i,l-1,l+1\rangle - \mid i,l,l+1\rangle\} & ,j=l-1 \\ 2S\sqrt{S(2S-1)}\{\mid i,l,l\rangle - \mid i,l+1,l+1\rangle\} & \\ \quad 2S(1-S)\{-\mid i,l-1,l+1\rangle + \mid i,l-1,l\rangle\} & ,j=l \\ 2S^2\{-\mid i,l-1,l+2\rangle + \mid i,l,l+2\rangle\} & ,j=l+1 \end{cases} \tag{C.4}$$

$$\widetilde{O}_l \mid i,j,j\rangle =$$

$$\frac{1}{2i}\begin{cases} 0 \mid i,j,j\rangle & ,i,\ j \neq l-1,l,l+1 \\ 2S^2\{-\mid l,j,j\rangle+\mid l+1,j,j\rangle\} & ,i=l-1 \\ 2S^2\{\mid l-1,j,j\rangle-\mid l+1,j,j\rangle\} & ,i=l \\ 2S^2\{-\mid l-1,j,j\rangle+\mid l,j,j\rangle\} & ,i=l+1 \\ 2S\sqrt{S(2S-1)}\{-\mid i,l-1,l\rangle+\mid i,l-1,l+1\rangle\} & ,j=l-1 \\ 2S\sqrt{S(2S-1)}\{\mid i,l-1,l\rangle-\mid i,l,l+1\rangle\} & ,j=l \\ 2S\sqrt{S(2S-1)}\{-\mid i,l-1,l+1\rangle+\mid i,l,l+1\rangle\} & ,j=l+1 \end{cases} \tag{C.5}$$

Equations for the Hamiltonian acting on the kets $\mid i,i,j\rangle$, $\mid i-1,i,j\rangle$ and $\mid i-2,i,j\rangle$ follow the forms of equations (C.5), (C.4) and (C.3) respectively. The equations for I_2 acting on states with two spin deviations on the same site, nearest neighbor sites, or second nearest neighbor sites, and the other deviation farther than second nearest neighbor from either of the other two deviations are found to be

$$\begin{aligned} I_2 \mid i,j,j+2\rangle = -\frac{1}{2i}\Big\{ & 2S^2[-\mid i+1,j,j+2\rangle+\mid i+2,j,j+2\rangle+\mid i-1,j,j+2\rangle \\ & -\mid i+1,j,j+2\rangle-\mid i-2,j,j+2\rangle+\mid i-1,j,j+2\rangle-\mid i,j,j+3\rangle+\mid i,j,j+4\rangle \\ & +\mid i,j,j+1\rangle-\mid i,j,j+3\rangle+\mid i,j-1,j+2\rangle-\mid i,j+1,j+2\rangle-\mid i,j-2,j+2\rangle \\ & +\mid i,j-1,j+2\rangle]+2S\sqrt{S(2S-1)}[-\mid i,j,j\rangle+\mid i,j+2,j+2\rangle] \\ & +2S(1-S)[\mid i,j+1,j+2\rangle-\mid i,j,j+1\rangle]\Big\} \end{aligned} \tag{C.6}$$

$$\begin{aligned} I_2 \mid i,j,j+1\rangle = -\frac{1}{2i}\Big\{ & 2S^2[-\mid i+1,j,j+1\rangle+\mid i+2,j,j+1\rangle+\mid i-1,j,j+1\rangle \\ & -\mid i+1,j,j+1\rangle-\mid i-2,j,j+1\rangle+\mid i-1,j,j+1\rangle-\mid i,j,j+2\rangle+\mid i,j,j+3\rangle \\ & -\mid i,j-2,j+1\rangle+\mid i,j-1,j+1\rangle]+2S\sqrt{S(2S-1)}[-2\mid i,j+1,j+1\rangle+2\mid i,j,j\rangle] \\ & +2S(1-S)[-\mid i,j+1,j+2\rangle+\mid i,j,j+2\rangle-\mid i,j-1,j+1\rangle+\mid i,j-1,j\rangle]\Big\} \end{aligned} \tag{C.7}$$

$$\begin{aligned} I_2 \mid i,j,j\rangle = -\frac{1}{2i}\Big\{ & 2S^2[-\mid i+1,j,j\rangle+\mid i+2,j,j\rangle+\mid i-1,j,j\rangle-\mid i+1,j,j\rangle \\ & -\mid i-2,j,j\rangle+\mid i-1,j,j\rangle]+2S\sqrt{S(2S-1)}[-\mid i,j,j+1\rangle+\mid i,j,j+2\rangle \\ & +\mid i,j-1,j\rangle-\mid i,j,j+1\rangle-\mid i,j-2,j\rangle+\mid i,j-1,j\rangle]\Big\} \end{aligned} \tag{C.8}$$

The operator I_2 acting on the states $|\, i-2,i,j\rangle$, $|\, i-1,i,j\rangle$ and $|\, i,i,j\rangle$ are similar to the above equations.

One can also find the effects of $\tilde{O}_l$ acting on kets with all three spin deviations on nearest neighbor sites or next nearest neighbor sites, or two spin deviations on nearest neighbor sites and the other deviation on a second nearest neighbor site.

$$
\begin{aligned}
&\tilde{O}_l \,|\, i-2,i,i+2\rangle = \\
&\begin{cases}
0\,|\, i-2,i,i+2\rangle & ,i \neq l-3,l-2,l-1,l,l+1,l+2,l+3 \\
2S^2\{-|\, l-5,l-3,l\rangle + |\, l-5,l-3,l+1\rangle\} & ,i=l-3 \\
2S^2\{|\, l-4,l-2,l-1\rangle - |\, l-4,l-2,l+1\rangle\} & ,i=l-2 \\
2S\sqrt{S(2S-1)}\{|\, l-3,l+1,l+1\rangle - |\, l-3,l-1,l-1\rangle\} & \\
\quad +2S(1-S)\{|\, l-3,l,l+1\rangle - |\, l-3,l-1,l\rangle\} & ,i=l-1 \\
2S^2\{|\, l-2,l-1,l+2\rangle - |\, l-2,l+1,l+2\rangle\} & ,i=l \\
2S\sqrt{S(2S-1)}\{|\, l+1,l+1,l+3\rangle - |\, l-1,l-1,l+3\rangle\} & \\
\quad +2S(1-S)\{|\, l,l+1,l+3\rangle - |\, l-1,l,l+3\rangle\} & ,i=l+1 \\
2S^2\{|\, l-1,l+2,l+4\rangle - |\, l+1,l+2,l+4\rangle\} & ,i=l+2 \\
2S^2\{-|\, l-1,l+3,l+5\rangle + |\, l,l+3,l+5\rangle\} & ,i=l+3
\end{cases}
\end{aligned}
\tag{C.9}
$$

$$\widetilde{O}_l \mid i-2,i,i+1\rangle =$$
$$\begin{cases} 0 \mid i-2,i,i+1\rangle & ,i \neq l-2,l-1,l,l+1,l+2,l+3 \\ 2S^2\{-\mid l-4,l-2,l\rangle+\mid l-4,l-2,l+1\rangle\} & ,i=l-2 \\ 2S\sqrt{S(2S-1)}\{-\mid l-3,l,l\rangle+\mid l-3,l-1,l-1\rangle\} & \\ \quad +2S(1-S)\{\mid l-3,l-1,l+1\rangle-\mid l-3,l,l+1\rangle\} & ,i=l-1 \\ 2S\sqrt{S(2S-1)}\{\mid l-2,l,l\rangle-\mid l-2,l+1,l+1\rangle\} & \\ \quad +2S(1-S)\{\mid l-2,l-1,l\rangle-\mid l-2,l-1,l+1\rangle\} & ,i=l \\ 2S\sqrt{S(2S-1)}\{\mid l+1,l+1,l+2\rangle-\mid l-1,l-1,l+2\rangle\} & \\ \quad +2S(1-S)\{\mid l,l+1,l+2\rangle-\mid l-1,l,l+2\rangle\} & ,i=l+1 \\ 2S^2\{\mid l-1,l+2,l+3\rangle-\mid l+1,l+2,l+3\rangle\} & ,i=l+2 \\ 2S^2\{-\mid l-1,l+3,l+4\rangle+\mid l,l+3,l+4\rangle\} & ,i=l+3 \end{cases} \tag{C.10}$$

$$\widetilde{O}_l \mid i-1,i,i+1\rangle =$$
$$\frac{1}{2i}\begin{cases} 0 \mid i-1,i,i+1\rangle & ,i \neq l-2,l-1,l,l+1,l+2 \\ 2S^2\{-\mid l-3,l-2,l\rangle+\mid l-3,l-2,l+1\rangle\} & ,i=l-2 \\ 2S\sqrt{S(2S-1)}\{-\mid l-2,l,l\rangle+\mid l-2,l-1,l-1\rangle\} & \\ \quad +2S(1-S)\{\mid l-2,l-1,l+1\rangle-\mid l-2,l,l+1\rangle\} & ,i=l-1 \\ 2\sqrt{S(2S-1)}(1-S)\{-\mid l-1,l-1,l+1\rangle+\mid l,l,l+1\rangle+\mid l-1,l-1,l\rangle & \\ \quad -\mid l,l+1,l+1\rangle-\mid l-1,l,l\rangle+\mid l-1,l+1,l+1\rangle\} & ,i=l \\ 2S\sqrt{S(2S-1)}\{\mid l,l,l+2\rangle-\mid l+1,l+1,l+2\rangle\} & \\ \quad +2S(1-S)\{\mid l-1,l,l+2\rangle-\mid l-1,l+1,l+2\rangle\} & ,i=l+1 \\ 2S^2\{-\mid l-1,l+2,l+3\rangle+\mid l,l+2,l+3\rangle\} & ,i=l+2 \end{cases} \tag{C.11}$$

The full Hamiltonian acting on these states are:

$$\begin{aligned} I_2 \mid i-2,i,i+2\rangle = -\frac{1}{2i}\Big\{ & 2S^2[-\mid i-2,i,i+3\rangle+\mid i-2,i,i+4\rangle+\mid i-2,i,i+1\rangle \\ & -\mid i-2,i,i+3\rangle+\mid i-2,i-1,i+2\rangle-\mid i-2,i+1,i+2\rangle+\mid i-3,i,i+2\rangle \\ & -\mid i-1,i,i+2\rangle-\mid i-4,i,i+2\rangle+\mid i-3,i,i+2\rangle] \\ & +2S\sqrt{S(2S-1)}[-\mid i-2,i,i\rangle+\mid i-2,i+2,i+2\rangle-\mid i-2,i-2,i+2\rangle \end{aligned}$$

$$+ \mid i,i,i+2\rangle] + 2S(1-S)[\mid i-2,i+1,i+2\rangle - \mid i-2,i,i+1\rangle + \mid i-1,i,i+2\rangle$$
$$- \mid i-2,i-1,i+2\rangle]\} \tag{C.12}$$

$$I_2 \mid i-2,i,i+1\rangle = -\frac{1}{2i}\{2S^2[-\mid i-2,i,i+2\rangle + \mid i-2,i,i+3\rangle + \mid i-3,i,i+1\rangle$$
$$- \mid i-1,i,i+1\rangle - \mid i-4,i,i+1\rangle - \mid i-3,i,i+1\rangle]$$
$$+ 2S\sqrt{S(2S-1)}[-\mid i-2,i+1,i+1\rangle + \mid i-2,i,i\rangle + \mid i-2,i,i\rangle$$
$$- \mid i-2,i+1,i+1\rangle - \mid i-2,i-2,i+1\rangle + \mid i,i,i+1\rangle]$$
$$+ 2S(1-S)[-\mid i-2,i+1,i+2\rangle + \mid i-2,i,i+2\rangle - \mid i-2,i-1,i+1\rangle$$
$$+ \mid i-2,i-1,i\rangle + \mid i-1,i,i+1\rangle - \mid i-2,i-1,i+1\rangle]\} \tag{C.13}$$

$$I_2 \mid i-1,i,i+1\rangle = -\frac{1}{2i}\{2S^2[-\mid i-1,i,i+2\rangle + \mid i-1,i,i+3\rangle - \mid i-3,i,i+1\rangle$$
$$+ \mid i-2,i,i+1\rangle] + 2S\sqrt{S(2S-1)}[-\mid i-1,i+1,i+1\rangle + \mid i-1,i,i\rangle$$
$$+ \mid i-1,i-1,i+1\rangle - \mid i,i,i+1\rangle] + 2S(1-S)[-\mid i-1,i+1,i+2\rangle$$
$$+ \mid i-1,i,i+2\rangle - \mid i-2,i,i+1\rangle + \mid i-2,i-1,i+1\rangle]$$
$$+ 2(1-S)\sqrt{S(2S-1)}[-\mid i-1,i-1,i+1\rangle + \mid i,i,i+1\rangle + \mid i-1,i-1,i\rangle$$
$$- \mid i,i+1,i+1\rangle - \mid i-1,i,i\rangle + \mid i-1,i+1,i+1\rangle]\} \tag{C.14}$$

$I_2 \mid i-1,i,i+2\rangle$ is similar to $I_2 \mid i-2,i,i+1\rangle$.

Next we find $\widetilde{O}_l$ acting on the kets $\mid i,i,i\rangle, \mid i,i,i+1\rangle$ and $\mid i,i,i+2\rangle$. Then the equations for I_2 acting on states with all three spin deviations on the same site, or two deviations of the same site and the other deviation on a nearest neighbor or next nearest neighbor site can be found.

$$\widetilde{O}_l \mid i,i,i+2\rangle =$$
$$\frac{1}{2i}\begin{cases} 0 \mid i,i,i+2\rangle & ,i \neq l-3,l-2,l-1,l,l+1 \\ 2S^2\{-\mid l-3,l-3,l\rangle + \mid l-3,l-3,l+1\rangle\} & ,i=l-3 \\ 2S^2\{\mid l-2,l-2,l-1\rangle - \mid l-2,l-2,l+1\rangle\} & ,i=l-2 \\ -2S\sqrt{3S(S-1)}\mid l-1,l-1,l-1\rangle + 2\sqrt{S(2S-1)}(1-S)\mid l-1,l,l+1\rangle & \\ \quad +2S(2S-1)\mid l-1,l+1,l+1\rangle - 2S(2-S)\mid l-1,l-1,l\rangle & \\ \quad ,i=l-1 & \\ 2S\sqrt{S(2S-1)}\{\mid l-1,l,l+2\rangle - \mid l,l+1,l+2\rangle\} & ,i=l \\ 2S\sqrt{S(2S-1)}\{-\mid l-1,l+1,l+3\rangle + \mid l,l+1,l+3\rangle\} & ,i=l+1 \end{cases} \tag{C.15}$$

$$\widetilde{O}_l \mid i,i,i+1\rangle =$$

$$\frac{1}{2i}\begin{cases} 0 \mid i,i,i+1\rangle & ,i \neq l-2,l-1,l,l+1 \\ 2S^2\{- \mid l-2,l-2,l\rangle + \mid l-2,l-2,l+1\rangle\} & ,i=l-2 \\ 2S\sqrt{3S(S-1)} \mid l-1,l-1,l-1\rangle - 2\sqrt{S(2S-1)}(1-S) \mid l-1,l,l+1\rangle & \\ \quad -2S(2S-1) \mid l-1,l,l\rangle + 2S(2-S) \mid l-1,l-1,l+1\rangle & \\ \quad ,i=l-1 & \\ 2S\sqrt{3S(S-1)} \mid l,l,l\rangle - 2\sqrt{S(2S-1)}(1-S) \mid l-1,l,l+1\rangle & \\ \quad -2S(2S-1) \mid l,l+1,l+1\rangle + 2S(2-S) \mid l-1,l,l\rangle & ,i=l \\ 2S\sqrt{S(2S-1)}\{- \mid l-1,l+1,l+2\rangle + \mid l,l+1,l+2\rangle\} & ,i=l+1 \end{cases} \tag{C.16}$$

$$\widetilde{O}_l \mid i,i,i\rangle =$$

$$\frac{1}{2i}\begin{cases} 0 \mid i,i,i\rangle & ,i \neq l-1,l,l+1 \\ 2S\sqrt{3S(S-1)}\{- \mid l-1,l-1,l\rangle + \mid l-1,l-1,l+1\rangle\} & ,i=l-1 \\ 2S\sqrt{3S(S-1)}\{\mid l-1,l,l\rangle - \mid l,l,l+1\rangle\} & ,i=l \\ 2S\sqrt{3S(S-1)}\{- \mid l-1,l+1,l+1\rangle + \mid l,l+1,l+1\rangle\} & ,i=l+1 \end{cases} \tag{C.17}$$

Therefore the effect of I_2 acting on states with all three spin deviations on the same site or two deviations on the same site and the other deviation on a nearest neighbor or a next nearest neighbor site are:

$$\begin{aligned} I_2 \mid i,i,i+2\rangle = -\frac{1}{2i}\Big\{ & 2S^2[- \mid i,i,i+3\rangle + \mid i,i,i+4\rangle + \mid i,i,i+1\rangle - \mid i,i,i+3\rangle] \\ & + 2S\sqrt{S(2S-1)}[\mid i-1,i,i+2\rangle - \mid i,i+1,i+2\rangle - \mid i-2,i,i+2\rangle + \mid i-1,i,i+2\rangle] \\ & - 2S\sqrt{3S(S-1)} \mid i,i,i\rangle + 2S(2S-1) \mid i,i+2,i+2\rangle \\ & + 2(1-S)\sqrt{S(2S-1)} \mid i,i+1,i+2\rangle - 2S(2-S) \mid i,i,i+1\rangle \Big\} \end{aligned} \tag{C.18}$$

$$\begin{aligned} I_2 \mid i,i,i+1\rangle = -\frac{1}{2i}\Big\{ & 2S^2[- \mid i,i,i+2\rangle + \mid i,i,i+3\rangle] + 2S\sqrt{S(2S-1)}[- \mid i-2,i,i+1\rangle \\ & + \mid i-1,i,i+1\rangle] + 4S\sqrt{3S(S-1)} \mid i,i,i\rangle - 4S(2S-1) \mid i,i+1,i+1\rangle \\ & + 2(1-S)\sqrt{S(2S-1)}[- \mid i,i+1,i+2\rangle - \mid i-1,i,i+1\rangle] \\ & + 2S(2-S)[\mid i,i,i+2\rangle + \mid i-1,i,i\rangle]\Big\} \end{aligned} \tag{C.19}$$

$$I_2 \mid i,i,i\rangle = -\frac{1}{2i}\Big\{2S\sqrt{3S(S-1)}[-\mid i,i,i+1\rangle+\mid i,i,i+2\rangle+\mid i-1,i,i\rangle-\mid i,i,i+1\rangle$$
$$-\mid i-2,i,i\rangle+\mid i-1,i,i\rangle]\} \qquad \text{(C.20)}$$

$I_2 \mid i-2,i,i\rangle$ is similar to $I_2 \mid i,i,i+2\rangle$ and $I_2 \mid i-1,i,i\rangle$ is similar to $I_2 \mid i,i,i+1\rangle$.

The full set of equations specifying the effect of I_2 on the complete set of orthonormal states are equations (C.2), (C.6) to (C.8), (C.12) to (C.14) and (C.18) to (C.20). The conversion of these equations to a more understandable form is done in section 5.3.

Bibliography

[1] P.A.M. Dirac, Proc. Roy. Soc. **112A**, 661 (1926).

[2] W. Heisenberg, Z. Phys. **49**, 619 (1928).

[3] S.T. Chiu-Tsao, Peter M. Levy, and C. Paulson, Phys. Rev. B **12**, 1819 (1975).

[4] R.J. Lee, *Three Magnon Excitations in One Dimensional Quantum Spin Chains*, M. Sc. Thesis, University of Manitoba (1993).

[5] H.A. Bethe, Z. Phys. **71**, 205 (1931).

[6] F.D.M. Haldane, J. Phys. C **15**, L1309 (1982).

[7] L.A. Takhtajan, Phys. Lett. **87A**, 479 (1982).

[8] H.M. Babujian, Phys. Lett. **90A**, 479 (1982).

[9] A.M. Tsvelik, Phys. Rev. B **42**, 779 (1990).

[10] R. Hoogerbeets, A.J. van Duyneveldt, A.C. Phaff, C.H.W. Swüste and W.J.M. de Jonge, J. Phys. C **17**, 2595 (1984).

[11] D.N. Haines and J.E. Drumheller, Phys. Rev. Lett. **58**, 2702 (1987).

[12] J.B. Torrance, Jr., and M. Tinkham, Phys. Rev. Series 2 **187**, 595 (1969).

[13] C. Benelli, A. Caneschi, D. Gatteschi, L. Pardi and P. Rey, Inorg. Chem. **29**, 4223 (1990).

[14] C.K. Majumdar, J. Math Phys. **10**, 177 (1969).

[15] I. Ono, S. Mikado and T. Oguchi, J. Phys. Soc. Japan **30**, 358 (1971).

[16] I. Gochev, Theor. and Math. Phys. (USA) **15**, 402 (1973).

[17] A.A. Bahurmuz and P.D. Loly, J. Phys. C **19**, 2241 (1986).

[18] B.W. Southern, T.S. Liu and D.A. Lavis, Phys. Rev. B **39**, 12160 (1989).

[19] A.J.M. Medved and B.W. Southern, Phys. Rev. B **43**, 816 (1991).

[20] P.J. Millet and H. Kaplan, Phys. Rev. B **10**, 3923 (1974).

[21] C. Kadolkar, D.K. Ghosh and C.R. Sarma, J. Phys.: CM **4**, 9651 (1992).

[22] R. Haydock, *The Recursive Solution of the Schrödinger Equation* in: Solid State Physics Vol. 35, edited by H. Ehrenreich, F. Seitz, and D. Turnbull, Academic Press, Inc., New York (1980).

[23] B.W. Southern, A.A. Kumar and J.A. Ashraff, Phys. Rev. B **28**, 1785 (1983).

[24] Yu.A. Izyumov and Yu.N.Skryabin, *Statistical Mechanics of Magnetically Ordered Systems*, Consultants Bureau, New York (1988).

[25] R. White, *Quantum Theory of Magnetism*, McGraw-Hill Book Company, New York (1970).

[26] E. Economou, *Green's Functions in Quantum Physics*, Springer-Verlag, Berlin (1983).

[27] P. Turchi, F. Ducastelle and G. Tréglia, J. Phys. C **15**, 2891 (1982).

[28] A.M. Tsvelik, JETP Letters **49**, 117 (1989).

[29] H. Frahm, J. Phys. A **25**, 1417 (1992).

[30] M. Grabowski and P. Mathieu, preprint, Los Alamos National Laboratory (1994).